Coupling geothermal energy capture with carbon dioxide sequestration in naturally permeable, porous geologic formations – a novel approach for expanding geothermal energy utilization.

A DISSERTATION
SUBMITTED TO THE FACULTY OF THE GRADUATE SCHOOL
OF THE UNIVERSITY OF MINNESOTA
BY

Jimmy Bryan Randolph

IN PARTIAL FULFILLMENT OF THE REQUIREMENTS
FOR THE DEGREE OF
Doctor of Philosophy

Martin O. Saar

August, 2011

Acknowledgements

Numerous people have earned my gratitude for their contribution to the completion of my dissertation. I would like to thank my adviser, Martin Saar, for his continuous support, encouragement, and excitement in pursuing diverse research opportunities as they arise, without which the carbon dioxide plume geothermal (CPG) concept would never have progressed.

To colleagues from around the University of Minnesota, I am grateful for countless inspiring research discussions and assistance in my endeavors – Calvin Alexander, Scott Alexander, Thomas Kuehn, Clay Parker, Melisa Pollak, William Seyfried, Russ Straate, Steven Taff, Harvey Thorleifson, and Elizabeth Wilson. I am grateful to have had the opportunity to work and consult with researchers from Lawrence Berkeley National Laboratory, the U.S. Geological Survey, and the University of North Dakota, including Karsten Pruess, Shaul Hurwitz, Christopher Farrar, and William Gosnold.

Moreover, I would like to thank fellow graduate students, undergraduate students, and post docs for extensive encouragement and innumerable research conversations – Ben Adams, Ravi Appana, Maria Davis, Andrew Luhmann, Joe Myre, Joseph Nelson, Andrew Smale, Ryan Toot, Benjamin Tutolo, and Stuart Walsh.

Funding for the research presented in this dissertation was generously provided by the Minnesota Legislature; the Initiative for Renewable Energy and the Environment, a signature program of the Institute on the Environment of the University of Minnesota; and the U.S. Department of Energy.

Finally, I thank my wife, Lauren Anderson, without whose unfailing love, support, and companionship this dissertation would not have been possible.

Abstract

This thesis research presents a new method to harness geothermal energy by combining it with geologic carbon dioxide (CO_2) sequestration. CO_2 is injected into deep, naturally porous and permeable geologic formations. The geothermally heated CO_2 is piped to the surface, used to produce electricity, and then returned to the subsurface. This new approach represents a radical shift in electric/heat power generation as it not only utilizes a renewable energy source but has a negative carbon footprint. This research explores the potential and applicability of the approach and related aspects of geologic fluid and heat flow.

Contents

List of Tables

List of Figures

Chapter 1

Introduction

1.1 The Carbon Dioxide (CO_2) Plume Geothermal (CPG) System

Carbon dioxide sequestration in deep saline aquifers and depleted hydrocarbon fields has been widely considered as a means for reducing anthropogenic CO_2 emissions to the atmosphere (e.g., 2007 IPCC Fourth Assessment [3]). Rather than treating CO_2 merely as a waste fluid in need of disposal, however, it could also be used as a working fluid in geothermal energy capture. CO_2's high heat extraction efficiency compared to water, demonstrated in Chapter 2, would be particularly beneficial in regions with low- to medium-grade geothermal heat resources, where traditional geothermal electricity production is not economically feasible. Therefore, this approach could vastly extend geothermal electricity generation worldwide. Moreover, this method would sequester CO_2 emitted from, for example, fossil fuel power plants, helping address a critical challenge of CO_2 capture and storage: cost [4].

Geothermal energy offers clean, consistent, reliable electric power with no need for grid-scale energy storage, unlike most renewable power alternatives. However, geothermal energy is often underrepresented in renewable energy discussions and has considerable room for growth (e.g., [5] [6]). New technology and methods will be critical for future investment, and rapid implementation of new techniques will be important to

ensure geothermal energy plays a significant role in the future energy landscape worldwide.

CO_2 has previously been proposed as a geothermal working fluid [7] [8] [9] [10] [11] [12], however, only in the context of engineered or enhanced geothermal systems (EGS), hereafter referred to as CO_2-based EGS. As opposed to naturally porous, permeable geologic formations (hereafter referred to as "reservoir" or porous medium systems), EGS are typically generated by hydraulic fracturing or stimulating of rock of low natural permeability, which may induce seismicity [13] [14]. Hence, despite potential for widespread future development [5], EGS must overcome significant socio-political resistance - as exemplified by the termination of EGS projects in 2009 (e.g., [15]) - in addition to technical obstacles. In contrast, the method described here does not rely on hydrofracturing or similar permeability-enhancement, rather it utilizes existing, high-permeability formations. Such natural reservoirs are typically much larger than hydro-fractured reservoirs (e.g., reservoirs in the Williston Basin, U.S., extend hundreds of kilometers [16], whereas the Soultz, France, EGS site has an extent of a few hundred meters [17]). Consequently, the CO_2 sequestration potential of the system described here is significantly larger than that of EGS. Therefore, I distinguish this approach from CO_2-based EGS and refer to it as a CO_2-plume geothermal (CPG) system.

CPG involves injecting supercritical CO_2 into deep, naturally porous, permeable geologic reservoirs overlain by low-permeability caprock (Figure 1.1), formations often prevalent worldwide (e.g., [19]). There, the CO_2 displaces native formation fluid (e.g., brine or hydrocarbons), as in standard CO_2 sequestration or enhanced oil recovery (EOR), and is heated by the natural in-situ heat and geothermal heat flux. A portion of the heated CO_2 is piped back to the surface and sent through an expansion device, powering an electrical generator, or a heat exchanger to provide heat for direct use and/or binary power systems. The CO_2 is then re-injected into the reservoir; long-term, all injected CO_2 is stored.

Prior to field implementation of CPG technology, several challenges must be addressed. Inherent in CPG are the challenges, as well as the opportunities, of geologic CO_2 sequestration; issues include preventing vertical CO_2 leakage, while benefits include reduced atmospheric CO_2 emissions and potential revenue from future carbon

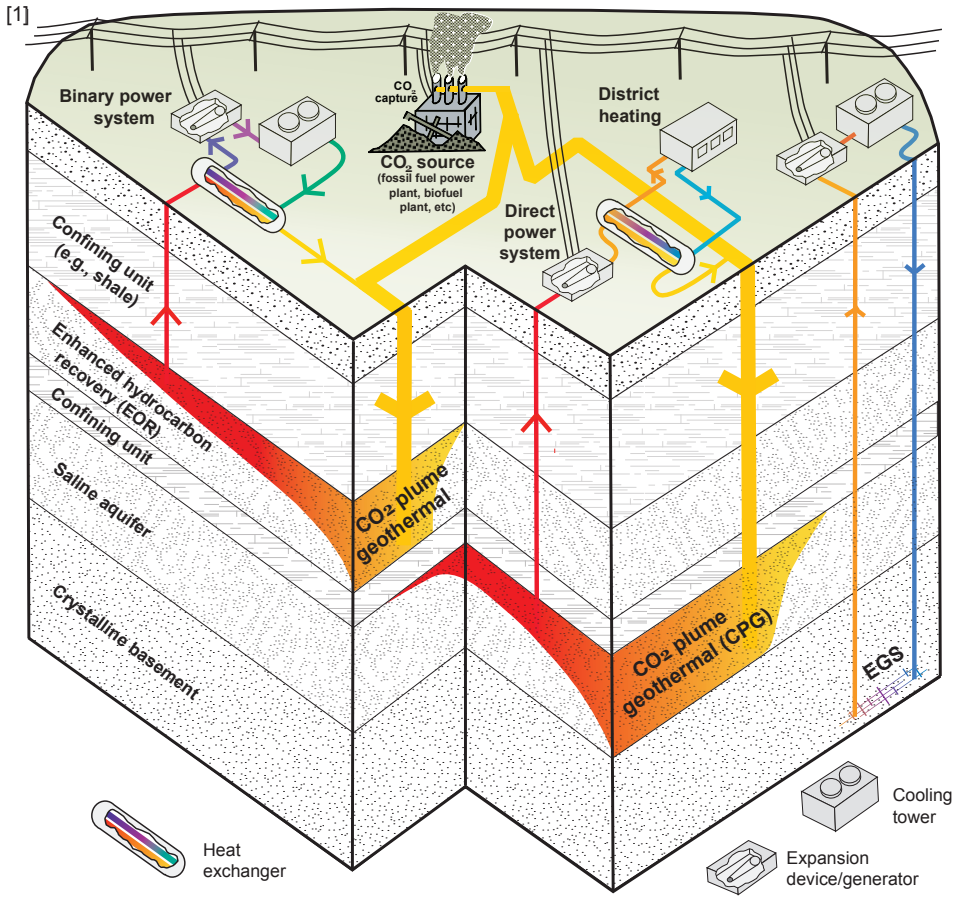

Figure 1.1: Envisioned implementations of CO_2-based geothermal systems. Included are CO_2-plume geothermal (CPG) systems established in saline aquifers or as components of enhanced oil/hydrocarbon recovery (EOR). Realizations include direct or binary cycles, various secondary working fluids, and multiple production/injection wells. CO_2 sources include fossil-fuel power plants, which would provide nearby electric-grid access for the geothermal facility, and biofuel plants. Geothermal energy could be used for electricity generation, district heating, and/or to power compressors during CO_2 sequestration or EOR, particularly in remote regions (e.g., off-shore). From [18].

emissions limitation policies. Extensive research worldwide is dedicated to CO_2 sequestration, thus for information on CO_2-sequestration-specific issues, see the literature (e.g., [20]). Specific to adding geothermal heat mining to geologic CO_2 sequestration, topics to be dealt with, together with possible approaches to addressing them, include: 1) acidic water saturated with CO_2 (may be addressed using corrosion-resistant materials, water separation technology, and/or binary cycle power systems) and 2) short circuiting or upconing of plume (may be addressed by careful reservoir management, including reservoir pressure and plume development through strategic geothermal fluid pumping). For additional discussion of CPG challenges and opportunities, see Chapter 3.

1.2 The Invention of CPG

This dissertation began as a fundamental study of fluid and heat flow in the subsurface; over time, it evolved into an examination of a new process to extract geothermal heat energy for power production or direct use – Carbon dioxide (CO_2) Plume Geothermal (CPG). Here, I relate the story of this evolution in thought and study, along the way introducing the chapters comprising this dissertation. The chapters reveal how the seemingly disparate concepts of subsurface fluid/heat flow and geologic CO_2 sequestration merged over the course of my graduate program into a single, novel geothermal energy capture technique.

At its onset (2006), my thesis research was structured around an examination of temperature as a function of depth, T(z), in a region of high geothermal heat flow, Long Valley Caldera (LVC), California. Chapter 6 briefly describes this project, with additional information on Long Valley and T(z) applications provided in Appendices F and E, respectively. As time progressed, I sought to explore subsurface heat and fluid flow locally in addition to studies in LVC; opportunities arose in the form of deep T(z) examinations in Minnesota for heat flow determination. LVC material in Chapter 6 is followed by a discussion of said local examinations.

In 2007, the Minnesota Legislature indicated interest in accessing the feasibility of geologic CO_2 sequestration in the state. The Minnesota Geological Survey (MGS) was tasked with producing a report on the potential for storage in the Midcontinental Rift

Sysem (MRS), which passes from Lake superior through Minnesota into Iowa. MGS director, Harvey Thorleifson, being familiar with research activities in the UMN Department of Earth Sciences (formerly, the Department of Geology and Geophysics), approached Dr. Martin Saar and myself regarding numerical modeling of CO_2 sequestration in the MRS. Having an interest in mitigation of anthropogenic greenhouse gas emissions, and given that CO_2 sequestration modeling involves similar techniques to general simulation of subsurface heat and fluid flow, I embarked upon a project to complete simple simulations of MRS CO_2 sequestration. The results of this study are provided in Appendix C.

Shortly after completion of the MGS CO_2 sequestration study, having developed a strong interest in the subject, I sought a way to continue studying geologic sequestration while simultaneously advancing my subsurface fluid and heat flow examinations, particularly related to geothermal energy. At that time (mid 2008), the Initiative for Renewable Energy and the Environment (IREE), a program of the Institute on the Environment (IonE) at the UMN, issued its first call for proposals in several years. IREE seeks to fund innovative research focused on renewable energy and mitigation of greenhouse gas emissions. I thought to submit two proposals to IREE, one regarding local geothermal energy potential and one, CO_2 storage modeling.

During a drive to the UMN Hydrogeology Field Camp site for a weekend of groundwater research, Martin Saar and I discussed how we might submit one proposal to IREE that combines geothermal and CO_2 storage research. The pieces of the puzzle came together – we wondered if CO_2 could be used as a geothermal heat capture fluid in the naturally permeable, porous formations typically considered for geologic CO_2 sequestration. Pondering the system, we began to see the potential of CO_2 as a geothermal working fluid (see, for e.g., Chapter 2). Significantly, a CO_2-based geothermal system would both produce power and sequester CO_2, resulting in power generation with negative CO_2 emissions. Returning to the UMN, we consulted Dr. Thomas Kuehn of the Department of Mechanical Engineering. He confirmed that a CO_2-based power system is indeed viable and could in fact have significant advantages over typical water-based systems (see, for example, Appendix B).

Attempting to verify the originality of the CO_2-geothermal concept, I conferred with Dr. Karsten Pruess of Lawrence Berkeley National Labs, a leading expect on CO_2

sequestration and geothermal modeling, and developer of the well-established geologic reservoir modeling code TOUGH2. He noted that recently, the use of CO_2 as the subsurface working fluid in enhanced geothermal systems (EGS) had been proposed [7]. However, he confirmed that beyond employing the same heat exchange fluid, EGS and sedimentary basin (i.e., naturally permeable, porous formation) CO_2-geothermal are significantly different, possessing widely disparate aspects of fluid flow, heat exchange, and reservoir development and maintenance.

Thus, Martin and I pursued IREE funding to explore what we termed CO_2 Plume Geothermal (CPG), bringing together a team to explore the full system, necessarily including mechanical engineers, economists, public policy experts, geologic modelers, geologists, and geochemists. The grant proposal – written primarily by Martin and myself with assistance from Dr. Kuehn, Dr. Elizabeth Wilson (UMN Humphrey Institute), Dr. Steven Taff (UMN Applied Economics), Dr. William Seyfried (UMN Geology and Geophysics), and Dr. Harvey Thorleifson (Minnesota Geological Survey) – was funded in early 2009 after extensive review (the first peer review of the CPG concept), providing momentum for the CPG research comprising the majority of this dissertation.

Given the innovative nature of CPG, the natural next step was to pursue patenting it. Should CPG research advance sufficiently that field demonstrations are deemed appropriate, a patent will be essential for attracting the large amounts of capital required for energy projects. With the assistance of the UMN Office for Technology Commercialization (OTC) with Leza Besemann and Russ Straate, we wrote and submitted a provisional patent application in March 2009. A year later, a full patent application was submitted (Appendix B), shortly prior to which OTC brought Clay Parker, a CEO in residence, onto the project to help guide CPG commercial development.

Following provisional patent submission, I embarked on numerical modeling exercises with the goal of determining in detail the geologic feasibility of CPG. Because of the novelty of the concept, it was critical to ensure that all models were extensively verified and cross checked with existing published literature (e.g., [9]) to ensure accurate and consistent operation. Furthermore, it was important to establish CPG as distinct from other geothermal approaches, which will ultimately be key attracting funding for field-scale demonstrations. As such, the pivotal CPG publication demonstrating the

technique's geothermal heat extraction viability followed full patent application by approximately one year (Chapter 2). Along the way, favorable aspects of the system were demonstrated, including improved heat extraction of CPG compared to EGS with CO_2 as the working fluid (Chapter 3), and the opportunity provided by CPG to offset costs of traditional carbon capture and storage (CCS) (Chapter 4).

For extensive detail on the modeling used to demonstrate the viability of the CPG approach, see Chapter 3. While CPG is very favorable in many respects, as previously noted, numerous challenges must be overcome prior to field implementation. Many of these challenges, together with approaches that may serve to address them, are also presented in Chapter 3.

Finally, if more recent work, I have sought to explore additional characteristics of the CPG system. Geologic reservoir permeability is a key parameter governing subsurface fluid flow and, particularly for fluids other than CO_2, the amount of energy required to produce reservoir fluid. Thus, in Chapter 5, I explore reservoir permeability versus net formation energy capture and conversion to electricity for several reservoir working fluids. Thereafter, Chapter 7 summaries the conclusions and main findings of this dissertation.

Chapter 2

Combining geothermal energy capture with geologic carbon dioxide sequestration

This chapter is largely based on Randolph and Saar, 2011 [18]. Here, the fundamental viability of the CO_2 Plume Geothermal approach is explored. For additional detail concerning the development of CPG numerical modeling capabilities, as well as challenges and opportunities associated with CPG, see Chapter 3.

2.1 Introduction

In this chapter, I demonstrate that CPG systems are capable of achieving improvements in heat extraction efficiencies well above those accomplished by replacing water with CO_2 as the working fluid in EGS.

The CPG approach has only become feasible of late, due to planned (and partially implemented) large-scale geologic CO_2 sequestration in natural reservoirs worldwide. Discussion of the challenges and opportunities of CO_2 sequestration or EOR, though inherent to CPG, are reserved for the extensive literature (e.g., [21] [22] [3]). Existing preliminary research on CO_2-based EGS [9] [11] [12], though a recently devised method itself, provides context to determine the feasibility of the new CPG approach. Hence, I

focus my investigation on comparing CPG with CO_2- and water-based EGS, and with conventional water-based geothermal reservoir systems.

2.2 Model characteristics and methods

Model parameters are summarized in Tables 2.1 and 2.2. A subsurface system initial temperature of $T = 100\ ^oC$ is chosen for base-case models, as it is often considered the lower limit for geothermal electricity production (e.g., [23]). In comparison, $T = 150\ ^oC$ is more typical for water-based geothermal systems, as 90% of the US geothermal electrical capacity operates on higher-temperature ($T > 150\ ^oC$) dry and flash-steam systems rather than lower-temperature ($100 < T < 150\ ^oC$) binary systems (unpublished data, 2010, available from the Geothermal Energy Association (http://geo-energy.org/plants.aspx) and the International Energy Agency (http://www.iea.org)). In a region of moderate heat flow (here characterized by a geothermal gradient of 30 - 35 ^oC/km), 100 ^oC corresponds to a formation depth of 2.5 km, depending on the local mean annual surface temperature and fluid-rock thermal conductivity. Fluid injection/production rates are determined by specifying downhole injection and production pressures 10 bars higher and lower, respectively, than formation pressure. The presence of subsurface CO_2 is assumed (naturally or from previous injection) and no other fluid occupies the pore space, analogous to CO_2-based EGS studies [9] [11]. While displacement of native fluid is of interest, it is beyond the scope of the present study. All simulations utilize the well-verified reservoir simulator TOUGH2 [24] with equation-of-state module ECO2N [25]. Conduction of heat between the domain and confining beds, a minor contribution to model heat budget [11], is approximated using the semi-analytic heat exchange method in TOUGH2 [26].

To ensure that models constructed for the present study function correctly, the EGS models and results of Pruess [9] were first reproduced (see Chapter 5). The symmetry of the employed five-spot computational grid reduces simulation requirements to 1/8th of the system domain (gridded region, inset, Figure 2.1). In EGS models, fracture/matrix heat exchange is accomplished via the multiple-interacting continua method [27]. Heat extraction rate, $H = Q(h - h_o)$, and fluid mass flow rate, Q, are monitored at a production well; h and h_o are specific enthalpy of the produced and injected fluids, respectively.

Parameter	Value
Geologic Formation	
Thickness	305 meters
Well separation	707.1 meters
Porosity (reservoir/EGS)	20% / 2%
Permeability, k (reservoir/EGS)	$5x10^{-14}$ m^2 / $2.5x10^{-14}$ m^2
Rock grain density	2650 kg/m^3
Rock specific heat	1000 J/kg/^{o}C
Thermal conductivity	2.1 W/m/^{o}C
Injection/Production Conditions	
Formation map-view area	1 km^2
Temperature of injected fluid	20 ^{o}C[a]
Well pattern (Figure 2.1, insert)	Five-spot
Injection/production rate	300 kg/s (variable)
Downhole injection pressure	260 bar
Downhole production pressure	240 bar
Formation Initial Condition	
Fluid in pore spaces	All CO_2 or all H_2O
Temperature	100 ^{o}C
Pressure	250 bar
Formation Boundary Conditions	
Top/sides	No fluid or heat flow
Bottom	Heat conduction, no fluid flow

Table 2.1: Parameters of Base Cases. [a]Downhole injection temperature is higher than the surface heat rejection temperature specified in Section 5.1, as Joule-Thomson heating occurs in the injection well [9]).

Case Number	Permeability (Reservoir/EGS)	Formation Pressure	Formation Temperature
1	$5x10^{-14}$/ $2.5x10^{-14}$ m^2 [a]	250 bar[a]	120 ^{o}C
2	$5x10^{-14}$/ $2.5x10^{-14}$ m^2 [a]	250 bar[a]	140 ^{o}C
3	$5x10^{-14}$/ $2.5x10^{-14}$ m^2 [a]	200 bar	100 ^{o}C[a]
4	$5x10^{-14}$/ $2.5x10^{-14}$ m^2 [a]	300 bar	100 ^{o}C[a]
5	$5x10^{-14}$ m^2	250 bar[a]	100 ^{o}C[a]

Table 2.2: Parameters of Cases for Exploration of Parameter Space. [a]Parameter is the same as in the base cases. Cases 1-4 apply to CPG, CO_2-based EGS, H_2O reservoir, and H_2O-based EGS. Case 5 applies only to CO_2-based EGS.

A representative value for permeability, k, of hydraulically stimulated rock (in EGS) of 2.5x10^{-14} m^2 is determined by averaging the reported values from EGS field sites - Soultz, France: 6x10^{-14} m^2 [13] [28]; Ogachi, Japan: 10^{-15} to 10^{-14} m^2 [5] - together with system-scale $k_{EGS} = 1.1\text{x}10^{-14}$ m^2, calculated via a network model from individual fracture permeabilities ([29] and Chapter 3).

2.3 Energy Recovery

Figure 2.1 presents temperatures from injection to production well after 10 simulated years of heat recovery, providing an intermediate snapshot of system behavior and illustrating heat extraction differences among CPG and CO_2-based EGS cases. Here, all simulations are performed with the same permeability (5x10^{-14} m^2, calculated in Randolph and Saar [29]) to ensure identical mass flow rates. As noted in Section 3, k_{EGS} is expected to be less than that of reservoir systems. Thus, results depicted in Figure 2.1 are conservative; Figure 2.2 includes results for $k_{EGS} < 5\text{x}10^{-14}$ m^2. Three EGS cases are considered, corresponding to fracture spacings of 70 m (primary grid block side length), 140 m, and 210 m. Such discrete fracture networks provide reasonable approximations of principal fluid flow conduits and heat extraction from fracture-dominated systems, as percolation theory, principal path analysis, and field tests often show that while systems may contain dense fracture networks, very few fractures accommodate the majority of fluid flow (e.g., [30]).

In the CPG case, temperature at the production well remains closer to the initial system temperature (100 ^{o}C) than in any EGS case (Figure 2.2), permitting more prolonged heat use in CPG. Furthermore, EGS production temperature decreases with increasing fracture spacing. These results indicate more thorough heat-sweeping capabilities of the CPG system than fractured formations, a consequence of the CO_2 being in contact with a larger specific surface area of host rock or sediment in CPG.

Time series of geothermal heat energy extraction rates are provided in Figure 2.2a. All rates are given for the full, 5-well domain. Two values for k_{EGS} are considered: 5x10^{-14} m^2, to allow direct comparison with reservoir-system simulations, and 2.5x10^{-14} m^2, more indicative of actual EGS implementations (Section 3). Heat extraction rates decrease with time as formation heat is depleted and production temperatures decrease.

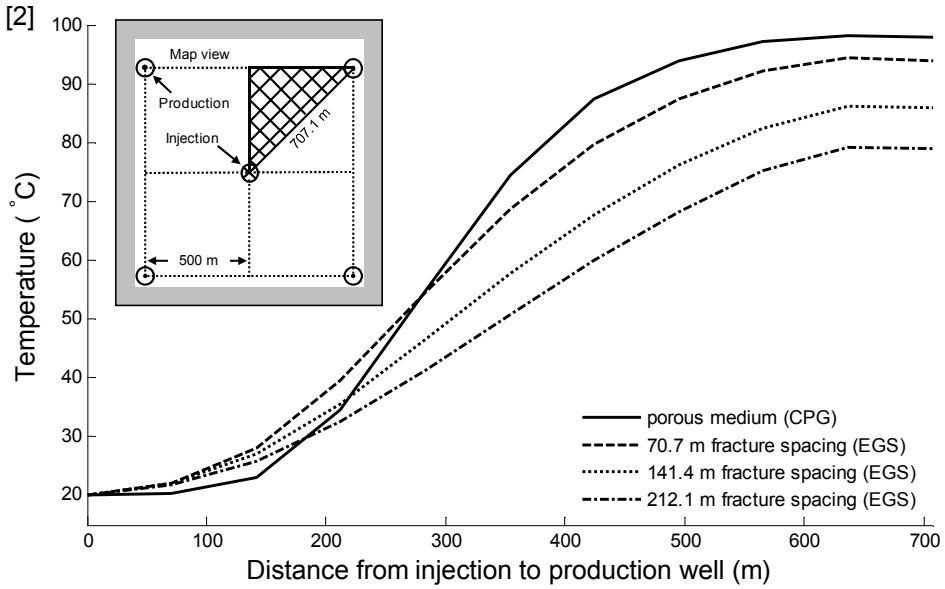

Figure 2.1: Temperature sections along direct lines from injection to production wells. All simulations have the same system-scale permeability, $k = 5\text{x}10^{-14}$ m^2. Simulation results are plotted after 10 years of CO_2 injection/production. The gridded section of the inset figure provides the model domain (in map view) and reveals the symmetry of the five-spot well system. From [18].

EGS models with lower permeabilities result in smaller mass flow rates, producing lower heat extraction rates, though slower formation cooling, than EGS with similar fracture spacing and higher permeability.

Fluid mobility - density divided by dynamic viscosity (i.e., inverse kinematic viscosity) - describes a fluid's tendency to preserve momentum. Hence, despite the lower heat capacity of CO_2 than water, 2.20 versus 4.16 J/g/K at 100 ^{o}C and 250 bar (NIST), CO_2's markedly higher mobility (Tables 2.3 and 2.4) permits higher fluid mass flow rates and, thus, higher heat extraction rates at a given reservoir permeability, k, and reduces the minimum k above which heat advection tends to dominate over conduction [31]. Moreover, a low natural-reservoir $k = 5\text{x}10^{-14}$ m^2 (conservative average calculated from several CO_2 storage sites [32] [16]) was utilized, suggesting that for actual implementation sites, CPG heat extraction rates could be greater.

Figure 2.2b compares CPG, water-based reservoir, and water- and CO_2-based EGS heat extraction potentials for a variety of formation temperatures and pressures. A conservative EGS fracture spacing of 70 m is specified, which represents the investigated spacing with heat-sweeping characteristics most similar to reservoir (CPG) cases, and $k_{EGS} = 2.5\text{x}10^{-14}$ m^2. CPG systems provide greater heat extraction rates compared to water-based systems (both reservoir and EGS) as temperature and pressure decrease, suggesting the CPG approach is particularly useful in, but not restricted to, relatively shallow geologic formations. Minimum depths are required, however, to ensure adequate subsurface temperatures and that CO_2 is supercritical.

2.4 Implications for geothermal development

2.4.1 Expansion of the geothermal resource base

Traditional water-based geothermal development requires three geologic conditions: 1) significant amounts of water, 2) a permeable formation to permit water extraction/reinjection, and 3) sufficient subsurface temperatures. EGS seeks to artificially generate Condition 2 and supply (water-based EGS) or avoid (CO_2-based EGS) Condition 1, thereby expanding geothermal heat mining prospects. In comparison, CPG provides an alternative working fluid (avoiding Condition 1) with high mobility compared to water (Tables 2.3 and 2.4), thus expanding the range of usable natural-formation permeabilities (Condition 2). Similarly, CO_2 lowers minimum thresholds of economically and technologically viable subsurface temperatures (Condition 3), as its high mobility enhances heat extraction efficiency.

Figure 2.3 quantifies the expansion of subsurface regions that may become viable for geothermal power production in the contiguous US when CO_2 rather than water is used as the reservoir-based (i.e., CPG) heat extraction fluid; similar expansions may be feasible worldwide. Although the technology exists to utilize water-based geothermal resources at temperatures < 100 ^{o}C, approximately 90% of US installed capacity uses dry-steam or flash power systems, which rely on subsurface temperatures > 150 ^{o}C. Our models indicate that a traditional water-based reservoir system, installed in a single five-spot pattern (inset, Figure 2.1), at 150 ^{o}C and 2.5 km depth with $k = 5\text{x}10^{-14}$ m^2 would, over 25 years, extract on average 46 MW of thermal energy, given

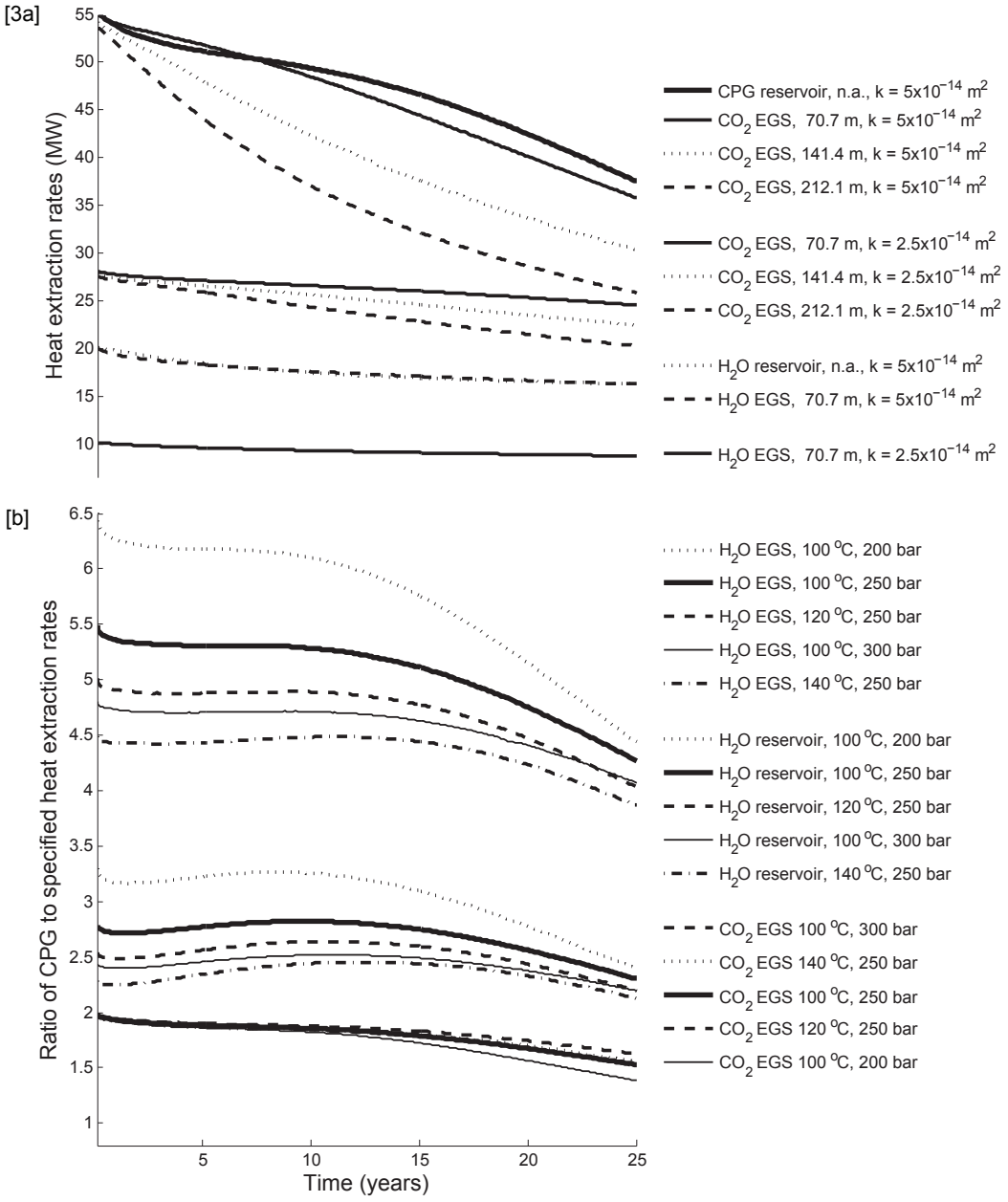

Figure 2.2: Time series of [a] geothermal heat extraction rates and [b] ratios of rates. CPG benefits over water-based systems are most pronounced at lower temperatures and pressures (i.e., shallower systems). Legend columns denote: [a] system type, fracture spacing if applicable, system permeability; [b] system type, temperature, pressure. In [b], reservoir system $k = 5\text{x}10^{-14}$ m^2 and $k_{EGS} = 2.5\text{x}10^{-14}$ m^2 (see main text). From [18].

Case Number	CPG	H_2O Reservoir	CO_2-Based EGS	H_2O-Based EGS
Base case	47.0	17.4	26.2	9.2
1	58.6	23.2	32.8	12.4
2	68.8	29.3	38.4	15.7
3	52.4	17.2	30.2	9.1
4	43.0	17.7	23.5	9.3
5	n.a.	n.a.	45.8	n.a.

Table 2.3: Results: Average Heat Extraction Rates (MW). Averages for 25 years of working-fluid injection/production and resultant heat energy recovery. Cases 1-4 apply to CPG, CO_2-based EGS, H_2O reservoir, and H_2O-based EGS. Case 5 applies only to CO_2-based EGS.

Case Number	CPG to H_2O Reservoir			CPG to CO_2 -Based EGS			CPG to H_2O -Based EGS		
	HE	M	MF	HE	M	MF	HE	M	MF
Base case	2.7	3.8	5.5	1.8	1.0	1.9	5.0	3.8	10.3
1	2.4	3.2	4.9	1.8	1.0	1.9	4.7	3.2	9.6
2	2.3	2.7	4.7	1.8	1.0	1.9	4.3	2.7	9.0
3	2.9	3.9	5.4	1.8	1.0	1.8	5.7	3.9	10.5
4	2.5	3.7	5.4	1.8	1.0	1.8	4.6	3.7	10.0
5	n.a.	n.a.	n.a.	1.0	1.0	1.0	n.a.	n.a.	n.a.

Table 2.4: Results: Ratios of Average Heat Extraction Rates (HE), Mobilities (M), and Mass Flow Rates (MF). Averages for 25 years of working-fluid injection/production and resultant heat energy recovery. Cases 1-4 apply to CPG, CO_2-based EGS, H_2O reservoir, and H_2O-based EGS. Case 5 applies only to CO_2-based EGS.

base-case parameters (Table 2.3). Applying a Carnot calculation with an annual average heat rejection temperature of 10 ^{o}C and assuming a power system efficiency of 50% (modified after Sanyal and Butler [33]), this translates to 5.2 MW of electrical generation. Our simulations show that a CPG system with identical parameters results in the same electrical production with geologic temperatures of only 98.2 ^{o}C. Applying similar considerations, a water reservoir system at 100 ^{o}C is required to provide the same electric power as a CPG system at only 65.8 ^{o}C. Note: as in traditional geothermal development, several CPG systems could be installed at a given site.

The just-discussed subsurface temperature pairs of 150 ^{o}C/ 98.2 ^{o}C (Figure 2.3a) and 100 ^{o}C/65.8 ^{o}C (Figure 2.3b) at 2.5 km depth illustrate the expanded regions of economically viable geothermal heat mining, should CO_2 be utilized rather than water and assuming suitable reservoirs exist. Figure 2.3 illustrates that while only black-shaded regions are viable for water-based reservoir geothermal systems, both gray- and black-shaded regions could be viable for CPG implementations. These comparisons do not include differences in Joule-Thomson heating/ cooling in wells between CO_2 and water [9]. Nonetheless, the CPG-viable regions may be considered conservative as they do not account for efficiency benefits when using CO_2, rather than water, in a power cycle (e.g., higher-than-atmospheric operating pressure leaving CO_2 turbines compared to near-vacuum pressure leaving steam turbines [12]). Moreover, CO_2 freezes at temperatures significantly below 0 ^{o}C, and thus in cool climates, the heat rejection temperature of CPG can be much lower and the electricity production potential, higher, than calculated. Also, the potential for a CO_2 thermosyphon [12] and associated, perhaps significant, reduction in pumping costs are not examined here.

2.4.2 Additional implications of CPG systems

Sales of CPG-produced energy could help offset the cost of CO_2 capture and storage; alternatively, in a carbon market, revenue from sequestration could enhance the competitiveness of CPG electricity [4].

Next, water-based EGS is confronted with challenges of loss and reactivity of injected water, as well as induced seismicity. EGS test sites have experienced water losses of up to 12% or more [5]. Clean, potable water is often limited, making such loss undesirable. In contrast, "loss" of injected CO_2 (i.e., sequestration) in saline - and thus unusable

- formations would be favorable. Furthermore, pure-phase CO_2, or CO_2 with little dissolved water, should be markedly less reactive than water in formations of interest for geothermal development [7] [12], limiting mineral dissolution/precipitation and "short-circuiting" of fluid flow pathways. Formation plugging is also less likely in a CPG system than in EGS, as percolation theory indicates that fluid flow pathways are more diverse and difficult to interrupt in a 3D porous medium than 2D or even 3D fracture systems (e.g., [30]).

Finally, meeting electricity demand by balancing baseload and peak power requirements is a challenge for expanding the use of renewable energies. Wind and solar are critical elements of the renewable energy landscape, but they have difficulty fulfilling baseload demand given the inconsistent nature of their energy sources. Geothermal can provide power both continuously and intermittently, helping meet baseload requirements or contributing to peak demands. Thus, alternative geothermal technology, such

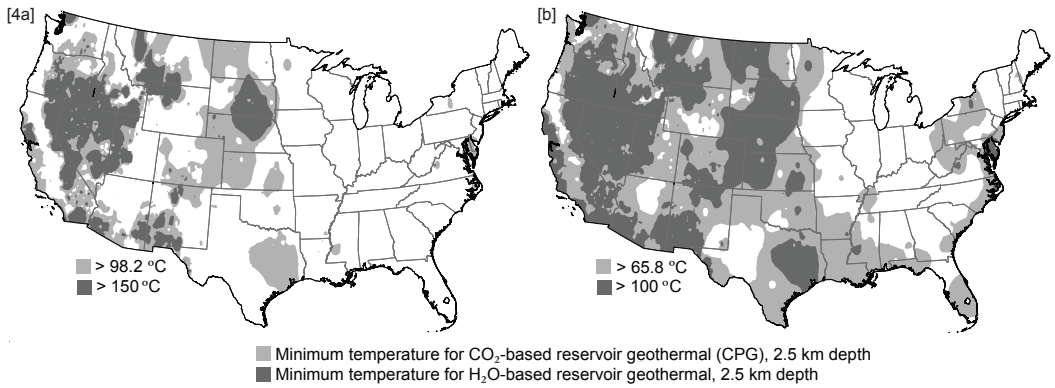

Figure 2.3: Expansion of viable geothermal regions using CPG. Temperature contours at 2.5 km depth illustrate the estimated expansion of regions viable for electricity production (if naturally permeable, porous reservoirs overlain by low-permeability caprocks exist), when replacing water with CO_2 as the subsurface geothermal heat extraction fluid (see main text), from dark-shaded to both dark- and gray-shaded regions. Maps were created using geothermal heat flow data from the Southern Methodist University heat flow database (2008, http://smu.edu/geothermal) together with the U.S.A. National Climate Data Center 30-year (1970-2000) mean annual surface temperature standard (2010, http://cdo.ncdc.noaa.gov). From [18].

as CPG, that expands our ability to capture geothermal energy beyond conventionally-viable regions, will become increasingly important.

2.5 Conclusions

We suggest that CO_2-plume geothermal (CPG) provides viable geothermal energy resources for electricity production, even in regions with relatively low geothermal temperatures and heat flow rates, where suitable reservoirs exist. Early-stage studies by several authors have indicated high potential for EGS with CO_2 as the subsurface working fluid [7] [9]. The work presented here, however, demonstrates that under a broad range of conditions, CPG results in significantly higher heat mining rates than even CO_2-based EGS, let alone traditional water-based reservoir or EGS methods, while simultaneously storing CO_2.

We recognize that inherent in the CPG approach are the challenges (and rewards) of geologic CO_2 sequestration. However, sequestration, both in saline aquifers and during Enhanced Oil Recovery (EOR), is extensively discussed in the literature and already occurring worldwide. Future work will investigate native formation fluid displacement by injected CO_2, fluid-mineral reactions, and upconing of the CO_2-brine interface. Adding geothermal energy capture to geologic CO_2 sequestration, i.e. the CPG approach, could improve the economic viability of sequestration by providing electricity for CO_2 injection and/or energy sales [4]. Simultaneously, opportunities for renewable electricity production could be expanded into regions far beyond those deemed economical for water-based geothermal.

Chapter 3

Comparing CPG with enhanced geothermal systems

This chapter is highly modified after Randolph and Saar, 2010 [29]. It provides many of the details behind the calculations and simulations that comprise the research discussed throughout this publication.

3.1 Introduction

Numerical simulations indicate at present that CPG systems provide significantly improved heat energy recovery over similar water-based systems. The purpose of the present investigation is 1) to compare CPG and EGS with CO_2 and 2) to provide extensive detail on the development of CPG numerical models. Furthermore, I explore the challenges associated with CPG systems and possible approaches for dealing with them.

While EGS with CO_2 is a recent development in geothermal technology, the existing preliminary research on the method provides context to determine the feasibility of the very new CPG approach presented here. With respect to comparing CPG systems and CO_2-based EGS, I focus here on the permeabilities and hydraulic characteristics of the various reservoirs and the consequential differences in geothermal heat energy extraction.

3.2 Permeability Comparison

3.2.1 General system parameters

Several geothermal reservoir and fluid injection/production characteristics are important in an early-stage comparison of CPG and CO_2-based EGS heat energy extraction, the most critical being reservoir permeability, temperature, pressure, size, and fluid injection/production rate. In a numerical exercise, we have the luxury of adjusting these parameters as desired within the limits of what may be encountered in natural systems.

For the purpose of investigating CO_2 geothermal potential in low-to-moderate geothermal heat flow regions (as comprise most of the Earth's surface [34]), reservoir (initial) temperature and pressure of 100 ^{o}C and 250 bar (2.5 km deep formation), respectively, are employed. While these values suggest a shallower and lower temperature field than typically targeted for EGS (e.g., Soultz, France [13]), such a site may be envisioned. Furthermore, such values may be encountered at several potential geologic CO_2 sequestration sites, including the Williston Basin of North Dakota and the Alberta Basin in Canada [16], which may be of interest as targets for CPG installations.

A five-spot well configuration (Figure 3.1) is utilized to facilitate comparison of numerical modeling results with existing CO_2-based EGS studies [9] [11]. The symmetry of the five-spot computational grid reduces modeling requirements to 1/8th of the system domain. The boundaries of the five-spot are no flow, as the configuration assumes the presence of additional five-spot systems surrounding the one simulated. The two-dimensional grid consists of 36 primary grid blocks, each with 70.71 m side length. For CPG simulations, blocks consist of a continuous porous medium matrix with a porosity of 20%, consistent with several CO_2 sequestration basins including the Williston and Alberta Basins [16]. EGS simulation reservoirs contain two orthogonal fracture sets imbedded in a matrix of negligible permeability, with a resulting system porosity of 2%. Fractures accommodate fluid flow while the matrix provides thermal energy storage; fracture/matrix heat exchange is accomplished via the multiple interacting continua (MINC) method [27].

Fluid injection and production rates are determined by specifying a 20 bar pressure difference between wells (bottom hole). Heat extraction rate (H) and fluid flow rate (Q) are monitored at a production well, with the former defined as $H = Q(h - h_o,$

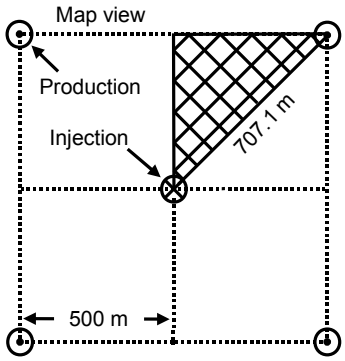

Figure 3.1: Five-spot well configuration for reservoir simulation. By symmetry, only the gridded section of the domain need be modeled. From [29].

where h is the enthalpy of the produced fluid and h_o is the enthalpy of the fluid at injection conditions ($T = 20^oC$). The system is assumed to contain CO_2 only; while the displacement of native formation brine or other fluid by CO_2 is important, it is not the focus of the current study. Rock characteristics loosely mirror those of the Soultz EGS site [9] and represent average values that may typically be encountered in EGS or CPG implementations. All simulations are completed utilizing the well-established reservoir simulator TOUGH2 [24] with the fluid property module ECO2N [25]. Table 3.1 provides a full list of model parameters and conditions.

3.2.2 Permeability

The remaining critical parameter to be defined for these simplified simulations is permeability. For CPG cases, the choice is straightforward - we select a value of $5x10^{-14}$ m^2, consistent with that measured at several CO_2 sequestration sites. Fields in the Illinois Basin report values ranging from $3.0x10^{-14}$ to $10x10^{-14}$ m^2 [32], whereas the saline aquifer systems of Alberta, Saskatchewan, North and South Dakota, and Montana have values ranging from $9.3x10^{-15}$ to $9.3x10^{-12}$ m^2 [16].

Permeabilities for CO_2-based EGS simulations are less readily defined. Approach 1: EGS model permeability could be selected to be the same as that of a CPG model,

which is useful for a comparison of thermal energy extraction between the two reservoir systems without the need to consider complications of hydraulic effects. Such an EGS permeability, however, is not necessarily representative of values found at actual EGS implementation sites. Approach 2: Thus, we also model EGS fracture permeability consistent with hydraulically stimulated basement rock.

Concerning Approach 2, the limited number of production-scale (water-based) EGS facilities hinders selection of a representative reservoir-scale permeability for CO_2-based EGS simulations. The Soultz, France, EGS site provides a post-stimulation, reservoir-scale value of $6x10^{-14}$ m^2 [13]. To provide at least one additional value, we employ

Reservoir formation	
Thickness	305 meters
Well separation	707.1 meters
Permeability	(variable)
Porosity (CPG)	20% (0.20)
Rock grain density	2650 kg/m^3
Rock specific heat	1000 $J/kg/^oC$
Thermal conductivity	2.1 $W/m/^oC$
Injection and production conditions	
Reservoir mapview area	1 km^2
Temperature of injected fluid	20 ^oC
Injection/production rate	max. 300 kg/s (variable)
Downhole injection pressure	260 bar
Downhole production pressure	240 bar
Injection/production duration	25 years
Initial conditions	
Reservoir fluid	All CO_2
Temperature	100 ^oC
Pressure	250 bar
Boundary conditions	
Top and sides	No fluid or heat flow
Bottom	No fluid flow, heat conduction

Table 3.1: TOUGH2 simulation parameters. Those defined as "variable" are described in detail in the text.

an analytical approach to approximate reservoir-scale permeability of a hydraulically-stimulated basement rock reservoir from core-scale, pre-stimulated basement rock samples.

3.2.3 Analytic permeability calculation

Intact core samples from the Soultz site have permeabilities that range from 10^{-18} to 10^{-16} m^2 [28] [13]. Of interest for future geothermal work in the interior North American continent, core samples from the Midcontinental Rift System at depths greater than 3500 m have an average permeability of 10^{-18} m^2 [35]. Choosing a pre-hydraulic-stimulation value of 10^{-17} m^2 and assuming stimulation increases permeability by approximately a factor of 200, as was the case at Soultz [13], post-stimulation core-scale EGS permeability would be $2x10^{-15}$ m^2.

To upscale core permeability (i.e., the permeability of an individual fracture) to bulk reservoir permeability, we apply electrical resistor theory to the five-spot EGS grid (with fracture spacing set to 70.71 m). Ohm's law, $I = \Delta V/R$, where I is current, ΔV is voltage difference, and R is electrical resistance, is analogous to Darcy's law, $q = -K\nabla h$, where q is Darcy velocity, ∇h is hydraulic head gradient, and $K = \rho g k/\mu$ is hydraulic conductivity with ρ denoting fluid density, g Earth's gravitational acceleration, k permeability, and μ dynamic fluid viscosity [36]. Assuming fluid density and dynamic viscosity are constant, R is analogous to permeability, k. Thus, we may apply Kirchoff's first rule - which states that the sum of currents entering a node must equal the sum of currents exiting a node in an electrical circuit - to a fracture network.

In the Multiple Interacting Continua (MINC) approach, fractures effectively exist along the boundaries of primary grid blocks; however, fractures connect between adjacent grid blocks [27]. Fracture connections, not fracture positions, are the important aspect in reservoir fluid flow and, hence, the analytic permeability calculation. Thus, the fracture network in Figure 3.2 comprises the permeable domain of the five-spot EGS model. Notice that the injection and production wells (i.e., nodes) have been connected by a non-resistive "wire," which closes the fracture circuit as required by Kirchoff's law. A "current" (i.e., fluid flow) of 1 amp is applied to the circuit to establish a "voltage" (i.e., hydraulic head) gradient across each fracture, and the injection well is grounded, to permit calculation of reservoir permeability.

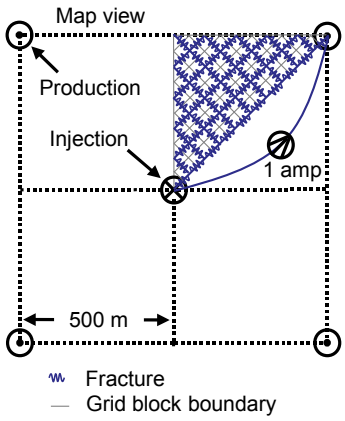

Figure 3.2: Network of connected fractures that comprise the permeable domain of EGS models in this study, here modified in order to complete the flow "circuit," permitting an analytical calculation of reservoir-scale permeability. From [29].

Consider Figure 3.3, a section of the fracture network from Figure 3.2. Applying Kirchoff's law to node 5 of the fracture network gives the equation $(V2-V5)/R+(V4-V5)/R+(V6-V5)/R+(V8-V5)/R=0$, where Vi is the "voltage" (i.e., hydraulic head) at node i and R is the "resistance" (i.e., permeability) of an individual fracture. Applying Kirchoff's law to each node in the fracture network except the injection well (for which we know the "voltage" $=0$) provides a system of 35 linear equations with 35 unknown voltages. Solving the system of linear equations, then solving Ohm's law with $I=1$ amp and $\Delta V=$ (voltage difference between production and injection wells), the effective "resistance" (i.e., permeability) of the fracture network can be determined for a given individual fracture permeability. We find that the bulk system permeability is a factor of 5.4 that of the permeability of an individual fracture.

Returning to the chosen core-scale EGS permeability of $2\text{x}10^{-15}$ m^2, the effective system-scale permeability is then $1.1\text{x}10^{-14}$ m^2. For the purpose of this numerical exercise, we average this value and measured EGS permeability from Soultz, resulting in a fracture system permeability of $3.5\text{x}10^{-14}$ m^2, which is used in Approach 2 to compare CPG and CO_2-based EGS. While more permeability values from EGS implementations

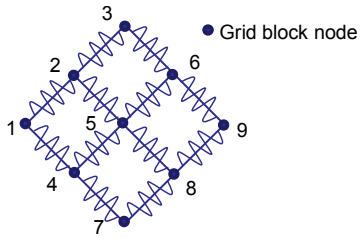

Figure 3.3: Expanded view of a section of the fracture network from Figure 3.2. From [29].

would be preferred, the preceding technique provides one method for comparing CO_2-based geothermal systems.

3.3 Numerical Modeling Methods

TOUGH2 [24] is an integral finite difference geologic reservoir simulator that has been extensively tested and verified for geothermal and geologic CO_2 sequestration numerical modeling applications. It is capable of simulating fully coupled multiphase, multicomponent geologic fluid and heat transfer. For the simulations employed in this study, the following flow equations are utilized.

For geologic fluid flow, flow of each fluid phase, β, is determined by the multiphase form of Darcy's law:

$$Q_\beta = -k\frac{k_{r\beta} * \rho_\beta}{\mu_\beta}(\nabla P_\beta - \rho_\beta * g)$$

where Q is volumetric Darcy velocity, k is permeability, k_r is relative permeability, ρ is density, μ is viscosity, P is pressure, and g is gravitational acceleration. For the small flow velocities in the scenarios investigated for this study, the assumptions of Darcy's law are valid. Note that, particularly for CO_2, ρ and μ are functions of temperature and pressure. Moreover, P_β is the sum of a reference phase (usually gas, i.e., CO_2 phase) pressure, P, and capillary pressure, $P_{c\beta}$:

$$P_\beta = P + P_{c\beta}$$

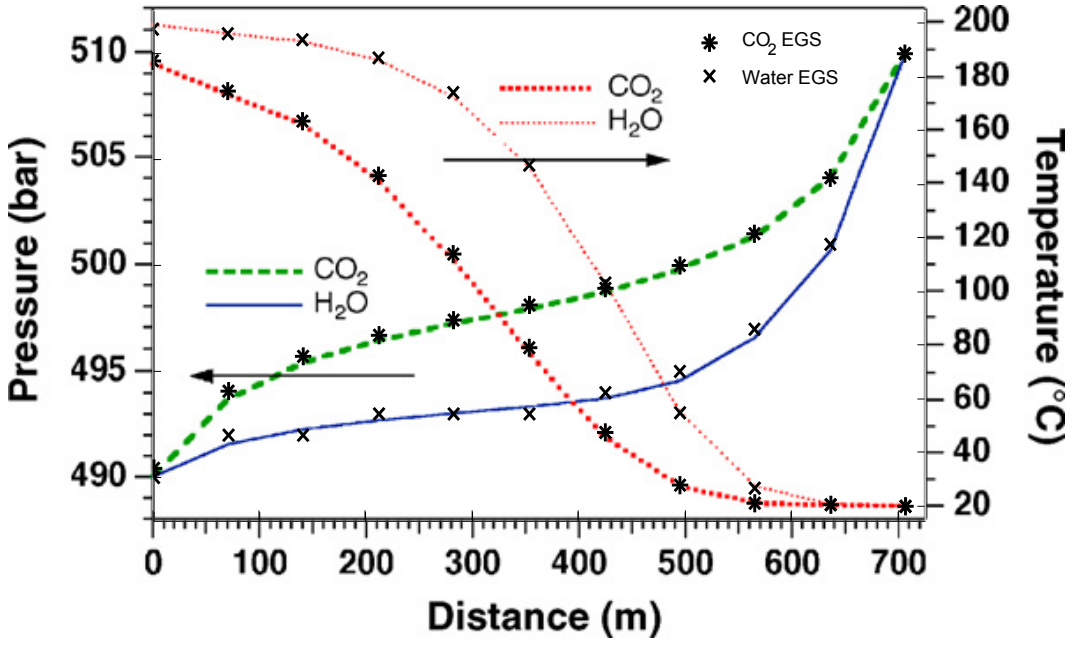

Figure 3.4: To verify numerical modeling capabilities for the present study, the models of Pruess [9] (colored lines) were reproduced. Symbols give the reproduced temperature and pressure profiles for CO_2- and water-based EGS from production to injection well after 25 years of system operation. Note the very good agreement between Pruess and reproduced profiles, ensuring correct use of the TOUGH2 simulator. Slight differences between Pruess results and reproductions are the result of small differences in modeling techniques, however, the results are fully consistent (confirmed in private communication with Pruess, 2010).

Heat flux is the sum of heat conduction and convection in each phase:

$$F = -k_T \nabla T + \sum_{\beta} h_\beta * Q_\beta$$

where k_T is thermal conductivity, h is specific enthalpy, and Q_β is Darcy velocity, given above. Note that for the geothermal systems in the current study, convection is far more significant than conduction (e.g., [9]).

3.3.1 Numerical model verification

To ensure numerical models for the present study function correctly, the TOUGH2 models and results of Pruess [9] were first reproduced. The Pruess models compare CO_2- and water-based enhanced geothermal systems in reservoirs at a depth of 5 km and temperature of 200 ^oC. Other model parameters are consistent with those in Table 3.1. Referring to Figure 3.4, the reproduced models match those of Pruess [9] very accurately, verifying modeling capabilities for this study.

3.3.2 CO_2 versus water mobility and heat capacity

As previously noted, CO_2 is of interest as a geothermal working fluid because, among numerous other benefits, its thermodynamic and fluid mechanical properties suggest it transfers heat from the subsurface more efficiently than water [9]. In particular, under the geologic conditions relevant for CPG or CO_2-based EGS, CO_2 mobility is higher than that of water. Mobility, fluid density divided by dynamic viscosity (the inverse of kinematic viscosity), describes a fluid's tendency to preserve momentum while flowing. Higher mobility implies greater geologic fluid flow, resulting in improved geothermal heat extraction. Therefore, using CO_2 as the working fluid in geothermal power systems may permit utilization of geologic formations that are deemed economically unviable with current water-based technology.

3.3.3 Two dimensional reservoir temperature evolution

Geothermal systems primarily mine the heat energy contained in subsurface materials, as the latent energy is generally much greater than the energy recharged via heat flow; continental heat flow ranges from 10 to, at most, a few hundred milliwatts per square meter [38]. As such, geothermal reservoirs decrease in temperature during heat mining operations, though they will recharge on human timescales once heat mining ceases. Figures 3.7 and 3.8 display reservoir temperature in map view for base case CPG and comparable water-reservoir systems at 5 year intervals during fluid injection/production. Similarly, Figures 3.9 and 3.10 display formation temperature for CO_2 and water-based EGS, assuming base case system parameters and 70.71 m fracture spacing (most similar to the reservoir cases).

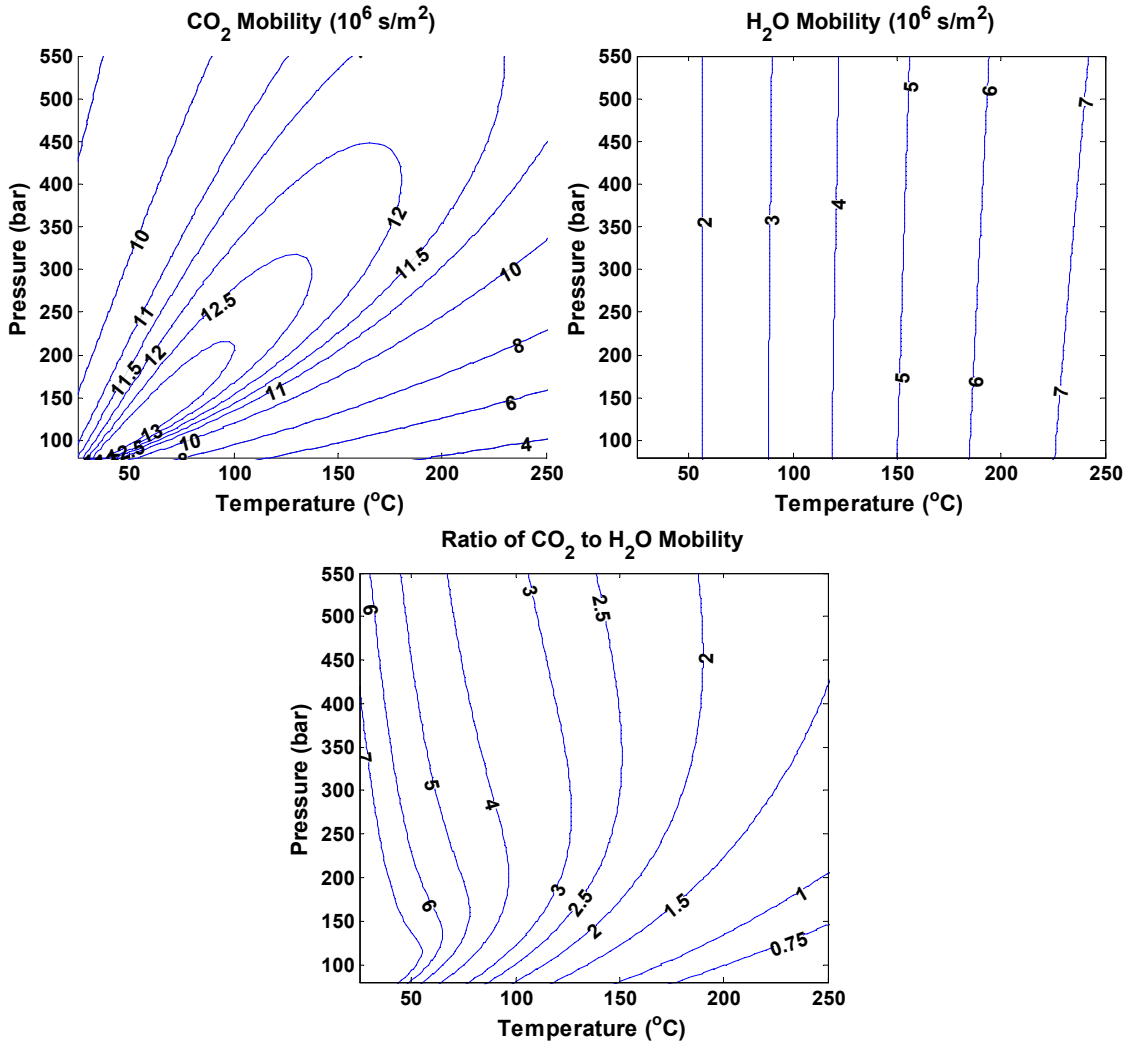

Figure 3.5: Plots of CO_2 and water mobilities over the range of temperatures and pressures of interest for geothermal development. Mobility, density divide by dynamic viscosity, describes a fluid's tendency to preserve momentum while flowing. The substantially higher mobility of CO_2 than water, particularly at temperatures and pressures relevant for CPG systems (e.g., 100 ^{o}C and 250 bar), results in higher subsurface fluid flow rates with CO_2 for a given pressure difference between injection and production wells. Moreover, the high mobility of CO_2 decreases pumping requirements, a substantial parasitic power requirement in traditional water-based geothermal systems. Data for figure generation is from the National Institute of Standards and Technology [37].

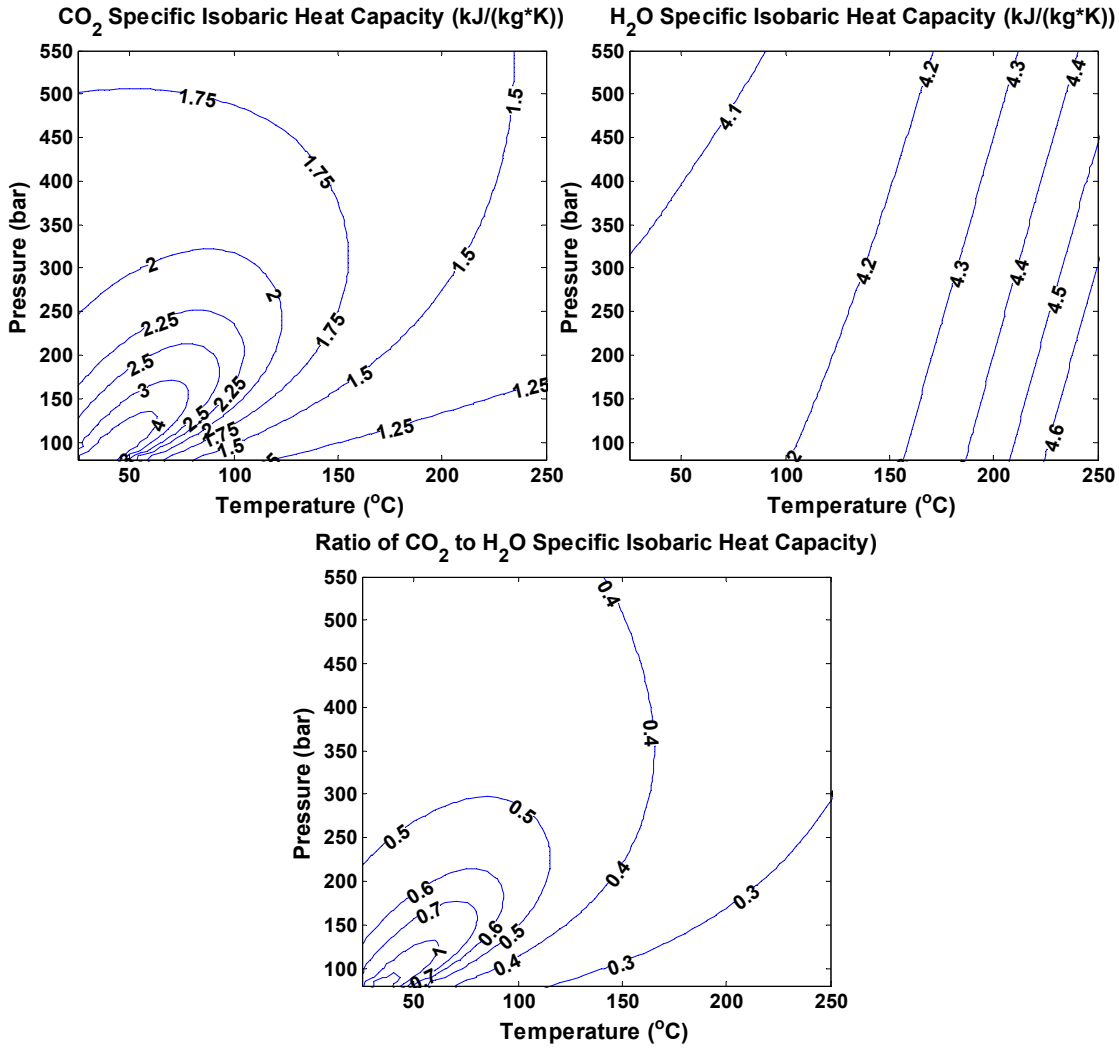

Figure 3.6: Heat capacities of CO_2 and water over the range of temperatures and pressures of interest for geothermal development. Because of the lower heat capacity of CO_2 than water, more CO_2 must be produced from a geothermal system in order to supply as much energy for electricity generation as comparable water-based systems. However, because of the high mobility of CO_2 (Figure 3.5), such higher flow rates are achievable. Data for figure generation is from the National Institute of Standards and Technology [37].

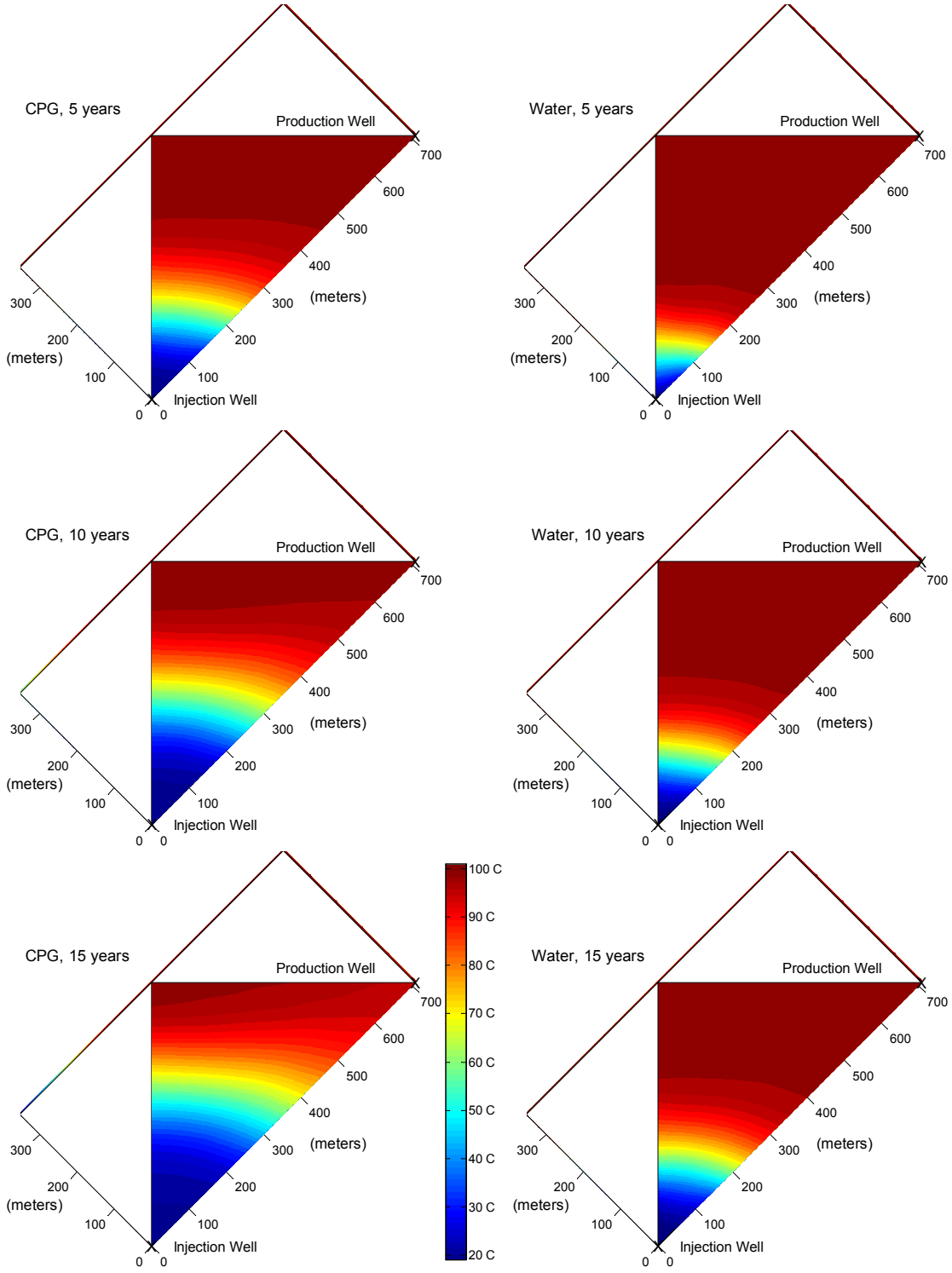

Figure 3.7: Temperature evolution of CPG and water-reservoir geothermal systems; 1.

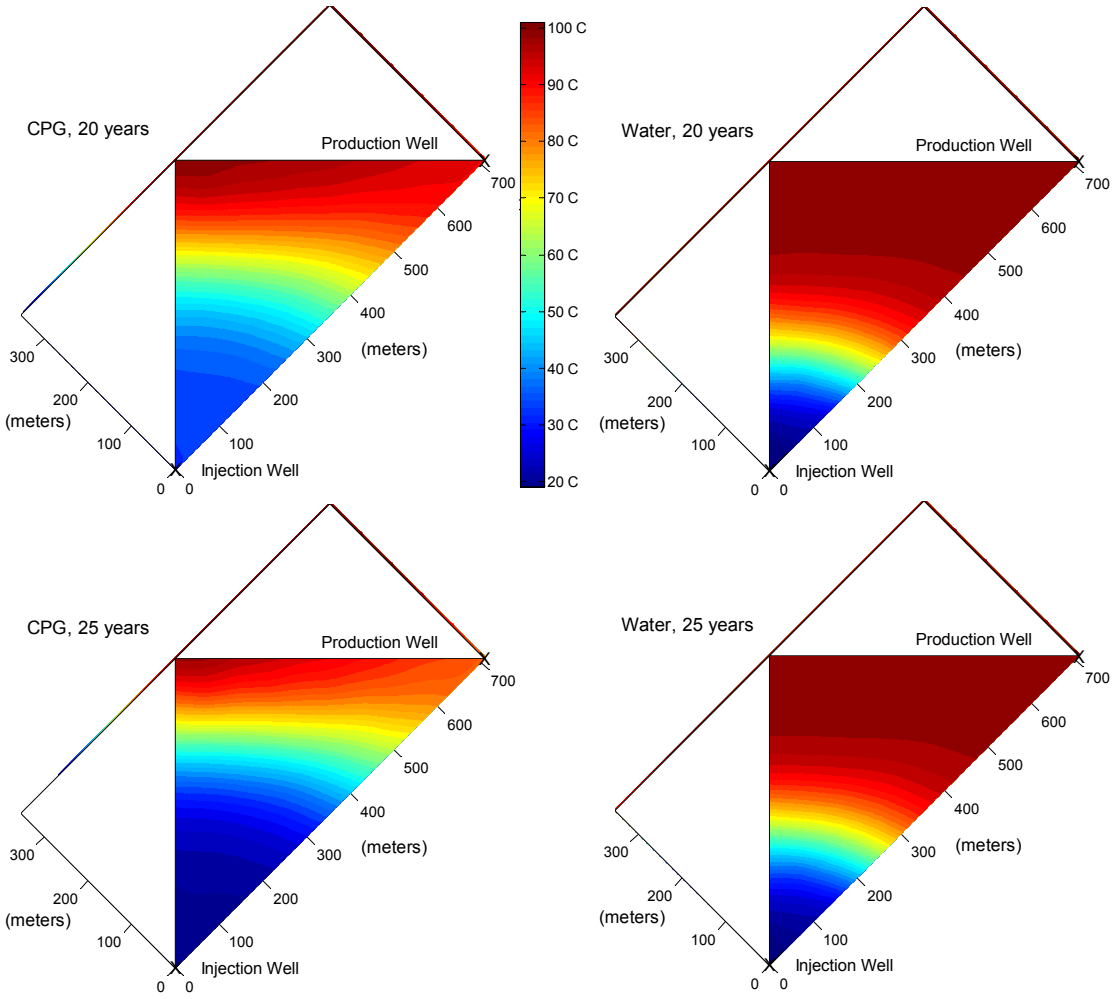

Figure 3.8: Temperature evolution of CPG and water-reservoir geothermal systems; 2.

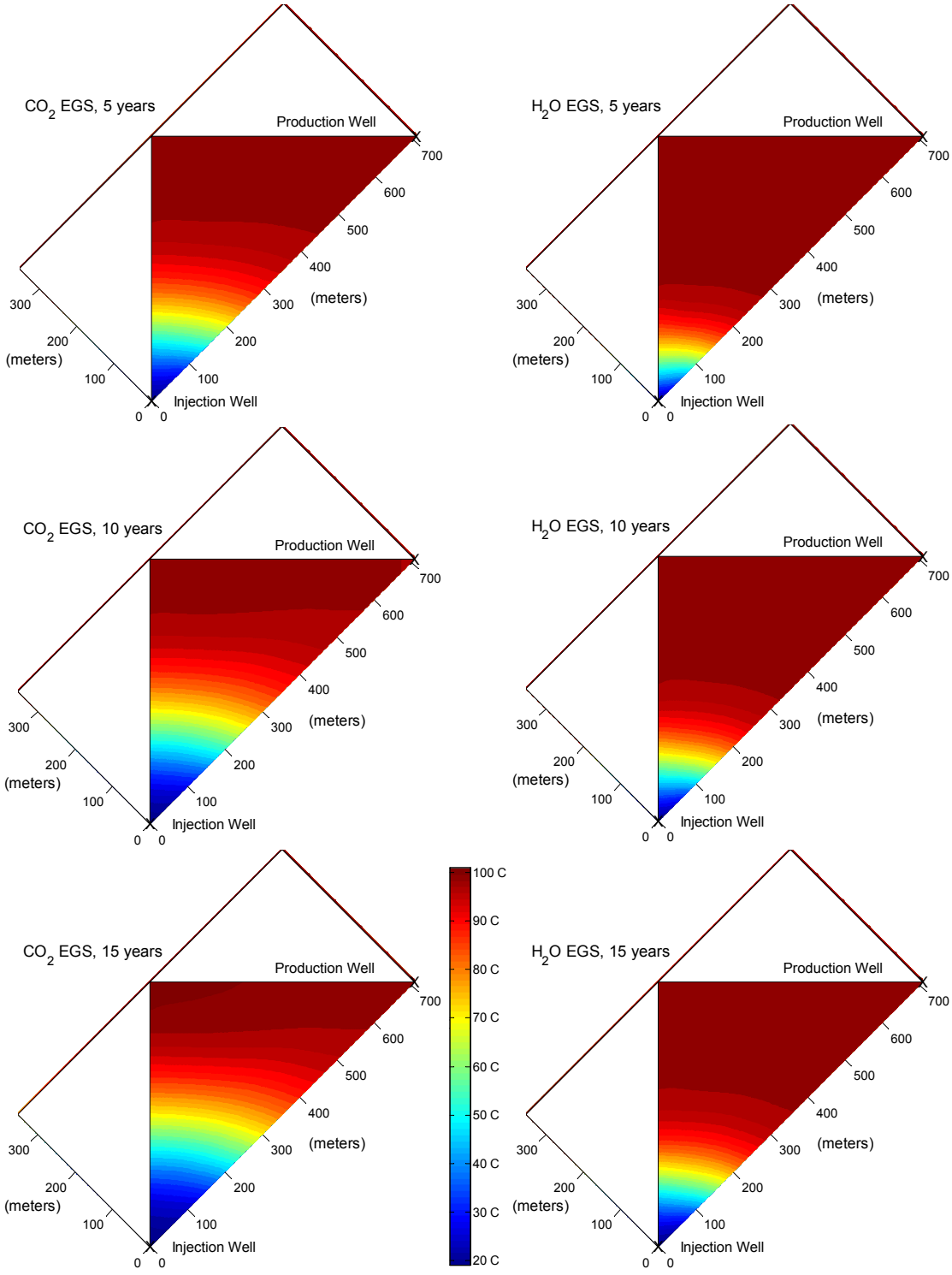

Figure 3.9: Temperature evolution of CO_2- and water-based enhanced geothermal systems; 1.

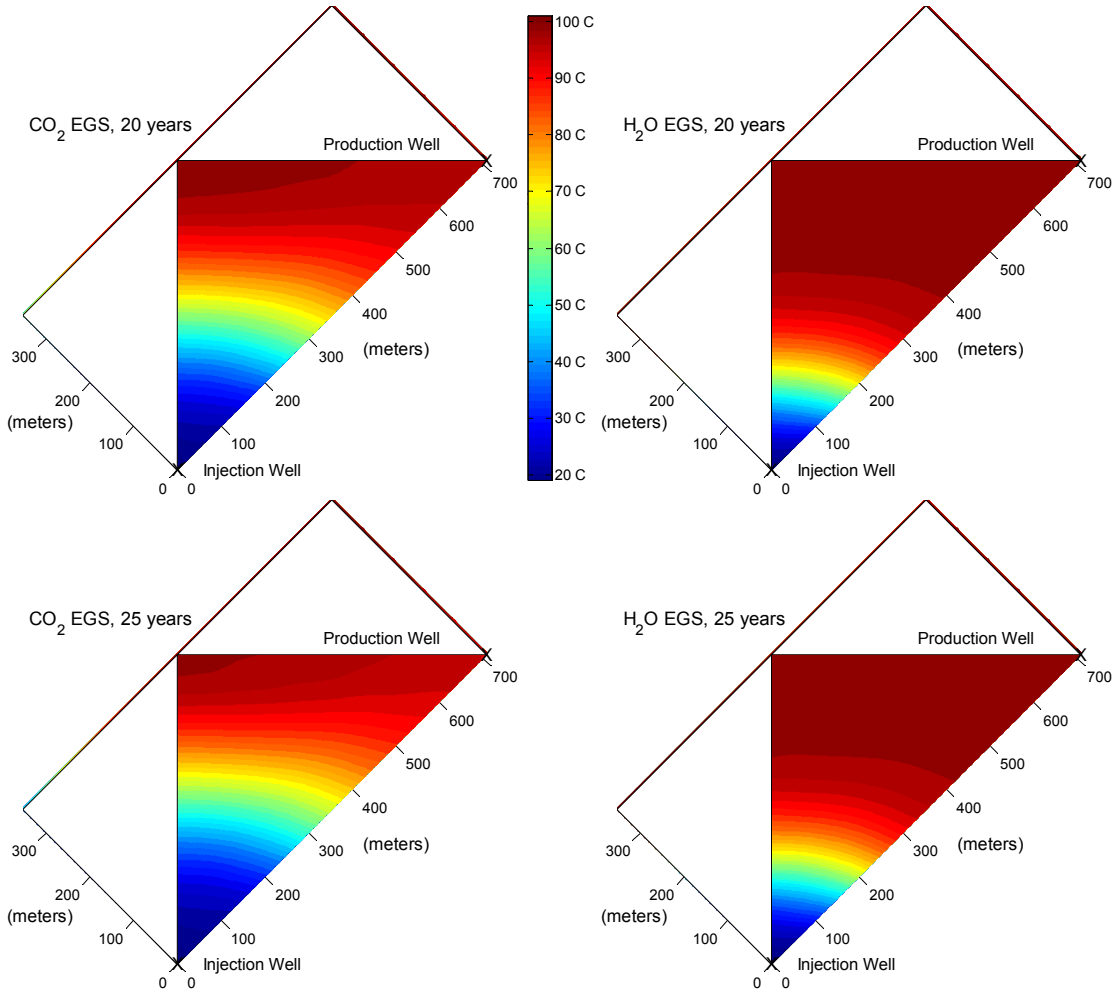

Figure 3.10: Temperature evolution of CO_2- and water-based enhanced geothermal systems; 2.

3.4 Energy Recovery from CO_2 Geothermal

Results of simulations corresponding to Approach 1, in which CPG and CO_2-based EGS reservoirs have the same system permeability of $5x10^{-14}$ m^2, are shown in Figure 3.11. Three EGS cases are considered, corresponding to fracture spacings of 70.71 m (chosen equal to the primary grid block side length), 141.42 m (i.e., 2 x 70.71 m), and 212.13 m (i.e., 3 x 70.71 m). Figure 3.11 displays temperatures along a line from injection to production well after 10 simulated years of CO_2 injection and production from the reservoir. Notice that the temperature at the production well in the CPG case is closer to the initial reservoir temperature (100 ^oC) than in any of the EGS cases, with EGS production well temperature decreasing with increasing fracture spacing. This result indicates more widespread heat mining in the CPG system than the EGS cases, a consequence of the CO_2 being in contact with more reservoir rock or sediment in CPG.

Time series of geothermal heat extraction for CPG and EGS cases are provided in Figure 3.13. All rates are given on a full-well basis (i.e., for the entire five-spot system). For a given case, heat extraction rates decrease with time as the reservoir system heat is depleted and the temperature at production wells decrease. Mass flow rates remain relatively constant with time. The CPG system provides more widespread heat mining than the EGS cases, thus maintaining higher temperatures at the production well for longer duration. Produced fluid temperature decreases with time more rapidly as EGS fracture spacing increases, a consequence of less reservoir material being in contact with heat exchange fluid.

In the EGS simulation corresponding to Approach 2, with system permeability of $3.5x10^{-14}$ m^2, heat energy extraction is considerably lower than in the CPG system and EGS with similar fracture spacing. Lower permeability results in smaller fluid mass flow rates, producing lower heat energy extraction rates.

3.5 Challenges Associated with CPG

As noted in this Chapter as well as Chapters 2, 4, and 5, the CPG system has numerous advantages over traditional and EGS geothermal techniques. However, numerous challenges must be overcome or dealt with before CPG systems can be implemented. Many of these challenges, together with possible approaches for dealing with them, are

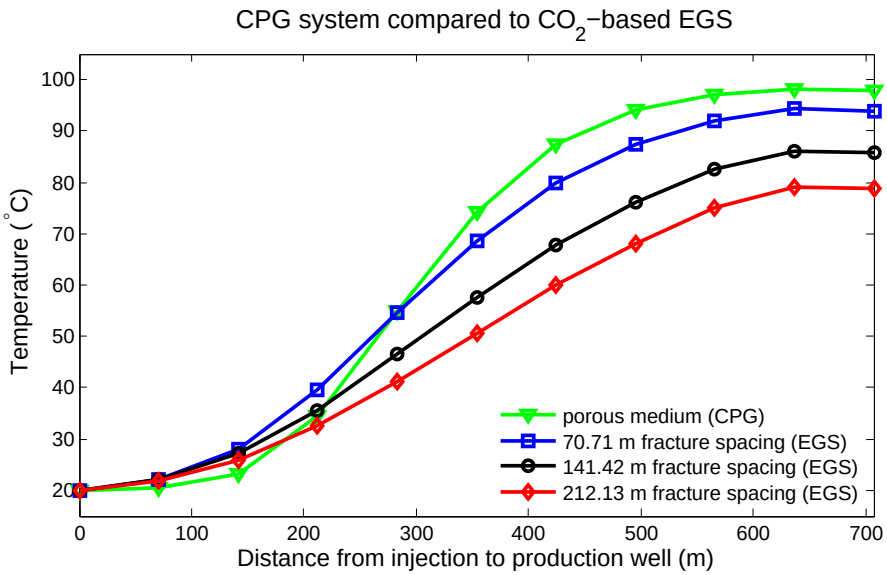

Figure 3.11: Temperature profiles along a line from injection to production well after 10 simulated years of injection and production; system permeability in all cases is $5x10^{-14}$ m^2. The higher CPG than EGS temperature at the production well indicates more widespread heat mining in the CPG case. From [29].

discussed here.

As with any subsurface fluid injection/production activity, there is some potential for inducing seismicity while operating a CPG system. However, the probability of inducing earthquakes with CPG is much lower than that with EGS technologies, because in the former, the subsurface pressure increase is small (see, for e.g., Table 2.1) while in the latter, the pressure increase is much larger because operators are intentionally attempting to exceed the local fracture threshold. Moreover, the risk of induced seismicity may be decreased by operating CPG with dynamic reservoir management, which involves pumping reservoir brine during CO_2 plume formation in order to limit formation pressure increase and control plume formation. Future research will examine this approach.

Induced seismicity is a challenge of geologic CO_2 sequestration in general, however

CPG has the advantage that pressure buildup is limited by CO_2 production. I recognize that the challenges of CO_2 sequestration are also associated with CPG, including preventing CO_2 leakage to the surface. Leakage most likely will occur along poorly-sealed, abandoned wells that penetrate the caprock (e.g., [39]), thus careful simulation of geologic formations prior to onset of injection together with extensive monitoring of field development are critical. CO_2 leakage through caprocks overlying an injection formation may be unlikely, as CO_2 geochemical reaction with typical caprock materials (shales) may result in mineral precipitation that clogs flow pathways (ongoing research at the University of Minnesota, Department of Earth Sciences). The challenges of CO_2 sequestration are extensively studied by hundreds of scientists worldwide (e.g., [40]), and as such, I focus the current investigation on those specific to adding geothermal heat extraction to a CO_2 sequestration development.

Vertical leakage of CO_2 from storage formations may also result in contamination of drinking water, another reason for careful assessment of potential CO_2 injection formations for caprock integrity prior to onset of injection. However, as noted in Chapter 2, using CO_2 as the geothermal working fluid rather than water preserves potentially scarce water resources. Similarly, as concerns the environmental impact of CPG systems, unlike many other power generation options, geothermal operations have very little surface expression. As such, geothermal power plants are minimally invasive and relatively simple to decommission.

Formations for CO_2 injection are only considered if their water is of non-drinking quality (typically greater than 10,000 ppm total dissolved solids, as defined by the Clean Water Act). Generally, deep saline aquifers are far saltier than seawater (e.g., [32]), therefore seawater would be desalinated for drinking purposes long before considering deep saline water. Injecting CO_2 into such saline formations does introduce challenges in a geothermal power system, however. Water saturated with CO_2 is acidic, thus if such water is produced during CPG power operations, care must be taken to ensure system components can handle the fluid. This may include using stainless steel or corrosion-resistant composite pipes and power system components, removing (i.e. drying) the CO_2 stream prior to sending it through a power system, or using a binary power system with a heat exchanger (e.g., Figure B.3). Acidic water may dissolve subsurface minerals, which may later precipitate in power equipment. However, pure supercritical

CO_2 appears to be fairly non-reactive, far less reactive than the brine in traditional geothermal developments, and nearly immiscible with water. Thus, it is anticipated that after water is flushed from a formation, the close-to-pure-phase CO_2 plume can be used for geothermal heat mining with minimal potential for reactivity or mineral scaling issues in the power system (e.g., [41]).

As heated CO_2 is produced from a deep geologic formation, it will expand in a production well because of its relatively high expansivity; this effect is known as Joule-Thomson cooling ([9] and Chapter 5). Therefore, unlike water, CO_2 cools as it rises to the surface, potentially decreasing the efficiency of the geothermal power system. However, the high expansivity of CO_2 results, favorably, in high fluid flow rates in production wells without the need (or with far less need than in comparable water-based systems) for pumping, a source of substantial parasitic power losses in traditional geothermal power systems [12]. Direct cycle two phase turbines that can operate efficiently with relatively low temperature geothermal fluids and turbines that can take advantage of the large pressure difference between CO_2 production and injection wellheads (a further result of the high expansivity or change in density of CO_2 with temperature) are capable of more than making up for the efficiency loss caused by CO_2 cooling with expansion. Moreover, direct turbines, in which the produced CO_2 is sent through the turbine without the need for a heat exchanger, can operate far more efficient than binary cycle turbines, which are required for water-based systems at low to moderate temperatures (generally, less than 150 ^{o}C and in practice, less than approximately 190 ^{o}C [42]), resulting in CO_2 power systems with higher efficiency than water-based systems.

Because geothermal power plants utilize relatively low-temperature fluids compared to fossil fuel power plants, regions of the world with high average surface temperatures offer challenges for geothermal power plant operations. Power plant heat-to-electricity conversion efficiency is a function of the difference between operating temperature and ambient temperature, ΔT (see Chapter 2 for a discussion of the Carnot efficiency) – the higher the ambient temperature, the lower the efficiency. As such, in high ambient temperature regions, geothermal power plants may only be operable at night, when ΔT is sufficient for economical power operation. However, when balanced with wind and solar power, which operate generally only during the day, such a geothermal operation can be very desirable. In regions without high average ambient temperatures, CPG

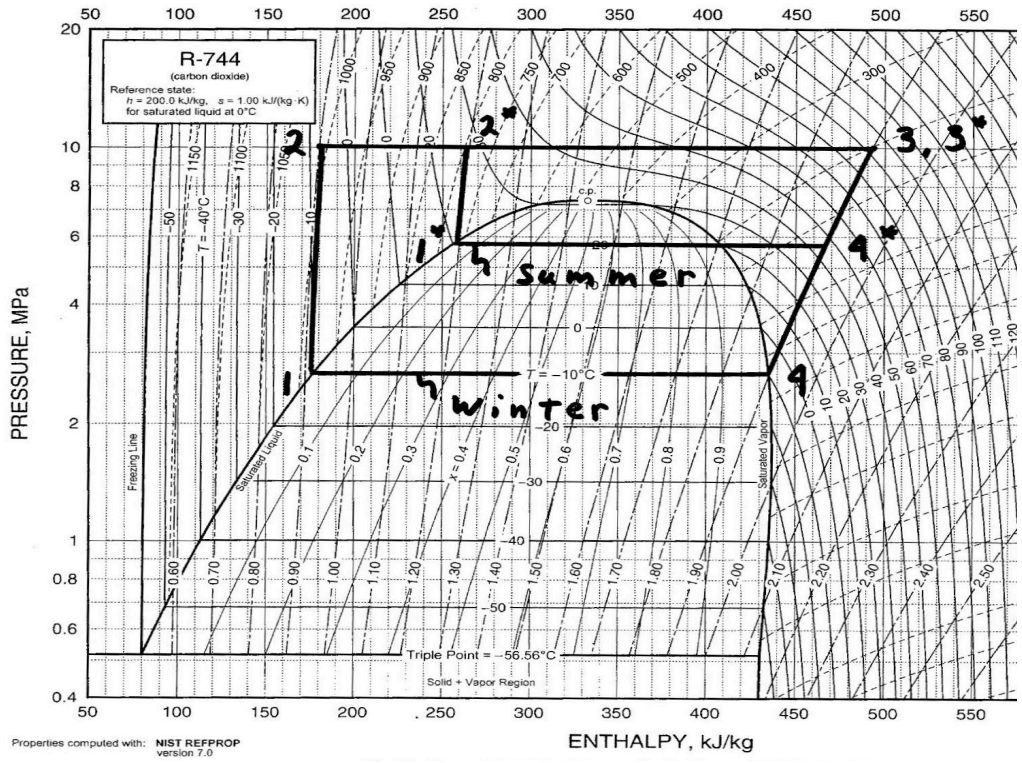

Figure 3.12: CO_2 power plant summer and winter phase diagram, assuming an average annual climate similar to Minnesota. Numbers correspond to elements of the power cycle: (1) is the injection well wellhead; (2) is the injection well well-bottom (assuming, here, isentropic fluid compression in the well); (3) is the production well well-bottom (assuming near-isobaric fluid heating in the reservoir); and (4) is the production well wellhead (assuming isentropic fluid expansion in the well). The summer and winter cycles differ because, with the very low freezing point of CO_2, the winter heat rejection temperature of the power cycle can approximately equal the average daily temperature (sub 0 ^{o}C). This offers substantial efficiency benefits to a CO_2 system, which are not available in a water-based power system. Data for figure generation is from the National Institute of Standards and Technology [37].

systems can provide both baseload and on-demand, dispatchable power. See Figure 3.12 for CO_2 power system phase diagram and power cycles.

To ensure economical geothermal power operation for several decades, reservoir heat

mining must be managed so as not to prematurely deplete formation heat (see Subsection "Two Dimensional Reservoir Temperature Evolution" for additional information). Excessive pumping or production may cause upconing at production wells, resulting in both brine and CO_2 being produced, as opposed to just CO_2. This effect will be limited by the high mobility and associated preferential flow of CO_2 (Figure 3.5). Excessive pumping may also cause short-circuiting of fluid flow paths, whereby CO_2 follows a few high permeability paths that are rapidly heat-depleted, rather than the entire reservoir. Because CPG systems operate in naturally high permeability formations, short circuiting is far less likely here than in EGS, in which a few fractures dominate flow [30]. Similarly, it is less likely that the three dimensional fluid flow pathways in CPG systems will be clogged by mineral precipitation than the approximately two dimensional flow pathways in EGS [30].

Finally, in certain situations, water-based geothermal systems may be more efficient than CPG systems in a given geologic formations (see, for e.g., Chapter 5, which describes certain reservoir pressure, temperature, and permeability combinations in which water-based systems are more efficient than CO_2-based). However, in such situations, there may nonetheless exist several reasons to use CO_2 rather than water in a geothermal development, such as limited water availability or desire to limit atmospheric CO_2 emissions. It is likely that CPG development will be driven by CO_2 emissions policy. With emission limits, CPG becomes more economically favorable even in cases where water would be a more efficient geothermal working fluid.

3.6 Concluding Remarks

While additional research is required, numerical modeling results at present suggest that geologic reservoirs with CO_2 as the heat mining fluid would be viable geothermal energy sources for power production, potentially even in regions with relatively low geothermal temperatures and heat flow rates. Early-stage studies by several authors have suggested the potential of enhanced geothermal systems (EGS) with CO_2 as the geothermal working fluid (e.g., [9] [12]). The work presented here, however, demonstrates that in certain situations, CO_2 plume geothermal (CPG) systems provide better geothermal heat energy recovery than EGS with CO_2.

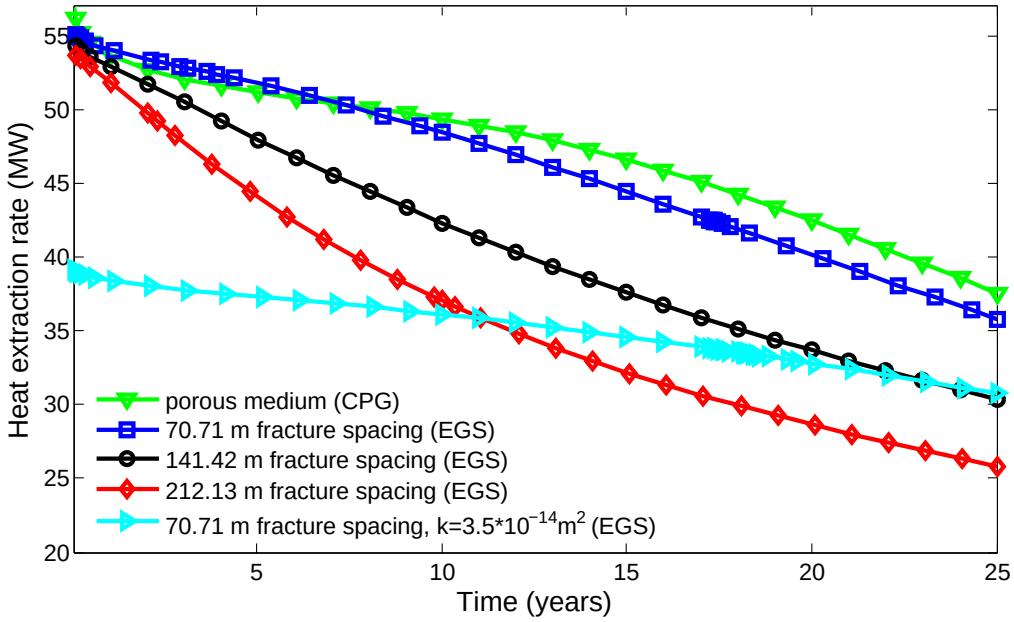

Figure 3.13: Time series of simulated geothermal heat energy extraction. Heat extraction rate is defined as the enthalpy difference between injected and produced fluid multiplied by the rate of fluid production. Unless otherwise noted, system permeability is 5x10^{-14} m^2. The CPG system maintains higher production temperatures for longer time than EGS with the same permeability, resulting in higher heat energy extraction rates. From [29].

Chapter 4

Economic Implications of CPG for CO_2 sequestration

This chapter is largely based on Randolph and Saar, 2011 [4].

4.1 Introduction and Background

Geologic CO_2 sequestration is often considered the primary approach with soon-to-be available technology by which anthropogenic CO_2 emissions to the atmosphere could be significantly reduced [3]. However, a challenge for large-scale implementation of sequestration is cost; CO_2 capture and storage (CCS) could add 20%, or more, to the cost of fossil-fuel-based electricity generation, assuming CCS costs of 0.02 $U.S.A. per kWh [43]. Advances in CCS technology and experience, together with legislation such as carbon cap and trade, will improve the economic feasibility of CCS, however, these advances may not be sufficient to encourage large-scale CCS implementation. Coupling CCS with renewable energy capture, electricity production, and/or district heating would further improve the economic viability of CCS, among numerous other advantages, as outlined in this contribution.

The present study is focused on the economic benefits of CPG with respect to carbon capture and storage (CCS), in particular, the potential for CPG to offset some of the costs associated with CCS. For detailed comparisons of the CPG approach to traditional water-based geothermal systems as well as to EGS, refer to [18] (Chapter 2)

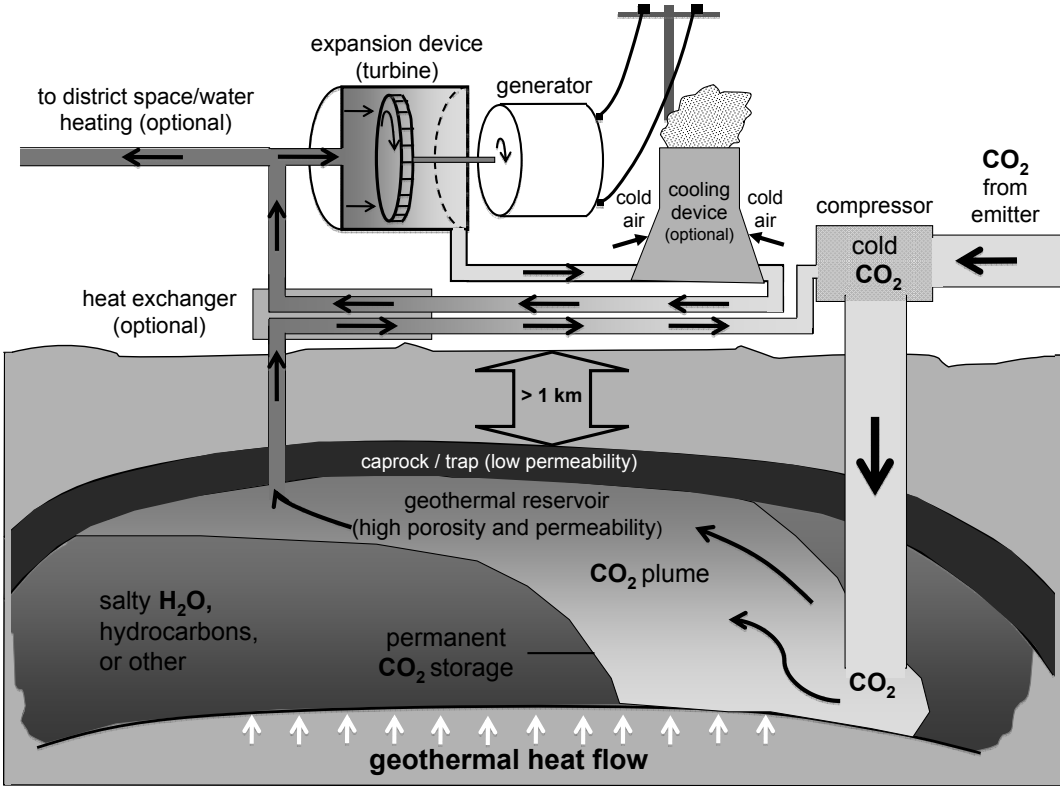

Figure 4.1: Simplified schematic of one possible implementation of a CO_2-plume geothermal (CPG) system, established in a deep saline aquifer or as a component of enhanced oil/hydrocarbon recovery (EOR) operations. Some components of the system are generalized or absent. As in traditional geothermal approaches, energy recovered from CPG systems could be used both for electricity generation and for space/water heating. Moreover, a wide range of realizations can be envisioned including direct and binary cycles, bottom cycles, and multiple secondary working fluids. Note that only one production well is shown here, while actual implementations would likely include multiple production, and possibly several injection, wells (see also Figure 2.1, insert, for a typical 5-spot well pattern). From [4].

[29] (Chapter 3). The current study is concerned primarily with North America, but its conclusions are applicable worldwide.

4.2 Methods

The viability of a geothermal system with CO_2 as the working heat exchange fluid in the subsurface has been demonstrated with regards to CPG systems (Chapters 2 and 3) and for CO_2-based EGS [9]. In particular, CPG can provide heat extraction rates up to a factor of three greater than those of traditional water-based systems ([18], Chapter 2). Here, we develop numerical simulations to estimate geothermal heat energy extraction in the CPG approach for the purpose of calculating the electricity provided per ton of sequestered CO_2. The most critical geothermal reservoir and fluid injection/production characteristics in an early-stage analysis are reservoir permeability, temperature, pressure, dimensions, and fluid injection/production rate. In a numerical exercise, we have the luxury of adjusting these parameters as desired within the limits of what may be encountered in natural systems.

Water-based geothermal electricity production has traditionally, but not exclusively, relied on relatively high temperature ($> 150^o$C), high heat flow (> 90 mW/m^2, approximately) regions. In the U.S.A., where currently most of the world's geothermal electricity production occurs [44], approximately 90% of the geothermal electricity generation capacity takes the form of higher-temperature dry and flash steam systems, as opposed to lower-temperature ($< 150^o$C) binary systems [44] [42]. High temperature systems are generally restricted to the western part of the continent. In contrast, large-scale implementation of CO_2 sequestration will require use of broader CO_2 reservoir targets that frequently will not serve as ideal, high-temperature geothermal reservoirs. Thus, for the purpose of this investigation, we choose, as a base case, a geologic reservoir with more moderate thermal characteristics, as may be encountered in moderate to low geothermal heat flow regions, as found throughout most of Earth's near-surface regions (e.g., [34]). Reservoir (initial) temperature and pressure of 100 ^{o}C and 250 bar (2.5km deep formation), respectively, are employed, as 100 ^{o}C is often considered the lower limit for geothermal electricity generation [23]. Such temperature and pressure values may be encountered at several potential geologic CO_2 sequestration sites worldwide, including

the Williston Basin of North Dakota, U.S.A., and the Alberta Basin in Canada [16]. In addition to the base case, several other temperature and pressure cases are considered for the purpose of exploring parameter space.

A five-spot well configuration (Figure 2.1, insert) is utilized, as is employed in several early-stage geothermal investigations in the literature (e.g., [9] [11]). To ensure models for the present study function correctly, the models and results of Pruess [9] were first reproduced (Figure 3.4). These models employed EGS characteristics, and once agreement was obtained, our simulations were modified to represent naturally porous, permeable systems. The symmetry of the five-spot computational grid reduces modeling requirements to $1/8^{th}$ of the system domain. The two-dimensional grid consists of 36 primary grid blocks, each with 70.71 m side length. Blocks consist of a continuous porous medium matrix with a porosity of 20%, in agreement with several CO_2 sequestration basins including the Williston and Alberta Basins [16].

Fluid injection and production rates are determined by specifying a 20 bar pressure difference between wells (bottom hole). Heat extraction rate (H) and fluid flow rate (Q) are monitored at a production well, with the former defined as $H = Q(h - h_o)$, where h is the enthalpy of produced fluid and h_o is the fluid enthalpy at injection conditions (at a temperature of 20 ^{o}C). For a given simulation, the system is assumed to contain CO_2 only. While the displacement of a formation's native brine or other fluid by CO_2 is important, it is not the focus of the current study. Rock thermal characteristics and permeability, the latter set to a conservative value of $5\text{x}10^{-14}$ m^2, are consistent with values that may typically be encountered at CO_2 sequestration sites (see Chapter 3 and [16]). Regarding permeability, fields in the Illinois Basin report values ranging from $3.0\text{x}10^{-14}$ to $10\text{x}10^{-14}$ m^2 [32], whereas the saline aquifer systems of Alberta, Saskatchewan, North and South Dakota, and Montana have values ranging from $9.3\text{x}10^{-15}$ to $9.3\text{x}10^{-12}$ m^2 [16]. All simulations are completed utilizing the well-established reservoir simulator TOUGH2 [24] with the fluid property module ECO2N [25]. Table 4.1 provides a complete list of model parameters and conditions.

Base Case Parameters	
Reservoir formation	
Thickness	305 meters
Well separation	707.1 meters
Permeability	$5x10^{-14}$ m^2
Porosity (CPG)	20% (0.20)
Rock grain density	2650 kg/m^3
Rock specific heat	1000 $J/kg/^oC$
Thermal conductivity	2.1 $W/m/^oC$
Injection and production conditions	
Reservoir mapview area	1 km^2
Temperature of injected fluid	20 ^oC
Injection/production rate	max. 300 kg/s (variable)
Downhole injection pressure	260 bar
Downhole production pressure	240 bar
Injection/production duration	25 years
Initial conditions	
Reservoir fluid	All CO_2
Temperature	100 ^oC
Pressure	250 bar
Boundary conditions	
Top and sides	No fluid or heat flow
Bottom	No fluid flow, heat conduction
Parameters for Additional Cases	
Case number Formation temperature/ depth	
1	150 ^oC / 4 km (400 bar)
2	100 ^oC / 1 km (100 bar)

Table 4.1: TOUGH2 simulation parameters. For the additional cases, all parameters not specifically defined are taken to be the same as for the base case.

4.3 Energy Recovery from CO_2-based Geothermal (CPG)

Results of simulations are presented in Table 4.2. Heat extraction rates are given on a full-well basis (i.e., for the entire five-spot system) and are averaged over the duration of fluid injection and production. For a given case, heat extraction rates decrease with time as the reservoir system heat is depleted and the temperature at production wells decrease. Mass flow rates remain relatively constant with time. Heat extraction rates in the CPG approach generally increase with formation temperature, as may be expected.

Note that Case 1 applies to a relatively deep reservoir in a moderate geothermal heat flow region; such a formation may be encountered in the afore-mentioned Williston Basin [16] but may be less common than the base case. Case 2 applies to a shallow reservoir in a high heat flow region, as may be encountered in the western U.S.A. (refer to Figures 4.2 and 4.3 for maps of subsurface temperatures and basins, respectively).

Simulation Results	
Case number	Heat extraction rate (25 year average)
Base case	47.0 MW
1	62.6 MW
2	64.1 MW

Table 4.2: Summary of simulation results for one five-spot well system. In practice, multiple such systems can be envisioned. Note: to determine the amount of electricity produced, system-specific energy losses have to be considered for conversion of heat energy to electricity, as discussed in the main text.

4.4 Economic Implications for Geologic CO_2 Sequestration

The geothermal energy harnessed in the CPG approach can be utilized for baseload or dispatchable (peak-demand) electricity production or to provide heat for district space/water heating. The highest energy utilization efficiencies can be achieved by providing both electricity and heat, although this restricts the locations of facilities to sites

near heat end-users such as industry and/or residences. In the CPG approach, electricity could be supplied to the grid or used onsite to help offset the energy requirements of CCS. Here, we estimate the value of the energy harnessed by CPG with respect to CCS, specifically calculating the value of energy harnessed per ton injected CO_2.

Applying the parameters relevant to the base case simulation (Table 4.1), we first calculate the total amount of CO_2 sequestered during 25 years of CPG power plant operation. As previously mentioned, displacement of native formation fluid by CO_2 injection is not the objective of the current investigation. The reservoir must be prepped by injecting CO_2 for a period of time prior to producing heated CO_2. For current purposes, we assume that prior to CO_2 withdrawal from production wells, the 1km by 1km by 305m reservoir must be 10% filled with CO_2, which corresponds to approximately 6 months of injection at 280 kg/sec. Thereafter, we assume that averaged over the duration of power plant operation (loss rates are expected to be higher during early plant operation and decrease with time [9]), 7% of injected CO_2 is not recoverable at the production well and must be continuously replaced. Non-recoverable CO_2 is considered permanently stored within the geologic formation, reflecting the CO_2 sequestration component of the system. Pruess [9] utilizes a value of 5% for fluid "loss" (i.e., CO_2 storage) from CO_2-based EGS, and a higher value may be expected in the naturally permeable formations considered here (future studies will examine rates of fluid loss in detail). Note that, eventually, all injected CO_2 is permanently sequestered (barring upward leakage through the caprock) because the CO_2 circulated through the aboveground power plant system is reinjected (Figure 4.1). Therefore, for the base case, total CO_2 sequestration is 2.0 x 10^7 tons over the simulated 25-year life of the CPG power plant.

Starting with the thermal energy extraction rate (Q), electricity production (W) can be estimated by applying the Carnot efficiency (C) and mechanical system utilization efficiency (E) as $W = C*E*Q$. The Carnot efficiency, the theoretical maximum heat energy that can be converted to mechanical work, is defined as $C = 1 - T_{rejection}/T_{reservoir}$, where for the base case, $T_{reservoir} = 373.15$ K and $T_{rejection}$ is taken to be 283 K (the approximate average annual surface temperature for regions of the northern U.S.A. [45]). Applying $E = 0.5$ (modified after [33]) and taking $Q = 47.0$ MW thermal (average value over the 25 year life of the system, full well basis), $W = 5.7$ MWe.

Gross revenue (R) generated by the sale of this electricity is calculated using $R = Wx(hours\ \ per\ \ year) * (value\ \ per\ \ MW * hour)$, where $(value\ \ per\ \ MW * hour)$ is taken to be 100 \$U.S.A. [46] and tax incentives are excluded. Power plant construction cost (including exploration, drilling, permitting, plant construction, and transmission) is set at 3 x 10^6 \$U.S.A per MW [46], and operating cost, at 6.5 x 10^4 \$U.S.A. per MW per year [47]. Net revenue, gross revenue minus construction and operating costs, is 8.6 x 10^7 \$U.S.A. over the life of the power plant. This translates, for the base case, to a net revenue of 4.4 \$U.S.A per ton CO_2 sequestered, again assuming a 25-year lifespan of the CPG system. Longer operation times would result in higher net revenue values due to fixed construction and low maintenance costs.

For comparison, Case 1 (temperature = 150 ^{o}C, reservoir depth = 4 km) gives a net revenue of 7.9 \$U.S.A per ton CO_2 sequestered whereas Case 2 (temperature = 100 ^{o}C, reservoir depth = 1 km) gives net revenue of 5.9 \$U.S.A per ton CO_2 sequestered.

Over the same time span, the net revenue from CPG provides, in the base case, approximately 7.3% of the cost of CCS, assuming a current CCS cost of 60 \$U.S.A. per ton CO_2 (CCS costs range from $16.6 - 91.3$ \$U.S.A. per ton for capture from a coal or natural gas power plants [3]). In Cases 1 and 2, the percentage increases to 13.1% and 9.8%, respectively.

More significantly, CPG (base case) could provide 53% to 730% of the cost of geologic CO_2 sequestration and monitoring/verification (excluding CO_2 capture), assuming storage and monitoring/verification costs of $0.6 - 8.3$ \$U.S.A. per ton CO_2 [3]. For Cases 1 and 2, the ranges are 95% to 1300% and 71% to 980%, respectively. While the CO_2 injection and partial sequestration component of enhanced hydrocarbon recovery is generally considered economically feasible, traditional deep saline aquifer CO_2 sequestration is not. These results suggest that combining geothermal energy capture with sequestration, i.e., CPG, vastly improves the economic feasibility of the CO_2 sequestration component in deep saline aquifer CCS.

Rather than considering the revenue generated by CPG in the context of the cost of CCS, we may also examine CPG with respect to the carbon price required to achieve certain reductions in atmospheric CO_2 emissions. According to the IPCC 2007 report [3], a carbon price of 31 \$U.S.A per ton CO_2 (the mean value of 12 scenarios) by 2030

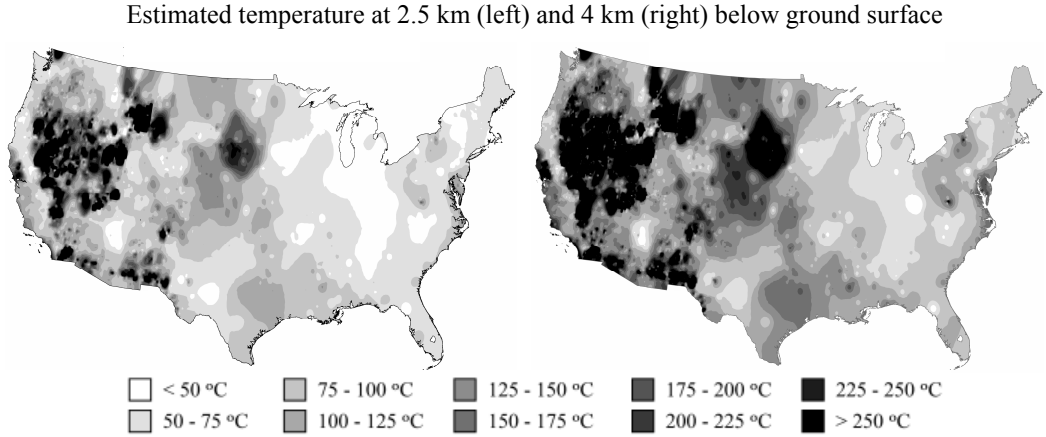

Figure 4.2: Contiguous U.S.A. temperature maps at 2.5 (left) and 4 km (right) depths. Comparing these maps with the locations of sedimentary basins in the U.S.A., shown in Figure 4.3, reveals that such basins are often present in regions with moderate to high subsurface temperatures. Thus, with regards to temperature, such sedimentary basins, if utilized for CO_2 sequestration, could also be employed for geothermal energy capture employing CPG systems. From [4].

delivers emissions trajectories that lead to stabilization of atmospheric CO_2 concentration at Category III levels (440 - 485 ppm). The CPG scenarios investigated here provide revenue in the range of $4.4 - 7.9$ \$U.S.A. per ton CO_2, or $14 - 25\%$ of the above indicated carbon price. With widespread utilization of CPG, therefore, lower carbon prices could provide the same incentive to sequester CO_2, and hence reduce atmospheric CO_2 emissions, as higher carbon prices without CPG. In general, lower carbon prices (i.e., taxes) should be easier to implement.

In addition to sequestering CO_2, the CPG approach avoids atmospheric emissions by supplying energy from non-CO_2-emitting, renewable energy sources, as geothermal energy may be considered renewable over human time scales, in stark contrast to hydrocarbon-based energy. Assuming a standard coal-fired power plant produces 30 tons CO_2 per MWe per day [21], the electricity supplied by the base case CPG power plant avoids 1.6 x 10^7 tons of CO_2 over the duration of power plant operation, similar in magnitude to the quantity of CO_2 directly sequestered.

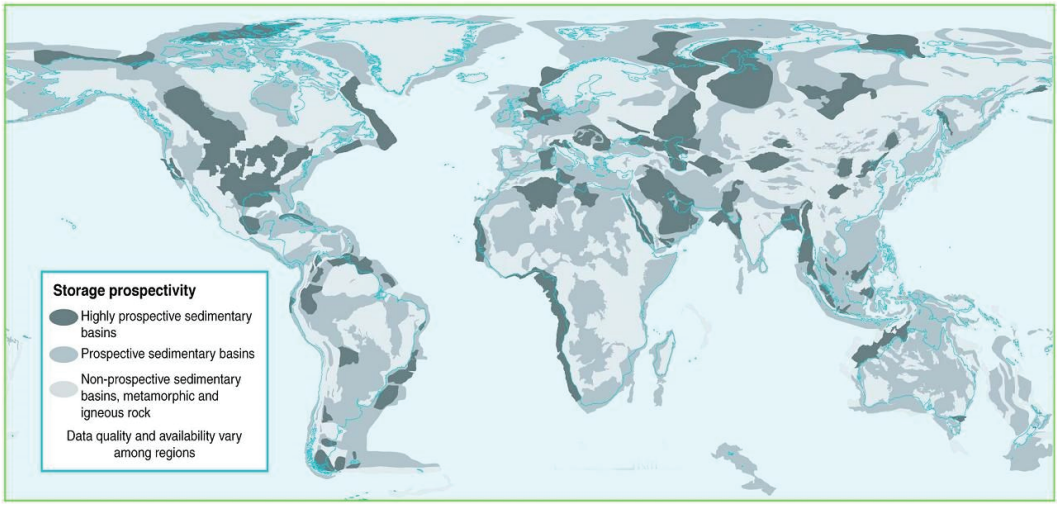

Figure 4.3: Map of sedimentary basins worldwide ([48]) that may serve as reservoirs for geologic CO_2 sequestration. For the work presented here, particularly note the locations of basins in the United States.

4.5 Concluding Remarks

While additional research is required, numerical modeling results at present suggest that geologic reservoirs with CO_2 as the subsurface heat mining fluid (i.e., CPG systems) could substantially offset the costs of CCS, and in particular the sequestration component of CCS. In addition, CPG systems would serve as clean, renewable geothermal energy sources for electric power production, potentially even in regions worldwide with moderate to low geothermal temperatures and subsurface heat flow rates.

Chapter 5

Impact of reservoir permeability on the choice of subsurface geothermal heat exchange fluid: CO_2 versus water and native brine

This chapter is largely based on Randolph and Saar, 2011 [49].

5.1 Introduction

Existing literature [29] (Chapter 3)) [18] (Chapter 2) has noted that the high mobility of CO_2 compared to water at the geologic conditions of interest for natural-reservoir-based geothermal development should permit CPG development in reservoirs with permeabilities lower than are viable for water-based geothermal (Condition 2, Chapter 2). Here, I explore geothermal heat extraction from naturally permeable, porous geologic formations as a function of reservoir permeability and subsurface heat exchange fluid.

5.2 Numerical simulation methodology

The purpose of the investigation detailed here is to isolate the effects of permeability and choice of subsurface heat extraction fluid on natural-reservoir-based geothermal energy production. To accomplish a comparison of reservoir behavior between fluids, numerous assumptions and simplifications to the system are incorporated into the numerical simulations.

First, we assume sufficient geologic formation injectivity/productivity in the immediate neighborhood of wells (bottom hole) for the specified injection/production rates. Though injectivity/productivity are important considerations, the current focus is on reservoir-scale properties. Insufficient well bottom-hole properties could be addressed in part through the use of limited hydraulic, thermal, or chemical stimulation or horizontal wells with long sections open to the reservoir. Similarly, technologies exist to increase the effective well bore diameter.

We simulate operation of geothermal reservoirs containing CO_2, pure water (henceforth called "water"), or 20% mass fraction NaCl brine (henceforth called "brine") over a variety of reservoir permeabilities, from 5 x 10^{-16} to 5 x 10^{-12} m^2 (see, e.g., [32] and [16] for sample CO_2 sequestration reservoirs with permeabilities covering this range and fluid compositions similar to this brine). In each numerical model, only one fluid occupies the pore space, analogous to previous CPG studies [29] (Chapter 3) [18] (Chapter 2) and CO_2-based EGS studies [9] [11]. Thus, in the case of CO_2 working fluid, the presence of subsurface CO_2 is assumed (naturally or from previous injection), and while displacement of native fluid - such as water, brine, or hydrocarbons - is of interest, it is beyond the scope of the present study. All reservoir simulations utilize the simulator TOUGH2 [24] with equation-of-state module ECO2N [25].

Of particular interest in the current study are low-temperature geothermal resources, as they provide an opportunity for widespread expansion of the geothermal power base. Therefore, a subsurface system initial temperature of $T = 100\ ^oC$, often considered the lower limit for geothermal electricity production (e.g., [23]), is chosen. In a region with low to moderate geothermal gradients (30-35 ^oC/km), $T = 100\ ^oC$ corresponds to a reservoir depth of 2.5 km, dependent upon local mean annual surface temperature and fluid/rock thermal conductivity. At such low reservoir temperatures and heat flow

Parameter	Value
Geologic Formation	
Formation map-view area	1 km^2
Thickness	305 meters
Permeability, k	5x10^{-14} m^2
Porosity	10%
Rock grain density	2650 kg/m^3
Rock specific heat	1000 J/kg/^oC
Thermal conductivity	2.1 W/m/^oC
Injection/Production Conditions	
Average annual surface temperature	12 ^oC
Surface heat rejection temperature	22 ^oC
Well separation	707.1 meters
Well pattern	Five-spot
Heat extraction rate	43.6 MW
Formation Initial Condition	
Fluid in pore spaces	All CO_2, H_2O, or brine
Temperature	100 ^oC
Pressure	250 bar
Formation Boundary Conditions	
Top/sides	No fluid or heat flow
Bottom	Heat conduction, no fluid flow

Table 5.1: Summary of parameters used in base-case models. Base-case parameters correspond, in general, to parameters utilized in previous studies [29] [4] [18]. The base-case simulations were utilized to determine mass-flow rate for each fluid at $k = 5$ x 10^{-14} m^2; this mass-flow rate was then fixed as permeability was varied. See text for additional details.

rates, it is reasonable to assume approximately hydrostatic fluid pressures [50]. Table 5.1 presents a list of formation and model parameters, which are generally consistent with previous publications concerning CPG [4] [18] [29] (Chapters 2 - 4). With such low formation temperatures, the geothermal power system is taken to be a binary system [50].

Long-term fluid behavior in injection and production wells, once rock surrounding

the wells has achieved near-equilibrium with well fluid temperatures, can be approximated as isenthalpic [9]. Accounting for isenthalpic expansion/compression, i.e. Joule-Thompson cooling/heating, is primarily important in CO_2 simulations (Figure 5.1). The temperature, T, and pressure, P, profiles for CO_2 in the injection well are calculated by Newtonian iteration starting from T, P values at the surface. Fluid injection surface T is set to 22 ^{o}C, which is 10 ^{o}C higher than the average annual atmospheric (i.e., power system heat rejection) temperature in St. Paul, MN [45]. This is a conservative assumption for heat rejection efficiency of binary geothermal systems [51]. Furthermore for CO_2, injection surface pressure is set to 10 bar above saturation pressure (60.0 bar) at injection wellhead temperature, ensuring single phase conditions in surface equipment (of particular value should the reader wish to compare this binary power system with a direct CO_2 turbine system). Because of the low compressibility/expansivity of water and brine, they are assumed to undergo isothermal well flow [9].

For simplicity, we assume constant fluid production temperature, a reasonable approximation for the first ten years of power plant operation at the specified reservoir and injection/production conditions (see Figure 5.2). Moreover, we ignore the pressure drop through surface equipment (we do, however, impose a mechanical system efficiency of 50%, modified after [33]). While important, this will be explored in future analyses. Note that in certain CPG systems, a throttling valve could be used to sufficiently decrease pressure between injection and production wellheads, whereas in water/brine and other CPG cases (e.g., very low reservoir permeability), additional pumping may be needed.

We account for injection and production pumping power using the approximation given in the U.S. Department of Energy Geothermal Electricity Technology Evaluation Model (GETEM) [52], where $pumping\ power = (total\ flow) * (\Delta P/\rho) * (pump\ efficiency)$. Here, ΔP is the required pressure rise to ensure the $total\ flow\ rate$, and ρ is fluid density. $Pump\ efficiency$ is set conservatively high, to 0.9 (modified from [50]). In CPG simulations, pumping power is assumed to be zero if the production wellhead pressure is higher than the injection wellhead pressure (i.e., a thermosyphon exists). Assuming use of downhole shaft pumps (as opposed to electric submersible pumps, which are not yet in extensive operation), pump depth is limited to 450 m [50]. Thus, for water and brine models, the assumption of approximately hydrostatic reservoir conditions imposes

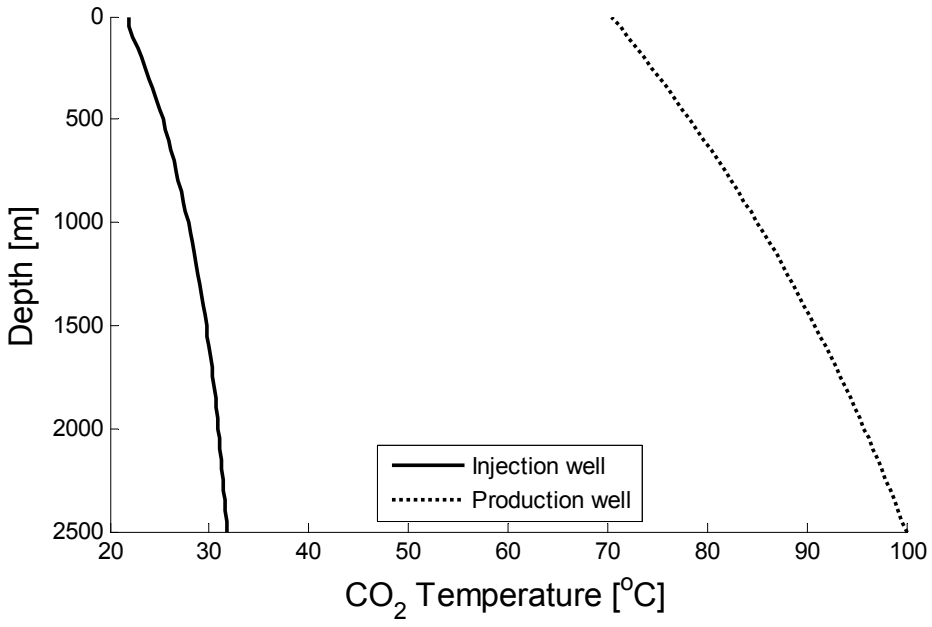

Figure 5.1: Isenthalpic CO_2 flow in geothermal injection and production wells. Because CO_2 is a relatively compressible supercritical fluid at the temperature and pressure conditions of interest, it compresses/ heats upon injection and expands/ cools during production. Water and brine (not shown), in contrast, are relatively incompressible liquids at the investigated conditions and, thus, experience essentially isothermal well flow. From [49].

a minimum pressure of 205 bar at the production well bottom hole such that the fluid will reach the downhole production pump. In simulations, the production bottom hole pressure is not permitted to fall below 210 bar and any additional fluid-driving pressure differential between injection and production wells must come from the injection side.

Reservoir thermal energy extraction rate, H, is calculated from specific enthalpy difference between produced, h, and injected, h_o, fluids, and the production fluid mass flow rate, Q, given as $H = Q(h - h_o)$. Electricity production rate, E, is then calculated by multiplying H by the Carnot efficiency - calculated using fluid wellhead temperature and the previously-stated mean annual surface temperature (12 ^{o}C) - and by a 50% mechanical system efficiency (modified after [33]).

Finally, there are many means that could be employed to compare the CO_2, water, and brine systems. For instance, we could use the same fixed bottom-hole pressure difference between injection and production wells for all fluids, as in other studies [9] [18] [29] (Chapters 2 - 4). Alternatively, we could set the production mass flow rate or the binary system power output to be the same for all fluids. However, in order to isolate the effects of reservoir permeability, k, from differences in mobility (inverse kinematic viscosity) and heat capacity of the fluids, we choose to fix the reservoir heat energy extraction rate between fluids for a given reservoir permeability (see Chapter 3 for additional information on fluid mobility differences and consequences for reservoir heat extraction). To determine a heat extraction rate to use in comparisons, we start (for consistency with previous literature [29] [18], Chapters 2 and 3) with the base case model parameters given in Table 5.1 (note, $k = 5 \text{ x } 10^{-14}$ m^2). Beginning with the CO_2 case, fluid flow is driven by a 20 bar pressure drop through the reservoir. The CPG heat extraction rate is then determined. For water and brine simulations at the same permeability, the pressure drop through the reservoir is adjusted to match the CO_2 heat extraction rate. The pressure drops specify a mass-flow rate for each fluid, which is fixed as permeability is varied.

Note that these simulations do not necessarily optimize power plant electricity production for each permeability and fluid. For example, a CPG reservoir with high permeability (e.g., $5 \text{ x } 10^{-12}$ m^2) would likely have a power system designed to operate at higher fluid mass-flow rates than that used in this set of simulations. However, in order to compare various reservoir fluids over a variety of permeabilities, fluid mass-flow rates are fixed.

5.3 Results: Electricity production efficiency versus reservoir permeability

Figure 5.2 presents geothermal electricity production efficiency versus reservoir permeability for CO_2, water, and brine subsurface working fluids. Electricity production efficiency is defined as the net electricity production rate, E_{net}, divided by the total heat energy extraction rate, H; E_{net} is the gross electricity production rate, E, minus injection/production pumping power requirements.

For reservoir permeabilities below approximately 2 x 10^{-14} m^2, CO_2 provides clearly higher electricity production efficiency than both water and brine (see [B] in Figure 5.2). For larger permeabilities of $k > 2$ x 10^{-14} m^2, pure water, and for $k > 5$ x 10^{-14} m^2 (see [A] in Figure 5.2), brine is more efficient than CO_2. At moderate to low permeabilities of about $10^{-16} < k < 10^{-13}$ m^2, CO_2's high mobility compared to water and brine [18] is particularly advantageous as it minimizes pumping power requirements while permitting high mass flow rates. Within this latter permeability range, some k values are so low that net electricity production with pure water, let alone brine, is not possible, while CO_2's efficiency is hardly diminished (Figure 5.2). However, at higher permeabilities, the relatively high heat capacity and low compressibility of liquid water and brine, compared to CO_2, result in water and brine having moderately more favorable electricity production efficiencies. At very high permeabilities of about $k > 5$ x 10^{-13} m^2, pumping power (for water and brine) nears zero (while CO_2 does not require pumping due to a strong thermosyphon effect) and electricity production efficiency ceases changing with k.

It should also be noted that aspects other than efficiency, such as undesirable subsurface loss of water versus desirable subsurface loss of CO_2, i.e. geologic storage, must be considered when selecting a subsurface working fluid. Particularly in arid regions and/or localities where large amounts of CO_2 need to be sequestered, CO_2 may be the preferable subsurface working fluid despite somewhat lower efficiencies than water at higher permeabilities.

The above efficiency results are reasonable in light of the common observation that significant advective heat transfer by water (or brine) appears to require minimum permeabilities of 5 x $10^{-17} < k_{min} < 10^{-15}$ m^2 (e.g., [53] [31]), given the hydraulic head gradients, water kinematic viscosities, and water heat capacities at temperatures and pressures of interest. Hence, Figure 5.2 shows how supercritical CO_2's differing kinematic viscosity (or mobility), heat capacity, and compressibility combine to provide improved geothermal heat extraction - and ultimately electricity production - efficiencies at permeabilities at or below k_{min} for water. In other words, k_{min} for CO_2 appears to be several orders of magnitude lower than that for water, and only at permeabilities above k_{min} is significant advective heat transfer, and resultant economical geothermal energy extraction, expected.

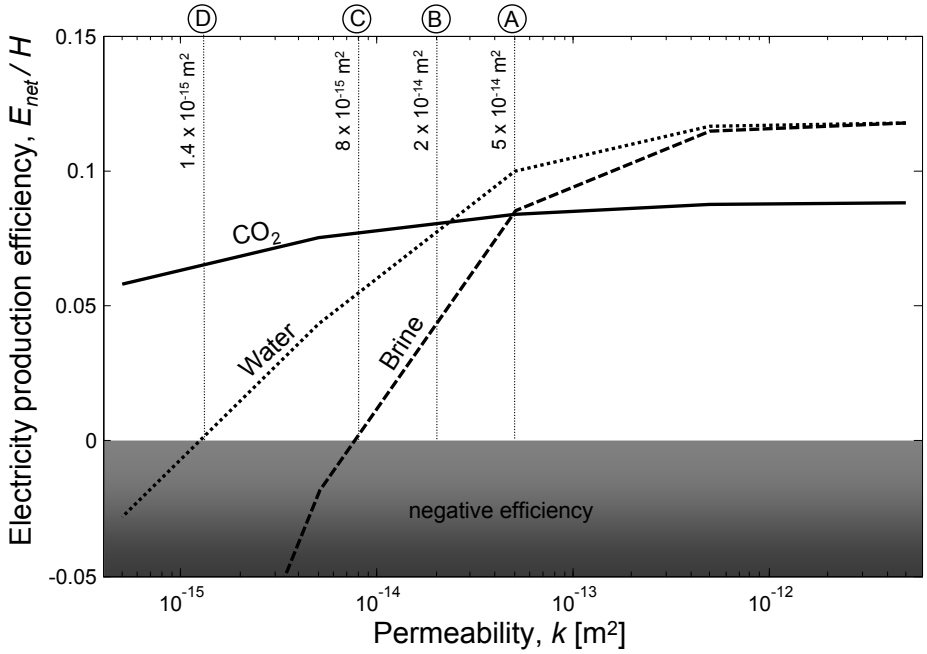

Figure 5.2: Results of numerical simulations of electricity production efficiency (net electricity production divided by thermal energy extracted from the reservoir) versus reservoir permeability, k, for CO_2, water, and 20% mass fraction NaCl brine working fluids. For $k < 5$ x 10^{-14} m^2 [A], CO_2 results in higher efficiencies than brine, and for $k < 2$ x 10^{-14} m^2 [B], CO_2 efficiencies are higher than those of water. At $k = 8$ x 10^{-15} m^2 [C], brine transitions into the negative efficiency field while CO_2 results in 50% higher efficiency than water. At about $k < 1$ x 10^{-15} m^2 [D], water results in negative efficiencies while CO_2 efficiencies remain relatively constant and high. This illustrates that CO_2 is particularly advantageous at somewhat low, but common, permeabilities where water or brine could not be used for geothermal electricity production. From [49].

In order to explore the effects of permeability on electricity production efficiency over a variety of temperature and pressure conditions, simulations are executed at several points along two different geothermal gradients, the results of which are given in Figure 5.3. In Panels [A], [B], and [C] of Figure 5.3, a geothermal gradient of 35 ^{o}C/km (with 12 ^{o}C as the average annual surface temperature) is utilized, representing a moderate geothermal heat flow as mentioned above. Note that Panel [B] provides the same results

as Figure 5.2, allowing comparison with other panels. Figure 5.3 Panels [D], [E], and [F] represent a geothermal gradient of 60 ^{o}C/km, consistent with a relatively high geothermal heat flow rate, more typical of tectonically and/or volcanologically active regions. Depending on temperature and pressure, Figure 5.3 shows that CO_2 provides higher electricity production efficiencies than water at permeabilities as high as 2 x 10^{-13} m^2 (Panel [A]) and than brine at permeabilities of up to 4 x 10^{-13} m^2 (Panel [A]).

At the other end of the spectrum (Panel [C]), water efficiency remains above that of CO_2 throughout the investigated permeability range, while brine efficiency is greater than that of CO_2 at permeabilities higher than 2 x 10^{-14} m^2 (panel [C]). Finally, in the high geothermal gradient case (Panels [D] through [F]) efficiencies of the three working fluids are very similar at greater depths and associated temperatures (Panels [E] and [F]). However, at shallower depths and lower temperatures (Panel [D]), to which drilling is more economical, CO_2 is more efficient than water at $k <$ 2 x 10^{-13} m^2 and than brine at $k <$ 3 x 10^{-13} m^2. As previously noted, in all cases, in addition to electricity production efficiency, availability and subsurface loss of water as well as availability and permanent subsurface storage of CO_2 must be considered when selecting a working fluid in real-world applications.

As geothermal development in sedimentary basins progresses, it is likely that at the depths required to achieve sufficient temperatures for economical geothermal development, permeability may be well below 2 x 10^{-14} m^2 as a results of 1) compaction (of sediments) and/or 2) hydrothermal alteration causing clogging of pore space (e.g., see Finley [32] and Steadman et al. [16] for permeabilities, k, of deep sedimentary basins). Moreover, in crystalline rocks, k can be small even at shallower depths. Thus, the results of this investigation are relevant for CPG-type development in sedimentary basins as well as moderately-permeable EGS in crystalline rocks.

5.4 Conclusions

Previous studies [18] [29] (Chapters 2 and 3) have shown that CO_2-plume geothermal (CPG) systems provide higher geothermal heat extraction rates from naturally permeable, porous geologic formations, such as sedimentary basins, than traditional water-based reservoir geothermal operations even at low subsurface temperatures. The work

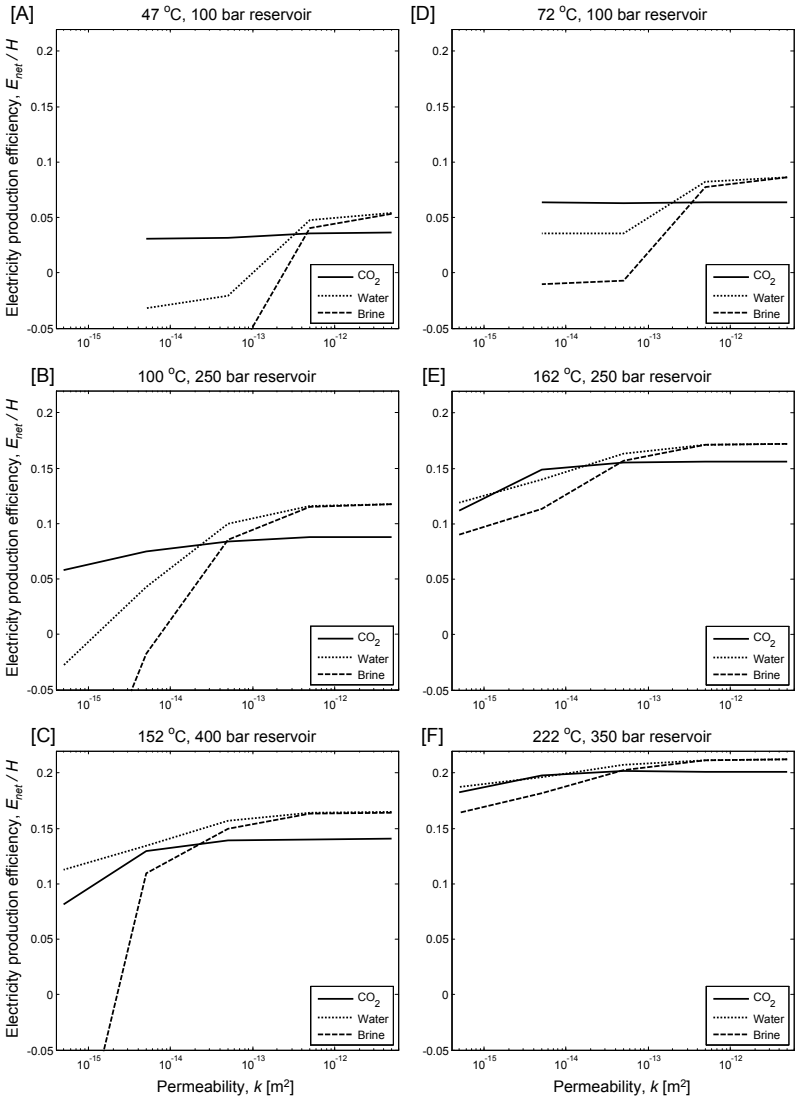

Figure 5.3: Electricity production efficiency versus permeability, k, for several T, P conditions along two geothermal gradients. In Panels [A], [B], and [C], a moderate geothermal gradient of 35 ^{o}C/km (with 12 ^{o}C average annual surface temperature) is utilized. Note that Panel [B] provides the same results as Figure 5.2. Panels [D], [E], and [F] represent a relatively high geothermal gradient of 60 ^{o}C/km. Depending on T, P, CO_2 provides higher electricity production efficiency than water at k as high as 2 x 10^{-13} m^2 [A]. Similarly, CO_2 provides higher electricity production efficiency than brine at permeabilities as high as 4 x 10^{-13} m^2 [A]. Note that in the shallow, low temperature cases (Panels [A] and [D]), TOUGH2 simulations did not converge for $k = 5$ x 10^{-16} m^2 because of the very high pressure gradients required to drive flow of cool, dense fluids in such low k reservoirs. From [49].

presented here demonstrates that CO_2 is particularly beneficial as a subsurface geothermal heat exchange fluid in moderate-to-low permeability ($k < 2$ x 10^{-14} to $k < 2$ x 10^{-13} m^2, depending on reservoir temperature and pressure) formations. Such geologic reservoirs, overlain by low-permeability caprocks, exist worldwide and are under consideration for geologic CO_2 sequestration (e.g., [16] [19] [32]). Furthermore, the present study shows that even at permeabilities higher than $k = 2$ x 10^{-14} to $k = 2$ x 10^{-13} m^2, CO_2's electricity production efficiency is only slightly lower than that of water or brine, depending on temperature and depth, while providing the additional benefits of preserving water and geologically sequestering CO_2.

Future work will explore the geothermal electricity production efficiency of CO_2, water, and brine accounting for optimization of the power cycle. At low resource temperatures ($T < 150$ ^oC), water- or brine-based geothermal operations are limited to binary power plants, often utilizing a form of Organic Rankine Cycle [42]. However, because of its low critical temperature (31.1 ^oC at 73.8 bar), CO_2 could be used directly in a turbine (tolerable levels of contaminants, such as water or sulfur, in the CO_2 will also be examined). Potentially, such a direct system would permit significantly higher electricity production efficiencies than those accounted for with the simple assumptions in the current study. For instance, in the base CO_2 case investigated above ($T = 100$ ^oC, $P = 250$ bar, $k = 5$ x 10^{-14} m^2), the net electricity production rate (E_{net}) is calculated to be 3,664 kW, and the production efficiency is 8.4%. In comparison, work, W, produced from a direct system is given by $W = (total\, mass\, flow) * (\Delta P/\rho)$, where ΔP is the pressure difference between injection and production wells (at wellheads) and ρ is fluid density. Assuming 93% turbine efficiency and 90% system efficiency [54], $E_{net} =$ 4,170 kW and the electricity production efficiency is 9.6%. At higher resource temperatures and pressures, where the wellhead pressure difference may be much larger, the direct system efficiency may be proportionally even larger.

Chapter 6

Temperature-depth, T(z), Profile Studies

As noted in Chapter 1, this dissertation began with an examination of temperature-depth, T(z), profiles in Long Valley Caldera (LVC), California. Thus, this research chapter begins by exploring the initiated project and motivation for said project. My study of temperature-depth profiles evolved to include T(z) examination locally, i.e., in Minnesota (MN), as I recognized that existing local heat flow data is limited and inaccurate. Discussion of the current state of this MN project follows the LVC section. For additional background information on T(z) profiles, see Appendix E.

6.1 Transient T(z) Study in Long Valley Caldera

It is widely recognized that subsurface heat and fluid flow fields can change with time. For example, Bodvarsson et al. [55] modeled the transient temperature evolution associated with the formation of a geothermal system, as might occur if faulting opens new pathways for fluid flow in a geothermally active area, and he specifically examined changes in T(z) profiles with time. Studies of near-surface transient temperature behavior are abundant, Suzuki in 1960 [56] and Birman in 1969 [57] being some of the first to discuss the impact of surface temperatures on the shallow subsurface with specific reference to T(z) profiles. Numerous other studies followed, many focusing on the use of shallow T(z) profiles to determine infiltration of surface waters (e.g., [58] [59] [60] [61]

[62] [63]). These near surface, surficial zone studies reveal the impact of annual surface temperature oscillations on ground temperatures, and a recent study [64] was capable of measuring the impact of diurnal oscillations in this same zone.

Long term (several hundreds of years) transient temperature variations in the geothermal zone, the result of changes in mean annual surface temperature, have long been recognized, with Birch in 1948 [65] being one of the first. To note, the geothermal zone [66] is the subsurface deeper than 30ft to approximately 130ft, depending on local geology and conditions (e.g., [67]), which is not affected by diurnal or annual surface temperature oscillations. Numerous climate-related studies have been completed since Birch [65] (e.g., [68] [69] [70] [71] [72] [73] [74] [75] [76]).

Despite the recognition of near-surface transient temperature conditions and long term deep temperature variations, for the vast majority of studies using T(z) profiles to study the geothermal zone, temperature data is recorded only once because travel to boreholes and logging of profiles is time consuming and expensive. Consequently, little research has been done to explore short term (hours to decades) transient T(z) profiles in the geothermal zone despite many studies' fundamental assumption of steady state conditions and the significant lack of research to verify this claim. One of the few studies to consider transient T(z) profiles was completed by Ingebritsen et al. (2001) [77] in which several profiles were obtained each year for several years in a single borehole in order to examine seasonal hydrologic behavior.

This project was conceived to begin filling the void in short term transient T(z) profile examinations of the geothermal zone. Further motivation was provided by transient variations observed in T(z) profiles in Long Valley Caldera. In particular, a steady increase in temperatures over the past twenty years has been observed in Well CH10B (see Figure 6.1), including a several degree Celsius jump that appeared to correlate with a series of relatively strong local earthquakes, and recently (2006) changes were noted in hot springs near the borehole [78]. To investigate future T(z) profile changes at CH10B, in the summer of 2006, Martin Saar installed a string of ten thermistors in the well to measure temperature at ten different depths every 15 minutes. The following year, I assisted in the design and installation of a ten-thermistor string in Borehole 35-28, also in Long Valley Caldera. Data collected thus far reveals clear transient temperature behavior in the two boreholes (see Figures 6.3 and 6.4).

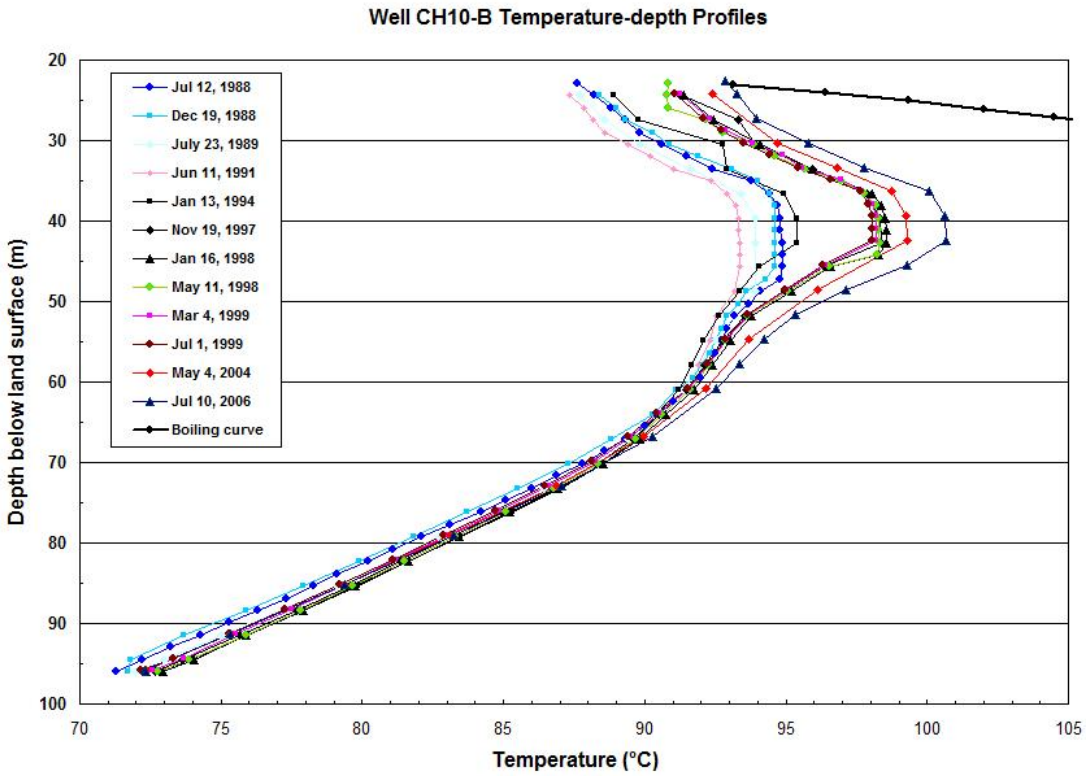

Figure 6.1: T(z) profiles that were hand-logged (as opposed to measured by the ten thermistor string installed in CH10B) from borehole CH10B in Long Valley Caldera. The high aquifer temperatures captured by these T(z) logs are strongly indicative of (near horizontal) flow of hot water. Notice a steady increase in temperature beginning in the mid 1990's. The most recent profile plotted here intersects the water boiling curve at depth; this intersection roughly corresponds in time with strongly-increased hot spring activity in the nearby Hot Creek [78]. Also note the several degree temperature increase in the flow zone (the bulged portion of the profile centered at a depth of approximately 40m) between the 1994 and 1997 profiles. This might correspond to strong local seismic activity in the late 1970's [79] inducing changes in fluid flow from the Long Valley hydrothermal reservoir, delayed by the time required for fluid to move from the reservoir to CH10B. Additional study is needed to confirm or deny this correlation. Finally, notice that all profiles tend to the same temperature at depth, suggesting that local geothermal heat flow has not changed. The negative gradient of the profiles at depth suggests the presence of a deep, cold aquifer.

Potential causes for the transient behavior observed in Long Valley Caldera T(z) profiles, including the observed diurnal signal in well CH10B and the general transient behavior evident in both wells 35-28 and CH10B, are discussed in the following. Techniques that could be employed to analyze the potential causes in the context of LVC profiles are described, though thorough analysis is reserved for future studies.

6.1.1 Increase in mean annual surface temperature.

Before discussing how we might look for surface warming effects in T(z) data, it is important to explain why we consider looking for these effects in data from Long Valley Caldera rather than elsewhere. One could argue that Long Valley is a poor site to look for surface warming effects in the subsurface thermal regime because the high local geothermal and hydrothermal heat fluxes (e.g., [80]) could drastically overprint the climate signal. However, Long Valley Caldera and its boreholes have been extensively studied in general and our well-instrumented boreholes in particular, providing significantly more data than available in other regions. Even though there are issues in Long Valley with convoluted surface and geothermal temperature signals, with the vast available information, we may be able to deconvolve the signals. The vast store of information and large set of boreholes provide a rare opportunity to search for effects of surface warming on the subsurface fluid and heat flow regimes in an area of high geothermal heat flow, which has not been widely accomplished and would be valuable in debates on the effects of climate change.

As mentioned above, it has long been recognized that ground surface temperature (GST) affects the subsurface thermal regime (e.g., [68] [81]). In areas without significant groundwater flow, the GST record is preserved as a time- damped signal in the subsurface [71] and can be read to estimate paleoclimate temperatures for up to 80,000 yr B.P. [72], limited by the depth of the borehole in which T(z) measurements are taken. The older the observed temperature signal, the more it is time-averaged because heat diffusion in geologic media dampens high-frequency temperature information [71]. The GST impacts subsurface temperatures everywhere, but in most locations the surface signal is nearly obscured, groundwater being the primary cause of signal loss [82]. Analysis of T(z) profiles to reconstruct past climate involves profile inversion to solve for the surface temperature (e.g., [74]), as original surface temperatures are not recorded.

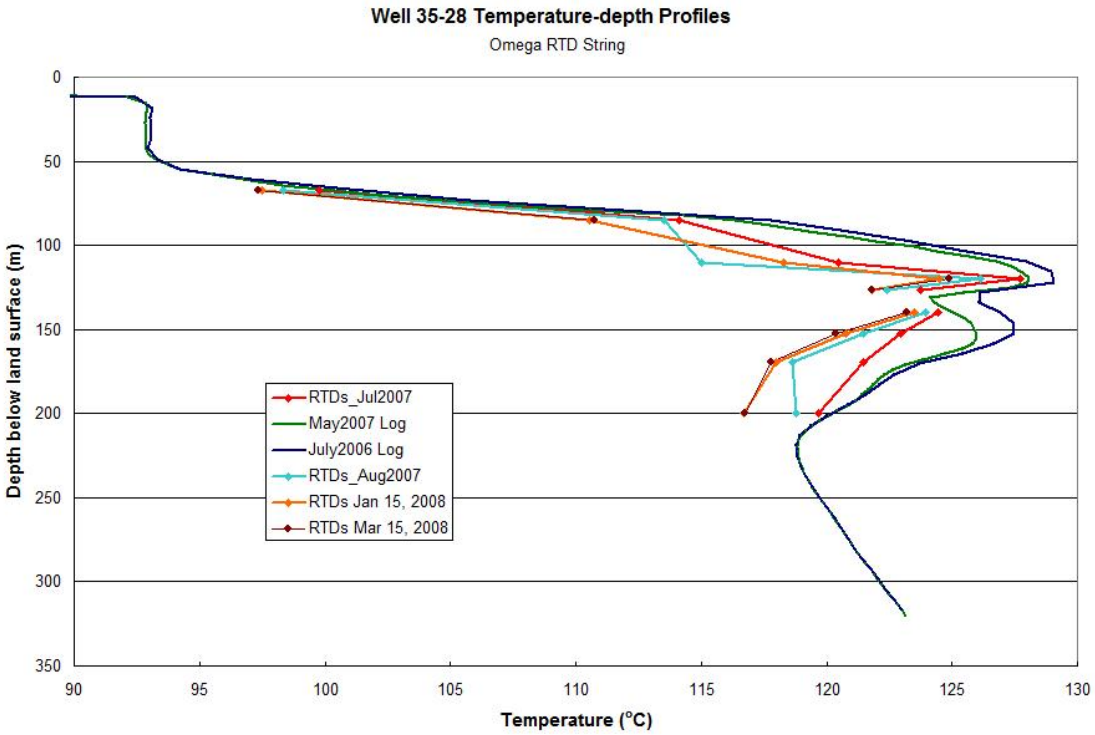

Figure 6.2: T(z) profiles from well 35-28 in Long Valley Caldera. The rightmost, smooth profiles were logged by hand while the four that are more coarse were logged by the ten thermistor string installed in the well. This plot highlights the spacial resolution that is lost when we gain temporal resolution using an installed thermistor string. Notice that the profiles show decreasing temperatures with time in the flow zone(s). 35-28 T(z) profiles reveal one large temperature deviation from the local geothermal gradient temperature in which are two small deviations, the latter perhaps caused by a narrow semiconfining layer within the hydrothermal aquifer at this location.

What might be considered the opposite approach, the study of effects of surface warming on groundwater, has seen limited application, though researchers have recognized its utility in addressing concerns over the impact of global warming upon water resources (e.g., [83]).

Typical climate studies using T(z) profiles assume GST impacts the subsurface thermal regime via conduction from the surface (e.g., [68]). Streambed studies using T(z) profiles, however, have recognized annual changes in subsurface thermal structures and attributed them to stream temperature variations (e.g., [58] [63]). Similarly, changes in mean annual surface temperature may contribute, via groundwater-surface water interaction, to T(z) changes in Long Valley. While it is unlikely that LVC boreholes could prove viable for historic surface temperature reconstruction (i.e., based on conduction from the surface) because of the strong hydrothermal flow system, surface temperature variations may influence changes in LVC T(z) profiles at depth.

In Long Valley, water of hydrothermal origin mixes with meteoric water as it moves from the site of upwelling from the thermal reservoir to the discharge location. Mixing could be confirmed by examining the transient T(z) records currently being obtained at CH10B (Figure 6.3) and 35-28 (Figure 6.4) for seasonal temperature oscillations (an indication of mixing of thermal waters with seasonal snow melt). Changes in surface temperature make for changes in the temperature of meteoric water (except for snow melt, which always recharges at zero degrees Celsius), and thus when meteoric water mixes with thermal water, the mixture should record damped changes in surface temperature.

This is difficult to test, however, because of the many possible sources of heat for the regional groundwater flow system – such as the local geothermal gradient, changes in hydrothermal flow paths and associated changes in heat input from the caldera hydrothermal reservoir, and the local geothermal power plant. Thus, we suggest testing the idea of surface temperature effects on the subsurface thermal regime theoretically, examining in a numerical model whether changes in meteoric water temperature could be observe in synthetic T(z) profiles and whether the decade-scale transient temperature behavior observed in Long Valley boreholes such as CH10B could be caused by surface warming. The model would be based upon characteristics of the Long Valley hydrothermal system, which are readily obtained (e.g., [84]). Meteoric water temperatures for the model can be taken from Long Valley meteorological station records. The extent of mixing of meteoric and thermal waters at various sites in the caldera can be estimated from chemical data (e.g., [85]). Finally, T(z) records from boreholes in the caldera but outside the main hydrothermal flow path or from multiple locations on the flow path

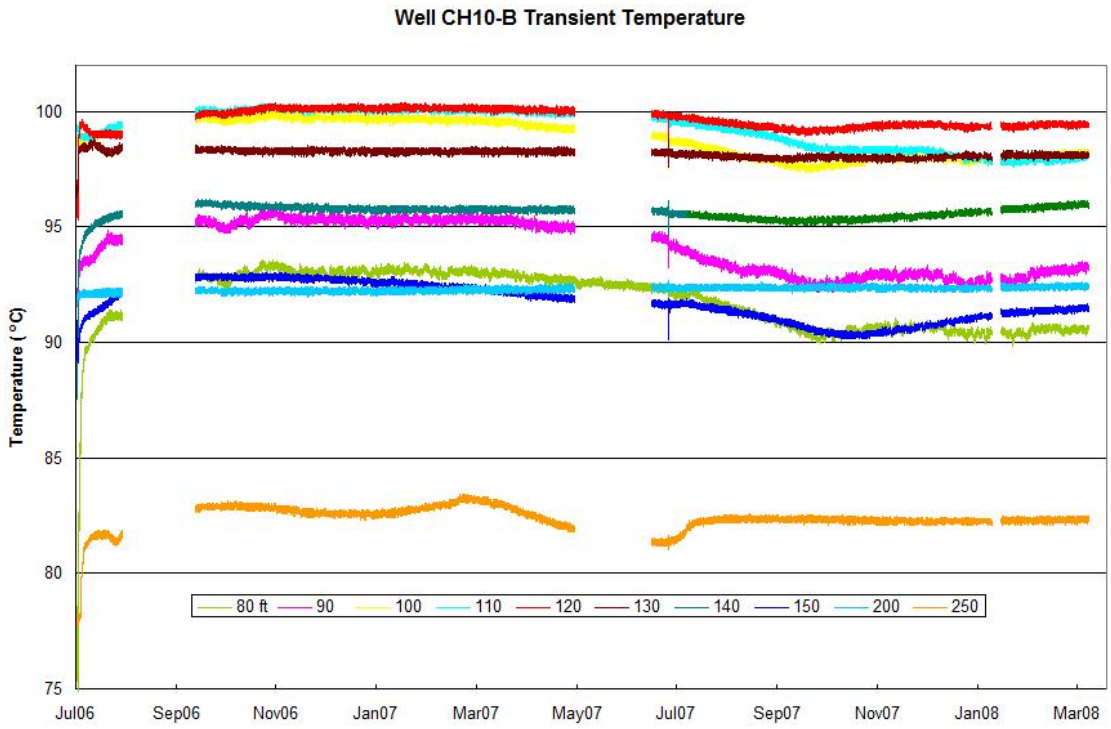

Figure 6.3: Data from the ten thermistor string installed in well CH10B. Each line corresponds to one thermistor at the indicated depth. Notice clear transient temperature behavior.

(and thus displaying different degrees of mixing) could be examined to strengthen model conclusions. And it may be of interest to examine, for comparison, boreholes near the caldera where snow melt does not significantly recharge the local groundwater system.

Regardless of whether T(z) changes can be reasonably attributed to surface temperature changes, other possible causes must be explored. If demonstrated, however, this approach could theoretically be applied to any borehole in which several T(z) profiles have been taken over many years, providing a more direct method of measuring surface temperature changes from T(z) profiles than currently available (i.e., inverting the conductive GST signal from profiles). Furthermore, it would reveal an impact of surface temperature changes upon groundwater, of value in global climate change discussions.

6.1.2 Other climatological effects, namely changes in precipitation and annual snow cover.

As mentioned, within Long Valley Caldera, hot waters in relatively near surface aquifers and at the surface are a mix of waters of hydrothermal origin and waters of meteoric origin (e.g., [84]). Much of the meteoric water falls as snow in the mountains surrounding the caldera, entering the caldera's groundwater system following the spring melt. This influx of cold water should be evident as a temperature drop in T(z) profiles; similar interaction has been noted elsewhere (e.g., [77]). Transient T(z) profiles, such as those we are collecting at boreholes CH10B (Figure 6.3) and 35-28 (Figure 6.4) in the caldera may reveal the presence of snow melt water and permit determination of lag time between melt and observation at distance. This time lag, combined with estimates of the distance between borehole location and snow recharge area, could help constrain hydraulic parameters (e.g., permeability) of local aquifers. A thermal constraint on hydraulic parameters is highly beneficial and could be applied to many regions (e.g., [64]).

Snow cover naturally varies from year to year, and assuming snow meltwater influences T(z) profiles, snow cover variations should be visible in transient profiles as temperature differences between subsequent years, caused by changing snowmelt/thermal water mixing ratios. Records from Long Valley Caldera meteorological stations should permit accurate determination of yearly precipitation, allowing correlation of precipitation records with transient T(z) data.

6.1.3 Energy production at the local geothermal power plant.

Long Valley Caldera contains a 40MW geothermal power plant that went into operation in 1985 (a 10MW unit) and 1990 (two 15MW units) (see Figure 6.5 for powerplant physical organization). In the facilities, heat is removed from thermal water at a temperature of 170 ^{o}C. The total hot water pumped by the three units is approximately 850kg/s; the water is cooled to 85 ^{o}C before being injected into the subsurface. The production zone is at a depth of 150m while the injection zone is at 600 m [1]. The two areas are separated in order to minimize cooling of the production reservoir. But since the start of pumping, the temperature in the production area has declined from a

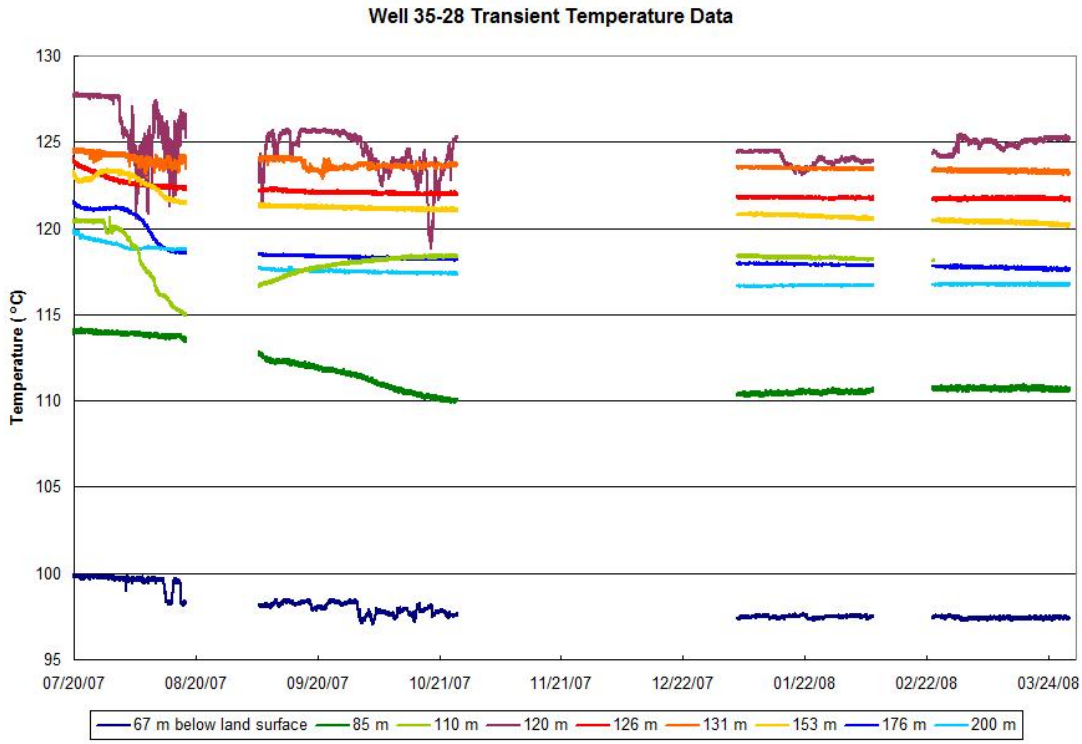

Figure 6.4: Data from the ten thermistor string installed in well 35-28. Each line corresponds to one thermistor at the indicated depth. Notice clear transient temperature behavior. The gaps in the data occurred because the data logger at 35-28 has limited storage capacity, so in the winter when 35-28 is difficult to access, data is lost. We intend to install in the near future a data logger with greater memory.

pre-1985 value of 140 ^{o}C (not 170 ^{o}C – temperatures are different between depth and the surface because of pressure variations) to 130^{o}C as a result of migration of cool fluid from the injection to the production area. The pressure in the production reservoir has decreased, the temperature in the injection zone has decreased by over 50 ^{o}C, and pressure in the injection zone has increased since energy production began [1]. Because of the decrease in pressure in the production area, the result of a decrease in the fluid volume in the production reservoir, boiling began to occur above the production reservoir. Relative subsidence of the power plant area coincides in time with the start of pumping and in space with the production reservoir (it actually extends beyond the

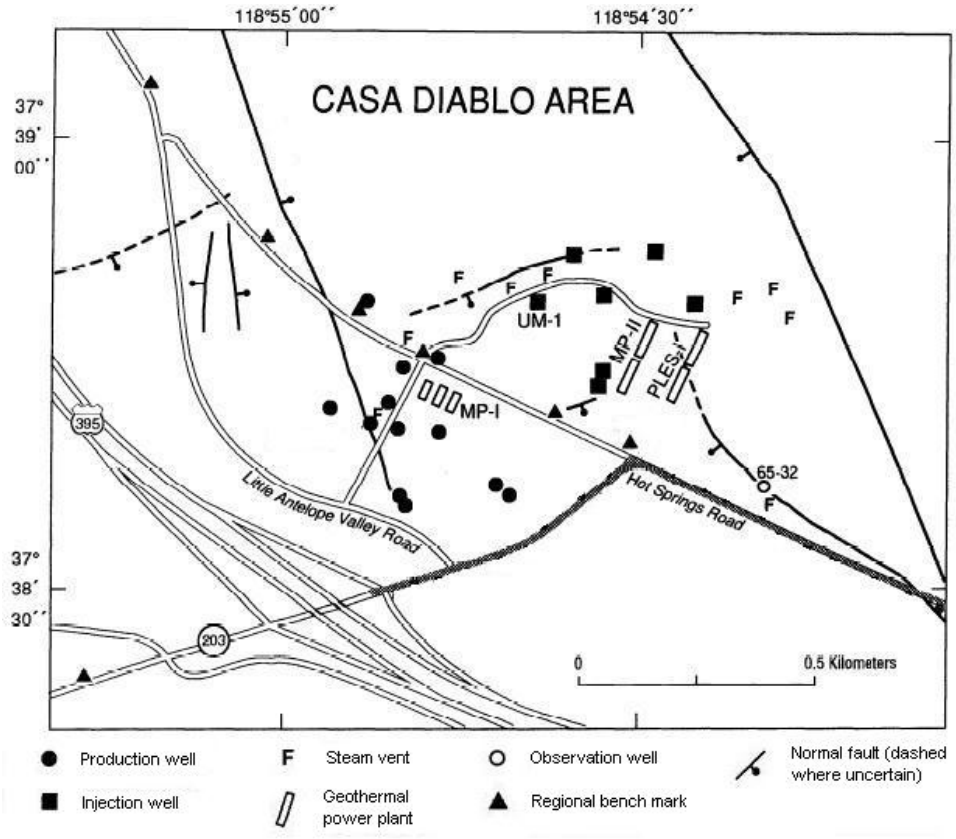

Figure 6.5: A map of the Casa Diablo area showing the Long Valley Caldera geothermal power plant and its wells. From [1].

reservoir to nearby faults). The area has also been tilting more rapidly than the rest of the nearby resurgent dome; tilt seems to have increased with increasing power production [1]. Recently (2007), the power plant began pumping at a series of new wells that are up-gradient in the hydrothermal system and produce water at higher temperature than the original production wells (personal communication with Christopher Farrar, USGS – who has worked extensively in Long Valley – May, 2007).

Following the onset of geothermal power production, the thermal landscape of Long Valley Caldera changed dramatically (from Christopher Farrar, May, 2007). Fumaroles and mudpits in the vicinity of the power plant dried up, and large areas of tree kill formed, generally along faults. Tree kill could be caused by subsurface heating or

CO_2 release, the result of subsurface boiling as geothermal power plant water pumping reduces pressures [1], permitting boiling and rapid transport of heat and gases from deep reservoirs to the surface. Changes in hydrothermal systems following the onset of geothermal energy production have been recognized in other areas, including The Geysers geothermal field in California [86].

It could be the case that the power plant is causing the observed T(z) changes in Long Valley boreholes. The mentioned changes in the local subsurface thermal regime suggest power plant influence, as do measured T(z) profiles from wells CH10B and 35-28. In particular, profiles in CH10B, which is down-gradient from the power plant, are relatively constant during the late 1980's and early 1990's (see Figure 6.1), but temperatures in the flow zone increased several degrees beginning in the mid 1990's and continuing through the most recent data. To note, temperatures below the flow zone in CH10B are essentially steady state, strongly suggesting that the observed temperature variations are not caused by changes in the local geothermal gradient. T(z) profiles from 35-28 also show temperature increases in the local hydrothermal fluid aquifer, though far fewer profiles have been taken there than in CH10B (see Figure 6.2). Upon first consideration, one might expect temperature decreases rather than increases due to power plant activity; however, induced subsurface boiling and the associated increased influx of heat could cause temperature increases above the power plant pumping zone.

To constrain whether the power plant is indeed the cause of the observed T(z) profile warming, it will be necessary to observe profiles both up the hydrothermal fluid gradient and down-gradient from the power plant pumping zone. Well 35-28 is up-gradient, and CH10B is down-gradient. Furthermore, velocity of thermal fluid must be determined and, from velocity, travel time from the power plant to observation wells, in order to confirm or deny correlation of power plant pumping and measured T(z) profile changes. Velocity can be determined from the measured profiles, perhaps using modifications to the theory of Ge [87], and confirmed against values calculated using tracers (e.g., [88]). Transient T(z) data from the ten thermistor strings in 35-28 (Figure 6.4) and CH10B (Figure 6.3) should be of value in assessing the impact of the power plant on the Long Valley thermal regime, particularly if they can be correlated with recent or future changes in power plant operation (such as pumping at new wells). Additional T(z) data from power plant observation and production wells may be accessible, in which

case transient temperature variations at the geothermal well field, if present, might be available for analysis.

Regardless of whether one can show that the power plant is affecting the Long Valley hydrothermal system, similar analysis could be applied to other geothermal power plants. As geothermal power is generally considered a desirable, environmentally friendly renewable energy source, it is very desirable to understand how a power plant affects (or does not affect) its surrounding space. Future studies may consider development of a numerical model to investigate the impacts of the Long Valley (or other) geothermal power plant on the caldera (or other) hydrothermal system. Finally, research concerning the effects of geothermal power production on local thermal structures helps determine the long-term feasibility of geothermal power plants.

6.1.4 Changes in heat flow from the regional thermal reservoir.

Changes in the local geothermal gradient, perhaps caused by magma chamber variations, or changes in the heat flow from the local hydrothermal reservoir – caused, for instance, by closing of flow paths through precipitation and opening of new fluid flow paths – could result in the observed gradual temperature increase in Long Valley T(z) profiles from CH10B (Figure 6.1) and 35-28 (Figure 6.2). Local geothermal gradient variations can be confirmed or denied by examining several T(z) profiles from a single borehole over time and observing whether they tend to the same temperature at depth. The measured profiles from CH10B (see Figure 6.1) and 35-28 (see Figure 6.2) show that this is the case, i.e. the local geothermal gradient has not changed.

In Long Valley, the area of hydrothermal fluid upwelling from the deep hydrothermal reservoir is relatively well characterized [80]. To determine whether the heat flow from this reservoir is changing, it will be necessary to examine T(z) profiles near the upwelling region. If profiles have not changed significantly over time, it should be safe to rule out the reservoir as the source of change. If they have changed, this changing convective heat flux is interesting in itself and would warrant searches for causes of the change (such as seismic events, which could open new flow paths). To note, in order to link source reservoir temperature changes (if they exist) to T(z) changes, it will be necessary to estimate the residence time of thermal fluid in the caldera, determinable from T(z)-calculated fluid velocities or chemical tracer information (e.g., [88]) and the known

distance from hydrothermal upwelling site (the western caldera) to the discharge site (Lake Crowley in the eastern caldera). This must be completed in order to ensure sufficient data is collected at the thermal source to pick up any associated temperature changes at CH10B or 35-28. Ready access to all T(z) profiles measured in Long Valley is available through, Shaul Hurwitz of the USGS, Menlo Park, California.

6.1.5 Solid earth tidal signals, barometric pressure fluctuations, and seismic events.

The first and second forces are considered here because in preliminary analysis of transient T(z) data from CH10B, a daily periodic signal was observed (see Figure 6.6). Earth tidal forces and barometric pressure fluctuations are theoretically capable of creating daily periodic signals in the subsurface (described shortly), and demonstrating their impact, whether upon borehole fluid specifically or the Long Valley groundwater system in general, would be significant.

Naturally-varying mechanical stresses have been shown to influence fluid flow, particularly in geyser systems but also in aquifers in general (e.g., [89] [90] [86]). Additionally, groundwater flow has been shown to vary mechanical stresses thereby inducing seismicity (e.g., [91] [89] [92]).

Theoretical work by Bredehoeft [93] revealed that tidal stresses can affect the specific storage (the change in the volume of fluid stored in a unit volume of porous medium per unit change in hydraulic head [86]) of aquifers causing variations in the water levels in wells. The theory requires that the horizontal stresses caused by tides be estimated, which can be accomplished using solid earth tide theory. Large error, perhaps 25%, is associated with calculations based on solid earth tide theory, but it is nonetheless possible to estimate aquifer response to stress. The equation that results from Bredehoeft's derivation is $\frac{p}{\rho * g} = \frac{\varepsilon_(t,d)}{S_s}$, where p is pore-fluid pressure, ρ is fluid density, g is gravitational acceleration, $\varepsilon_(t, d)$ is the sum of stresses in the principle directions (tidal dilatation), and S_s is the aquifer's specific storage [90].

Much of the work done relating naturally-varying stresses to fluid flow involves geysers. It seems reasonable to expect that forces that influence geyser activity affect other fluid flow systems since geysers are simply hot springs driven by steam or other gases [86]. Changing natural mechanical stress induces changes in fluid storage and

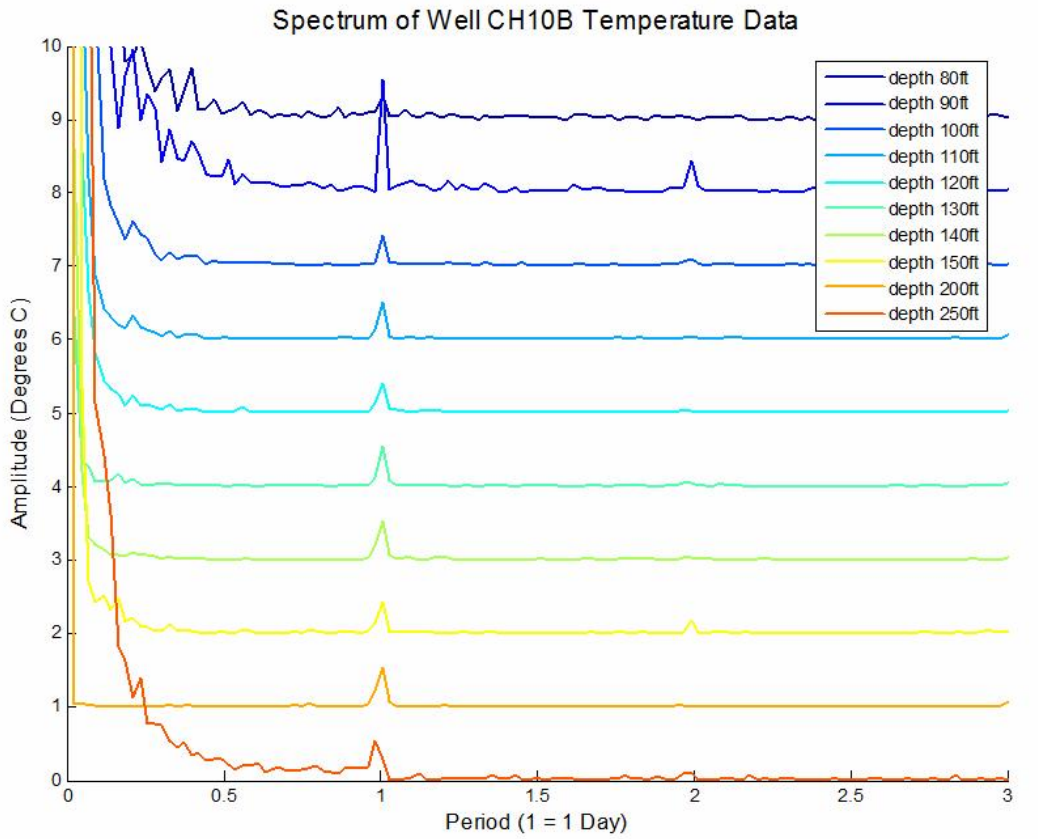

Figure 6.6: The results of Fourier transform of the transient temperature data from CH10B, showing a strong daily periodicity at all depths, which could be caused by barometric pressure or solid earth tide oscillations. To note, the baselines for the transforms have been shifted to allow all curves to be plotted on a single graph.

flow pathways, varying fluid behavior. Rinehart [89] noted correlations between the interval between geyser eruptions in three United States geysers for which there exist long activity time series (Old Faithful of Yellowstone, Old Faithful of California, and Riverside in Yellowstone) and barometric pressure variations, tidal cycles, and seismic activity. He noted a statistically significant negative correlation of interval between geyser activity and barometric pressure. Periodicity in both processes is present on a yearly scale with a phase lag between the two of approximately 70 days.

Snow loading and rainfall have been related to seismicity. Seasonal seismicity has

been found in many volcanic areas, and in all cases the maxima in seismic activity have occurred between one and six months after the majority of snow melt (e.g., [92]). Of particular relevance to this discussion is evidence of seasonal seismicity in Long Valley caldera. In this area, the regional tectonism provides the close-to-critical stress that is necessary for seasonal water fluctuation to trigger earthquakes [91]. Using at least 20 years of continuous earthquake data and six month bins (that is, comparing the number of earthquakes in six continuous months to the number in previous and following groups of six months), Christiansen et. al. [91] determined that both the Mammoth Mountain area and the south moat of Long Valley show statistically strong evidence for seasonality of seismicity. Considering earthquakes in only the top three km of the crust – three km is rather an arbitrary choice, but the closer an earthquake hypocenter is to the surface, the more likely groundwater will affect the earthquake's triggering – Mammoth Mountain earthquakes show periodicity of 365.25 days and south moat earthquakes, very close to that [91].

Using the change in water table elevations in Long Valley, Christiansen et. al. [91] calculated that groundwater recharge causes pressure to change by between 18 and 123kPa at seismogenic depths beneath Mammoth Mountain, more than sufficient to trigger earthquakes according to laboratory experiments by Lockner et. al. [94]. Tidal variations and barometric pressure changes cause much smaller pressure changes at depth (< 5kPa), generally too small to induce seismicity.

Clearly, naturally-varying mechanical forces are capable of inducing periodicity in groundwater behavior, and groundwater is able to affect stress fields. Little work has been done concerning whether mechanical forces or groundwater behavior induces periodicity in heat flow, though this might be expected particularly in areas of high heat and groundwater flux such as Long Valley Caldera. Future work may look for statistically significant correlations between transient T(z) data and barometric pressure, tidal forces, or seismic events (the required pressure, tidal, and seismic data is readily obtainable from the USGS).

To conclude, some correlations are expected between measured transient T(z) behavior in Long Valley and one or more of the afore-mentioned potential explanations, significantly improving understanding of coupled heat and fluid flow and providing a base for examination of hydrothermal systems other than Long Valley. However, if no

correlation can be made, it is simply of interest to report the transient behavior we see in 35-28 and CH10B, since transient T(z) information is very limited, and note that it cannot be linked to any single cause, affirming the complexity of natural hydrothermal systems.

6.2 Deep T(z) Profiles in MN

With funding assistance from the Minnesota Legislature, under a project led through the University of North Dakota (William Gosnold) and the University of Minnesota - Duluth (Steve Hauck), I began examining geothermal heat flow in Minnesota. The study began in summer 2009 and will continue into 2012, with most results available at the project's conclusion.

6.2.1 Project background information

Future geothermal energy development in the U.S. will likely target unconventional resources, such as regions with relatively low geothermal heat flow and deep crystalline rocks (i.e., enhanced geothermal systems (EGS)). EGS could provide 100 GWe or more cost-competitive generating capacity in the next 50 years at sites throughout the U.S. [5] where geothermal heat transfer conditions, rock stability, and appropriate reservoir environments are present at depths (generally) greater than 5 km (although much shallower depths may be feasible if CO_2, rather than water is utilized as the working fluid [18]). The cost of geothermal power in general tends to be far less than that of wind- or solar-generated electricity and competitive with power produced from coal or natural gas, even without accounting for costs associated with emissions or carbon capture and sequestration (CCS) (e.g., [5]).

Unfortunately, if the current heat flow map for Minnesota is left to represent the state's geothermal possibilities, MN is unlikely to adopt new geothermal power technology because the map greatly underestimates the state's potential geothermal heat flow (see Figure 6.7). This underestimation stems from the method that was employed to collect the little available data, which was biased towards sampling in low heat flow regions and confounded by climate forcing factors that adversely affected heat flow measurements. 93 of the 94 state data points were collected in lakes (largely Lake Superior,

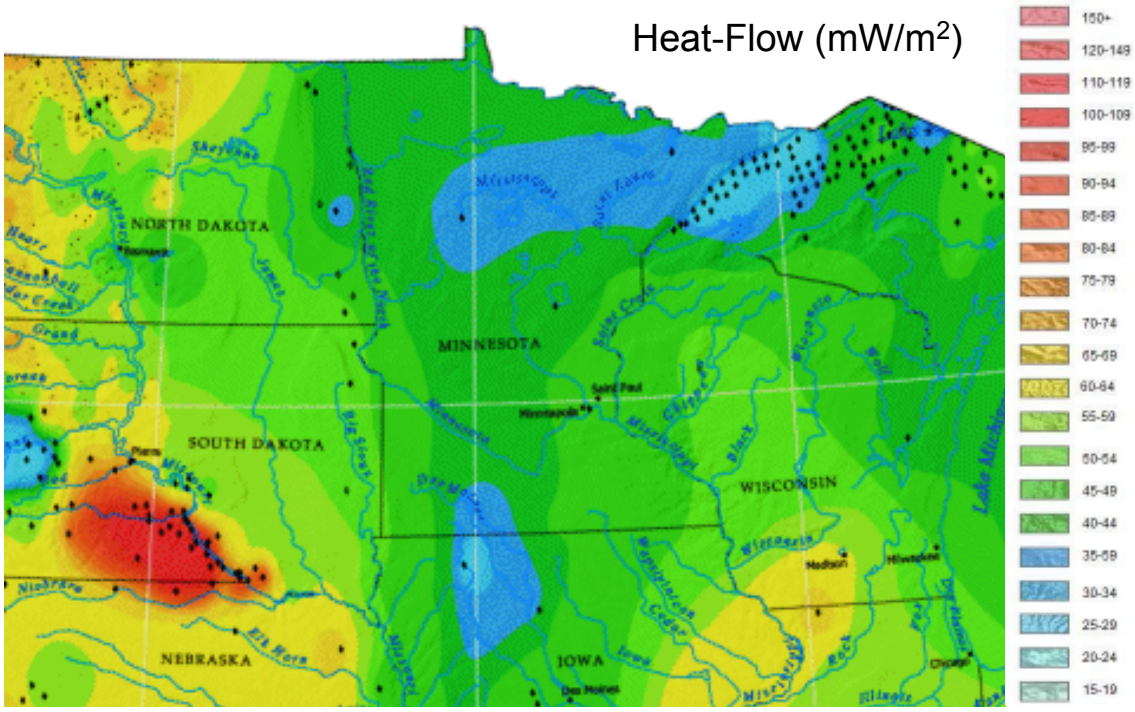

Figure 6.7: Map of geothermal heat flow in Minnesota, where black dots are points where measurements were taken. Note the lack of data points, in particular that most are in Lake Superior (and were taken in the shallow lake bottom). Most measurements are biased towards low heat flow sites, underestimating the geothermal potential of the region. Modified after [34].

as well as some intra-state lakes) and only 2.5 m below lake beds; associated poor heat flow results were then extrapolated over all of MN.

6.2.2 Description of project results

This project includes measuring temperature at depth in existing MN wells (DNR Waters and USGS water well databases), new deep water wells (DNR Waters 2010 LCCMR drilling project), and mineral exploration drill holes. 175 representative borehole and granite outcrops will be sampled by project completion, in order to measure thermal

gradient and thermal conductivity, respectively. See Figure 6.8 for a sample borehole profile. Measurements will span the state, and climate forcing factors will be minimized via careful data collection. As its primary product, the full project will generate a new heat flow map for Minnesota to far more accurately gauge the state's true potential for future geothermal development. All data will be incorporated into the National Geothermal Data System, permitting full public access.

In producing the heat flow map and report, the fully coordinated project involves: 1) locating deep wells or boreholes at 125 locations statewide using available well databases; 2) evaluating sample site conditions (thermal stability at depth, quality of hole for down-hole measurements, availability of rock samples for thermal conductivity measurements, etc.); 3) constructing a new temperature-depth measurement device (Section 6.2.3) to use in conjunction with a device from the University of North Dakota; 4) measuring and recording temperature at different depths; 5) collecting rock samples and determining their thermal conductivity; 6) collecting granite samples from boreholes and outcrops for radiogenic isotope determinations; 7) calculating heat flow rates from temperature-depth and thermal rock conductivity data; 8) assessing MN heat flow conditions relative to neighboring areas; and 9) summarize Minnesota's potential for pursuing geothermal power generation.

Likely, the new map will show that MN has substantially higher heat flow rates than previously thought, more similar to regions to the West and South. With evidence of higher heat flow, the prospect for geothermal power development in the state should significant increase, benefited by local geologic stability, groundwater resources (for water-based operations and for power plant cooling systems), and high potential for power use without massive transmission infrastructure. New maps will provide local energy companies with extensive baseline data to evaluate the economics of constructing geothermal plants for baseload and/or dispatchable electricity production.

6.2.3 Equipment development

Ideal wells for measurement of geothermal heat flux are deeper than 600 meters, as T(z) profiles taken in such wells extend below most MN aquifers that interact extensively with the surface, as well as below thermal perturbations caused by the most recent glaciation [95]. However, MN lacks an abundance of deep wells, in part because of limited local

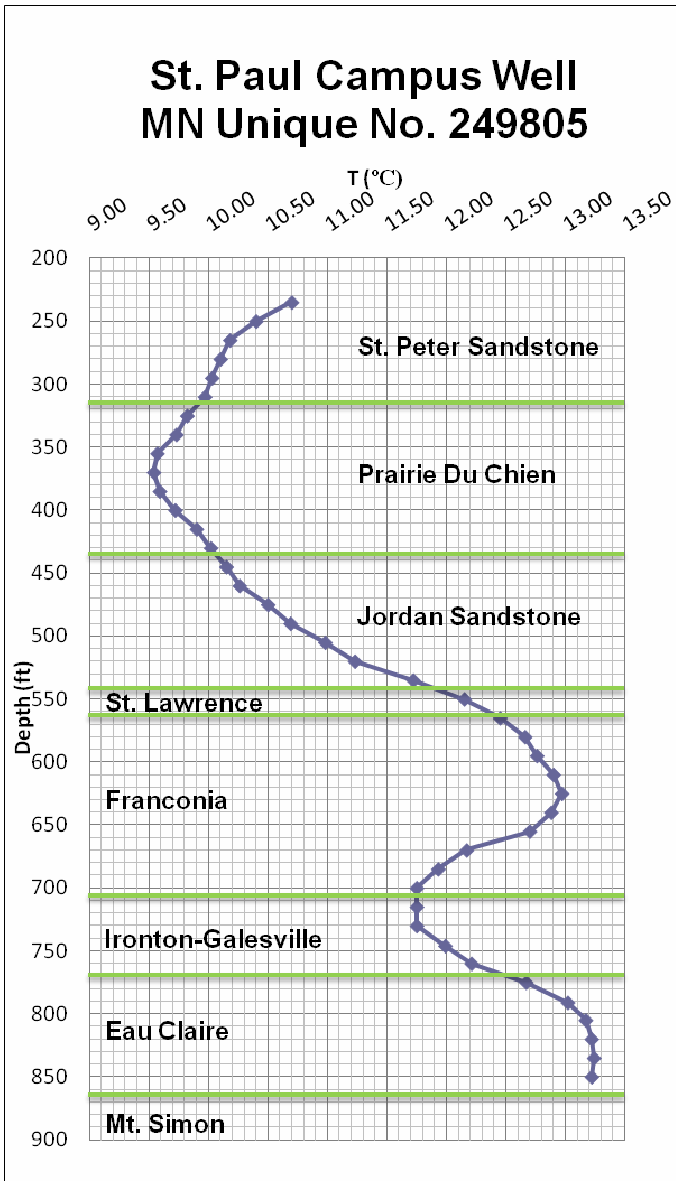

Figure 6.8: T(z) profile taken the St. Paul, MN, University of Minnesota campus. The well passes through several permeable aquifers, as indicated by the deviation in profiles from linear. Because of the extensive groundwater flow at this site, a deep geothermal gradient cannot be accurately estimated. However, the profile is useful in examining groundwater flow and demonstrating the product of T(z) measurements.

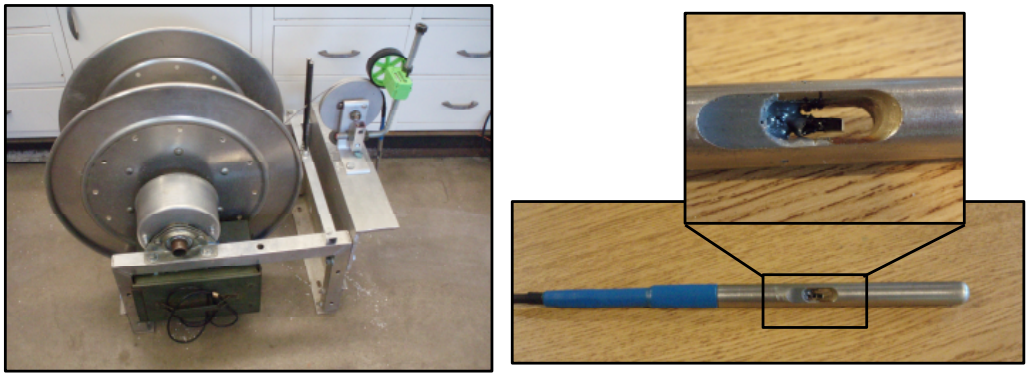

Figure 6.9: Equipment developed for measurement of temperature-depth (T(z)) profiles in Minnesota. At left, the full T(z) cable reel and data collecting equipment, at right, a close-up of the platinum Resistivity Temperature Device (RTD) probe. Photographs by Ben Tutolo, 2010.

hydrocarbon and deep mineral exploration. Thus, wells deeper than 150 meters may be used, as the extinction point for seasonal and daily variations in subsurface temperature is about 30 meters, depending on sediment/rock thermal conductivity [95]. In such wells, then, at least 120 meters of the profile are usable for heat flow determination (see Appendix E for additional details). Preferably, wells should be fully cased in order to preserve the temperature profile within deep aquifers, which may be thermally equilibrated with the surrounding formation (if groundwater flow is minimal).

In partial fulfillment of the project objective to measure heat flow around MN, a T(z) logging device was custom built. The temperature probe (Figure 6.9) developed for use here utilizes a 1000 Ohm platinum thin-film Resistance Temperature Device (RTD) from U.S. Sensor. The RTD is sealed with 3M Scotch-Weld Epoxy Adhesive, liquid electrical tape, and shrink tubing into a metal housing to ensure electrical connections are water proof and the sensor is sufficiently durable to survive extensive downhole use. The probe uses a Whitmor/Wirenetics cable 350 m long and spooled on a large-arbor, aluminum reel. The custom wire contains a kevlar strength member to prevent stretching, a braided shield to allow repeated spooling, and a teflon coating to ensure high heat tolerance. Temperature measurements are obtained using a calibrated Campbell

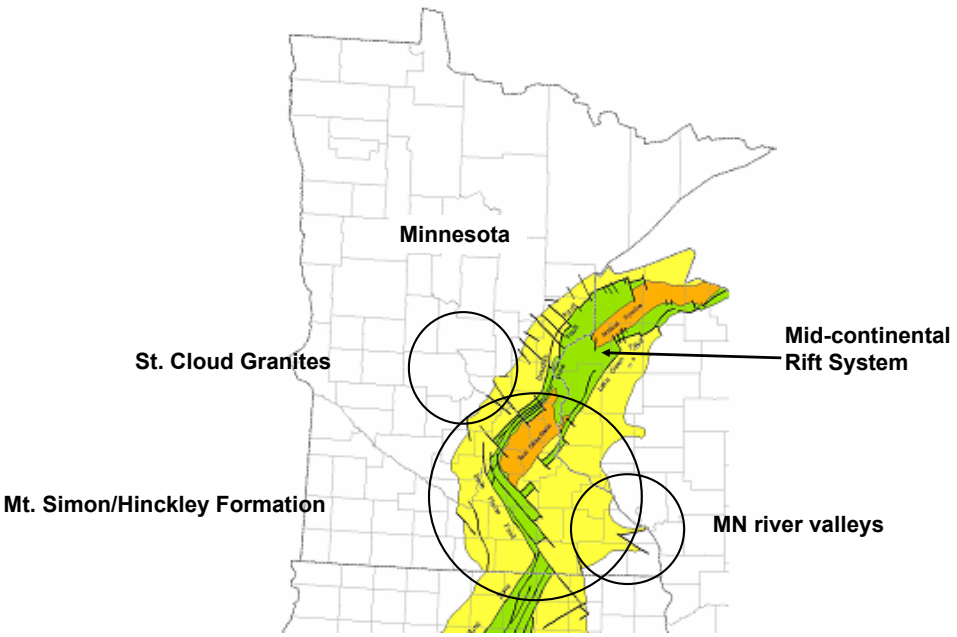

Figure 6.10: Several sites in Minnesota of interest for T(z) analysis and heat flow measurement. Sites include the Midcontinental Rift System (MRS), which contains deep sediments potentially viable for CO_2 sequestration or future geothermal development; large river valleys, where diffusive heat flux from large regions may be focused by groundwater flow prior to discharging into rivers; and regions underlain by granites, which might exhibit locally high heat flow due to radioactive decay. Modified after [35].

Scientific, Inc. (CSI) CR800 data logger with a 4-wire Kelvin connection to the RTD leads. Depth measurements are made using a rotating analog wheel, and provisions have been made for future use of Hall Effect sensors to provide accurate, bidirectional, digital measurements of probe depth.

6.2.4 Ongoing investigations

Ongoing research is adding to the accuracy and precision of the MN deep T(z) data, both by utilizing an RTD calibration bath with milliCelcius precision and by testing and incorporating a very stable T(z) probe-to-data logger electronic connection (the Kelvin connection, which display far better stability than the standard Wheatstone

connection – see [96], in preparation). Furthermore, several regions around MN of potentially interesting geothermal heat flux are being logged: the UMN Rosemount site (for future large-scale geothermal heat pump deployment), the MN river valley (where extensive groundwater flow may focus heat), and regions underlain by old granites (with potentially high radiogenic heat production), see Figure 6.10.

Chapter 7

Conclusions

The major findings of this dissertation are summarized in the following sections, which are modified after the abstracts or conclusions of the original publications presented in this thesis.

7.1 Demonstration of CO_2 Plume Geothermal (CPG) Geologic Viability

Geothermal energy offers clean, renewable, reliable electric power with no need for grid-scale energy storage, yet its use has been constrained to the few locations worldwide with naturally high geothermal heat resources and groundwater availability. I present a novel approach with the potential to permit expansion of geothermal energy utilization: heat extraction from naturally porous, permeable formations with CO_2 as the injected subsurface working fluid. This technique is termed CO_2 Plume Geothermal (CPG) to distinguish it from traditional water-based reservoir geothermal (i.e., hydrothermal), as well as water- and CO_2-based enhanced geothermal systems (EGS).

Fluid-mechanical simulations reveal that the significantly higher mobility of CO_2, compared to water, at the temperature/pressure conditions of interest makes CO_2 an attractive heat exchange fluid. I show numerically that, compared to conventional water-based and engineered geothermal systems, the proposed approach provides up to factors of 2.9 and 5.0, respectively, higher geothermal heat energy extraction rates. Furthermore, simulations reveal that the CPG system provides more widespread heat

mining than EGS, thus maintaining higher temperatures at geothermal production wells for longer duration. Moreover, produced fluid temperature decreases with time more rapidly as EGS fracture spacing increases, a consequence of less reservoir material being in contact with heat exchange fluid. These results suggest improved economic viability for CPG operations compared to both water- and CO_2-based EGS.

Net geothermal electricity generation is highly influenced by subsurface formation permeability. Thus, I explore CPG heat extraction as a function of reservoir permeability and in comparison to water and brine geothermal heat extraction. I show that, for reservoir permeabilities below 2 x 10^{-14} to 2 x 10^{-13} m^2, depending on formation temperature and pressure, CPG provides better electric power production efficiency than both water- and brine-based systems.

Field implementation of CPG systems will likely be dependent on societal drive to eliminate atmospheric CO_2 emissions. CO_2 sequestration in deep saline aquifers and exhausted oil and natural gas fields has been widely considered as a means for reducing said emissions. Energy production and sales in conjunction with sequestration would improve the economic viability of CO_2 sequestration, a critical challenge for large-scale utilization of the technology. I present the results of early-stage calculations demonstrating some of the implications of the geothermal energy capture potential of CO_2-based geothermal systems for the economic viability of geologic CO_2 sequestration. In particular, simulations indicate that the net revenue from CPG could provide in the cases here considered, approximately 7.3% to 13.1% of the cost of CCS. More significantly, CPG could provide 53% to 1300% of the cost of geologic CO_2 sequestration and monitoring/verification (excluding CO_2 capture), depending on reservoir temperature and pressure conditions.

As a consequence of CO_2 Plume Geothermal (CPG) development, more regions worldwide could be economically used for geothermal electricity production. Furthermore, as the injected CO_2 is eventually geologically sequestered, such power plants would have negative carbon footprints.

7.2 Temperature-depth, T(z), Profile Studies

Correlations are expected between measured transient temperature-depth, T(z), behavior in Long Valley Caldera and one or more of the several potential causes of transient temperature signals that have been described, improving understanding of coupled heat and fluid flow and providing a base for examination of hydrothermal systems other than Long Valley. If, however, no correlation can be made, it is simply of interest to report the transient behavior observed in Long Valley Caldera Wells 35-28 and CH10B, since transient T(z) information is very limited, and note that it cannot be linked to any single cause, affirming the complexity of natural hydrothermal systems.

T(z) examinations in Minnesota will produce a new geologic heat flow map of the state. It is anticipated that the new map will show that MN has substantially higher heat flow rates than previously measured, more similar to regions to the West and South. With evidence of higher heat flow, the prospect for geothermal power development in the state should increase, benefited by local geologic stability, groundwater resources (for water-based operations and/or for power plant cooling systems), and high potential for power use without massive transmission infrastructure. A new map will provide local energy companies with extensive baseline data to evaluate the economics of constructing geothermal plants for baseload and/or dispatchable electricity production.

References

[1] M. L. Sorey, C. D. Farrar, G. A. Marshall, and J. F. Howle. Effects of geothermal development on deformation in the Long Valley Caldera, eastern California. *Journal of Geophysical Research*, 100(B7):486, 1995.

[2] R. A. Bailey. Geologic map of Long Valley Caldera, Mono-Inyo Craters volcanic chain, and vicinity, eastern California. Technical Report I-1933, 1989.

[3] Intergovernmental Panel on Climate Change (IPCC). *Contribution of Working Group III to the Fourth Assessment Report of the Intergovernmental Panel on Climate Change*. Cambridge University Press, Cambridge, GB and New York, NY, US, 2007.

[4] J. B. Randolph and M. O. Saar. Coupling carbon dioxide sequestration with geothermal energy capture in naturally permeable, porous geologic formations: Implications for CO_2 sequestration. *Energy Procedia*, 4:2206–2213, 2011.

[5] J. W. Tester, B. J. Anderson, A. S. Batchelor, D. D. Blackwell, R. DiPippo, E. M. Drake, J. Garnish, B. Livesay, M. C. Moore, K. Nichols, S. Petty, M. N. Toksz, and R. W. Veatch Jr. The future of geothermal energy: Impact of enhanced geothermal system (EGS) on the United States in the 21st century. *Rep. INL/EXT-06-11746, Massachusetts Institute of Technology, Cambridge, MA*, 2006.

[6] C. F. Williams, M. J. Reed, R. H. Mariner, J. DeAngelo, and S. P. Galanis Jr. Assessment of moderate- and high-temperature geothermal resources of the united states. *USGS Fact Sheet 2008-3082, United States Geological Survey*, 2008.

[7] D. Brown. A hot dry rock geothermal energy concept utilizing supercritical CO_2 instead of water. *Proceedings of the Twenty-Fifth Workshop on Geothermal Reservoir Engineering, Stanford University, Stanford, CA*, pages 233–238, 2000.

[8] C. Fouillac, B. Sanjuan, S. Gentier, and I. Czernichowski-Lauriol. Could sequestration of CO_2 be combined with the development of enhanced geothermal systems? *Third Annual Conference on Carbon Capture and Sequestration, Alexandria, VA*, 2004.

[9] K. Pruess. Enhanced geothermal systems (EGS) using CO_2 as working fluid - a novel approach for generating renewable energy with simultaneous sequestration of carbon. *Geothermics*, 35:351–367, 2006.

[10] K. Pruess. Role of fluid pressure in the production behavior of enhanced geothermal systems with CO_2 as working fluid. *GRC Transactions*, 31:307–311, 2007.

[11] K. Pruess. On production behavior of enhanced geothermal systems with CO_2 as working fluid. *Energy Conversion Management*, 49:1446–1454, 2008.

[12] A. D. Atrens, H. Gurgenci, and V. Rudolph. CO_2 thermosyphon for competitive geothermal power generation. *Energy & Fuels*, 23:553–557, 2009.

[13] K. F. Evans, H. Moriya, H. Niitsuma, R. H. Jones, W. S. Phillips, A. Genter, J. Sausse, R. Jung, and R. Baria. Microseismicity and permeability enhancement of hydrogeologic structures during massive fluid injections into granite at 3 km depth at the Soultz HDR site. *Geophysics Journal International*, 160:388–412, 2005.

[14] E. L. Majer, R. Baria, M. Stark, S. Oates, J. Bommer, B. Smith, and H. Asanuma. Induced seismicity associated with enhanced geothermal systems. *Geothermics*, 36:185–222, 2007.

[15] J. Glanz. Quake threat leads Swiss to close geothermal project. *The New York Times, Dec 11*, 2009.

[16] E. N. Steadman, D. J. Daly, L. L. de Silva, J. A. Harju, M. D. Jensen, E. M. O'Leary, W. D. Peck, S. A. Smith, and J. A. Sorensen. Plains CO_2 Reduction

(PCOR) Partnership (phase 1) final report/July-September 2005 quarterly report. *Energy & Environmental Research Center, University of North Dakota, Grand Forks, ND*, 2006.

[17] C. Dezayes, A. Genter, and G. R. Hooijkaas. Deep-seated geology and fracture system of the EGS Soultz reservoir (France) based on recent 5 km depth boreholes. *World Geothermal Congress, Antalya, TR*, 2005.

[18] J. B. Randolph and M. O. Saar. Combining geothermal energy capture with geologic carbon dioxide sequestration. *Geophysical Research Letters*, 38:L10401, 2011.

[19] Intergovernmental Panel on Climate Change (IPCC). *IPCC Special Report on Carbon Dioxide Capture and Storage*. Cambridge University Press, Cambridge, GB and New York, NY, US, 2005.

[20] S. Bachu. Sequestration of CO_2 in geological media: Criteria and approach for site selection in response to climate change. *Energy Conversion and Management*, 41(9):953–970, 2000.

[21] B. Hitchon, editor. *Aquifer Disposal of Carbon Dioxide*. Geoscience Publishing, Ltd., Sherwood Park, Alberta, CA, 1996.

[22] S. Bachu. Screening and ranking of sedimentary basins for sequestration of CO_2 in geological media in response to climate change. *Environmental Geology*, 44:277–289., 2003.

[23] J. B. Hulen and P. M. Wright, editors. *Geothermal energy: Clean, sustainable energy for the benefit of humanity and the environment*. Energy & Geoscience Institute, University of Utah, Salt Lake City, UT, 2001.

[24] K. Pruess. The TOUGH codes - a family of simulation tools for multiphase flow and transport processes in permeable media. *Vadose Zone Journal*, 3:738–746, 2004.

[25] K. Pruess. ECO2N: A TOUGH2 fluid property module for mixtures of water, NaCl, and CO_2. *Rep. LBNL-57952, Lawrence Berkeley National Laboratory, Berkeley, CA*, 2005.

[26] K. Pruess, C. Oldenburg, and G. Moridis. TOUGH2 user's guide, version 2.0. *Rep. LBNL-43134, Lawrence Berkeley National Laboratory, Berkeley, CA*, 1999.

[27] K. Pruess and T. N. Narasimhan. A practical method for modeling fluid and heat flow in fractured porous media. *Society of Petroleum Engineers Journal*, 25:14–26, 1985.

[28] S. A. Shapiro, P. Audigane, and J. J. Royer. Larger-scale in-situ permeability tensor of rocks from induced seismicity. *Geophysics Journal International*, 137:207–213, 1999.

[29] J. B. Randolph and M. O. Saar. Coupling geothermal energy capture with carbon dioxide sequestration in naturally permeable, porous geologic formations: A comparison with enhanced geothermal systems. *GRC Transactions*, 34:433–438, 2010.

[30] B. Berkowitz. Characterizing flow and transport in fractured geological media: A review. *Advances in Water Resources*, 25:861–884, 2002.

[31] M. O. Saar. Review: Geothermal heat as a tracer of large-scale groundwater flow and as a means to determine permeability fields. *Hydrogeology Journal*, 19:31–52, 2011.

[32] R. Finley. An assessment of geologic carbon sequestration options in the Illinois basin, phase 1 final report. *Midwest Geological Sequestration Consortium, Illinois State Geological Survey, Champaign, IL*, 2005.

[33] S. K. Sanyal and S. J. Butler. An analysis of power generation prospects from enhanced geothermal systems. *World Geothermal Congress, Antalya, TR*, 2005.

[34] D.D. Blackwell and M. Richards. Geothermal map of North America. *American Association of Petroleum Geologists (AAPG)*, 2004.

[35] J.B. Randolph and M.O. Saar. Preliminary numerical modeling of CO_2 injection and storage in deep saline aquifers: Current research, scenarios, and required data, in potential capacity for geologic carbon sequestration in the Midcontinent Rift System in Minnesota, Thorleifson, L. H. *Minnesota Geological Survey Open File Report OFR-08-01*, 2008.

[36] I. Fatt. The network model of porous media III. Dynamic properties of networks with tube radius distribution. *Petroleum Transactions, AIME*, 207:164–181, 1956.

[37] National Institute of Standards and Technology. NIST Reference Fluid Thermodynamic and Transport Properties Database (REFPROP): Version 9.0, 2011.

[38] H. N. Pollack, S. J. Hurter, and J. R. Johnson. Heat flow from the earth's interior; analysis of the global data set. *Reviews of Geophysics*, 31(3):267–280, 1993.

[39] S. E. Gasda, J. M. Nordbotten, and M. A. Celia. A hybrid numerical-analytical model for wellbore leakage in reservoir-scale simulations. *American Geophysical Union Fall Conference*, 2007.

[40] R. T. Okwen, J. M. Nordbotten, M. T. Stewart, and J. A. Cunningham. Analytical model for screening potential repositories for subsurface sequestration of CO_2. *American Geophysical Union Fall Conference*, 2007.

[41] K. Pruess and N. Mueller. Formation dry-out from CO_2 injection into saline aquifers. *part* 1, effects of solids precipitation and their mitigation. *Water Resources Research*, 2008.

[42] Geothermal Energy Association. Geothermal power plants - U.S.A., 2010.

[43] J. David and H. Herzog. The cost of carbon capture. *Fifth International Conference on Greenhouse Gas Control Technologies, Cairns, Australia*, 2000.

[44] International Energy Agency. Renewable energy essentials: Geothermal, 2010.

[45] U.S.A. Department of Commerce (DOC). National Oceanic and Atmospheric Administration (NOAA), National Environmental Satellite, Data, and Information Service (NESDIS), National Climate Data Center (NCDC), U.S.A. climate normals 1971-2000, 2000.

[46] J. Cross and J. Freeman. U.S.A. Department of Energy 2008 geothermal technologies market report. *DOE/GO-102009-2864*, 2009.

[47] C. O'Donnell, P. Baumstark, V. Nibler, K. Corfee, and K. Sullivan. Renewable energy cost of generation update, PIER interim project report. *CEC-500-2009-084, California Energy Commission*, 2009.

[48] J. Gale, J. Bradshaw, Z. Chen, A. Garg, D. Gomez, H. Rogner, and et al. *Carbon dioxide capture and storage*. Cambridge University Press, Cambridge, GB and New York, NY, US, 2005.

[49] J. B. Randolph and M. O. Saar. Impact of reservoir permeability on the choice of subsurface geothermal heat exchange fluid: CO_2 versus water and native brine. *GRC Transactions, In Press*, 35, 2011.

[50] S. K. Sanyal, J. W. Morrow, and S. J. Butler. Net power capacity of geothermal wells versus reservoir temperature - a practical perspective. *Thirty-Second Workshop on Geothermal Reservoir Engineering, Stanford University, Stanford, CA*, 2007.

[51] R. DiPippo. Ideal thermal efficiency for geothermal binary plants. *Geothermics*, 36:276–285, 2007.

[52] D. J. Entingh. DOE Geothermal Electricity Technology Evaluation Model (GETEM): Volume I – Technical reference manual. *GETEM-TEHCNICAL-MANUAL-dje-July-06-2006, U.S. Department of Energy, Washington, DC, and The National Renewable Energy Laboratory, Golden, CO*, 2006.

[53] C.E. Manning and S. E. Ingebritsen. Permeability of the continental crust: implications of geothermal data and metamorphic systems. *Reviews of Geophysics*, 37, 1999.

[54] V. Dostal, M. J. Driscoll, and P. Hejzlar. A supercritical carbon dioxide cycle for next generation nuclear reactors. *Rep. MIT-ANP-TR-100, Massachusetts Institute of Technology, Cambridge, MA*, 2004.

[55] G. S. Bodvarsson, S. M. Benson, and P. A. Witherspoon. Theory of the development of geothermal systems charged by vertical faults. *Journal of Geophysical Research*, 87(B11):9317–9328, 1982.

[56] S. Suzuki. Percolation measurements based on heat flow through soil with special reference to paddy fields. *Journal of Geophysical Research*, 65(9):2883–2885, 1960.

[57] J. H. Birman. Geothermal exploration for ground water. *Geological Society of America Bulletin*, 80(4):617–630, 1969.

[58] M. Taniguchi. Evaluation of vertical groundwater fluxes and thermal properties of aquifers based on transient temperature-depth profiles. *Water Resources Research*, 29(7):2021–2026, 1993.

[59] J. Constantz, C. L. Thomas, and G. Zellweger. Influence of diurnal variations in stream temperature on streamflow loss and ground water recharge. *Water Resources Research*, 30(12):3253–3264, 1994.

[60] A. Tabbagh, H. Bendjoudi, and Y. Benderitter. Determination of recharge in unsaturated soils using temperature monitoring. *Water Resources Research*, 35(8):2439–2446, 1999.

[61] M. Taniguchi, J. Shimada, T. Tanaka, I. Kayane, Y. Sakura, Y. Shimano, S. Dapaah-Siakwan, and S. Kawashima. Disturbances of temperature-depth profiles due to surface climate change and subsurface water flow; 1, An effect of linear increase in surface temperature caused by global warming and urbanization in the Tokyo metropolitan area, Japan. *Water Resources Research*, 35(5):1507–1517, 1999.

[62] M. Taniguchi, D. R. Williamson, and A. J. Peck. Disturbances of temperature-depth profiles due to surface climate change and subsurface water flow; 2, An effect of step increase in surface temperature caused by forest clearing in Southwest Western Australia. *Water Resources Research*, 35(5):1519–1529, 1999.

[63] J. E. Constantz and D. A. Stonestrom. Heat as a tracer of water movement near streams; heat as a tool for studying the movement of ground water near streams. Technical Report C 1260, 2003.

[64] H. R. Bravo, F. Jiang, and R. J. Hunt. Using groundwater temperature data to constrain parameter estimation in a groundwater flow model of a wetland system. *Water Resources Research*, 38(8):14, 2002.

[65] A. F. Birch. The effects of Pleistocene climatic variations upon geothermal gradients. *American Journal of Science*, 246(12):729–760, 1948.

[66] M. P. Anderson. Heat as a groundwater tracer. *Ground Water*, 43(6):951–968, 2005.

[67] M. L. Sorey. Measurement of vertical ground-water velocity from temperature profiles in wells. *EOS, Transactions, American Geophysical Union*, 52(4):206, 1971.

[68] A. H. Lachenbruch and B. V. Marshall. Changing climate; geothermal evidence from permafrost in the Alaskan Arctic. *Science*, 234(4777):689–696, 1986.

[69] R. N. Harris and D. S. Chapman. Climate change on the Colorado Plateau of eastern Utah inferred from borehole temperatures. *Journal of Geophysical Research*, 100(B4):6367–6381, 1995.

[70] R. N. Harris and D. S. Chapman. Borehole temperature and a baseline for 20th-century global warming estimates. *Science*, 275(5306):1618–1621, 1997.

[71] R. N. Harris and W. D. Gosnold. Comparisons of borehole temperature-depth profiles and surface air temperatures in the northern plains of the USA. *Geophysical Journal International*, 138(2):541–548, 1999.

[72] D. Y. Demezhki and V. A. Shchapov. 80,000 years ground surface temperature history inferred from the temperature-depth log measured in the superdeep hole SG-4 (the Urals, Russia). *Global and Planetary Change*, 29:219–230, 2001.

[73] L. Bodri, V. Cermak, and Ilmo T. Kukkonen. Climate change of the last 2000 years inferred from borehole temperatures: data from Finland; Inference of climate change from geothermal data. *Global and Planetary Change*, 29(3-4):189–200, 2001.

[74] L. Bodri and V. Cermak. Borehole temperatures, climate change and pre-observational surface air temperature mean; allowance for hydraulic conditions; reply [modified]. *Global and Planetary Change*, 48(4):315–316, 2005.

[75] G. Ferguson and A. D. Woodbury. The effects of climatic variability on estimates of recharge from temperature profiles. *Ground Water*, 43(6):837–842, 2005.

[76] H. N. Pollack, S. Huang, and J. E. Smerdon. Five centuries of climate change in Australia; the view from underground; Integrating high-resolution past climate records for future prediction in the Australasian region. *Journal of Quaternary Science*, 21(7):701–706, 2006.

[77] S. E. Ingebritsen, D. L. Galloway, E. M. Colvard, M. L. Sorey, and R. H. Mariner. Time-variation of hydrothermal discharge at selected sites in the Western United States; implications for monitoring. *Journal of Volcanology and Geothermal Research*, 111(1-4):1–23, 2001.

[78] S. Hurwitz, C.D. Farrar, J.B. Randolph, and M.O. Saar. Anomalous hydrothermal activity in Hot Creek Gorge area, Long Valley Caldera, California, USA. 2006.

[79] D. P. Hill, J. O. Langbein, and S. Prejean. Relations between seismicity and deformation during unrest in Long Valley Caldera, California, from 1995 through 1999; Crustal unrest in Long Valley Caldera, California; new interpretations from geophysical and hydrologic monitoring and deep drilling. *Journal of Volcanology and Geothermal Research*, 127(3-4):175–193, 2003.

[80] M. L. Sorey, G. A. Suemnicht, N. C. Sturchio, and G. A. Nordquist. New evidence on the hydrothermal system in Long Valley Caldera, California, from wells, fluid sampling, electrical geophysics, and age determinations of hot-spring deposits. *Journal of Volcanology and Geothermal Research*, 48(3-4):229–263, 1991.

[81] C. Clauser. A climatic correlation on temperature gradients using surface-temperature series of various periods; Terrestrial heat flow studies and the structure of the lithosphere. *Tectonophysics*, 103(1-4):33–46, 1984.

[82] T. Kohl. Palaeoclimatic temperature signals; can they be washed out?; Heat flow and the structure of the lithosphere; IV. *Tectonophysics*, 291(1-4):225–234, 1998.

[83] M. Sophocleous. Global and regional water availability and demand; prospects for the future. *Natural Resources Research*, 13(2):61–75, 2004.

[84] D. D. Blackwell. A transient model of the geothermal system of the Long Valley Caldera, California; special section on Long Valley Caldera, California [modified]. *Journal of Geophysical Research*, 90(B13):11–11,241, 1985.

[85] R. H. Mariner and L. M. Willey. Geochemistry of thermal waters in Long Valley, Mono County, California. *Journal of Geophysical Research*, 81(5):792–800, 1976.

[86] S. Ingebritsen, W. Sanford, and C. Neuzil. *Groundwater in Geologic Processes*. Cambridge University Press, 2006.

[87] S. Ge. Estimation of groundwater velocity in localized fracture zones from well temperature profiles. *Journal of Volcanology and Geothermal Research*, 84(1-2):93–101, 1998.

[88] W. C. Evans, T. D. Lorenson, M. L. Sorey, and D. Bergfeld. Transport of injected isobutane by thermal groundwater in Long Valley Caldera, California, USA. *Proceedings - Eleventh International Symposium on Water-Rock Interaction*, 11:125–129, 2004.

[89] J. S. Rinehart. Fluctuations in geyser activity caused by variations in earth tidal forces, barometric pressure, and tectonic stresses. *Journal of Geophysical Research*, 77(2):342–350, 1972.

[90] P. A. Hsieh, J. D. Bredehoeft, and S. A. Rojstaczer. Response of well aquifer systems to earth tides; problem revisited. *Water Resources Research*, 24(3):468–472, 1988.

[91] L. B. Christiansen, S. Hurwitz, M. O. Saar, S. E. Ingebritsen, and P. A. Hsieh. Seasonal seismicity at western United States volcanic centers. *Earth and Planetary Science Letters*, 240(2):307–321, 2005.

[92] M. O. Saar and M. Manga. Seismicity induced by seasonal groundwater recharge at Mt. Hood, Oregon. *Earth and Planetary Science Letters*, 214(3-4):605–618, 2003.

[93] J. D. Bredehoeft. Response of well-aquifer systems to earth tides. *Journal of Geophysical Research*, 72(12):3075–3087, 1967.

[94] D. A. Lockner and N. M. Beeler. Premonitory slip and tidal triggering of earthquakes. *Journal of Geophysical Research*, 104(B9):20,151, 1999.

[95] W. Gosnold and J. Majorowicz. The post-glacial warming signal in heat flow. *24th General Assembly of the International Union of Geodesy and Geophysics (IUGG 2007), University of Perugia, Perugia, Italy*, 2007.

[96] R. Toot, J. B. Randolph, B. Tutolo, S. A. Alexander, and M. O. Saar. A comparison of the Wheatstone Bridge and Kelvin Connection for high-precision temperature measurements in geologic applications. *to be submitted to Ground Water or Geophysical Research Letters*, 2011.

[97] Y. K. Kharaka, D. R. Cole, S. D. Hovorka, W. D. Gunter, K. G. Knauss, and B. M. Freifeld. Gas-water-rock interactions in Frio formation following CO_2 injection; implications for the storage of greenhouse gases in sedimentary basins. *Geology (Boulder)*, 34(7):577–580, 2006.

[98] W. J. Plug and J. Bruining. Capillary pressure for the sand-CO_2-water system under various pressure conditions. Application to CO_2 sequestration. 2007.

[99] M. O. Saar and M Manga. Permeability-porosity relationship in vesicular basalts. *Geophysical Research Letters*, 26(1):111–114, 1999.

[100] C. Tsang, J. T. Birkholzer, and Q. Zhou. Pressure propagation and brine displacement in CO_2 storage formations: The role of sealing units. *American Geophysical Union Fall Conference*, 2007.

[101] T. Xu, J. A. Apps, and K. Pruess. Mineral sequestration of carbon dioxide in a sandstone-shale system; geochemical aspects of CO_2 sequestration. *Chemical Geology*, 217(3-4):295–318, 2005.

[102] Q. Zhou, J. T. Birkholzer, C. Tsang, and J. Rutquist. Quick assessment of CO_2 storage capacity in pressure-constrained saline aquifers with different hydrogeologic properties. *American Geophysical Union Fall Conference*, 2007.

[103] J. T. Birkholzer, J. A. Apps, Y. Zhang, L. Zheng, and T. Xu. Prediction of groundwater quality changes in response to CO_2 leakage from deep geologic storage. *American Geophysical Union Fall Conference*, 2007.

[104] S. P. White, R. G. Allis, J. Moore, T. Chidsey, C. Morgan, W. Gwynn, and M. Adams. Simulation of reactive transport of injected CO_2 on the Colorado Plateau, Utah, USA; geochemical aspects of CO_2 sequestration. *Chemical Geology*, 217(3-4):387–405, 2005.

[105] T. Xu and K. Pruess. Mineral dissolution, enhanced CO_2 solubility trapping and convective mixing. *American Geophysical Union Fall Conference*, 2007.

[106] J. M. Nordbotten, M. A. Celia, and S. Bachu. Injection and storage of CO_2 in deep saline aquifers; analytical solution for CO_2 plume evolution during injection. *Transport in Porous Media*, 58(3):339–360, 2005.

[107] H. E. Huppert. Fluid mechanical modeling of carbon dioxide sequestration. *American Geophysical Union Fall Conference*, 2007.

[108] M. Szulczewski and R. Juanes. Upscaling of capillary traping in a buoyant plume: application to CO_2 sequestration in aquifers. *American Geophysical Union Fall Conference*, 2007.

[109] M. A. Hesse, H. A. Tchelepy, and F. M. Orr. The effect of residual trapping and slope on gravity currents in confined aquifers. *American Geophysical Union Fall Conference*, 2007.

[110] W. Han and B. McPherson. Evaluation of CO_2 injection into brine formations below oil reservoir. *American Geophysical Union Fall Conference*, 2007.

[111] L. Chiaramonte, M. D. Zobac, J. Friedmann, and V. Stamp. Fluid flow simulation for CO_2-EOR and sequestration utilizing geochemical constraints - Teapot Dome oil field. *American Geophysical Union Fall Conference*, 2007.

[112] J. Kim. Development of a fully coupled multiphase thermo-hydro-mechanical numerical model and its application to geological storage of carbon dioxide. *American Geophysical Union Fall Conference*, 2007.

[113] C. Wang, G. Yeh, and M. Li. A numerical model of coupled fluid flows, thermal transport, and reactive chemical transport in fractured and porous media. *American Geophysical Union Fall Conference*, 2007.

[114] S. K. Garg and D. R. Kassoy. *Convective heat and mass transfer in hydrothermal systems*. Geothermal systems; principles and case histories. John Wiley and Sons, Chichester, United Kingdom (GBR), 1981.

[115] W. S. Keys and R. F. Brown. The use of temperature logs to trace the movement of injected water. *Ground Water*, 16(1):32–48, 1978.

[116] A. Tabbagh and D. Trezeguet. Determination of sensible heat flux in volcanic areas from ground temperature measurements along vertical profiles; the case study of Mount Etna (Sicily, Italy). *Journal of Geophysical Research*, 92(B5):3635–3644, 1987.

[117] C. S. Slichter. Field measurements of the rate of movement of underground waters. Technical Report W 0140, 1905.

[118] W. D. Collins. Temperature of water available for industrial use in the United States. Technical Report W 0520-F, 1925.

[119] C. E. Van Orstrand. Some possible applications of geothermics to geology. *Bulletin of the American Association of Petroleum Geologists*, 18(1):13–38, 1934.

[120] R. W. Stallman. Computation of ground-water velocity from temperature data; Methods of collecting and interpreting ground-water data. Technical Report W 1544-H, 1963.

[121] J. D. Bredehoeft and I. S. Papadopulos. Rates of vertical groundwater movement estimated from the Earth's thermal profile. *Water Resources Research*, 1(2):325–328, 1965.

[122] R. W. Stallman. Steady one-dimensional fluid flow in a semi-infinite porous medium with sinusoidal surface temperature. *Journal of Geophysical Research*, 70(12):2821–2827, 1965.

[123] M. K. Hubbert. The theory of ground-water motion. *Journal of Geology*, 48(8):785–944, 1940.

[124] R. W. Stallman. Flow in the zone of aeration. *Advances in Hydroscience*, 4:151–195, 1967.

[125] D. Kunii and J. M. Smith. Heat transfer characteristics of porous rocks, 11; Thermal conductivities of unconsolidated particles with flowing fluid. *AIChE Journal*, 7(1):29–34, 1961.

[126] A. H. Lachenbruch and J. H. Sass. Heat flow in the United States and the thermal regime of the crust; the Earth's crust; its nature and physical properties. *Geophysical Monograph*, (20):626–675, 1977.

[127] M. Reiter, J. K. Costain, and J. Minier. Heat flow data and vertical groundwater movement, examples from southwestern Virginia. *Journal of Geophysical Research*, 94(B9):12,423–12,431, 1989.

[128] R. Schneider. Relation of temperature distribution to ground-water movement in carbonate rocks of central Israel. *Geological Society of America Bulletin*, 75(3):209–215, 1964.

[129] K. Cartwright. Groundwater discharge in the illinois basin as suggested by temperature anomalies. *Water Resources Research*, 6(3):912–918, 1970.

[130] H. I. Nightingale. Ground-water recharge rates from thermometry. *Ground Water*, 13(4):340–344, 1975.

[131] K. Cartwright. Redistribution of geothermal heat by a shallow aquifer. *Geological Society of America Bulletin*, 82(11):3197–3200, 1971.

[132] K. Cartwright. Tracing shallow groundwater systems by soil temperatures. *Water Resources Research*, 23:847–855, 1974.

[133] P. A. Domenico and V. V. Palciauskas. Theoretical analysis of forced convective heat transfer in regional ground-water flow. *Geological Society of America Bulletin*, 84(12):3803–3814, 1973.

[134] J. P. Ziagos, D. D. Blackwell, and R. C. Edmiston. A model for the effect of horizontal fluid flow in a thin aquifer on temperature-depth profiles; Geothermal energy; the international success story. *Geothermal Resources Council Transactions*, 5:221–223, 1981.

[135] J. P. Ziagos and D. D. Blackwell. A model for the transient temperature effects of horizontal fluid flow in geothermal systems. *Journal of Volcanology and Geothermal Research*, 27(3-4):371–397, 1986.

[136] A. D. Woodbury and L. Smith. On the thermal effects of three-dimensional groundwater flow. *Journal of Geophysical Research*, 90(B1):759–767, 1985.

[137] N. Lu and S. Ge. Effect of horizontal heat and fluid flow in the vertical temperature distribution in a semiconfining layer. *Water Resources Research*, 32(5):1449–1453, 1996.

[138] M. Reiter. Using precision temperature logs to estimate horizontal and vertical groundwater flow components. *Water Resources Research*, 37(3):663–674, 2001.

[139] G. Bodvarsson. On the temperature of water flowing through fractures. *Journal of Geophysical Research*, 74(8):1987–1992, 1969.

[140] M. L. Parsons. Groundwater thermal regime in a glacial complex. *Water Resources Research*, 6(6):1701–1720, 1970.

[141] Z. A. Saleem. A computer method for pumping-test analysis. *Ground Water*, 8(5):21–24, 1970.

[142] C. B. Andrews and M. P. Anderson. Thermal alteration of groundwater caused by seepage from a cooling lake. *Water Resources Research*, 15(3):595–602, 1979.

[143] A. D. Woodbury and L. Smith. Simultaneous inversion of hydrogeologic and thermal data; 2, Incorporation of thermal data. *Water Resources Research*, 24(3):356–372, 1988.

[144] J. M. Boyle and Z. A. Saleem. Determination of recharge rates using temperature-depth profiles in wells. *Water Resources Research*, 15(6):1616–1622, 1979.

[145] M. A. Arriaga and D. I. Leap. Using solver to determine vertical groundwater velocities by temperature variations, Purdue University, Indiana, USA. *Hydrogeology Journal*, 14(1-2):253–263, 2006.

[146] W. W. Lapham. Use of temperature profiles beneath streams to determine rates of vertical ground-water flow and vertical hydraulic conductivity. Technical Report W 2337, U. S. Geological Survey, Reston, VA, United States, 1989.

[147] A. K. Keshari and M. Koo. A numerical model for estimating groundwater flux from subsurface temperature profiles. *Hydrological Processes*, 21(25):3440–3448, 2007.

[148] I. T. Kukkonen, V. Cermak, and J. Safanda. Subsurface temperature-depth profiles, anomalies due to climatic ground surface temperature changes or groundwater flow effects. *Global and Planetary Change*, 9(3-4):221–232, 1994.

[149] A. J. Mansure and M. Reiter. A vertical groundwater movement correction for heat flow. *Journal of Geophysical Research*, 84:3490–3496, 1979.

[150] K. Cartwright. Temperature prospecting for shallow glacial and alluvial aquifers in Illinois. *Circular - Illinois State Geological Survey*, page 41, 1968.

[151] M. Taniguchi, J. V. Turner, and A. J. Smith. Evaluations of groundwater discharge rates from subsurface temperature in Cockburn Sound, Western Australia. *Biogeochemistry*, 66(1-2):111–124, 2003.

[152] R. A. Bailey, G. B. Dalrymple, and M. A. Lanphere. Volcanism, structure, and geochronology of Long Valley Caldera, Mono County, California. *Journal of Geophysical Research*, 81(5):725–744, 1976.

[153] M. L. Sorey, V. S. McConnell, and E. Roeloffs. Summary of recent research in Long Valley Caldera, California; Crustal unrest in Long Valley Caldera, California; new interpretations from geophysical and hydrologic monitoring and deep drilling. *Journal of Volcanology and Geothermal Research*, 127(3-4):165–173, 2003.

[154] T.H. Dixon, A. M., M. I. Bursik, M. B. Heflin, J. Langbein, R. S. Stein, and F. H. Webb. Continuous monitoring of surface deformation at Long Valley Caldera, California, with GPS. *Journal of Geophysical Research*, 102(B6):12–12,034, 1997.

[155] D. P. Hill, R. A. Bailey, and A. S. Ryall. Active tectonic and magmatic processes beneath Long Valley Caldera, eastern California; an overview; Special section on Long Valley Caldera, California [modified]. *Journal of Geophysical Research*, 90(B13):11–11,120, 1985.

[156] A. F. White and M. L. Peterson. Chemical equilibrium and mass balance relationships associated with the Long Valley hydrothermal system, California, U.S.A. *Journal of Volcanology and Geothermal Research*, 48(3-4):283–302, 1991.

[157] M. L. Sorey, R. E. Lewis, and F. H. Olmsted. The hydrothermal system of Long Valley Caldera, California. Technical Report P 1044-A, U.S. Geological Survey, 1978.

[158] M. L. Sorey and R. E. Lewis. Convective heat flow from hot springs in the Long Valley Caldera, Mono County, California. *Journal of Geophysical Research*, 81(5):785–791, 1976.

[159] M. L. Sorey. Evolution and present state of the hydrothermal system in Long Valley Caldera; Special section on Long Valley Caldera, California [modified]. *Journal of Geophysical Research*, 90(B13):11–11,228, 1985.

Appendix A

Acronyms

A.1 Acronyms

Table A.1: Acronyms

Acronym	Meaning
CCS	Carbon Capture and Storage
CO_2	Carbon dioxide
CPG	CO_2 Plume Geothermal
DOE	Department of Energy
DNR	Department of Natural Resources
EGS	Engineered or Enhanced Geothermal System
EOR	Enhanced Oil Recovery
EPA	Environmental Protection Agency
IonE	Institute on the Environment
IREE	Initiative for Renewable Energy and the Environment
LVC	Long Valley Caldera
MGS	Minnesota Geological Survey
MRS	Midcontinental Rift System
MW	Megawatts of energy

Continued on next page

Table A.1 – continued from previous page

Acronym	Meaning
MWe	Megawatts of electrical energy
NIST	National Institute of Standards and Technology
NOAA	National Oceanic and Atmospheric Administration
OTC	Office for Technology Commercialization
PCOR	Plains CO_2 Reduction Partnership
RTD	Resistivity Temperature Device
UMN	University of Minnesota
USGS	United States Geological Survey

A.2 Mathematical terminology

Table A.2: Commonly-used Mathematical Terms

Mathematical term	Definition [typically-employed units]
ρ	density [kg/m^3], generally specified for a fluid
μ	dynamic viscosity [Pa*sec], specified for a fluid
E	energy [J]
h	enthalpy [kJ/kg]
H	thermal energy extraction rate [J/sec]
k	permeability [m^2]
K	hydraulic conductivity [m/s]
P	pressure [bar]
Q	fluid mass flow rate [kg/sec]
t	time [sec]
T	temperature [^{o}C]
T(z)	temperature as a function of depth, i.e. temperature-depth, measurements
W	work [J/sec]

Appendix B

Pending Patent - Carbon Dioxide-Based Geothermal Energy Generation Systems and Methods Related Thereto

Document Type and Number: WIPO Patent Application WO/2010/104599
Inventors: SAAR, Martin O. (1916 Princeton Ave, St. Paul, MN, 55105, US)
RANDOLPH, Jimmy Bryan (4610 Blaisdell Ave, Minneapolis, MN, 55419, US)
KUEHN, Thomas H. (4 Williams Wood Road, Mahtomedi, MN, 55115, US)

Application Number: US2010/000756

Publication Date: September 16, 2010

Filing Date: March 12, 2010

International Classes: F25B30/06; F24J3/08; F25B27/00

This application claims the benefit under 35 U.S.C. 119 (e) of U.S. Provisional Application Serial No. 61/159,948 filed on March 13, 2009, hereby incorporated by reference in its entirety.

B.1 Background

[0001] In light of global climate change and in response to an increased desire to reduce dependence on foreign oil supplies, renewable energy systems, such as wind, solar and geothermal-based systems are being increasingly researched and developed. However, many such systems have only limited potential due to, for example, high costs, overall process inefficiencies, possible adverse environmental impact, and the like.

[0002] What is needed, therefore, are cost effective renewable energy systems which are not only efficient, but can improve the environment.

B.2 Summary

[0003] The inventors recognize the need for providing a cost effective carbon dioxide based geothermal energy system which, in some embodiments, provides added benefits for the environment by sequestering and containing excess carbon dioxide. In one embodiment, a system comprising one or more injection wells for accessing one or more reservoirs having a first temperature, wherein the one or more reservoirs are located below one or more caprocks and are accessible without using large-scale hydrofracturing, each of the one or more injection wells having an injection well reservoir opening; one or more production wells, each having a production well reservoir opening, wherein a non-water based working fluid can be provided to the one or more injection wells at a second temperature lower than the first temperature and exposure of the non- water based working fluid to the first temperature can produce heated non-water based working fluid capable of entering each of the one or more production well reservoir openings; and an energy converting apparatus connected to each of the one or more injection wells and the one or more productions wells, wherein thermal energy contained in the heated non- water based working fluid can be converted to electricity, heat, or combinations thereof, in the energy converting apparatus is provided.

[0004] In various embodiments, each of the one or more injection wells and each of the one or more production wells are located in the same channel and the system further comprises one or more injection pipes and one or more production pipes connected to the channel.

[0005] In various embodiments, the system further comprises a non-water based working fluid source, such as carbon dioxide (e.g., supercritical carbon dioxide) obtainable from a power plant (e.g., ethanol plant or fossil-fuel based power plant) or an industrial plant. In one embodiment, the energy converting apparatus comprises one or more expansion devices and one or more generators, one or more heat exchangers or a combination thereof. In one embodiment, the one or more generators can provide electricity to an electricity provider and the system further comprises the electricity provider. Additionally, in one embodiment, each of the one or more heat exchangers can provide heat to a heat provider and the system further comprises the heat provider, such as a direct use provider or a ground heat pump.

[0006] In one embodiment, the system further comprises one or more cooling units fluidly connected to the one or more production wells and the one or more injection wells.

[0007] In one embodiment, a method comprising accessing one or more underground reservoirs having a natural temperature, the one or more reservoirs located beneath one or more caprocks; introducing a non- water based working fluid (e.g., carbon dioxide, such as supercritical carbon dioxide) into the one or more reservoirs; exposing the non-water based fluid to the natural temperature to produce heated fluid; and extracting thermal energy from the fluid, without using large-scale hydrofracturing, is provided.

[0008] In various embodiments, the heated fluid also contains native fluid present in the one or more reservoirs. In one embodiment, the one or more caprocks each have a permeability ranging from about 10^{-16} m^2 to about 0 m^2 and the one or more reservoirs each have a porosity ranging from about one (1)% to about 50% and a permeability ranging from about 10^{-16} m^2 to about 10^{-6} m^2 , with each of the one or more reservoirs having a natural temperature between about -30 ^{o}C and about 300 ^{o}C.

[0009] In one embodiment, the thermal energy is used to produce electricity, to heat a working fluid in one or more heat exchangers, to provide condensed fluid to the one or more reservoirs, to provide cooled fluid to the one or more reservoirs, to

provide shaft power to one or more pumps or compressors, or a combination thereof. In various embodiments, the electricity is produced either by providing the hot fluid to one or more expansion devices or by providing the working fluid heated in the one or more heat exchangers to the one or more expansion devices, wherein the one or more expansion devices produces shaft power to one or more generators, which, in turn, produce the electricity.

[0010] In one embodiment, the working fluid heated in the one or more heat exchangers provides heat for direct use, for groundwater heat pumps, for a Rankine power cycle, or a combination thereof. In various embodiments, the method further comprises choosing the underground reservoir; transporting a non- water based working fluid source to an area proximate to the injection well; converting the non- water based working fluid source into a non-water based working fluid; and providing the heat energy to a customer.

[0011] The geothermal energy obtained using the novel systems and methods described herein can be used for a variety of applications, including, but not limited to, electricity generation and/or direct uses (e.g., aquaculture, greenhouse, industrial and agricultural processes, resorts, space and district heating (wells to structures) and/or ground-source heat pumps. Furthermore, cascading systems can be used to draw off energy at decreasing temperatures, thus allowing a single geothermal resource to be used for multiple purposes.

[0012] The ability to also geologically sequester carbon dioxide from various sources and use it to generate energy and, optionally, store excess carbon dioxide, means that the novel systems and methods described herein can also serve as a means to mitigate global warming. Additionally, the novel embodiments described herein can increase carbon-sequestration-based revenue potential from carbon offset sales in carbon cap and trade and similar markets.

B.3 Brief Description of the Drawings

[0013] Figure B.1 is a simplified schematic diagram of an energy generation system according to an embodiment of the invention.

[0014] Figure B.2 is a simplified schematic diagram of an alternative energy generation system according to an embodiment of the invention.

[0015] Figure B.3 is a simplified schematic diagram of another alternative energy generation system according to an embodiment of the invention.

[0016] Figure B.4 is a simplified schematic diagram of yet another alternative energy generation system according to an embodiment of the invention.

[0017] Figure B.5 is a cross-section of Minnesota's Rift System (MRS).

[0018] Figure B.6 is an enlarged view of a portion of Figure B.5 taken from within box 6-6 according to an embodiment of the invention.

[0019] Figure B.7 is an illustration of a geological structure used for a numerical model of a power generation system according to an embodiment of the invention.

[0020] Figure B.8 is a geological model showing dimensions and solute concentration according to an embodiment of the invention.

[0021] Figure B.9 is an illustration of an exemplary geometrical configuration according to an embodiment of the invention.

[0022] Figure B.10 is a graph showing temperature versus distance from an injection well to a production well for a porous medium in a carbon dioxide (CO_2) plume geothermal (CPG) system and various fracture spacings in an enhanced geothermal system (EGS) system according to an embodiment of the invention.

[0023] Figure B.11 is a graph showing heat extraction rate versus time for a porous medium in a CPG system and various fracture spacings in an EGS system according to an embodiment of the invention.

[0024] Figure B.12 is a graph showing heat extraction rate versus time for a CPG system as compared to a water system according to an embodiment of the invention.

[0025] Figure B.13 is a graph showing density versus distance from injection well to production well for a CPG system as compared to a water system according to embodiments of the invention.

[0026] Figure B.14 is a graph showing Rayleigh number versus distance from injection well to production well for a CPG system as compared to a water system according to an embodiment of the invention.

[0027] Figure B.15 is a graph showing Prandtl number versus distance from injection well to production well for a CPG system as compared to a water system according to

an embodiment of the invention.

B.4 Detailed Description

[0028] In the following detailed description, reference is made to the accompanying drawings that form a part hereof, and in which is shown by way of illustration, specific embodiments in which the invention may be practiced. These embodiments are described in sufficient detail to enable those skilled in the art to practice the invention, and it is to be understood that other embodiments may be utilized. It is also to be understood that structural, procedural, chemical and system changes may be made without departing from the spirit and scope of the present invention. The following detailed description is, therefore, not to be taken in a limiting sense, and the scope of the present invention is defined by the appended claims and their equivalents.

[0029] The detailed description begins with a definition section followed by a brief overview of conventional geothermal energy technology, a description of the embodiments, an example section and a brief conclusion.

[0030] In one embodiment, novel carbon dioxide-based geothermal energy generation systems, i.e., carbon plume geothermal (CPG) systems, and methods are provided. With the novel systems and methods described herein, geothermal energy can now be provided at lower reservoir temperatures and at locations other than hot, dry rock formations, without negatively impacting the surrounding area through use of large-scale hydrofracturing. Use of a carbon dioxide-based geothermal system further provides a means for sequestering and storing excess carbon dioxide, rather than having it released to the atmosphere.

B.4.1 Conventional Geothermal Energy Technology

[0031] Geothermal energy is heat energy stored within the earth (or any other planet), which can be "mined" for various uses, including to produce electricity, for direct use, or for ground-source heat pumps. Geothermal energy sources are relatively constant with heat energy replenished on human time scales after being "mined," and further require no storage other than the earth.

[0032] Potential uses of conventional geothermal energy are generally temperature

dependent, with cascading systems utilizing a single geothermal resource for multiple purposes. Current water-based geothermal systems (i.e., conventional water-based enhanced geothermal systems (EGS) and conventional non-EGS water-based), which use water as a working fluid, require very high temperatures. For example, electricity generation at water-based geothermal power plants typically requires temperatures which can exceed 150 ^{o}C. Direct uses, such as aquaculture, greenhouse, industrial and agricultural processes, resorts, space and district heating (wells to structures) from such systems utilize more moderate temperatures of about 38 to 150 ^{o}C when water is the subsurface geothermal working fluid. Residential and commercial building ground-source heat pumps from water-based geothermal systems, which may use a secondary heat exchange fluid (e.g., isobutene) in order to transfer geothermal heat energy from the ground for use, generally require temperatures between about 4 and 38 ^{o}C.

B.4.2 Definitions

[0033] The terms "subterranean" or "subsurface" or "underground" as used herein, refer to locations and/or geological formations beneath the Earth's surface.

[0034] The term "in situ" as used herein, refers to a natural or original position or place of a geologic feature which may be above ground or underground, such that it is located in a place where it was originally formed or deposited by nature and has remained substantially undisturbed over time, such that it is in substantially the same original condition. A geologic feature can be rock, mineral, sediment, reservoir, caprock and the like, or any combination thereof. A geologic feature is further considered to remain "in situ " following minor manmade disturbances used to create and/or position components, such as channels such as injection wells and/or production wells, within, around or near the feature. A feature is also considered to remain "in situ " following minor man-initiated disturbances, such as causing a controllable or limited amount of rock, mineral, sediment or soil to become dislodged as a result of the minor manmade or natural disturbance. In contrast, a feature is not considered to remain "in situ " following any type of large-scale manmade disturbances, including large-scale hydrofracturing (such as to create an artificial reservoir), or man-initiated disturbances, such as permanent deformation of a geologic feature, earthquakes and/or tremors following large-scale hydrofracturing, all of which can have a further negative impacts on groundwater flow

paths, habitats and man-made structures.

[0035] The term "large-scale hydrofracturing" as used herein refer to a known method for creating or inducing artificial fractures and/or faults in a feature, such as a rock or partially consolidated sediments, typically during operation of an enhanced geothermal system (EGS). See, for example, U.S. Patent No. 3,786,858 to Potter, which employs water for hydraulic fracturing of rock to create a thermal geological reservoir from which fluid is transported to the surface. Large-scale hydrofracturing is known to create unintended fluid flow pathways that can result in fluid loss or "shortcutting," which in turn decreases geothermal heating efficiencies of the working fluid. Large-scale hydrofracturing can also cause (micro-)seismicity and damages to natural and/or manmade structures.

[0036] The term "rock" as used herein, refers to a relatively hard, naturally formed mineral, collection of minerals, or petrified matter. A collection of rocks is commonly referred to as a "rock formation." Various types of rocks have been identified on Earth, to include, for example, igneous, metamorphic, sedimentary, and the like. A rock can erode or be subject to mass wasting to become sediment and/or soil proximate to or at a distance of many miles from its original location.

[0037] The term "sediment" as used herein, refers to a granular material eroded by forces of nature, but not yet to the point of becoming "soil." Sediment may be found on or within the Earth's crust. A collection of sediments is commonly referred to as a "sediment formation." Sediment is commonly unconsolidated, although "partially consolidated sediments" are often referred to simply as "sediments" and are therefore considered to be included within the definition of sediment.

[0038] The term "soil" as used herein, refers to a granular material comprising a biologically active, porous medium. Soil is found on, or as part of, the uppermost layer of the Earth's crust and evolves through weathering of solid materials, such as consolidated rocks, sediments, glacial tills, volcanic ash, and organic matter. Although often used interchangeably with the term "dirt," dirt is technically not biologically active.

[0039] The term "fluid" as used herein, refers to a liquid, gas, or combination thereof, or a fluid that exists above the critical point, i.e., a supercritical fluid. A fluid is capable of flowing, expanding and/or accommodating a shape of its physical surroundings. A

fluid can comprise a native fluid, a working fluid, or combinations thereof. Examples of fluid include, for example, air, water, brine (i.e., salty water), hydrocarbon, CO_2, magma, noble gases, or any combination thereof.

[0040] The term "native fluid" as used herein, refers to a fluid which is naturally resident in a rock formation or sediment formation. A native fluid includes, but is not limited to, water, saline water, oil, natural gas, hydrocarbons (e.g., methane, natural gas, oil), and combinations thereof. Carbon dioxide can also be a naturally present in the rock or sediment formation and thus constitute a native fluid in this case.

[0041] The term "working fluid" as used herein, refers to a fluid which is not native to a rock formation or sediment formation and which may undergo a phase change from a gas to a liquid (energy source) or liquid to gas (refrigerant). A "working fluid" in a machine or in a closed loop system is the pressurized gas or liquid which actuates the machine. A working fluid includes, but is not limited to ammonia, sulfur dioxide, carbon dioxide, and non-halogenated hydrocarbons such as methane. Water is used as a working fluid in conventional (i.e., water-based) heat engine systems. A working fluid includes a fluid in a supercritical state as the term is understood in the art. Different working fluids can have different thermodynamic and fluid-dynamic properties, resulting in different power conversion efficiencies.

[0042] The term "pore space" as used herein, refers to any space not occupied by a solid (rock or mineral). Pore space can be the space formed between grains and/or the space formed by fractures, faults, fissures, conduits, caves, or any other type of non-solid space. Pore space can be connected or unconnected and it may, or may not, evolve over time due to changes in solid space volume and/or size (which could come from reactions, deformations, etc.). A pore space is filled with fluid, as the term is understood in the art.

[0043] The term "CO_2 plume" as used herein, refers to a large-scale (meters to several kilometers to tens of kilometers in diameter) CO_2 presence within subsurface pore spaces (as defined above, where a significant percentage of the fluid in the pore space is CO_2.

[0044] The term "reservoir" or "storage rock formation" or "storage sediment formation" as used herein, refers to a rock formation and/or sediment formation capable of storing an amount of fluid substantially "permanently" as that term is understood

in the geological arts.

[0045] The term "geothermal heat flow" as used herein, refers to any kind of heat transfer in the subsurface and consists of conductive and/or advective (sometimes referred to as convective) and/or radiative heat transfer, with radiative heat transfer typically being negligible in the subsurface. A "low" heat flow is generally considered to be less than about 50 milliwatts per square meter. A "moderate" heat flow is generally considered to be at least about 50 to about 80 milliwatts per square meter. A "high" heat flow is generally considered to be greater than 80 milliwatts per square meter.

[0046] The term "injection well" as used herein, refers to a well or borehole which is optionally cased (i.e., lined) and which may contain one or more pipes through which a fluid flow (typically in a downwardly direction) for purposes of releasing that fluid into the subsurface at some depth. An injection well may exist in the same borehole as a production well.

[0047] The term "production well" as used herein, refers to a well or borehole which is optionally cased (i.e., lined) and which may contain one or more pipes through which a fluid can flow (typically in an upwardly direction) or purposes of bringing fluids up from the subsurface to (near) the Earth's surface. A production well may exist in the same borehole as an injection well.

[0048] The term "enhanced geothermal system" (EGS) as used herein, refers to a system in which a manmade (i.e., artificial) reservoir is created, usually by means of hydrofracturing the subsurface, i.e., inducing fractures to create space which may contain significant amounts of fluid. Such artificial reservoirs are typically much smaller than natural reservoirs

[0049] The term "conventional water-based geothermal system" as used herein, refers to a geothermal system that utilizes water as the (subsurface) working fluid. This could be in natural reservoir systems or in hydrofractured (i.e., EGS) systems.

[0050] The term "conventional CO_2-based EGS" refers to a conventional EGS system which uses carbon dioxide as the working fluid.

B.4.3 Description of Embodiments

[0051] In one embodiment, a system 100 generates energy from a source, such as a carbon dioxide (CO_2) source 110 using a CO_2 sequestration component 112 and a geothermal

energy production component 114, as shown in Figure B.1. In one embodiment, the energy generated is thermal energy (i.e., heat), although the invention is not so limited. In one embodiment, the energy produced is used to generate electricity, as shown in Figure B.1. In an alternative embodiment, the energy is drawn off as heat, as shown in Figure B.2. In yet other embodiments, the energy is used to provide electricity and heat, as shown in Figure B.3, or to provide heat to operate a separate power cycle, such as an organic Rankine cycle, as shown in Figure B.4. Other variations and embodiments are possible, as discussed herein.

[0052] The source (e.g., CO_2 source 110) can be any suitable fluid (including a fluid containing solids, in dissolved or non-dissolved form, capable of absorbing thermal energy from its surroundings, and further releasing the thermal energy as described herein. In most embodiments, the source may be a waste stream from a power plant, such as a fossil fuel power plant (e.g., coal plant, natural gas plant, and the like), or any type of plant capable of producing fuel, such as biofuel (e.g., ethanol plant) or any type of industrial plant, such as a cement manufacturer, steel manufacturer, and the like. In one embodiment, the fluid is further capable of being transported via any suitable means, (e.g., pipe, various transportation means, such as truck, ship or rail), over a desired distance. Although the source, such as the CO_2 source 110 can, in most instances, be used "as is", in some instances, further processing may be used prior to introducing the CO_2 source 110 to a compressor 132 to produce a working fluid, such as cold CO_2 138, as shown in Figure B.1. For example, some waste streams may require dewatering and/or drying. In one embodiment the CO_2 source 110 is stored on site or off site for a period of time. In one embodiment, the cold CO_2 138 is supercritical CO_2.

[0053] In one embodiment, the system 100 is located at a site (i.e., in a position) configured to provide access to a target formation, the target formation comprising a caprock 118 located above a reservoir 120 as shown in Figure B.1. In one embodiment, the reservoir 120 has a natural temperature higher than a temperature of the working fluid. In the embodiment shown in Figure B.1, the natural temperature in the reservoir 120 is affected by geothermal heat 124 flowing up from below.

[0054] A top layer 116 may be located above the caprock 118 and reservoir 120 as shown in Figure B.1. The top layer 116 may comprise any number of layers and types of natural deposits and/or formations. For example, the top layer 116 may contain one

or more features such as a reservoir (e.g., reservoir 120) or caprock (e.g., caprock 118) having the features as described herein. In one embodiment, the top layer 116 additionally or alternatively contains additional areas suitable for injection of the working fluid, such as the cold CO_2 138 shown in Figure B.1. In one embodiment, the top layer 116 additionally or alternatively further comprises any type of rocks, including rocks or sediments in layers, rock or sediment formations, and the like, or any combinations thereof. In one embodiment, the top layer 116 additionally or alternatively comprises a top layer or layers of sediment and/or soil of varying depths. The permeability and/or porosity of the top layer 116 may vary widely, as long as drilling can be performed to insert the injection well 136 and production well 160 as described below, without using large-scale hydrofracturing.

[0055] In one embodiment, the top layer 116 can include a variety of geologic features, including, but not limited to, soil, sand, dirt, sediment, and the like, or combinations thereof. The top layer 116 may further have a wide range of depths (i.e., "thickness") sufficient to ensure working fluid introduced into the reservoir 120 remains in the desired state, such as a supercritical state. In one embodiment, the depth of the top layer 116 is at least 100 meters (m) or more, up to one (1) kilometer (km), further including more than one (1) km, such as up to three (3) km, four (4) km, five (5) km, or more, such as up to 10 km or over 15 km including any range there between, such as one (1) to five (5) km, below the Earth's surface (i.e., below or within a given topography in an area, which may or may not be exposed to the atmosphere). In most embodiments, however, it is expected that the target formations are located between about 800 m and about four (4) km beneath the Earth's surface.

[0056] Factors that can be considered in selecting reservoir depths can also vary according to local geology (e.g., specific rock type, geothermal heat flow rates, subsurface temperatures), access to working fluid (e.g., carbon dioxide from fossil fuel burning power plants, ethanol plants), drilling and operation costs, and sociopolitical circumstances (e.g., consumer locations, constructs, electric grid locations, and the like).

[0057] The target formation, comprising the caprock 118 and reservoir 120, can be made up of a variety of rock types, including, but not limited to, igneous rock, metamorphic rock, limestone, sedimentary rock, crystalline rock, and combinations thereof. In one embodiment, the target formation is a sedimentary basin having a substantially

bowl or convex shape as shown in Figure B.4. In other embodiments, the target formation have another shape, such as the substantially dome or concave shape as shown in Figures B.1-B.3, although the invention is not limited to the shapes depicted in Figure B.1-B.4. In one embodiment, the target formation is a saline aquifer or a saline water-filled rock formation (e.g., reservoir 120) containing a native fluid which is inhibited or prevented from escaping upwardly, due to the presence of the caprock 118. It is further understood that a target formation may contain a fault which can offset the target formation or a portion of the target formation, thereby forming a geological trap, as the term is understood in the art. In another embodiment, the target formation is a reservoir containing natural gas and/or oil and/or fresh water.

[0058] In one embodiment, CO_2, such as the cold CO_2 138 shown in Figure B.1, is used as the working fluid in combination with a reservoir 120 located at least about 0.1 km, to about 4 km deep. Such a combination can minimize upward leakage of the working fluid, since additional caprocks 118 may be present between the reservoir 120 and the Earth's surface. Additionally, higher natural reservoir temperatures (i.e., greater than about 70 ^{o}C) and higher pressures (i.e., greater than about 8 MPa) may be encountered at such depths. Larger depths can also increase the likelihood of the presence of dissolved salts and other minerals in the native fluid, which may reduce the likelihood that such native fluid would otherwise be useful for drinking and irrigation applications.

[0059] The caprock 118 shown in Figure B.1 is a geologic feature having a very low permeability, i.e., below about 10^{-16} m^2 . Such a low permeability allows the caprock 118 to essentially function as a barrier for fluid contained in the reservoir 120 below. Permeability may also be dependent, in part, on the depth (i.e., thickness) of the caprock 118, as well as the depth of the top layer 1 16 above. The porosity of the caprock 118 can vary widely. As is known in the art, even if a rock is highly porous, if voids within the rock are not interconnected, fluids within the closed, isolated pores cannot move. Therefore, as long as the caprock 118 exhibits permeability sufficiently low to allow it to prevent or inhibit fluid leakage from fluid in the reservoir 120, the porosity of the caprock 118 is not limited.

[0060] The thickness of the caprock 118 can vary, but is generally substantially less than the thickness of the top layer 116. In one embodiment, the top layer 116 has a

thickness on the order of 10, or 10 to 100, up to 1000 times the thickness of the caprock 118, further including any range there between, although the invention is not so limited. In one embodiment, the thickness of the caprock 118 can vary from about one (1) cm up to about 1000 m or more, such as between about five (5) cm and 1000 m, such as between about one (1) m and about 100 m. In one embodiment, the caprock 118 represents more than one caprock 118, such that multiple caprocks are present which partially or completely cover one another and may act jointly as a caprock 118 to prevent or reduce upward leakage of the working fluid from the reservoir 120.

[0061] The reservoir 120 can be one or more natural underground rock reservoirs capable of containing fluids. In one embodiment, the reservoir 120 is a previously-created manmade reservoir or a portion of a previously-created manmade reservoir, such as, for example, shale formations remaining from shale fracturing for hydrocarbon removal. In one embodiment, the reservoir 120 is also capable of storing carbon dioxide on a substantially "permanent" basis, as this term is understood in the art. In most embodiments, the reservoir 120 is sufficiently porous and permeable to be able to sequester fluids, such as carbon dioxide, and to receive and retain geothermal heat 124. In contrast to conventional enhanced geothermal systems, there is no requirement that the reservoir 120 be a hot dry rock reservoir, as that term is understood in the art, although, as noted herein, the such a reservoir can optionally be used

[0062] In one embodiment, the reservoir 120 is sufficiently permeable to allow multidirectional routes for dispersion or flow of fluid at relatively high rates, including lateral dispersion or flow. The presence of the caprock 118 above the reservoir 120 further enhances the dispersion capabilities of the reservoir 120. In one embodiment, the porosity of the reservoir 120 ranges from between about four (4)% to about 50% or greater, such as up to about 60%.

[0063] The reservoir 120 is also sufficiently permeable to allow fluids to flow relatively easily, i.e., at a rate of about 0.1 to about 50 liters/minute (L/min). In one embodiment, the reservoir 120 has a permeability of about 10^{-16} m^2 to about 10^{-9} m^2 , or greater, such as up to about 10^{-6} m^2 .

[0064] In an exemplary embodiment, the reservoir 120 has a porosity of at least about (4) % and a permeability of at least about 10^{-15} m^2 , with the caprock 118 having a maximum permeability of about 10^{-16} m^2. (See also Example 1).

[0065] The reservoir 120 can have any suitable natural temperature. In one embodiment, the natural temperature of the reservoir 120 is at least about 90 ^{o}C, although the invention is not so limited. In one embodiment, natural temperatures below 90 ^{o}C, such as down to 80 ^{o}C or 70 ^{o}C, further including down to 30 ^{o}C, including any range there between, are present. Natural temperatures greater than 90 ^{o}C may also be present, with the highest temperature limited only by the amount of geothermal heat 124 provided and the ability of the reservoir 120 to capture and retain the geothermal heat 124. It is possible that temperatures greater than about 300 ^{o}C may be present in the reservoir 120.

[0066] In one embodiment, a specific desired natural temperature is obtained by varying the depth of the injection well 136 or the production well (i.e., recovery well) 160. In one embodiment, higher natural temperatures are obtained by increasing the depth of the injection well 136, with or without increasing the depth of the production well 160. Unlike conventional geothermal energy systems which utilize water as the working fluid, **however, the natural temperatures used to generate energy in the novel non-water based geothermal systems described herein, in amounts sufficient to produce electricity, for example, are much lower.**

[0067] The depth of the reservoir 120 can vary as noted above. Additionally, the overall size of the reservoir 120 can also vary.

[0068] The geothermal heat 124 can flow at any suitable rate, including at a high rate as is present in "high geothermal heat flow regions", as the term is understood in the art. Conventional water-based systems are known to require high geothermal heat flow in most instances. As a result, as compared to conventional systems using water as the working fluid, the novel systems described herein can operate in a wider range of locations, including low and moderate geothermal heat flow regions. Also in contrast to conventional water-based systems which may choose to operate in areas containing little natural water (e.g., American Southwest), thus requiring importation of water, the novel systems described herein do not rely on water as the working fluid, and thus do not import water for use as a working fluid. **It is to be understood, that areas having medium or low geothermal heat flow rates can also be used.**

[0069] Additionally, water in a conventional EGS tends to react extensively with rocks causing mineral precipitation and/or wall rock dissolution reactions. In contrast,

substantially pure CO_2 (for example, CO_2 in the center of the CO_2 plume 122) is expected to result in very limited to no rock/mineral-fluid reactions. Some limited reactions may occur at the (narrow) H_2O-CO_2 interface. Extensive fluid- mineral/rock interactions can have often have adverse effects due to fluid flow path modifications, since flow constrictions can be formed due to mineral /rock/sediment precipitations with "short-circuiting" resulting from mineral/rock/sediment dissolution. However, limited reactions can have beneficial effects in the form of permeability and/or porosity enhancement.

[0070] As noted above, the system 100 of Figure B.1 comprises a CO_2 sequestration component 112 and a geothermal energy production component 114. CO_2 sequestration is accomplished by providing the CO_2 source 110 to an optional compressor 132 to produce compressed CO_2 111 (i.e., CO_2 having a temperature of about zero (0) to about 50 ^{o}C and pressure of about three (3) to about seven (7) MPa). The compressed CO_2 11 lean optionally pass through a first cooling unit 134 to produce a working fluid, such as cold CO_2 138 (i.e., saturated liquid CO_2 having a temperature less than about 30 ^{o}C and pressure of about three (3) to about seven (7) MPa), before entering the injection well 136, as shown in Figure B.1, where it flows in a substantially downwardly direction below the Earth's surface. Upon its release at an injection well reservoir opening 170, the cold CO_2 138 permeates the reservoir 120 forming a CO_2 plume. Upon exposure to the temperatures present in the reservoir 120 (which are higher than the temperature of the cold CO_2 138), the cold CO_2 138 absorbs heat from the reservoir 120, thus causing an upwardly-migrating CO_2 plume 122, which, in one embodiment, may be laterally advected due to nonzero groundwater flow velocities within the reservoir 120, as shown in Figure B.1. In one embodiment, lateral migration occurs additionally or alternatively due to the CO_2 plume spreading, as additional CO_2 exits the injection well 170.

[0071] The CO_2 plume 122, which can further contain an amount of native fluid (partially dissolved in the CO_2 plume or included as individual bubbles or fluid pockets), migrates, is transported (such as in a closed loop system as described herein) and/or flows and/or spreads towards the production well 160, entering a production well reservoir opening 172 as hot CO_2 140 (i.e., fluid CO_2 having a temperature greater than about 30 0 C). The CO_2 plume 122 can move at any suitable rate in a substantially horizontal manner across the reservoir 120. In one embodiment, the CO_2 plume 122

moves at a rate of about 0.1 to about one (1) m/day, such as about 0.4 to about 0.6 m/day, although the invention is not so limited. When the CO_2 plume 122 reaches the production well reservoir opening 172 as hot CO_2 140, it can be transported and/or buoyantly move in a generally upwardly direction towards the Earth's surface. In the embodiment shown in Figure B.1, the hot CO_2 140 enters an expansion device 142 to produce shaft power 144 which can be provided to a generator 146 to produce electricity 148 and to the compressor 132.

[0072] Warm CO_2 150 (i.e., gaseous CO_2 having a temperature between about zero 0 ^{o}C and about 30 ^{o}C and a pressure between about three (3) and about seven (7) MPa) is also drawn off the expansion device 142 for use within the system 100, to provide part of the required load used during operation, thus providing a "power cycle." As such, the warm CO_2 150 is provided to the second cooling unit 152, where exhaust 154 (warmed air or water or water vapor) is released, while cooled CO_2 157 can be provided to the first cooling unit 134 to repeat the power cycle, after optionally passing through a pump 156.

[0073] A variety of working fluids can be employed in the novel systems and methods described herein. The working fluid used in the carbon dioxide sequestration component 1 12 of the system 100 shown in Figure B.1, is cold CO_2 138 obtained from a CO_2 source 110. Such a working fluid can further contain entrained contaminants. In contrast, the working fluid useful in the substantially above-ground geothermal energy production component 114 of the system 100 may be any suitable secondary working fluid 250 as is understood in the art. (See Figures B.2-B.4). In one embodiment, the working fluid for either the CO_2 sequestration component 112 or the geothermal energy production component 114 with a non water-based fluid, i.e., any fluid which is thermodynamically more favorable than water (i.e., having a higher condensing pressure and higher vapor density at ambient temperature). In one embodiment, one or more supercritical fluids are used as the working fluid for either or both components, 112 and 114.

[0074] In a particular embodiment, supercritical carbon dioxide is used as the working fluid in the CO_2 sequestration component 112 and/or the geothermal energy production component 114. Supercritical carbon dioxide has an increased density, as compared with other working fluids, such as gaseous carbon dioxide, such that a greater amount can be stored in a smaller volume, thus increasing system efficiency. Additionally, and

in particular for the CO_2 sequestration component 112, supercritical carbon dioxide has favorable chemical properties and interaction characteristics with water (such as saline water), as is known in the art. Supercritical carbon dioxide can also be used in colder conditions, as compared with water-based geothermal systems, since it has a lower freezing point of about -55 ^{o}C (as compared to approximately 0 ^{o}C for water) depending on pressure. As such, a carbon dioxide-based system can be used in temperatures much lower than 0 ^{o}C, such as down to -10 ^{o}C or -20 ^{o}C or -30 ^{o}C or below, down to about -55 ^{o}C, including any range there between. A larger temperature differential between the heat sink (atmosphere or ambient air) and the heat source (reservoir 120), also increases the overall efficiency of the system. The use of carbon dioxide, in one embodiment, as the working fluid in the CO_2 sequestration component 112 allows for sequestering of carbon dioxide.

[0075] In one embodiment, the working fluid in the CO_2 sequestration component 112 (e.g., cold CO_2 138) is released directly into the reservoir 120 where it becomes a CO_2 plume 122, which is allowed to flow through natural pores, fractures and conduits present in the reservoir 120 in the area between the injection well reservoir opening 170, where it eventually becomes hot CO_2 140, before entering a production well reservoir opening 172 of the production well 160, as shown in Figure B.1. Such a flow pattern is referred to herein as an "open" flow cycle. In this embodiment, the working fluid can displace and/or commingle with any native fluid(s) present. In this embodiment, heat exchange between the reservoir 120 and the working fluid (e.g., cold CO_2 138) is facilitated and heat energy extraction is increased, as compared to a "closed" system in which the working fluid travels only through manmade pipes located in the reservoir 120 between the injection well reservoir opening 170 and the production well reservoir opening 172. Additionally, any fluid loss occurring in an open cycle is simply sequestered in the reservoir 120. In one embodiment, a partially open cycle is used. In one embodiment a closed cycle is used. The injection well reservoir opening 170 and the production well reservoir opening 172, the production well 160 are, in one embodiment, located at a distance sufficiently apart from one another to permit adequate heating of the cold CO_2 138 to the desired temperature.

[0076] The compressor 132 can comprise any suitable compressor or compressors known in the art. In one embodiment any suitable type of pump replaces the compressor

132. In one embodiment, no compressor 132 is used, such as when the CO_2 source 110 is provided at a sufficiently high pressure (i.e., greater than about six (6) MPa). In one embodiment, no compressor 132 (or pump) is used and the first cooling unit 134 is a condenser which provides a saturated liquid at ambient temperature and corresponding saturation pressure (e.g., CO_2) for injection into the injection well 136, thus maximizing the density of the working fluid as well as the thermosyphon effect within the injection well 136.

[0077] In one embodiment, when the ambient temperature rises, and thus the corresponding saturation pressure also rises in the condenser or second cooling unit 152, the decrease in liquid density provided to the injection well reduces the hydrostatic head in the injection well. In one embodiment, as described in the Example section, the higher condensing pressure surprisingly compensates for this decreased density effect at a level sufficient to maintain the deep rock cavity (i.e., reservoir 120) pressure regardless of changing surface conditions without using a compressor 132 (or pump). Such a configuration allows for reduced start-up and operating costs.

[0078] Use of the first cooling unit 134 ensures that all of the carbon dioxide injected into the injection well 136 will be fluid at the same pressure and temperature, regardless of whether it comes from the CO_2 source 110 or as cooled CO_2 157 from the power cycle. Any suitable type or types of cooling unit can be used for the first cooling unit 134. The first cooling unit 134 further minimizes the amount of pumping action needed to increase pressure at the injection well 136, since less power is needed to pump a liquid to a higher pressure than a gas. Use of the first cooling unit 134 also helps to maximize any natural thermosyphon effect present (i.e., passive heat exchange based on natural convection which circulates liquid), by providing the injection well 136 with cold CO_2 138 at all times, although the invention is not so limited. In one embodiment, there is no first cooling unit 134. In one embodiment, the first cooling unit 134 is a condenser cooled by any suitable cooling means, such as with a water-antifreeze solution (e.g., glycol), with the cooling means in turn cooled by ambient air in the condenser.

[0079] The injection well 136 can be any suitable type of channel that allows the working fluid to move substantially downwardly. In one embodiment, the injection well 136 comprises more than one injection well. Depending on a particular site's history of heat extraction and on the geologic circumstances in the area (e.g., geologic

layers at depth, geothermal temperatures and heat flow rates), as well as the socio-political circumstances (instance to users and/or electrical grid, CO_2 source availability and distance, etc.), multiple injection wells may be located in patterns and inject the working fluid (CO_2) at various depths and rates to maximize the energy output of the power plant, maximize CO_2 sequestration, minimize subsurface heat depletion or a combination thereof.

[0080] In one embodiment, the injection well 136 and the production well 160 comprise a single channel or shaft with two or more pipes extending there from. In this embodiment, the injection "pipe" is deeper than the production "pipe."

[0081] Similarly, the production well 160 can be any suitable type of channel that allows the working fluid to move substantially upwardly. In one embodiment, the production well 160 comprises more than one production well. As with the injection well 136, patterns, depths, and CO_2 extraction rates of the production well 160 may be optimized.

[0082] In one embodiment, the injection well 136 comprises more than one injection well distributed in various locations and one or more production wells 160 are more centrally located. In this embodiment, the ambient temperature liquid coming out of the first cooling unit 134 can be provided to the sites of the various injection wells 136 through gravity-sloped small pipes (e.g., high density, low volumetric flow rate) with little or no thermal insulation required. The hot vapor, such as the hot CO_2 140 in the production well 160 is provided more directly to the geothermal energy production component 114, wherein pipe sizes may need to be larger to handle the higher volumetric flow rate and thermal insulation required.

[0083] The locations of the injection well 136 in relation to the production well 136 can be determined by any suitable means, including accessing geological data, such as from the U.S. Geological Survey pertaining to the particular target formation, and performing computer modeling, such as described in the Example section, in order to be able to predict and optimize conditions within the reservoir 120, such that, for example, the production well reservoir opening 172 of the production well 160 is at a point where the CO_2 plume 122 is at a sufficiently high temperature to become hot CO_2 140. In one embodiment, the injection well 136 and production well 160 are located at a distance sufficient to ensure that the working fluid (e.g., the cold CO_2 138) increases

in temperature by at least about 10 ^{o}C from the injection well reservoir opening 170 and the production well reservoir opening 172. Such distance can be a lateral distance, a vertical distance, or a combination thereof.

[0084] In one embodiment, the roles of the injection and production wells, 136 and 160, respectively, are reversed after a period of time to improve subsurface heat exchange within the reservoir 120. In one embodiment, the injection and production wells are reversed every few months or about every one (1) year up to about every five (5) years or any period there between.

[0085] The expansion device 142 can comprise any suitable type of expansion device 142 known in the art, including any type of turbine, although the invention is not so limited. In contrast to conventional water-based geothermal systems which produce low pressure steam at high volumetric flow rates, the use of a conventional turbine in higher pressure CO_2 geothermal energy systems and methods described herein, is an option, rather than a requirement.

[0086] In one embodiment, the expansion device 142 is one or more piston- cylinder devices. In one embodiment, the expansion device 142 is one or more scroll, screw or rotary compressors designed to run in reverse as engines. In one embodiment, the expansion device 142 comprises more than one expansion device 142. In one embodiment, multiple expansion devices 142 run in parallel, with some running pumps or compressors directly and others producing electric power for sale.

[0087] The generator 146 can be any suitable generator known in the art, to produce electricity 148. The second cooling unit 152 can be any suitable type of cooling unit as is known in the art. In one embodiment, the second cooling unit 152 is a dry cooling tower in which the exhaust 154 is released to ambient air. In one embodiment, the second cooling unit 152 is a wet cooling tower in which the exhaust 154 is released into the air by also evaporating a volume of water. In one embodiment, a dry cooling tower is used during colder conditions and a wet cooling tower is used during warmer conditions. Use of a wet cooling tower during warmer conditions can increase plant efficiency, as is known in the art.

[0088] The pump 156 shown in Figure B.1 is also optional and may be any suitable type of pump 156 as is known in the art to move the cooled CO_2 157 (e.g., direct lift, displacement, velocity, buoyancy, gravity, and the like) exiting the second cooling unit

152 prior to its return to the first cooling unit 134.

[0089] **In an alternative embodiment, the reservoir 120 is also used as a cooling unit to cool warm CO_2 150 exiting the expansion device 142, with the appropriate piping and pumps provided as is known in the art.**

[0090] In one embodiment, a geothermal energy system is provided, comprising a subterranean fluid transport system comprising an ingress channel (into the reservoir) and egress channel (out of the reservoir), each of the ingress and egress channels having respective proximal ends and distal ends relative to the surface; a natural subterranean porous in situ rock formation; a working fluid, the supercritical fluid being introduced into the rock formation starting at the proximal end and moving toward the distal end of the ingress channel. The fluid is withdrawn in part at the distal end of the ingress channel so as to form a subterranean fluid reservoir integral with the rock formation; and wherein the fluid is heated by the rock formation prior to transport toward the surface and proximal end 1 of the egress channel.

[0091] The system can comprise a compressor located in-line and integrated as part of the ingress channel to facilitate movement of the fluid toward the rock formation (i.e., reintroduction). The heated plume is formed as part of the migration through the rock toward the intake at the egress channel distal end. In the interim, the fluid absorbs the natural geothermal heat associated with the rock formation. Once the heated fluid travels toward the surface, the egress channel proximal end can be associated with a turbine and generator system, whereby electrical energy is produced and distributed to the consumer(s). Alternatively, the heat energy can be incorporated into system for district space and water heating applications (not illustrated).

[0092] In one embodiment, the subsurface-heated working fluid, as a primary working fluid, can be directly introduced into a turbine assembly as part of a turbine-generator system to generate electricity. In this embodiment, it is preferable to remove water or other ingredients as might be present within the primary working fluid.

[0093] In an additional embodiment, a plurality of ingress channels can be employed in combination with a single egress channel. Alternatively, a plurality of egress channels can be constructed, using a single ingress channel. Further yet, both a plurality of ingress channels and a plurality of egress channels can be constructed within a unitary system. Various arrangements are possible with the invention. Arrangements using multiple

systems at a land surface area using different parts of the same rock formation strata, or using separate and distinct rock formations at different depth and space parameters are contemplated.

[0094] In an additional embodiment of the invention, an additional transport channel can be constructed for the transport of external carbon dioxide sources. Examples of external carbon dioxide sources include, but are not limited to, fossil fuel power plants, ethanol plants, and the like. When direct turbine-generator systems are used, a water removal component may be incorporated into the system.

[0095] In one embodiment, the novel systems and methods described herein are constructed to permit maintenance desired for optimal operation of the system. For example, the working fluid supply channel (ingress channel) can be structured to permit its removal for maintenance (e.g., cleaning), or intermittent removal for a period of time to create a temporary closed cyclic system. The system can also be constructed to receive and accommodate multiple industrial carbon dioxide supply lines from different sources as part of the system.

[0096] In an alternative embodiment, as shown in Figure B.2, the hot CO_2 140 passes through a heat exchanger 202 where it is used to warm a secondary working fluid 250 also cycling through the heat exchanger 202 (through the second cooling unit 152 and pump 255 as shown). The heated secondary working fluid (temp ¿ about 30 ^{o}C) is released as heat 204, which can be used in any direct use application and/or as a ground-source heat pump, using components well known in the art. A portion of the heated secondary working fluid enters the expansion device 142 to produce shaft power 144 which is provided to the compressor 132 where the cycle is repeated. Meanwhile, the hot CO_2 140 exits the heat exchanger 202 as cooled CO_2 159 (i.e., CO_2 having a temperature of two (2) and seven (7) MPa that may be condensed liquid), passing through an optional pump or compressor 156 and finally returned to the first cooling unit 134, where it may be further cooled to become cold CO_2 138, thus repeating the cycle.

[0097] In another alternative embodiment, as shown in Figure B.3, both electricity 148 and heat 204 are produced. In this embodiment a second cooling unit (not shown) (e.g., 152 in Figures B.1 and B.2) is used and the heat exchanger 202 as described above is also retained.

[0098] In another alternative embodiment, as shown in Figure B.4, electricity 148 is produced and the a portion of the heat exiting the heat exchanger 202 is provided to a separate Rankine power cycle 405 having the components as understood in the art. With a Rankine cycle 405, the condensing pressure is typically subcritical and the highest pressure during the heat addition may be either supercritical or subcritical.

[0099] In one embodiment, a novel method is provided comprising pumping CO_2 from an emitter (e.g., ethanol or coal-fired power plant) underground into a geothermal reservoir. At certain depths (e.g., about 0.4 to about two (2) km), the reservoir contains salty groundwater unlikely to be used for irrigation or consumption. Alternatively, the reservoir may contain hydrocarbons (oil, natural gas) and the injected CO_2 is supercritical CO_2 which serves to enhance oil recovery (EOR). As noted above, the target formation comprises a reservoir located underneath at least one very low permeability caprock that prevents the working fluid, e.g., supercritical CO_2, from rising to the surface (similar to a natural gas trap). In addition, the depth of the reservoir reduces the chance of CO_2 reaching the surface, as multiple other low-permeability layers are likely present above the reservoir.

[00100] In one embodiment, CO_2 in the reservoir is heated by Earth's geothermal heat flow, which partially replenishes the heat energy transmitted to the CO_2. In one embodiment, a small portion of the geothermally-heated CO_2 is brought back to the surface where it drives an expansion device and generator, such as a turbine-generator combination. The cooled CO_2 can thereafter be returned to the reservoir. In one embodiment, the energy used to pump the CO_2 to the subsurface is a small fraction (e.g., **substantially zero (0)% to about five (5)%**) of the energy provided by the geothermal heat and may also be small in comparison to the electricity produced by the system (e.g. **substantially zero (0)% to about 25%**).

[00101] The various individual components of the system of the invention can be obtained and constructed using conventional equipment and techniques readily available to those in the (geothermal) power plant and carbon dioxide sequestration industries. Site locations can be determined using geological survey data for various regions throughout a given country in combination with the porosity and permeability parameters described herein as suitable for the method and system of the invention.

[00102] The specific materials and designs of additional minor components necessary

to perform the process, e.g., valves, pumps, lines, and the like, are understood in the art will not be described herein. The apparatus and method of the invention can further be implemented using a variety of specific equipment available to and understood by those skilled in process control art. For example, means for sensing temperature, pressure and flow rates in all of the flow lines may be accomplished by any suitable means. It will also be appreciated by those skilled in the art that the invention can include a system controller.

[00103] Specifically, the system controller can be coupled to various sensing devices to monitor certain variables or physical phenomena, process the variables, and output control signals to control devices to take necessary actions when the variable levels exceed or drop below selected or predetermined values. Such amounts are dependent on other variables, and may be varied as desired by using the input device of the controller. Such sensing devices may include, but are not limited to, devices for sensing temperatures, pressures and flow rates, and transducing the same into proportional electrical signals for transmission to readout or control devices may be provided for in all of the principal fluid flow lines. Such a controller may be a local or remote receiver only, or a computer, such as a laptop or personal computer as is well-known in the art. In one embodiment, the controller is a personal computer having all necessary components for processing input signals and generating appropriate output signals as is understood in the art. These components can include a processor, a utility, a driver, an event queue, an application, and so forth, although the invention is not so limited. In one embodiment, the controller has a non-volatile memory comprised of a disk drive or read only memory device that stores a program to implement the above control and store appropriate values for comparison with the process variables as is well known in the art.

[00104] In one embodiment, these components are all computer programs executed by a processor of the computer, which operates under the control of computer instructions, typically stored in a computer-readable media such as a memory. In this way, useful operations on data and other input signals can be provided by the computer's processor. The controller also desirably includes an operating system for running the computer programs, as can be appreciated by those within the art. The system controller may also comprise a machine coupled to a control panel. Buttons and dials can

be provided on the control panel to allow modification of the values and to control of the carbon dioxide-based energy generating system to take the desired steps described herein. The system controller can also be programmed to ignore data from the various sensors when the operator activates certain other buttons and dials on the control panel as he/she deems necessary, such as fill override or emergency stop buttons. Alternatively, or in addition to the foregoing, the control panel can include indicator lights or digital displays to signal an operator as to the status of the operation. Indicator lights can also be used to signal that a certain variable level is outside the desired range, therefore alerting the operator to the need for corrective action. In such an embodiment, the corrective action is not automatic, but requires the operator (who may be located remotely and optionally controlling more than one system substantially simultaneously) to initiate corrective action either by pushing a specific button or turning a specific dial on the control panel, or by manually adjusting the appropriate valve or device.

[00105] Additionally, as is known in the art, in implementing the system described herein, general chemical, mechanical and physical engineering principles must be adhered to, including accounting for the various types of energy and materials being input to and output from the system, in order to properly size the system. This includes not only the energy associated with mass flow, but also energy transferred by heat and work. In some embodiments, the system is optimized for maximum performance utilizing any known optimization methods known in the art.

[00106] The invention will be further described by reference to the following examples, which are offered to further illustrate various embodiments of the present invention. It should be understood, however, that many variations and modifications may be made while remaining within the scope of the present invention.

B.5 Example 1

[00107] Numerical modeling of carbon dioxide migration and storage was conducted using two-dimensional solute (carbon dioxide) injection schemes employing the multiphysics modeling environment COMSOL (available from Comsol AB, Burlington, Massachusetts).

[00108] A generic cross-section of Minnesota's Rift System (MRS) was provided by

the Minnesota Geological Survey (MGS) and is shown in Figure B.5. Figure B.6 provides an enlarged view of a portion of Figure B.5, taken from within box 6-6, which is an area that includes the Oronto Group of geological formations, estimated to be about 2.65 million years old. Within the Oronto Group, an area is noted that contains a target formation 600 which includes a caprock 618 and an aquifer 620 which was used for a numerical model of an energy generation system, as described herein. The model can permit estimation of the potential of the Midcontinent Rift System (MRS) for a carbon plume geothermal (CPG) system and the amount of time required for carbon dioxide to move from an injection to a production well.

[00109] A carbon dioxide injection model was designed and used to evaluate the spread of injected material over time and to determine whether the caprock 618 can effectively seal a reservoir, such as the aquifer 620 shown in Figure B.6.

[00110] Figure B.7 is an illustration of the target formation 600, containing the caprock 618 and aquifer 620. A simulated injection well 736 can be seen within the aquifer 620. Since no deep wells exist in Minnesota to provide geometric configurations of aquifer and caprock units, the cross-section was used only to verify that the estimated rift structure was sufficiently deep for carbon dioxide storage and to estimate depths for storage units. Due to the lack of measured data, a rectangular aquifer 50 meters (m) thick (in height) and several km in length was assumed and illustrated in Figure B.7.

[00111] The model geology was expanded by placing a capping material, i.e., caprock 618 dimensionally equivalent to the aquifer 620, immediately above the aquifer 620. The aquifer and caprock are then encased in a surrounding material that extends vertically to the ground surface with the aquifer at a depth of about 2500 m, and horizontally several kilometers beyond the aquifer and caprock (See, for example, Figure B.6). The extent of surrounding material was chosen such that the upper and lower boundaries were far enough from the aquifer to realistically assume that no fluid flow occurs across the boundaries during the simulated time interval while the left and right boundaries were chosen to be sufficiently far from the modeling domain of interest to assume hydrostatic fluid pressure conditions (i.e., constant pre-injection fluid pressure conditions). The surrounding unit's permeability was valued at 10^{-19} m^2, and the pore fraction was 0.04 (i.e., 4%) based on the data provided by the MGS. Fluid flow was permitted through the top and bottom of the aquifer to simulate natural conditions.

[00112] A solute solution of one (1)% CO_2 was injected (the remaining content being water), with a solute weight approximately equivalent to supercritical CO_2 at a depth of 2500 m, in the center of the aquifer for a period of one year. The injection rate can be varied to approximate injection of all CO_2 produced by a large (e.g., about 250 megawatt (MW) to about 1000 MW) fossil fuel-fired power plant. Carbon dioxide as a solute in water was assumed for injection into a water aquifer because the solute approach simplified modeling as compared with pure carbon dioxide fluid. Future modeling may include use of pure carbon dioxide fluid.

[00113] Approximately 30 scenarios were run (see Figure B.8 for a visualization of a sample injection), with varying injection rates and aquifer and caprock permeabilities and porosities. The results are set forth below in Tables B.1 and B.2.

[00114] The model indicated that the matrix permeability of the caprock in the rift was sufficiently low, ranging between 10^{-21} m^2 to 10^{-18} m^2. This was sufficient to serve as an effective reservoir caprock in the absence of large-scale hydro fracturing. Furthermore, deep geological sequestration and carbon plume geothermal (CPG) system would be possible in the reservoir of the rift, provided that large sandstone bodies with porosities in the range of 0.04 to 0.2 (i.e., about four (4)% to 20%) and permeabilities in the range of 10^{-15} m^2 to 10^{-13} m^2 (with an uncertainty of about a factor of 10) would eventually be located in the rift at depths greater than 800 m below a caprock with the above properties.

[00115] The model also indicated that the horizontal spread of solute was generally less than about ten (10) km from the injection point, which is a relatively small distance, and the result was interpreted to indicate reasonable storage space for aquifers having the previously defined properties. The results also suggest that in a CPG scenario, carbon dioxide would travel from injection to production wells, which could be a few hundred meters to several kilometers apart, within a relatively short period of time (typically less than a year to a maximum of approximately three (3) years).

[00116] Additional modeling demonstrated that the porosity of caprock units can be in a range from between about 0.06 to about 0.16 (i.e., about six (6)% to about 16%, respectively). Note that this range overlaps with that of the aquifer porosity. The models also indicated that porosity overlap would not be problematic for carbon dioxide storage, provided caprock permeability is several orders of magnitude lower than aquifer

	aquifer porosity			
		max concentration of solute in aquifer (kg/m^3)	distance in aquifer from injection well horizontally to liquid with a concentration of 1 kg/m^3 (m)	leakage through caprock?
value used when other parameters are varied:	0.1			
range:	0.02	150	14000	yes
	0.04	150	13139	no
	0.06	150	11588	no
	0.08	150	10214	no
	0.1	150	9075	no
	0.12	150	8150	no
	0.14	150	7391	no
	0.16	150	6749	no
	0.18	150	6225	no
	0.2	150	5761	no
	aquifer permeability			
value used when other parameters are varied:	10^{-13} m^2			
range:	10^{-13}	150	9075	no
	10^{-14}	153	8927	no
	10^{-15}	186	7665	some
	10^{-16}	430	3656	some
	10^{-17}	1261	1167	yes
	10^{-18}	3472	360	yes
	10^{-19}	14080	170	yes
	10^{-20}	62970	123	yes
	pumping rate			
value used when other parameters are varied:	5 m^3/s			
range:	5	150	9075	no
	10	292	9101	no
	15	499	9134	no
	20	623	9150	some

Table B.1: Injection Rates and Aquifer and Caprock Permeabilities and Porosities

	caprock porosity			
		max concentration of solute in aquifer (kg/m^3)	distance in aquifer from injection well horizontally to liquid with a concentration of 1 kg/m^3 (m)	leakage through caprock?
value used when other parameters are varied:	0.08			
range:	0.02	150	9160	yes
	0.04	150	9133	yes
	0.06	150	9101	some
	0.08	150	9075	no
	0.1	150	9031	no
	0.12	150	9024	no
	0.14	150	8997	no
	0.16	150	8963	no
	caprock permeability			
value used when other parameters are varied:	10^{-18} m^2			
range:	10^{-18}	150	9075	no
	10^{-19}	158	8904	no
	10^{-20}	192	7820	no
	10^{-21}	317	5684	no

Table B.2: Injection Rates and Aquifer and Caprock Permeabilities and Porosities (cont'd)

permeability. This preliminary study further provides support for providing a single injection well to accommodate all the carbon dioxide produced by an approximately 1000 MW coal-fired power plant using the novel systems described herein.

[00117] These results provide support for using a reservoir having a porosity of at least about (4) % and a permeability of at least about 10^{-15} m^2 or greater for sequestration within the MRS assuming presence of a caprock having a maximum permeability of about 10^{-18} m^2, although permeabilities as low as 10^{-16} m^2 may be used in certain instances. These results are consistent with ranges defined by the MGS using a compilation of current carbon dioxide storage studies worldwide and are also within the ranges that might be found in the MRS.

B.6 Example 2

[00118] In this example, a model of various CO_2-based geothermal systems in a naturally porous, permeable aquifer, i.e., the novel CO_2 Plume Geothermal (CPG) system is compared to a conventional CO_2-based engineered EGS and a conventional water-based (i.e., non-EGS) geothermal system.

[00119] For all sample models, the geometry as shown in map view in Figure B.9 is utilized. The system is (horizontally) one kilometer square and 305 m thick with one injection well at the center and four production wells, one at each corner of the square, as shown in Figure B.9. By symmetry, only l/8th of the system need be modeled, as shown in the gridded area of Figure B.9. This geometry is typical of early- stage geothermal system models and approximates real-world, water-based geothermal installations. The model thus provides a direct comparison to water- based geothermal power generation systems as well as CO_2-based EGS systems.

B.6.1 Parameters for Sample Models

[00120] Unless otherwise noted, the following parameters are used in the models of CPG formations that provide the results shown in the figures.

[00121] Table B.3 shows details of the modeled geothermal reservoir.

B.6.2 CPG System Compared to CO_2-Based EGS System.

[00122] Figure B.10 is a graph showing temperature versus distance from the injection well to a production well for various fracture spacings in the EGS cases (the CPG system does not contain specific fractures but rather a granular porous medium). Specifically, Figure B.10 compares the novel CPG system (top line) with several conventional CO_2-based EGS systems using various average fracture spacings (200 m, 100 m and 50 m, from bottom to second from the top), thus providing a cross section through the model geometry from injection well to production well. As such, Figure B.10 displays a temperature "snapshot" after 10 years of injection and production in this very low temperature geothermal environment. (The low temperature scenario was simulated to illustrate performance at commonly unfavorable low-temperature conditions. System

Geothermal reservoir	
Thickness	305 meters
Distance between injection and production wells	707.1 meters
Permeability	10^{-14} m^2
Porosity	20% (i.e., 0.20)
Rock grain density	2600 kg/m^3
Rock specific heat	1000 $J/kg/^oC$
Rock thermal conductivity	2.51 $W/m/^oC$
System initial and boundary conditions	
Reservoir fluid	All CO_2 or all water
Temperature	100 ^oC
Pressure	250 bar
Top and side boundaries	No fluid or heat flow
Bottom boundary	No fluid flow, heat conduction
Injection and production conditions	
Reservoir area	1 km^2
Temperature of injected fluid	20 ^oC
Injection/production rate	300 kg/s
Down hole injection pressure	250 bar
Down hole production pressure	240 bar
Injection/production duration	30 years

Table B.3: Geothermal Reservoir Specifics

performance increases for higher temperatures).

[00123] Surprisingly, there are substantial differences between the CPG and EGS models. With respect to the CPG case, near pre-production temperatures (and in general higher temperatures) were maintained at the production well for much longer than in the EGS models. These results indicated there was a more thorough thermal energy recovery in CPG systems as compared to the conventional EGS models. Hence, it is expected that, in use, a CPG system will achieve higher efficiency and maintain economic viability longer (due to longer-term production of high-temperature fluids) than a conventional EGS.

[00124] Additionally, after ten (10) years of injection and production, the maximum temperature in the reservoir in the CPG system occurred at the production well, which was not the case for the EGS system. As electrical energy production efficiency (and viability of system implementation) is directly related to fluid temperature, the CPG systems provided higher efficiency than EGS.

[00125] Finally, as the EGS cases revealed, the wider the average fracture spacing, the lower the temperature of produced fluid with time. Thus, all else being equal, CPG systems can be implemented in lower temperature formations (therefore, in more areas worldwide) than (even CO_2-based) EGS (let alone water- based EGS). The substantial differences in produced fluid temperatures between CPG systems and CO_2-based EGS were surprising and unexpected.

[00126] Figure B.11 shows a CPG system in comparison with several CO_2-based EGS examples, showing heat energy production as a function of time. In these examples, for a given pressure differential between injection and production wells, the CPG system produced over 1.75 times more heat energy than a comparable CO_2-based EGS. To produce comparable amounts of heat energy, EGS required a much higher (more than factor of two) pressure difference between the injection well and the production well. Thus, the EGS had a much greater pumping energy requirement and lower power production efficiency than the CPG systems.

B.6.3 CPG System Compared to Water-Based Non-EGS Geothermal System

[00127] Figure B.12 compares thermal energy extraction rates between a CPG system and a water-based regular (i.e., non-EGS, meaning a reservoir/non-hydro fractured) geothermal system, everything else being equal. Surprisingly, thermal energy extraction rates are 1.7 to 2.7 times larger with CO_2 than water, which appears to be primarily a result of CO_2 mass flow rates being up to 5 times greater than those of water, given a fixed pressure difference between injection and production wells. Interestingly, based on conventional wisdom, it was expected that CO_2 energy extraction rates would be up to 1.5 times larger than those of water. See, for example, Pruess, **"Enhanced geothermal systems (EGS) using CO_2 as working fluid - a novel approach for generating renewable energy with simultaneous sequestration of carbon, "** Geothermics 35 (4), pp. 351-367, 2006 [9]. Therefore, the above result is surprising in that conventional practices predict different results, thus teaching away from such a system. Additionally, these results show the widespread potential for CPG implementation in areas previously inaccessible to geothermal energy extraction by traditional, water-based means.

[00128] CO_2 mass flow rates can be largely attributed to high CO_2 mobility (density to dynamic viscosity ratio, ρ/μ). To note, real -world geothermal installations typically operate on a fixed differential production pressure, as has been included in the above models.

[00129] Figure B.13 provides density profiles from injection well to production well, comparing CO_2 and H_2O cases for two different reservoir depths. These plots are applicable to both naturally porous, permeable (CPG) systems and to EGS. Use of CO_2-based systems (lower two lines indicating different reservoir depths) compared to water-based systems (upper two curves indicating different reservoir depths) allows for a large density change in CO_2 between injection and production points. A drop in density from injection to production wells drives fluid flow through the subsurface system, an effect known as a thermosyphon, which reduces pumping requirements, a substantial energy draw in geothermal systems. Hence, the CO_2 system has much lower pumping energy requirements than a comparable water-based system.

[00130] As a result of these findings, scenarios may be envisioned where a CPG system does not even require a pump. Additionally, and surprisingly, the two CO_2

curves in Figure B.14 reveal that the injection to production density difference is much larger for CO_2 at shallower depths, while the water curves reveal little change with depth. This result applies to both EGS and CPG systems. Therefore, as EGS (with CO_2 or water) typically target much deeper reservoirs than are proposed for CPG systems, CPG demonstrates increased thermosyphon properties as compared with EGS.

[00131] Dimensionless numbers can be utilized to further describe the properties of CO_2 as compared to water in naturally porous, permeable (i.e., non- EGS) geothermal systems. For example, the above plot reveals that the CO_2 Rayleigh number is much higher than that of water, indicating CO_2 more readily advects/convects (circulates due to heat energy recovery) through the reservoir than water (all else being equal).

[00132] As the water Prandtl dimensionless number indicates in Figure B.15, as compared to the Prandtl number for CO_2, water more readily diffuses momentum than heat. Hence, CO_2 more easily moves through a geothermal reservoir than water, and the increased mobility of CO_2 (see also statement about mobility of CO_2 above) ultimately leads to the improved heat energy recovery of CO_2-based compared to water-based systems.

[00133] Surprisingly, the CPG system is able to increase power production efficiency by utilizing CO_2'S low freezing point. Since CO_2 does not freeze at 0 ^oC, unlike water, a CO_2 power cycle can use sub 0 ^oC condensing temperatures in its power system, increasing power production efficiency on top of efficiency improvements acquired in the geothermal reservoir.

B.6.4 Exemplary Reservoir Parameter Ranges

[00134] As a result of the above modeling, various exemplary reservoir parameters were determined as useful in the embodiments described herein. Of course, other parameters are also possible, which can be determined with additional modeling, proto-type testing and full-scale testing, including the testing described below in Prophetic Example 3.

B.7 Example 3 (Prophetic)

B.7.1 Modeling of CO_2 Reservoir Formation

[00135] Modeling of the formation of a CO_2 plume in a geologic structure will be performed. It is expected that numerical models of CO_2 injection into a brine or hydrocarbon filled geologic formation will show that a large (on the order of a kilometer in area and several tens to hundreds of meters thick), near-pure CO_2 plume can be established via displacement of the native fluid. The time period from onset of injection to CO_2 recovery at production wells is expected to be on the order of several months to two years (maximum 3 years), depending on site characteristics.

[00136] It is expected that initial plume formation will require a sequence of injection rates and durations designed to ensure thorough displacement of the native reservoir fluid and avoidance of so-called fingering or short-circuiting effects. It is expected that about 50% to about 95%, such as about 65% to 75%, such as approximately 70% of the injected CO_2 will be recoverable at production wells and cycled through the surface power system. The remaining fraction of injected CO_2 will be permanently geologically sequestered, as this term is understood in the art.

B.7.2 Reactive Transport and Poroelastic Modeling

[00137] In addition to physical experiments, modeling of the chemical reactions among injected CO_2, native reservoir brine or hydrocarbons, and reservoir rock is useful for understanding the function and the ranges of viable parameters for CPG systems. Similarly, modeling of the physical responses of a natural aquifer, including pore and matrix deformation and pressure propagation will be performed.

Permeability	$0.5x10^{-15}$ - $1x10^{-11}$ m^2
Porosity (i.e., pore fraction)	0.05 - 0.4
Depth below surface	800 - 5000 m
Temperature	70 - 300 ^oC

Table B.4: Exemplary Reservoir Parameters

[00138] One geochemical consequence of CO_2 injection into a naturally porous, permeable geologic formation overlain by a caprock (likely shale) that we expect to see from our modeling is fluid heating from exothermic reactions. Unique to some CPG systems, and something that is not possible in water-based geothermal systems and likely not possible in EGS (even CO_2-based EGS which would typically not include a caprock), are CO_2 reactions with some caprock minerals that produce heat. Because comparable water reactions are rare in geologic reservoir environments and EGS likely will not encounter native rocks that allow such reactions, CPG systems are uniquely able to make use of such geochemical behavior to enhance heat energy recovery. CO_2 injected into a geologic formation will naturally rise to the top of the formation, where it will rest against/underneath the local caprock. Should exothermic reactions occur, they would impart heat to the CO_2, which could be recovered to produce electricity as the fluid cycles through the CPG system. At the same time, these CO_2 -mineral reactions can be volume- increasing thereby serving to (further) seal the caprock. Such reactions may not occur in the reservoir itself if the reservoir rocks/minerals/sediments are of a different composition than the caprock materials.

B.7.3 Coupled Reservoir- Wellbore Modeling

[00139] Modeling fluid flow from the geologic reservoir through the wellbores is useful for the calculation of pumping requirements and permits estimation of fluid heating or cooling in the wells. It is expected that, because of the (greater) depths and temperatures typically targeted for EGS compared to those used for CPG systems, CPG systems will result in less CO_2 cooling than CO_2-based EGS as the heated fluid moves from the reservoir to the surface, showing further energy recovery improvements of CPG as compared to EGS.

B.7.4 Layered Reservoirs

[00140] Future models will account for fluid movement through the vertical dimension of a geologic formation, whereas models to date assume primarily lateral flow. It is expected that accounting for the third dimension (i.e., vertical dimension) will reveal additional features, such as improved heat recovery in CPG systems, as compared with

CO_2-based EGS (and water-based EGS and non-EGS systems) because in the CPG system, the heat transfer fluid will encounter considerably more heated rock.

B.7.5 Geochemical Reaction Experiments

[00141] Other experiments will examine geochemical reactions among CO_2, brine or hydrocarbons, and rock under temperature, pressure, and composition conditions that would be encountered in CPG systems or CO_2-based EGS. It is expected that the sedimentary rock reservoirs that would very often be used for CPG systems (because of depth, porosity, permeability, and existence of traps (reservoir with overlaying caprock that may also include a low permeability feature such as fault in some instances)), among other reasons, will show lower reactivity than the reservoirs typically accessible for EGS (because of the greater depths targeted for EGS). As such, EGS reservoirs are expected to be more easily clogged by mineral precipitation or short-circuited due to mineral/rock/sediment dissolution reactions which both can render such systems unusable.

B.7.6 Conclusion

[00142] The carbon dioxide-based energy generating system described herein provides a novel means for producing renewable energy, while further providing for carbon dioxide sequestration, thus providing a process with a negative carbon footprint. In one embodiment the geothermal power plant has a negative carbon dioxide output, thus providing the first electricity-generating power scheme with a negative carbon footprint. Carbon dioxide sequestration also provides added revenue to a power plant under a carbon-trading market. In contrast to conventional EGS (conventional water-based EGS and conventional CO_2-based EGS) sites which utilize large-scale hydro fracturing of rocks to create a usable reservoir, the embodiments described herein rely on natural or previously created reservoirs (including previously fractured natural gas formations) in combination with only minor disturbances at most, such that the target formation remains in situ, thus minimizing the negative effects of large-scale hydrofracturing described herein and known in the art. In one embodiment, a global warming reduction system is provided.

[00143] In embodiments which utilize supercritical carbon dioxide, the excellent

thermodynamic, fluid dynamic, and chemical properties of this working fluid provide new ways of generating electric power in regions formerly unimaginable for this purpose, such as the eastern and mid- western parts of North American may now be considered for renewable, clean, geothermal electricity production. This approach further enhances the efficiency of geothermal power plants, particularly during colder months, as compared to traditional water-based systems, thereby potentially allowing electricity production in such low heat flow regions, such as, for example, Minnesota, and other climatologically and geologically similar locations in a sustainable and highly efficient manner. Such plants are also expected to be more compact than water-based versions, thereby reducing the plant's spatial and environmental footprint.

[00144] Compared to water, carbon dioxide can be cooled well below zero (0)^{o}C (above atmospheric pressure), such as about -55 ^{o}C, without freezing. Carbon dioxide additionally allows the whole system to be run under pressures higher than ambient pressures. In contrast, water systems apply partial vacuums in parts of the cycle, which are prone to leaks. Additionally, the increased pressure allows for higher fluid densities, as compared to water, and thus smaller piping and other components reducing capital investment costs.

[00145] In one embodiment, the system is a closed loop carbon dioxide system without a carbon dioxide sequestration component. In other embodiments, the ability to contain carbon dioxide with use of an open loop or partially open loop system further enhances the efficiency of the system and provides a means to sequester carbon dioxide from, for example, a conventional power plant. In fact, by not recovering all of the carbon dioxide, some or most of the carbon dioxide (e.g., from about five (5)% to about 95%, can be sequestered. Additionally, these same systems and methods can also be applied to providing geothermal energy to heat pumps for space heating or for direct use, as described herein. In contrast to wind and solar power systems, geothermal systems are highly scalable and can provide base-load and dispatchable (peak) power as desired. Similarly, on a human-time scale, geothermal energy is a renewable energy resource and it is cheaper than coal, wind, nuclear, etc. and comparable in cost to natural gas.

[00146] The carbon dioxide-based geothermal energy generating system can be used to produce energy for a number of uses, including for commercial sale, process load (to operate the geothermal power or CO_2 sequestration system) and electricity generation.

In the exemplary embodiments described in detail herein, the system is designed to generate energy in quantities sufficient to provide electricity, to provide heat for on- or off-site uses, to provide shaft power to operate the on-site equipment, or combinations thereof, and the like. In this way, the use of fossil fuels, such as natural gas, is limited, while operational costs are reduced.

[00147] Embodiments of the novel system and methods described herein provide, for the first time, the ability to provide electricity from a geothermal source at temperatures much lower than are required for conventional water-based geothermal systems, although higher operating temperatures may optionally be used.

[00148] Embodiments of the novel systems and methods described herein are efficient, economical and relatively simple in operation. In one embodiment, the process uses a production waste product (CO_2) that must otherwise be properly disposed of, sometimes at significant costs. Various embodiments also allow an operating liability to be turned into a business asset, while simultaneously providing environmental benefits.

[00149] Embodiments of the invention can be employed as part of a simplified cost-effective geothermal energy system using natural state rock formations as subterranean in situ rock reservoirs. Various embodiments can also be used for subterranean carbon sequestration and permanent storage of CO_2. The use of saline aquifers and saline water-filled rock formations in one embodiment further allows water to be utilized which is unlikely to be used for consumption or irrigation. Embodiments may further be part of an enhanced oil recovery (EOR) scheme and other hydrocarbon extraction methods, thereby enhancing hydrocarbon recovery (in addition to providing geothermal energy and to providing a means to sequester CO_2).

[00150] In one embodiment, the source of the carbon dioxide and carbon dioxide-based geothermal energy generating system are located on the same site or less than about one (1) km of each other, although the invention is not so limited. In one embodiment, the energy generation system is in close proximity to the carbon- dioxide producing source, such that energy which is generated with the system described herein is consumed partially or completely as power to the facility itself, thus eliminating the need for an elaborate and expensive piping system. In other embodiments, the energy produced with the energy generating system is piped any desired distance to be utilized in any desired manner. In yet other embodiments, some or all of the energy is used to

power other types of manufacturing facilities and/or is sold to a local utility, and/or is used to generate electricity on-site.

[00151] Although specific embodiments have been illustrated and described herein, it will be appreciated by those of ordinary skill in the art that any arrangement that is calculated to achieve the same purpose may be substituted for the specific embodiments shown. For example, although the embodiments have been described with carbon dioxide as the working fluid, in other embodiments, fluids other than carbon dioxide, having the properties, may be used. Additionally, a working fluid may be injected as part of an enhanced oil recovery (EOR) or enhanced natural gas or other hydrocarbon recovery scheme. This application is intended to cover any adaptations or variations of the invention. It is intended that this invention be limited only by the following claims, and the full scope of equivalents thereof.

B.8 Claims

WHAT IS CLAIMED IS:

1. A system comprising: one or more injection wells for accessing one or more reservoirs having a first temperature, wherein the one or more reservoirs are located below one or more caprocks and are accessible without using large-scale hydrofracturing, each of the one or more injection wells having an injection well reservoir opening; one or more production wells, each having a production well reservoir opening, wherein a non-water based working fluid can be provided to the one or more injection wells at a second temperature lower than the first temperature and exposure of the non-water based working fluid to the first temperature can produce heated non- water based working fluid capable of entering each of the one or more production well reservoir openings; and an energy converting apparatus connected to each of the one or more injection wells and the one or more productions wells, wherein thermal energy contained in the heated non-water based working fluid can be converted to electricity, heat, or combinations thereof, in the energy converting apparatus.

2. The system of claim 1 wherein each of the one or more injection wells and each of the one or more production wells are located in the same channel and the system further comprises one or more injection pipes and one or more production pipes connected to

the channel.

3. The system of claims 1 or 2 further comprising a non- water based working fluid source.

4. The system of claim 1 wherein the non- water based working fluid source is carbon dioxide obtainable from a power plant or an industrial plant.

5. The system of claim 4 wherein the power plant is an ethanol plant or a fossil-fuel based plant and the system further comprises the power plant or the industrial plant.

6. The system of claim 1 wherein the carbon dioxide is supercritical carbon dioxide, further wherein the energy converting apparatus comprises one or more expansion devices and one or more generators, one or more heat exchangers or a combination thereof.

7. The system of claim 6 wherein the one or more expansion devices and the one or more generators can provide electricity to an electricity provider and the system further comprises the electricity provider.

8. The system of claims 6 or 7 wherein each of the one or more heat exchangers can provide heat to a heat provider and the system further comprises the heat provider.

9. The system of claim 8 wherein the heat provider is a direct use provider or a ground heat pump.

10. The system of any one of claims 1, 2, 4, 5, 6, and 7, further comprising one or more cooling units fluidly connected to the one or more production wells and the one or more injection wells.

1 1. A method comprising: without using large-scale hydrofracturing, accessing one or more underground reservoirs having a natural temperature, the one or more reservoirs located beneath one or more caprocks; introducing a non-water based working fluid into the one or more reservoirs; exposing the non-water based fluid to the natural temperature to produce heated fluid; and extracting thermal energy from the fluid.

12. The method of claim 11 wherein the non-water based working fluid is carbon dioxide.

13. The method of claim 12 wherein the carbon dioxide is supercritical carbon dioxide.

14. The method of claim 11 wherein the heated fluid also contains native fluid present in the one or more reservoirs.

15. The method of any one of claims 11 to 14 wherein the one or more caprocks each have a permeability ranging from about 10^{-16} m^2 to about zero (0) m2 and the one or more reservoirs each have a porosity ranging from about one (1)% to about 50% and a permeability ranging from about 10^{-16} m^2 to about 10^{-6} m^2.

16. The method of claim 11 wherein the natural temperature is between about - 30 ^oC and about 300 ^oC.

17. The method of any one of claims 11, 12, 13, 14, and 16 wherein the thermal energy is used to produce electricity, to heat a working fluid in one or more heat exchangers, to provide condensed fluid to the one or more reservoirs, to provide cooled fluid to the one or more reservoirs, to provide shaft power to one or more pumps or compressors, or a combination thereof.

18. The method of claim 17 wherein the electricity is produced either by providing the hot fluid to one or more expansion devices or by providing the working fluid heated in the one or more heat exchangers to the one or more expansion devices, wherein the one or more expansion devices produces shaft power to one or more generators, which, in turn, produce the electricity.

19. The method of claim 17 wherein the working fluid heated in the one or more heat exchangers provides heat for direct use, for groundwater heat pumps, for a Rankine power cycle, or a combination thereof.

20. The method of any one of claims 11, 12, 13, 14, and 16, further comprising: choosing the underground reservoir; transporting a non-water based working fluid source to an area proximate to the injection well; converting the non-water based working fluid source into a non-water based working fluid; and providing the heat energy to a customer.

B.9 Abstract

Novel carbon dioxide-based geothermal energy generation systems, i.e., carbon plume geothermal (CPG) systems, and methods are provided. With the novel systems and methods described herein, geothermal energy can now be provided at lower temperatures and at locations other than hot, dry rock formations, without negatively impacting the

surrounding area through use of large-scale hydrofracturing. Use of a carbon dioxide-based geothermal system further provides a means for sequestering and storing excess carbon dioxide, rather than having it released to the atmosphere.

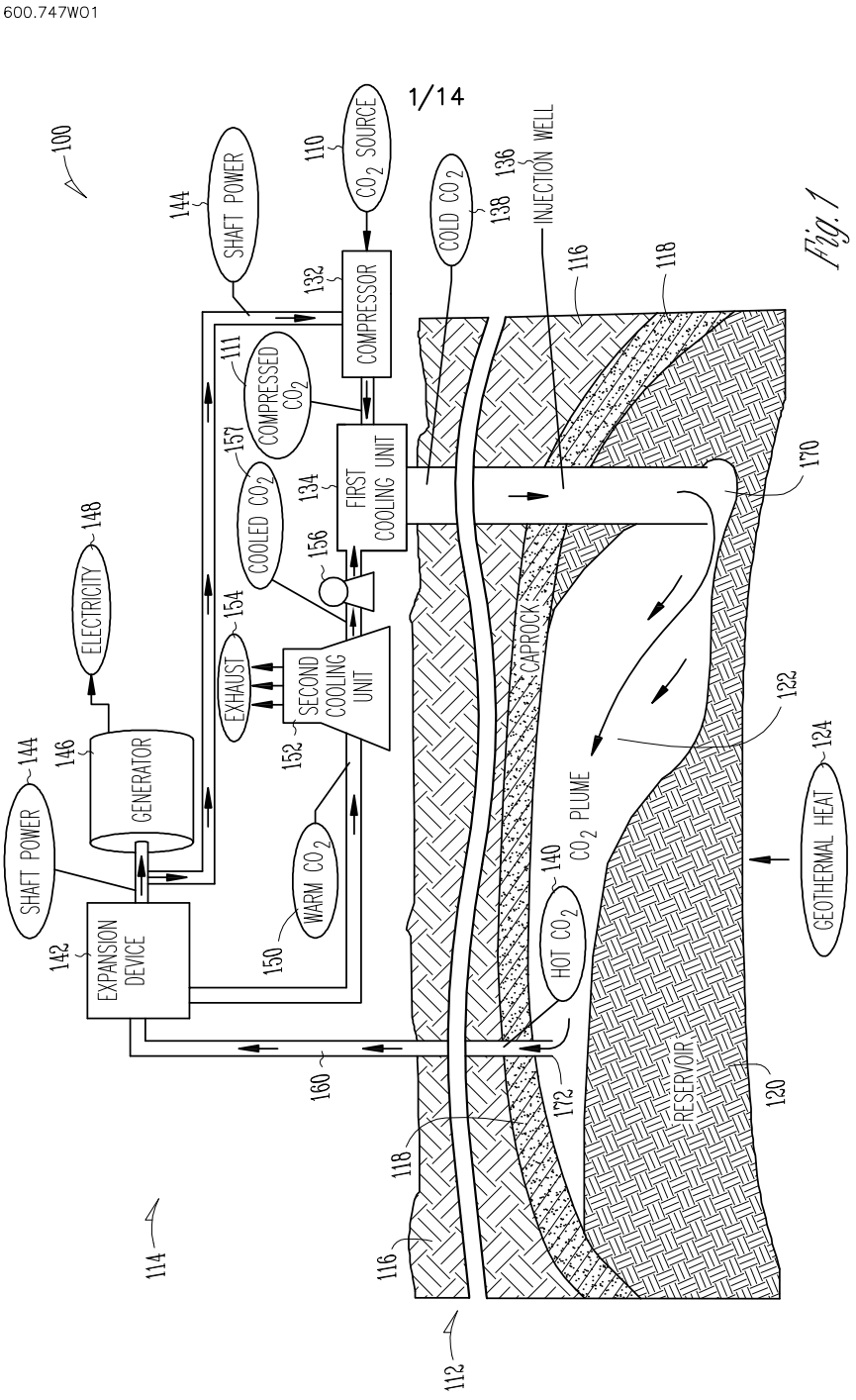

Figure B.1: A simplified schematic diagram of an energy generation system according to an embodiment of the invention.

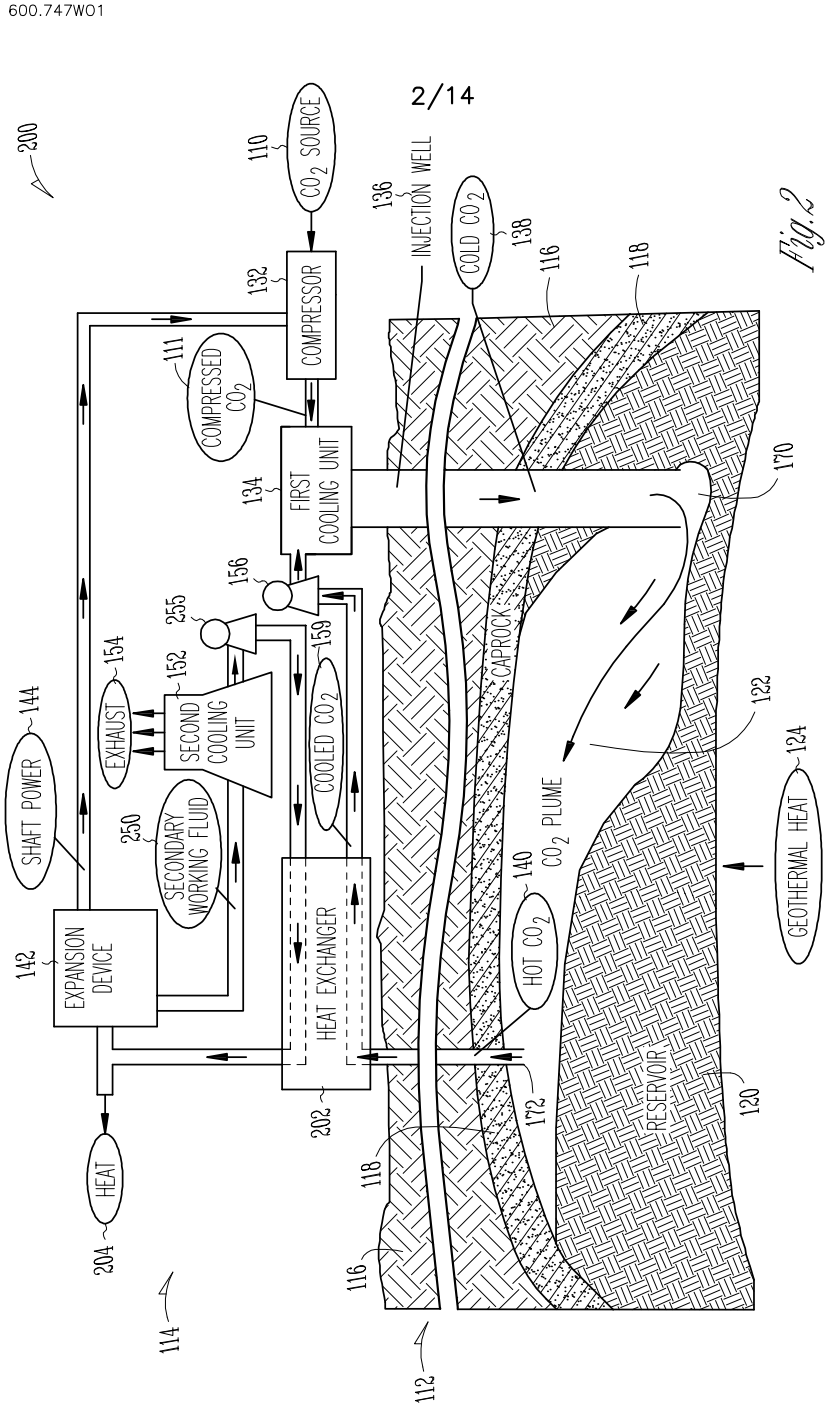

Figure B.2: A simplified schematic diagram of an alternative energy generation system according to an embodiment of the invention.

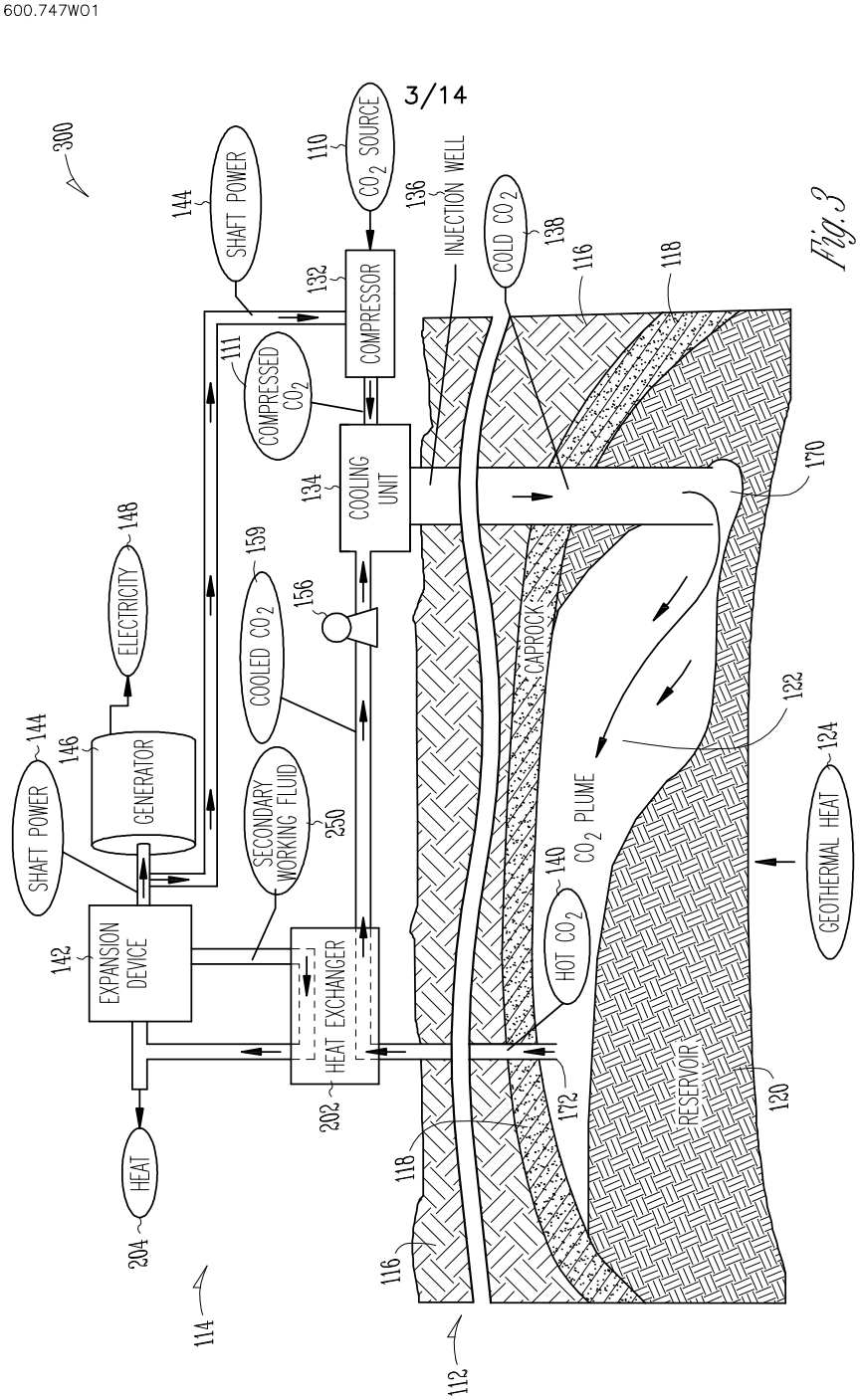

Figure B.3: A simplified schematic diagram of another alternative energy generation system according to an embodiment of the invention.

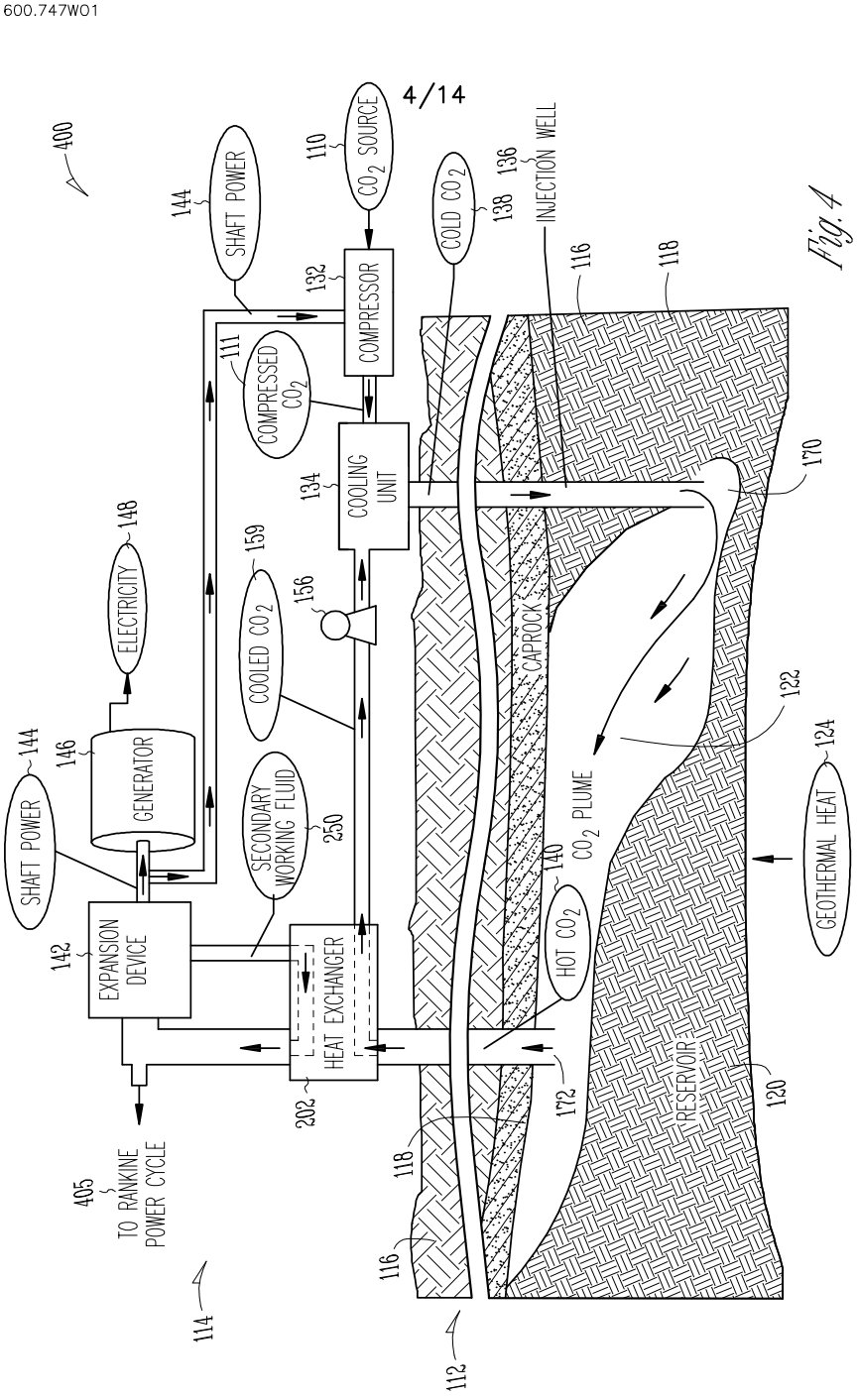

Figure B.4: A simplified schematic diagram of yet another alternative energy generation system according to an embodiment of the invention.

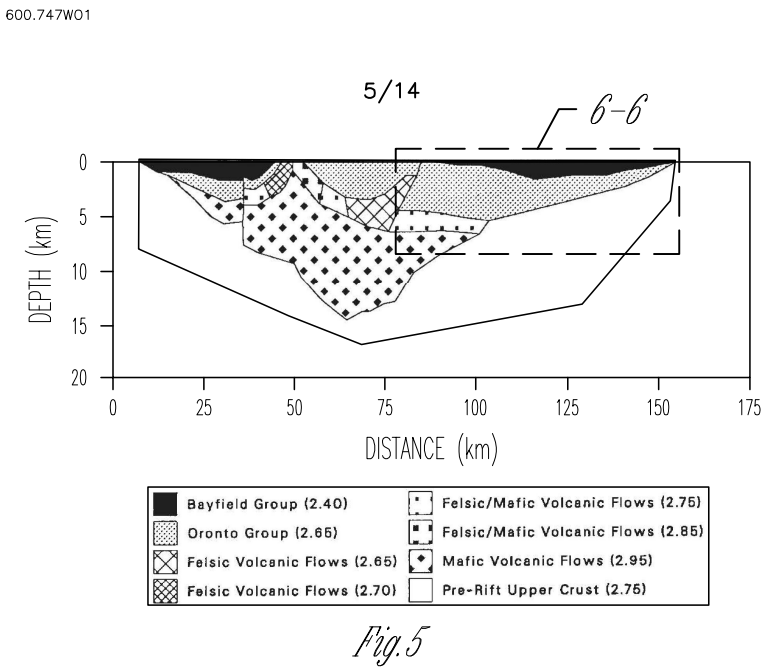

Fig. 5

Figure B.5: A cross-section of Minnesota's Rift System (MRS).

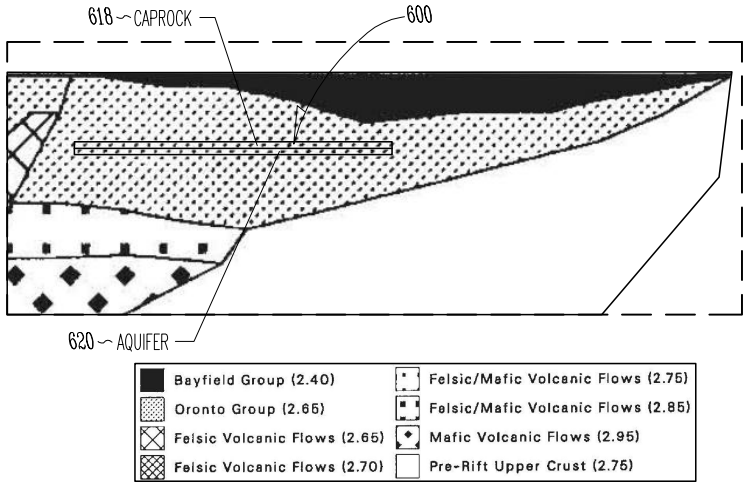

Fig. 6

Figure B.6: An enlarged view of a portion of Figure B.5 taken from within box 6-6 according to an embodiment of the invention.

600.747WO1

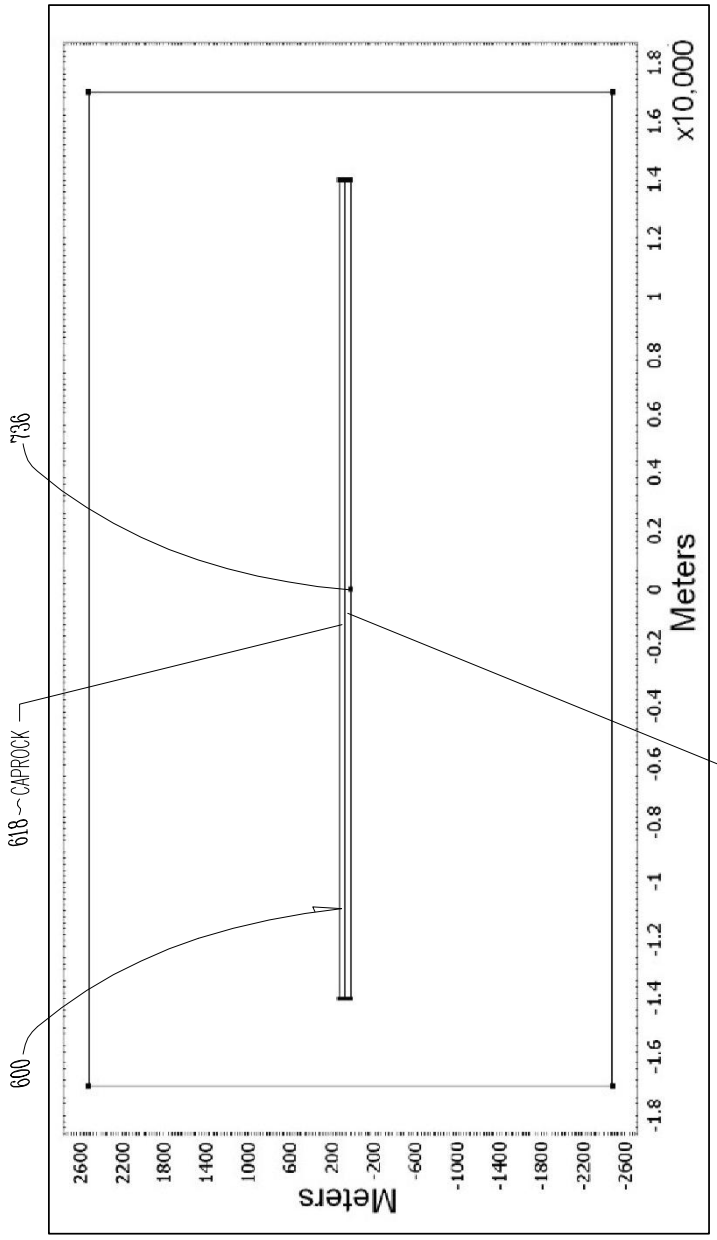

Fig. 7

Figure B.7: An illustration of a geological structure used for a numerical model of a power generation system according to an embodiment of the invention.

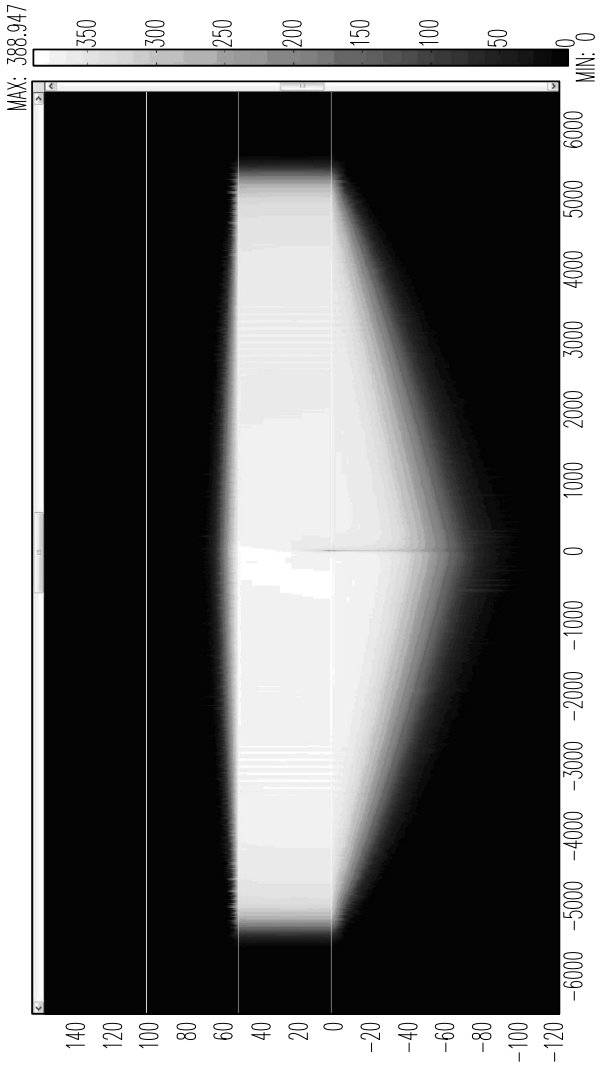

Fig.8

Figure B.8: A geological model showing dimensions and solute concentration according to an embodiment of the invention.

600.747WO1

8/14

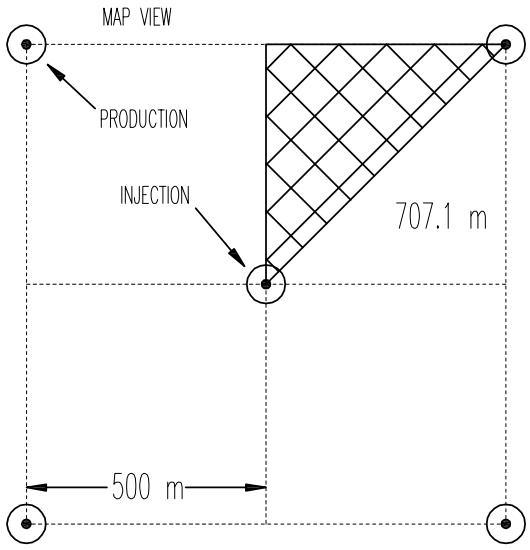

Fig.9

Figure B.9: An illustration of an exemplary geometrical configuration according to an embodiment of the invention.

600.747W01

9/14

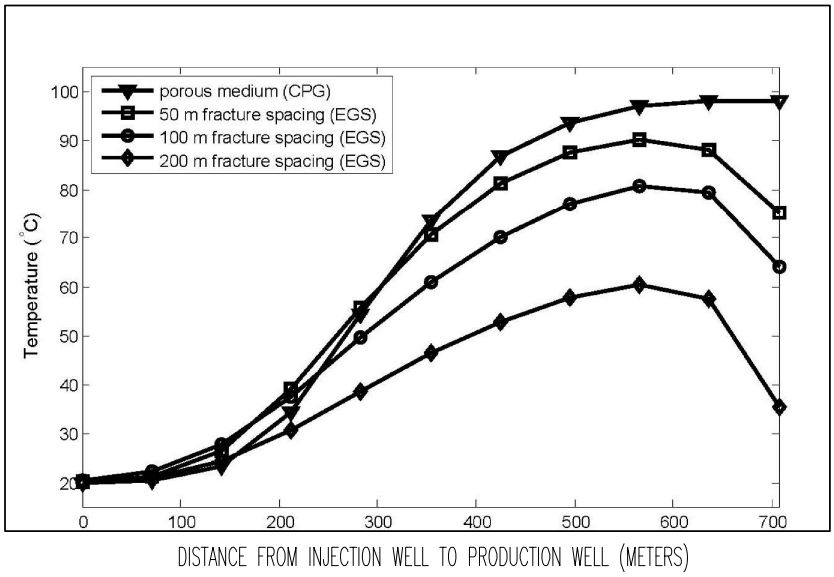

Fig. 10

Figure B.10: A graph showing temperature versus distance from an injection well to a production well for a porous medium in a carbon dioxide (CO_2) plume geothermal (CPG) system and various fracture spacings in an enhanced geothermal system (EGS) system according to an embodiment of the invention.

600.747W01

10/14

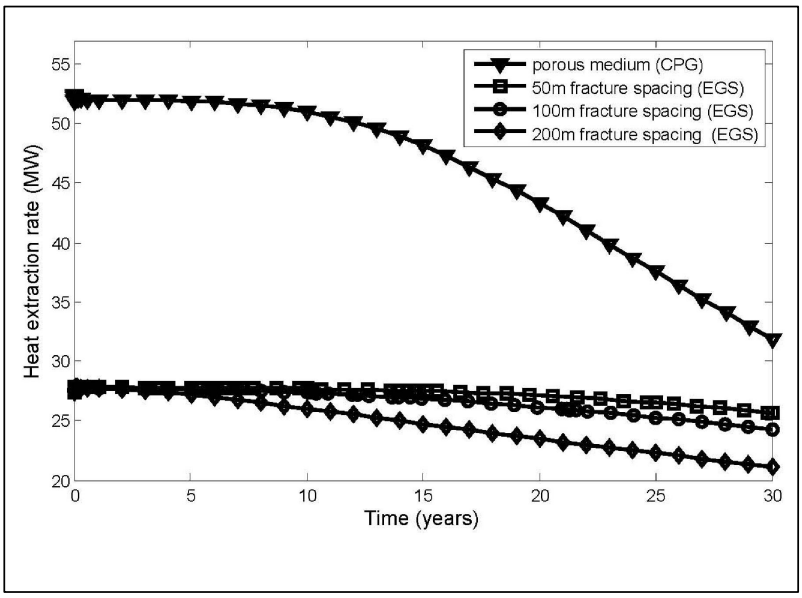

Fig. 11

Figure B.11: A graph showing heat extraction rate versus time for a porous medium in a CPG system and various fracture spacings in an EGS system according to an embodiment of the invention.

600.747W01

11/14

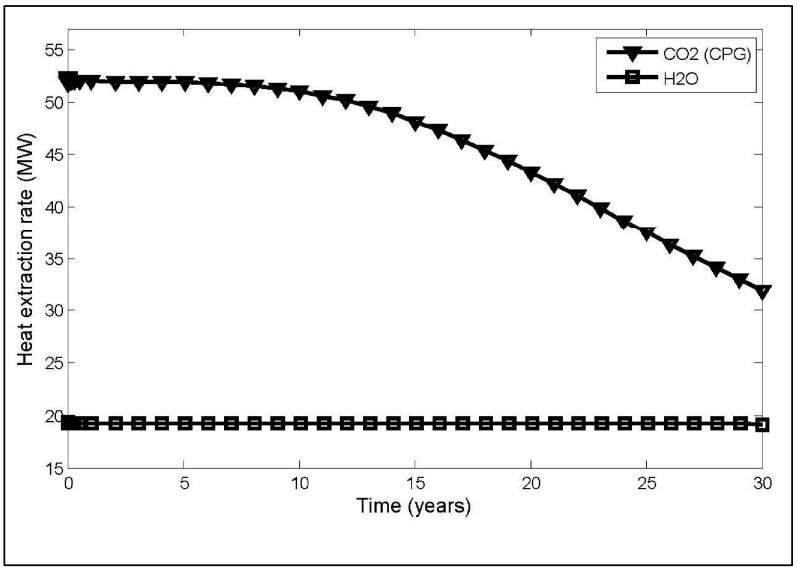

Fig. 12

Figure B.12: A graph showing heat extraction rate versus time for a CPG system as compared to a water system according to an embodiment of the invention.

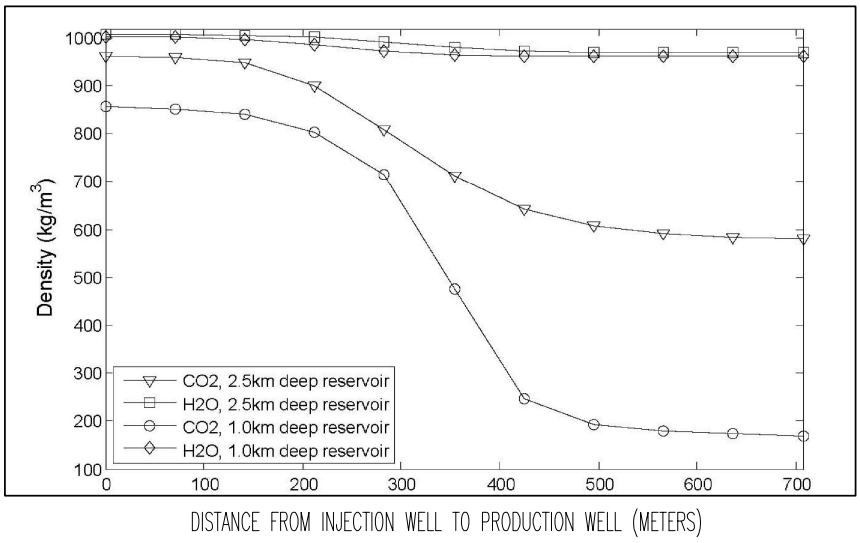

Fig. 13

Figure B.13: A graph showing density versus distance from injection well to production well for a CPG system as compared to a water system according to embodiments of the invention.

600.747W01

13/14

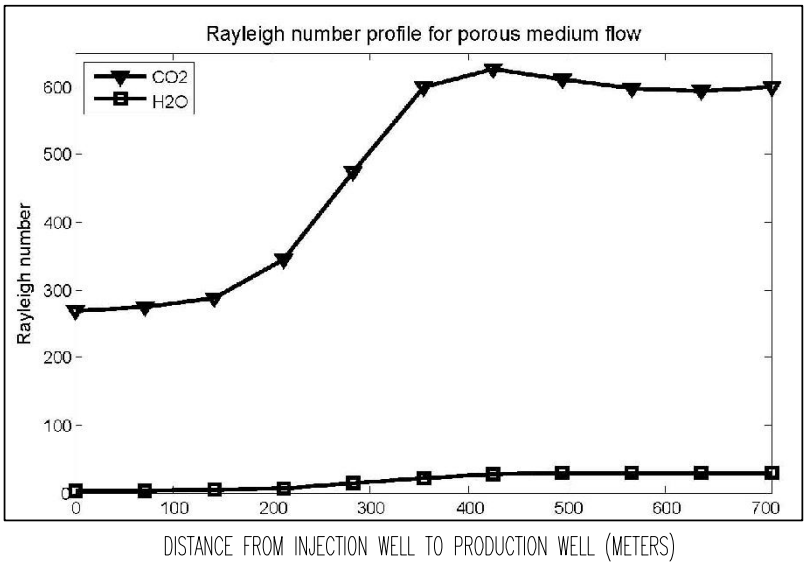

Fig. 14

Figure B.14: A graph showing Rayleigh number versus distance from injection well to production well for a CPG system as compared to a water system according to an embodiment of the invention.

600.747WO1

14/14

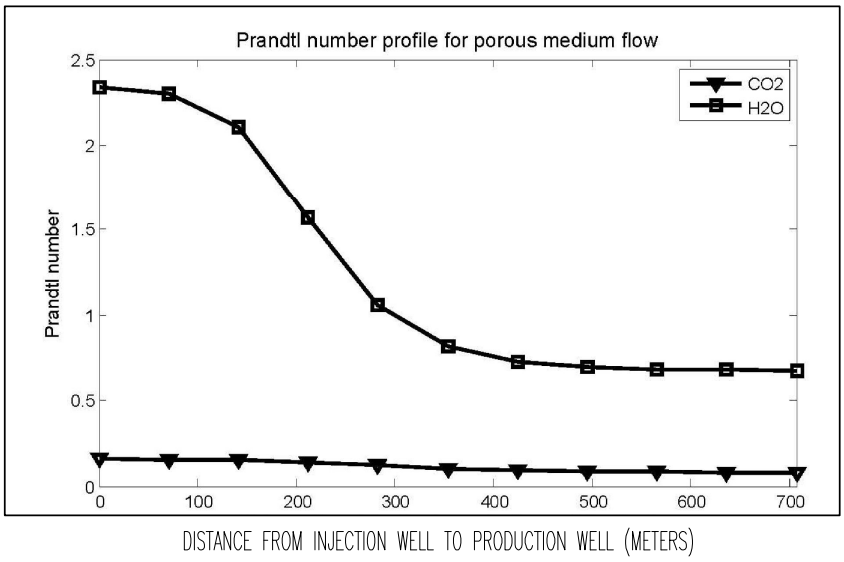

Fig. 15

Figure B.15: A graph showing Prandtl number versus distance from injection well to production well for a CPG system as compared to a water system according to an embodiment of the invention.

Appendix C

Preliminary Numerical Modeling of CO_2 Injection and Storage in Deep Saline Aquifers: Current Research, Scenarios, and Required Data

This chapter is largely based on Randolph and Saar, 2008 [35].

C.1 Introduction - The Purpose of Numerical Modeling of CO_2 Injection and Storage

Numerical modeling is an essential element of the process of determining whether an aquifer is a good candidate for CO_2 injection, of the risk assessment associated with injection, and of injection itself.

CO_2 injection and storage in deep saline aquifers falls naturally in the geosciences, with its study encompassing the disciplines of hydrogeology (CO_2 and aquifer brine fluid flow, heat flow, and solute transport), geochemistry (reactions among injected

CO_2, brine, and rock), geodynamics (subsurface pressure changes associated with injection, compression, and fracturing), as well as seismology and geophysics (both essential for gaining information about subsurface structures via seismic, electromagnetic, and gravity studies). Numerical modeling provides the framework for linking these different disciplines and determining how the various geologic conditions and processes within the CO_2 injection and storage problem affect the feasibility of the whole project.

Comprehensive experimental investigations of deep geologic processes are difficult, if not impossible, and expensive because of associated depths and the large, three-dimensional spatial extent requiring investigation. In addition, due to often complex feedback mechanisms that can act over long time spans, temporal effects of CO_2 injection would have to be studied in the field for up to thousands of years after (experimental) injection ceases (explained further in later sections). Clearly, such long durations of experimental investigation are impractical. Furthermore, detailed first-hand observation of deep aquifer behavior is typically impossible and remote observation techniques (e.g., equipment in deep wells, seismic/gravity/electromagnetic surveys) are expensive but provide essential (yet indirect) information of subsurface conditions. While the expense of some experimental studies is fully justifiable if a subsurface region appears promising for CO_2 injection and storage, viability of such experimental analysis cannot be determined without some initial study.

Numerical modeling of CO_2 injection and storage, while not without its own limitations that are predominantly caused by limited geologic information (as explained below), is a promising method for completing such initial - as well as subsequent - investigations. In fact, exploration of geologic parameters, numerical modeling based on those parameters, and field experiments complement each other. Each of these three approaches provides necessary background information for the next, more detailed level of study conducted by the other approaches. This iterative process of geologic exploration, numerical modeling, and field tests should then be continued until reasonable, predefined confidence levels regarding the feasibility of CO_2 injection and storage have been reached.

At the very start of a CO_2 injection and storage project, numerical modeling permits analysis of whether a particular deep saline aquifer (our proposed storage method, as explained later) holds promise for storage. From there, numerical models can be

developed to test a variety of injection and storage scenarios for ranges of geologic parameters and their three-dimensional distribution. Storage aquifer and surrounding unit characteristics can be modified as desired and as information from drilling, seismic studies, and other methods becomes available. This approach permits ever improving approximations of how actual CO_2 may behave upon subsurface injection. Models can be developed to assess the risks (e.g., CO_2 leakage, induced seismicity, effects on other aquifers) associated with CO_2 injection, aiding risk minimization in actual projects. Finally, numerical models allow assessment of long term (hundreds to thousands of years) behavior of injected CO_2, far beyond what physical experiments permit. Thus, while numerical models can only be as good as the (always limited) three-dimensional subsurface geologic information provided as input from field measurements, they are ultimately a key method in determining complex, spatially expansive, and long-term subsurface processes and behaviors, such as the effects of CO_2 injection and storage in geologic formations.

Geologic storage of CO_2 generally refers to permanent CO_2 trapping in oil reservoirs, coal beds, or deep saline aquifers. CO_2 injection into oil reservoirs helps maintain reservoir pressure thus improving oil recovery, and because such reservoirs trap oil, they readily store CO_2. CO_2 injected into coal beds bonds to coal, resulting in release of the methane that is typically bound to coal, which can be captured. Saline aquifers, described in detail in the next section, permit CO_2 trapping by a variety of mechanisms including dissolution of CO_2 into aquifer fluid and precipitation of carbon-containing minerals. Both oil reservoir and coal bed storage are profitable CO_2 reduction strategies, and oil reservoir CO_2 injection has been practiced for over 30 years [97]. Injection of CO_2 in saline aquifers, however, is purely a reduction strategy. Then why consider saline aquifer storage? Of the three geologic storage scenarios, only deep saline aquifers are abundant and large enough to trap a significant fraction of global emissions from fossil fuel power plants [98]. Considering global CO_2 emissions through 2050, coal beds worldwide could store approximately 2% of emissions (40 to 150 billion tons, or Gtons), oil reservoirs could store approximately 42% of emissions (up to 920 Gtons), and saline aquifers could store approximately 500% of emissions (up to 10,000 Gtons [98]. Furthermore, saline aquifers are very prevalent worldwide, offering favorable proximity to large CO_2 sources; oil reservoirs and coal beds, by comparison, are sparsely distributed.

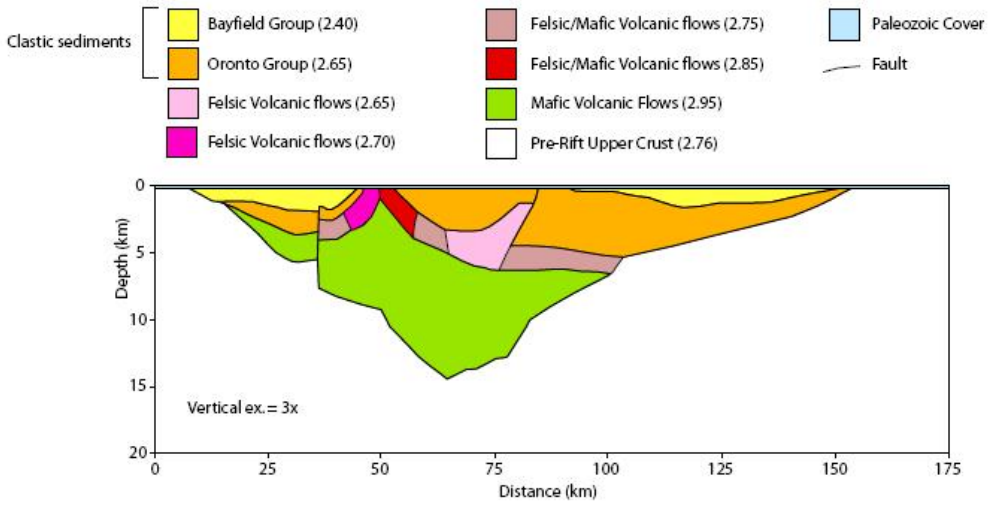

Figure C.1: An approximate/generic cross section through the Mid Continental Rift System in Minnesota, provided by the Minnesota Geological Survey. The geologic units of interest for CO_2 injection and storage are the Bayfield and Oronto groups.

Because of the significant advantages of geologic CO_2 storage via deep saline aquifers, the following discussion of numerical modeling of CO_2 injection and storage is primarily constrained to this method.

C.2 Currently Used Procedures for Numerical Modeling

Recent numerical modeling of CO_2 injection and storage has been accomplished using a variety of techniques; both individual, detailed aspects of the process (e.g., CO_2 leakage around abandoned wells or chemical reactions associated with CO_2 injection into a brine) and simplifications of entire injection scenarios are being modeled. In what follows, we describe a selection of recent literature regarding modeling of CO_2 injection and storage in deep saline aquifers, including much that is in progress.

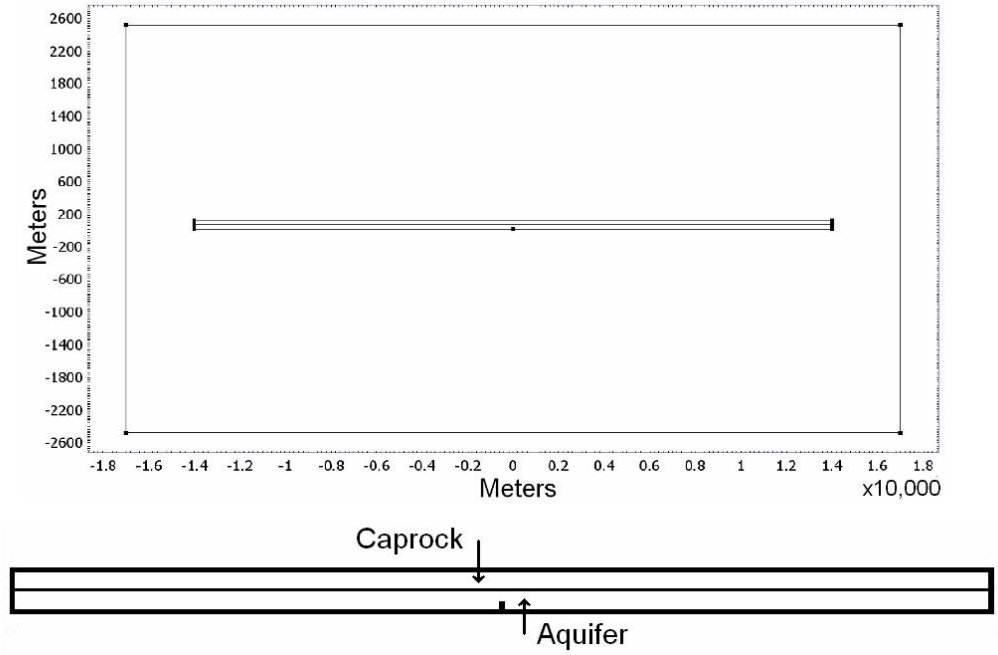

Figure C.2: At top is the geologic structure used in the stage 1 numerical model. A long, thin aquifer is placed below a capping rock of similar shape and both are imbedded in a surrounding material. At bottom is an expanded view of the aquifer and caprock.

C.2.1 Numerical modeling of multiphase fluid flow

We begin by describing the basic geologic structure of a potential CO_2 storage aquifer (Figures C.1 to C.2). An aquifer is a porous, permeable geologic unit containing water. Porosity is the fraction of aquifer space that is not rock; the more porous a rock, the more fluid (liquid or gas) the rock can hold. A porosity of 0.30 (i.e., 30%) indicates a very porous rock and one that would be excellent for CO_2 storage, if its permeability is high as well. Permeability is a measure of how readily a material allows fluid to pass through itself. Porous rocks do not necessarily have high permeabilities - for example, a rock with abundant but unconnected pores would have a low permeability and thus would not facilitate fluid flow through it. While higher porosities tend to result in higher permeabilities, this trend does not always hold true (e.g., [99]). As far as CO_2 injection, flow, and storage are concerned, a porosity of at least 0.04 (i.e., 4%) and a permeability

of at least 10^{-13} m^2 is currently considered reasonable for a CO_2 storage aquifer while permeabilities of 10^{-20} m^2 or less permit essentially no fluid movement (e.g., [100]). It may be possible to store CO_2 in lower porosity and permeability formations than those mentioned above, however, significantly more fundamental (computer modeling and field testing) research regarding injection schemes, rock hydrofracturing methods, reactive CO_2 flow modeling, and other approaches must be conducted to test such hypotheses. A recent Department of Energy (DOE) Office of Science workshop report entitled "Basic Research Needs for Geosciences: Facilitating 21st Century Systems" (published in July 2007) illustrates some of the basic science and engineering research necessary to better understand CO_2 injection and storage in the subsurface. The proposed 3-year computer simulation budget in Section with research conducted at the University of Minnesota, a public university, would allow such necessary fundamental research as well as applied research that is specific to CO_2 injection and storage in the Mid-Continental Rift System in Minnesota.

In a CO_2 storage scenario, one desires to permanently trap CO_2 in the subsurface. To accomplish this, storage aquifers must have virtually impermeable capping (or sealing) rocks above them. To complete the basic geology, the aquifer and caprock are encompassed by some surrounding material.

CO_2 storage in a deep saline aquifer is inherently a multiphase problem and hence, multiphase modeling is a principle aspect of CO_2 storage modeling. 'Multiphase' indicates that the aquifer system has more than one fluid present, in this case the naturally occurring aquifer brine (highly salty water, greater than 10,000 ppm solutes, which is the EPA drinking water maximum [101]), supercritical CO_2, and gaseous CO_2. A supercritical fluid is a fluid at sufficiently high temperature and pressure that it is neither a liquid nor a gas, though it behaves very similar to a liquid. The supercritical state of CO_2 is beneficial for storage because CO_2 in this state is considerably denser than gaseous CO_2, permitting storage of larger quantities of CO_2 in a relatively small volume. To achieve pressure and temperature conditions at which CO_2 is supercritical, depths of at least 800 m ($\tilde{2}$500 ft) are necessary; thus, deep aquifers are commonly proposed for CO_2 injection and storage. Furthermore, most drinking water supplies are relatively shallow while deep aquifers tend to have salinity far beyond drinking standards. Consequently, proposed CO_2 storage aquifers are typically deep and saline even though

salinity is not required for storage. Salinity will, however, affect fluid-mineral reactions in these aquifers. Finally, deep saline aquifers are prevalent worldwide and, therefore, could provide substantial CO_2 storage without directly interfering with drinking water supplies (that is, assuming no CO_2 leaks upwards from injection aquifers into overlaying fresh-water aquifers, which is discussed in Section 2).

Modeling of multiphase fluid flow in a porous medium (i.e., material that contains a certain fraction of open space and the remainder is solid, such as most rock) is more complex than single phase flow modeling because in addition to the interactions between fluid and the rock matrix, fluid-fluid interactions must be simulated. While considerable fundamental research is required to improve our understanding of multiphase flow processes, particularly with respect to CO_2 injection and storage as mentioned previously, a large body of work is already available concerning the multiphase fluid flow aspects of CO_2 injection and storage in deep (saline) aquifers. We note some of the work in this section, and considerably more falls naturally into subsequent sections.

With sufficient simplifications - a homogeneous (aquifer composition is constant throughout space), isotropic (aquifer properties are the same in all directions), and perfectly horizontal aquifer; no capillary forces (described in detail in later sections); no deformation of geologic units following injection - the multiphase fluid flow behavior of CO_2 injection and storage can be modeled analytically (e.g., [40]). Here, 'analytical' refers to the methodology of finding/developing exact mathematical solutions without requiring approximations; approximations are common with numerical modeling approaches. Analytical methods can provide upper bound estimates for post-injection pressure buildup and spread of injected material (e.g., [40]). Furthermore, they can be used to estimate displacement of native brine (e.g., [102]). However, because of the simplifying assumptions required to find analytical solutions, analytical models cannot capture all complex multiphase behavior. Real-world multiphase systems are prone to feed-back mechanisms where the outcome of such interactive processes is often considerably different from expectations at the outset or from results provide by necessarily simplified analytical models. Therefore, for the majority of real-world systems, numerical models are needed to approximate a range of possible outcome scenarios. Hence, while inexact and strongly dependent on the quality of field-measured input parameters, numerical models can often provide upper and lower bounds as well as estimates

of average behaviors and process outcomes. Such bounds and mean values help in the development of best/worst case scenarios and anticipated average system behavior.

The vast majority of numerical models related to CO_2 storage have focused on the behavior of injected CO_2 as opposed to the native brine in a deep saline aquifer. However, the brine must also be considered as it is displaced by the injected CO_2. Birkholzer et al. [103] are currently modeling brine flow using a radially symmetric geology and a 30-year, 1.5 million tons of CO_2 per year injection scheme that is followed by 70 years of non-injection fluid flow. This approach is similar to many other numerical modeling scenarios (e.g., [104], [105]). Displaced brine flows toward natural aquifer outlets and is accommodated by aquifer pore space provided by pore and brine compressibility, by caprock pore space, and by leaks in sealing units. Thus, aquifer, caprock, and fluid compressibility - none of which are included in simple models - as well as accurate approximations of caprock permeability and porosity are necessary to estimate brine flow. Birkholzer et al. [103] found that lateral brine velocities induced by CO_2 injection are of similar magnitude to natural groundwater flow velocities, suggesting that brine displacement will not affect injection regions.

C.2.2 Modeling of physical CO_2 trapping

Immediately following CO_2 injection, CO_2 is trapped in deep saline aquifers primarily by stratigraphic trapping. Supercritical CO_2 is less dense than saline brines, so CO_2 floats above the brine. Because the caprock above an injection aquifer is impermeable, injected CO_2 pools against the bottom of the caprock; this is known as stratigraphic trapping. Numerous numerical models (e.g., [106], [101], [107]) capture this behavior. As time progresses, other physical trapping mechanisms become important.

For example, capillary forces contribute to permanent trapping of CO_2 in saline aquifers. In a system with multiple fluids, one fluid may improve or limit the ability of another fluid to move through a material. As such, the interface between fluids is not a sharp line. In the case of CO_2 injection into a brine, at the CO_2/brine interface, capillary forces draw CO_2 into the brine in shapes resembling fingers (a process thus known as fingering). While CO_2 injection maintains high pressures behind the CO_2 interface, these 'fingers' may move through an aquifer faster than the interface. But after injection ceases and pressures stabilize, capillary forces tend to trap and permanently

store CO_2 at the interface [108]. Including capillary forces in a numerical model can increase model computation time significantly; however, this process is included more frequently in CO_2 storage simulations (e.g., [108]).

In addition to permanently trapping CO_2 along the injection interface, capillary forces contribute to residual trapping. Following CO_2 injection, the shape of the CO_2 plume evolves as brine displaces CO_2 and injected CO_2 displaces brine. This behavior is particularly prominent in an aquifer with some angle to the horizontal (which most natural aquifers have) in which buoyancy forces move CO_2 up the inclined aquifer. When brine displaces CO_2, capillary forces trap a percentage of CO_2 in pore space; hence, this behavior is of interest in current numerical modeling of CO_2 storage [109].

The percentage of CO_2 stored by residual trapping is debatable. A more substantial means by which CO_2 is trapped permanently in brine is solubility trapping - CO_2 dissolves into brine at a CO_2/brine interface and is thus stored in the aquifer. This type of trapping is considered permanent because deep saline aquifers tend to have lengthy residence times, that is, brine frequently stays in these units for long periods of time (several thousand years). Numerical models have found that more than 25% of injected CO_2 can be permanently trapped in this manner (e.g., [110]). Solubility trapping is relatively fast, making it the dominant and thus a very important form of permanent trapping immediately following injection. To note, the solubility of CO_2 in water - which is salinity-dependent - is much less than its solubility in oil. Therefore, CO_2 injected in a saline aquifer below an oil reservoir will rise (if not trapped in the aquifer) until it reaches the oil where it likely becomes permanently trapped. Numerical studies (e.g., [110]) are currently investigating the effectiveness of oil reservoirs as permanent CO_2 traps in this manner, though far fewer regions include such dual aquifer and oil reservoir systems than saline aquifers alone.

C.2.3 Reactive transport modeling

A significant aspect of modeling CO_2 storage in deep saline aquifers is the modeling of chemical reactions that occur following injection. However, as these are not a key component of this dissertation, they are not discussed here.

C.2.4 CO_2 leak assessment modeling

Methods of investigating deep geologic structures can sample only a small percentage of a potential CO_2 storage reservoir rendering CO_2 leak assessment a challenging problem. Reasonable estimates of the CO_2 storage viability of natural units in themselves may be provided. However, the effects of human-made reservoir perforations, namely by deep wells, can be more difficult to quantify. While deep wells can potentially provide high-permeability CO_2 pathways to the ground surface, the effective integrity of abandoned wells, their casing materials, and their plugs are often poorly constrained. In regions with high concentrations of abandoned deep wells, such as oil fields, it is essential to model the effects of injected CO_2 on the integrity of well systems and the potential for CO_2 leakage around such wells. Numerical-analytical hybrid models (e.g., [39]) have been developed to study well leakage; additional work is ongoing. To note, CO_2 storage projects in the Mid Continental Rift System are at a considerable advantage in this respect to many other storage projects in development worldwide because the rift is not punctured by numerous deep wells whereas most other sites are in (or near) explored oil fields.

Leakage modeling must also be concerned with pore-fluid pressure changes because injection into an aquifer alters the aquifer's rock matrix stress field, generally resulting in increased pore-fluid pressures. Pore-fluid pressure refers to the pressure exerted by the fluid in an aquifer's host rock on the rock matrix. Changes in pore-fluid pressure can induce fault slip (e.g., [92]) on pre-existing faults or fracture an aquifer or sealing unit rock (referred to as hydrofracturing), resulting in leakage if faults or fractures act as high permeability pathways for injected CO_2. Birkholzer et al. [103] model pore-fluid pressure build-up in a deep saline aquifer following CO_2 injection. He notes that build-up is highly dependent on caprock permeability, aquifer and caprock compressibility, and fluid compressibility, with pressure build-up tending to extend beyond the extent of a CO_2 plume. Other recent modeling (e.g., [111]) seeks to determine CO_2 injection pressures required to induce fault slip or rock fracturing as well as estimate safe pressure ranges. To develop a useful pressure-inclusive CO_2 injection model, the pre-injection rock stress and pore-fluid pressure field of an aquifer and caprock need to be known from field measurements at aquifer depths.

While fracturing can cause CO_2 leakage, minor fracturing can improve the storage

potential of an aquifer (e.g., [111]). If pore-fluid pressure variations following CO_2 injection cause minor aquifer fracturing, aquifer permeability might increase, improving transport of CO_2 away from an injection site and increasing storage potential.

C.2.5 Comprehensive modeling

As the previous discussion suggests, considerable modeling of the various elements of CO_2 injection and storage has been completed. Additionally, some work has integrated individual elements to create more comprehensive models with real-world geologic geometries. For example, Kim [112] developed a fully coupled multiphase thermo-hydro-mechanical numerical model of CO_2 storage. This model accounts for CO_2 flow, heat transport, and ground deformation.

The work of Xu and Pruess [105], for example, couples multiphase fluid flow with reactive transport permitting examination of CO_2 flow, formation of aqueous species, and mineral precipitation. However, their work uses very simple, radially symmetric injection aquifers and sealing units. Wang et al. [113] models heat transport in addition to reactive transport and multiphase fluid flow, as do Xu et al. [101]. In the work of Wang et al. [113], groundwater density and viscosity are dependent on chemical composition and chemical reactions are temperature dependent (to note, most models assume the simplified case of constant temperature). Further, precipitation of minerals from solution and dissolution of host rock affect aquifer porosity and permeability in addition to hydrodynamic dispersion (essentially the spreading of a solute), all of which are necessary for inclusive modeling scenarios.

Comprehensive numerical modeling of CO_2 injection and storage incorporates several geologic fields - hydrogeology (multiphase fluid, solute, and heat flow); geochemistry (chemical reactions); geodynamics (host rock stress and pore-fluid pressure build-up, hydrofracturing, and rock matrix deformation); and seismic and geophysical studies (to gain information about deep geologic structures) - resulting in a complex but interesting problem. Extensive modeling has been completed to date but much has yet to be done, particularly, combining individual fields into fully inclusive, thorough numerical models. Such models, for specific sites where field-measured model input data are available, would improve the previously mentioned upper and lower confidence bounds regarding the amount of possible geologic CO_2 injection and storage as well as associated risks

and costs.

C.3 Modeling Scenarios and Information Required

Due to the necessary integration of numerous geologic processes, modeling CO_2 injection and storage is complex and is made more so by the natural variability of geologic structures. As such, numerical modeling should begin with very simplified injection scenarios and geologic units, gradually evolving as information regarding geologic structures becomes more abundant and realistic and as different types of model parameters are added. At each stage in the modeling process, we gain additional information about the storage reservoir and injected fluid and, eventually, obtain a general sense of how CO_2 will behave following injection.

For much modeling, we restrain our geologic units to two dimensions for simplicity. The third dimension adds considerable complexity and computation time to models while without variation of parameters (e.g., aquifer or brine characteristics) in this dimension, no additional information can be gained from modeling the third dimension. Thus, except where noted, modeled geologic units extend vertically and in only one horizontal direction, i.e., they represent a vertically oriented, two-dimensional cross section through a potential injection region.

In the following, we provide the principal stages - with increasing complexity - involved in an ultimately comprehensive numerical modeling program for CO_2 injection and storage.

C.3.1 Stage one - CO_2 solute transport in porous media

Model with impermeable caprock: In the simplest case, the behavior of a solute (here CO_2) dissolved in water and injected into a pure water aquifer is investigated. The information required by the model is aquifer permeability and porosity, injection rate and duration, solute concentration, and aquifer geometry; each of these parameters can be varied as desired. The aquifer is assumed to be homogenous (porosity and permeability are constant throughout space), isotropic (permeability is direction independent), of constant thickness, and horizontal.

A solute rather than pure CO_2 is injected because solute flow behavior is much

simpler. Recall that for deep saline aquifer storage, CO_2 exists as a supercritical fluid and, hence, requires a multiphase model. For initial modeling, the aquifer system is simplified by using a single fluid phase.

The geology consists of an aquifer alone - a long, thin unit in which water is allowed to flow through the sides but not the top or bottom. This is a reasonable first approximation for a CO_2 storage aquifer because any potential storage unit is capped (at the top) by an essentially impermeable rock, is large (several kilometers to several hundred kilometers in some direction), and discharges fluid far from CO_2 injection points. Furthermore, aquifers are typically relatively thin (tens of meters) compared to their horizontal spread. At this stage of detail, tilting the aquifer does not provide significant new information. Finally, were pure CO_2 injected, it would rise to the top of the aquifer, affirming the assumption of no-leakage through the bottom of the aquifer.

A solute, which is sufficiently dilute (1% CO_2, the remainder water) to permit solution of the solute transport equations, is injected in the center of the aquifer. The solute is weight-equivalent to pure CO_2 and is adjusted to equal in quantity the amount of CO_2 produced by a coal-fired power plant (of any desired size). Injection progresses for several years (e.g., 25 years), and the solute is tracked for many years thereafter (e.g., 75 years or even hundreds of years). From this model it is possible to determine the simplified transfer and dispersion (i.e., spreading) of injected material with time. Thus, with field-measured data for aquifer permeability, porosity, and geometry, one can develop a first, rough estimate as to whether an aquifer may be feasible for considerable, long-term CO_2 storage.

Model with caprock of finite permeability: To investigate CO_2 leakage following injection, the model geology is expanded to include a caprock above the injection aquifer and material surrounding the aquifer and caprock units. This model requires input data regarding the permeability, porosity, thickness, and extent of the aquifer, caprock, and surrounding material. Injection modeling then continues as in the previous case but with fluid flow permitted through the top and bottom of the aquifer (not, however, the top and bottom of the surrounding material) so that potential leakage can be observed. Caprock permeability and porosity are varied to evaluate their impact upon CO_2 leakage. Thus, in addition to CO_2 transport, this model imparts a sense of the possible extent of solute leakage. With data including caprock structure above

an aquifer of interest, this model refines estimates of whether regional geology permits effective CO_2 storage. However, this model also requires significantly more field data from deep boreholes and other geologic and geophysical surveying techniques than the previous model.

C.3.2 Stage two - multiphase fluid flow in porous media

Injection of pure CO_2: Injecting a CO_2 solution rather than pure, supercritical CO_2 restricts the applicability of a numerical model, the primary limitations arising from low solute concentration and lack of multiphase behavior. Concerning the former, because we are injecting a solution, much more material is injected than in the case of pure CO_2. Regarding the latter, multiphase flow is different from, and more varied than, solute transport. Thus, the model evolves by replacing injection of a solute with pure, supercritical CO_2 injection.

As with all fluids, the density and viscosity of supercritical CO_2 depend on pressure and temperature. In addition to the information necessitated by the previous model, in the current case of multiphase modeling, the injection depth within the aquifer (which provides pore-fluid pressure) and the local geothermal gradient (the change in temperature with depth below ground surface, providing temperature at injection depths) are required - note that because of the latter, a borehole temperature-versus-depth measurement device is included in the modeling budget. Further, the aquifer's brine density and viscosity, parameters that depend on brine composition (as well as on pressure and temperature), are needed and determined using water samples taken from deep boreholes.

In a multiphase model, pure CO_2 is injected into a saline (i.e., salt-containing) aquifer - in quantities equal to those produced by fossil fuel power plants - and allowed to spread as in the solute models. At this stage, the brine (water plus salt) and CO_2 are assumed immiscible, i.e., they do not mix. This model provides an improved picture of aquifer storage capacity, the horizontal spread of CO_2 with time, and a caprock's ability to serve as a CO_2 barrier (stratigraphic CO_2 trapping). Additionally, local variations in caprock permeability can be included, simulating fractures or wells penetrating the caprock and causing CO_2 leaks.

Brine-CO_2 miscibility: Immiscibility of brine and CO_2 restricts the previous

model's applicability because brine and CO_2 are in fact miscible. This CO_2 dissolution in brine is a primary means by which injected CO_2 is permanently stored in a saline aquifer (solubility CO_2 trapping). Thus, improved models allow brine/CO_2 miscibility, which depends on brine salinity. Relative permeability - the permeability experienced by one fluid as the other fluid facilitates or limits its movement through the aquifer matrix - now becomes important and is non-trivial. In addition to the information provided in preceding models, this modeling environment reveals the quantity of CO_2 stored by different trapping mechanisms as a function of time. Stratigraphic trapping tends to be the primary storage mechanism immediately following injection, but it may not be permanent as buoyancy forces may cause CO_2 leakage through a caprock with finite permeability. In contrast, solubility trapping, following stratigraphic trapping, provides permanent storage.

C.3.3 Stage three - reactive transport coupled to multiphase fluid flow

Three dimensional models: Once a multiphase model is developed, much of the behavior of injected CO_2 in a deep saline aquifer can be deduced and an aquifer's storage potential may be estimated. If additional information in the third dimension is available - for example, regarding aquifer/caprock porosity, permeability, host rock composition, or geometric variations; brine parameters; and/or geothermal/pressure gradients - the model can be expanded from two to three dimensions. As discussed in the following paragraphs, numerical modeling is expanded to include reactive transport, rendering models more representative of the real world and providing new information relevant to an aquifer's CO_2 storage potential.

Reactive transport in the form of host-rock dissolution and mineral precipitation: Because CO_2 in solution increases water acidity, reaction modeling necessarily includes rock dissolution and, hence, requires pre-injection aquifer and caprock composition. Furthermore, brine composition is required because, as CO_2 and rock minerals move in and out of brine and as brine pH changes, composition-dependent reactions and mineral precipitation occur. Reactions arise within days of injection, yet significant mineral trapping of CO_2 can take hundreds to thousands of years [104]. Thus, reactions such as rock dissolution, mineral precipitation, and associated transport of elements and minerals within brine are spatially and temporally variable, providing

a challenging CO_2 storage simulation problem.

Using the final multiphase model from the previous section, multiphase flow is now coupled with reactive transport. Fluid flow proceeds similar to before, though permeability and porosity can now change as a result of host rock dissolution and mineral precipitation, altering flow patterns. To capture long-term reactions and precipitation, model runs need to represent several hundreds to thousands of years. This approach allows estimation of permanent CO_2 trapping via carbon-containing mineral precipitation (mineral trapping of CO_2). Further, this modeling stage allows evaluation of mineral precipitation in the vicinity of CO_2 injection wells. These numerical simulations may thus be employed to evaluate if brine and rock composition likely cause reactions that significantly decrease aquifer permeability near such wells and, hence, diminish the CO_2 injection and storage potential over time. Reaction models can also help refine assessments of a caprock's ability to serve as a CO_2 barrier. Specifically, they permit investigations of whether reactions following injection generate pathways for CO_2 through the rock or seal pre-existing pathways. With the development of reactive transport models, estimates of the CO_2 storage potential of deep saline aquifers can be significantly improved.

C.3.4 Stage four - additional model parameters

Hydrofracturing and capillary forces: A numerical model of reactive transport and multiphase fluid flow in porous media accounts for much of the post CO_2 injection behavior in a deep saline aquifer. As deep wells, seismic studies, and geophysical studies provide additional data concerning subsurface conditions, other parameters can be incorporated into models. For instance, with information on pre-injection host-rock stress and deformation, one can numerically investigate pore-fluid pressure changes and the possibility of resultant fracturing of a storage aquifer's host rock matrix. By simulating a variety of injection scenarios under a range of geologic conditions, modeling can help constrain fluid injection pressures that are unlikely to exceed such hydrofracturing thresholds. In addition, this type of so-called poroelasticity modeling allows estimation of aquifer matrix deformation (which occurs even without hydrofracturing) and associated possible land surface deformation, which is critical in evaluating if fluid injection

could affect human-made structures on the land surface. Additionally, including capillary forces into numerical models refines estimates of CO_2 migration with time and an aquifer's CO_2 storage potential via capillary trapping.

Heat flow: Finally, just as density and viscosity of supercritical CO_2 and brine are temperature-dependent, chemical reactions, dissolution, and precipitation rates depend on temperature. Thus, permitting heat flow (which, to note, also affects pore-fluid pressures and host rock stresses) in numerical models improves their real world applicability and accuracy, particularly with respect to buoyancy-driven flow and associated CO_2 migration over time. Therefore, we include in the numerical modeling budget resources for measuring temperature-versus-depth within boreholes.

As the discussed complexity of multiphase fluid flow and reaction behavior in a host rock suggests, numerical modeling is essential to the process of determining a deep saline aquifer's potential for CO_2 injection and storage and associated risks. From the simplest solute flow model through comprehensive models that incorporate hydrogeology, geochemistry, geodynamics, seismology, heat flow, and geophysics, each stage of the modeling process adds to our understanding of the CO_2 injection and storage process. The following section provides some preliminary modeling results through the beginning of stage two, conducted by the Hydrogeology and Geofluids research group in the Department of Geology and Geophysics at the University of Minnesota -Twin Cities.

C.4 Some Preliminary Numerical Models

To date, we have developed a set of very preliminary models, encompassing stage one and the start of stage two as described in Section 3, to start exploring the potential for CO_2 injection and storage in the Mid Continental Rift System in Minnesota (Figure C.1). As evident from the preceding section, developing a comprehensive CO_2 storage model for a given location requires considerable geologic and geochemical information. Unfortunately, relatively little geologic data exists for the Mid Continental Rift System through Minnesota and elsewhere. For the most basic numerical model, we require aquifer and caprock permeability, porosity, and thickness of the sedimentary units of interest for storage (the Bayfield/Oronto sandstone), all of which are most readily collected via deep wells. Few wells in Minnesota or elsewhere intersect these units at sufficient

depths for CO_2 injection. The data used in the following models is derived from deep boreholes in Iowa (the Iowa Deep Drilling Project) and relatively shallow sections of the rift in Minnesota (data provided by the Minnesota Geological Survey) that we assume for now is applicable to deep sedimentary units in Minnesota. Eventually, several deep boreholes to potential storage aquifers depths as well as other geologic surveying techniques (seismic, electromagnetic, gravity, etc.) will be required to better constrain input parameters for numerical models. To encompass the range of likely values for aquifer and caprock permeabilities and porosities, we model CO_2 injection numerous times, systematically varying aquifer and caprock parameters each time (a modeling procedure called exploring parameter space). Aquifer permeability varies from 10^{-20} to 10^{-13} m^2, aquifer porosity from 0.05 to 0.20 (i.e., 5 to 20%), caprock permeability from 10^{-21} to 10^{-18} m^2, and caprock porosity from 0.05 to 0.16 (i.e., 5 to 16%).

C.4.1 Stage one

We begin numerical modeling of CO_2 storage by building a two dimensional solute injection model - stage one in Section 3. The commercially available multiphysics modeling environment COMSOL is used. Figure C.1 shows a generic cross section of the rift system in Minnesota which was provided by the Minnesota Geological Survey (MGS). Because no deep wells exist in Minnesota to provide geometric configurations of aquifer and caprock units, we use the cross section only to verify that the estimated rift structure is sufficiently deep for CO_2 storage and estimate depths for storage units. Due to lack of measured data, we assume a rectangular aquifer that is 50 meters thick and several kilometers long (Figures C.2 and C.3). These parameters are adjustable as desired once better-constrained estimates are provided. At this stage, the model consists of the injection aquifer alone; fluid is allowed to flow through the sides but not the top or bottom of the unit. We inject a 1% CO_2 solute solution, with the solute weight approximately equivalent to supercritical CO_2 at a depth of 2500 m, in the center of the aquifer. The injection rate can be varied to approximate injection of all CO_2 produced by a large (e.g., 250 MW to 1000 MW) coal-fired power plant.

This model provides an extremely simplified CO_2 injection scheme from which we can upscale to a more realistic geometry immediately and when more detailed subsurface

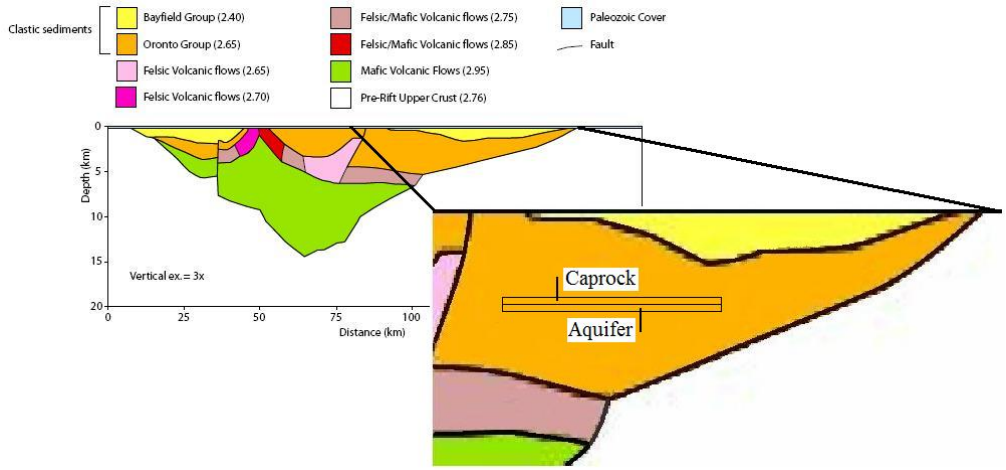

Figure C.3: A conceptual model of the aquifer and caprock structure we use for the initial stage 1 and stage 2 modeling. Because of the lack of information, we assume a long, thin aquifer below a capping unit. The aquifer is within one of the sedimentary units of the Mid Continental Rift System of interest for CO_2 storage and is at a depth sufficient for storage.

data is available. The model geology is expanded by placing a capping material, dimensionally equivalent to the aquifer, immediately above the aquifer. Then, the aquifer and caprock are encased in a surrounding material that extends vertically to the ground surface (with the aquifer at a depth of 2500 m) and horizontally several kilometers beyond the aquifer/caprock (Figure C.2). The extent of the surrounding material is chosen such that the upper and lower boundaries are far enough from the aquifer to assume no fluid flows across them while the left and right boundaries are sufficiently far to assume hydrostatic fluid pressure conditions (i.e., constant pre-injection fluid pressure conditions). The surrounding unit's permeability is 10^{-19} m^2 and the pore fraction is 0.04 (i.e., 4%), as provided by the MGS. Fluid flow is now permitted through the top and bottom of the aquifer to better approximate real-world conditions. Aquifer, caprock, and injection ranges are the same as the previous scenario.

This CO_2 injection model is developed to help us understand the spread of injected material with time and whether the capping unit could effectively seal the storage

aquifer. Ultimately, this model provides the first, very preliminary, indications concerning the viability of the Mid Continental Rift's CO_2 storage potential. We inject a solution for one year, choosing a relatively short time period because, when employing a solute (and not a pure CO_2) injection model, we inject considerably more material per year than an actual, pure CO_2 storage project would. The large injection volumes result from the necessity (for very simple models only) to maintain a dilute solution, as described previously. Therefore, the amount injected is equivalent to what would be injected by an actual CO_2 project over a much longer time period. Approximately 30 scenarios were run (see Figure C.4 for the visualization of a sample injection), varying injection rate and aquifer and caprock permeability and porosity (see Tables C.1 and C.2 for a summary of results). Our modeling indicates that the matrix permeability of potential caprock in the rift is sufficiently low, 10^{-21} to 10^{-18} m^2, to serve as an effective reservoir caprock (without consideration of fractures that would, however, increase caprock permeability). We also find that deep geologic sequestration would be possible in the strata of the rift if large sandstone bodies with porosities in the range 0.04 to 0.20 (i.e., 4% to 20%) and permeabilities in the range 10^{-15} to 10^{-13} m^2 (with uncertainty of approximately one order of magnitude) are eventually located in the rift at depths greater than 800 meters below a caprock with the above-described properties. The horizontal spread of solute modeled was generally less than ten kilometers from the injection point, a relatively small distance and interpreted in this initial study to indicate reasonable storage space for aquifers with the previously defined properties. Porosity of potential caprock units would need to be in the range 0.06 to 0.16 (i.e., 6% to 16%). Note that this range overlaps with that of aquifer porosity; our models indicate that porosity overlap is not problematic for CO_2 storage as long as caprock permeability is several orders of magnitude lower than aquifer permeability. Finally, our preliminary models indicate that a single injection well can support the injection of all the CO_2 produced by a 1000 MW coal fired power plant, given a subsurface system with the above-described characteristics is found.

To summarize, our results are very preliminary but suggest that potential CO_2 storage bodies will have to have a minimum of about 4% porosity and a permeability of 10^{-15} m^2 or higher for sequestration to be considered feasible, if a caprock with a maximum permeability of approximately 10-18 m2 is present. These results are in good

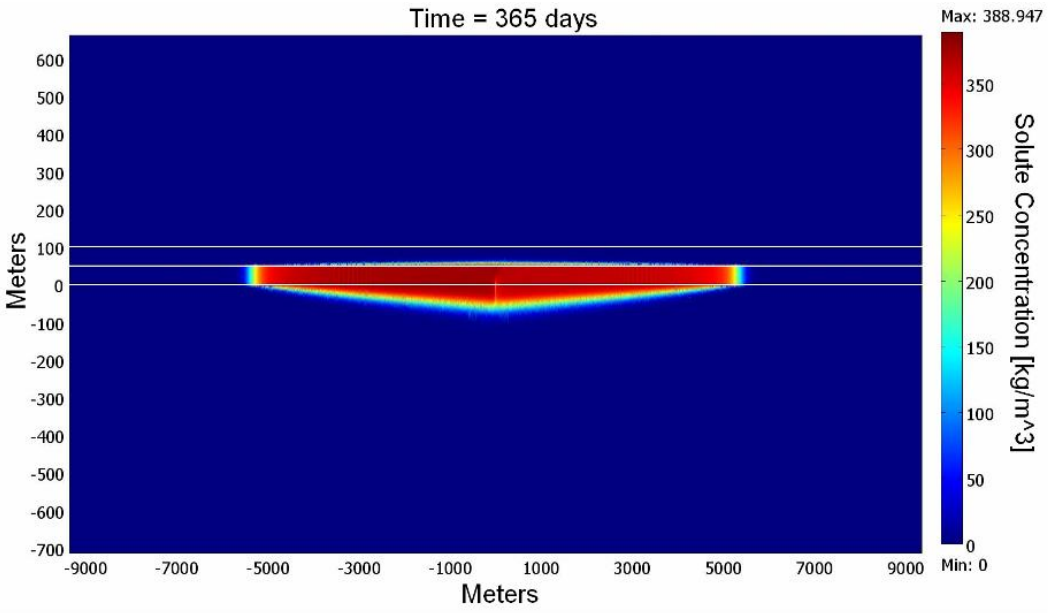

Figure C.4: One year of dilute solution injection into the center of a 50 m thick, several kilometer long fresh-water (for simplicity as actual injection would be in a brine) aquifer that is capped by a highly impermeable unit. The following model parameters were used: aquifer porosity = 0.10, aquifer permeability = 10^{-13} m^2, caprock porosity = 0.08, caprock permeability = 10^{-21} m^2, and injection rate = 5 m^3/s. Color indicates solute concentration. Notice that some solute leaks into the material below the aquifer. This would not be problematic in a real, pure CO_2 injection project because the CO_2 would be trapped in the subsurface as if it were in the aquifer. However, in a real scenario, it is unlikely that such leakage would occur because pure CO_2 rises above aquifer brine, causing injected CO_2 to pool against the bottom of sealing units (caprocks). Also visible are minor leaks into (but not through) the caprock.

agreement with ranges defined by the MGS using a compilation of current CO_2 storage studies worldwide.

Substantial field surveys, borehole drilling, and numerical studies are needed to determine whether the Mid Continental Rift System indeed exhibits favorable characteristics for CO_2 injection and storage. Our current model is in the very initial stages of the type of modeling required in a comprehensive CO_2 project because a wide range of geologic unit geometries and conditions as well as injection and storage scenarios

have yet to be fully explored. Therefore, these modeling results should be viewed as a means of guiding us toward significantly more detailed studies, both in the field and via numerical modeling, that are necessary to evaluate the potential of the rift for CO_2 injection and storage.

C.4.2 Stage two - initial study

The CO_2 solute injection model of the previous section, though a highly useful and informative exercise, cannot capture the multiphase aspects of pure CO_2 injection in a deep saline aquifer, as discussed in Section 3. Thus, we proceed to the second stage of numerical modeling (refer to Stage 2 in Section 3). We are in the process of developing a numerical framework to permit modeling of multiphase, miscible fluid transport in porous media (Figure C.2). Currently we employ the computer code COMSOL to develop all numerical models. However, future numerical modeling will also employ TOUGH2 and TOUGHREACT to allow comparison of model results and to improve our ability to develop insightful numerical models for CO_2 storage in the rift system. Additionally, we are strongly interested in concurrent numerical and analytical modeling of geologic phenomena and, hence, are considering analytical models to further improve CO_2 storage modeling capabilities.

At this point in our stage-2-type scenario, we inject pure, supercritical CO_2 into a fresh-water (not yet brine) aquifer that is modeled as an open conduit (work is underway to convert this model to more representative porous medium fluid flow conditions where porosities and permeabilities can be assigned to geologic units as in the previous solute model). This results in a system with more than one fluid phase, i.e., a multiphase model, consisting of the CO_2 and water phases (dark red and blue, respectively, in Figure C.5) that are considered immiscible for now. The model is symmetric about the right edge so that only the left half of the model needs to be simulated and visualized. This choice of symmetry permits relatively simple expansion of the model to three dimensions - the displayed geometry (Figure C.5) would be rotated about the right edge to create a cylindrically-shaped aquifer (referred to as radial symmetry). CO_2 is injected into the model at the lower-right corner. The model clearly shows that the higher buoyancy of injected, supercritical CO_2 relative to fresh-water causes the CO_2 to rise and effectively pond underneath the caprock near the center of the aquifer (represented at the right

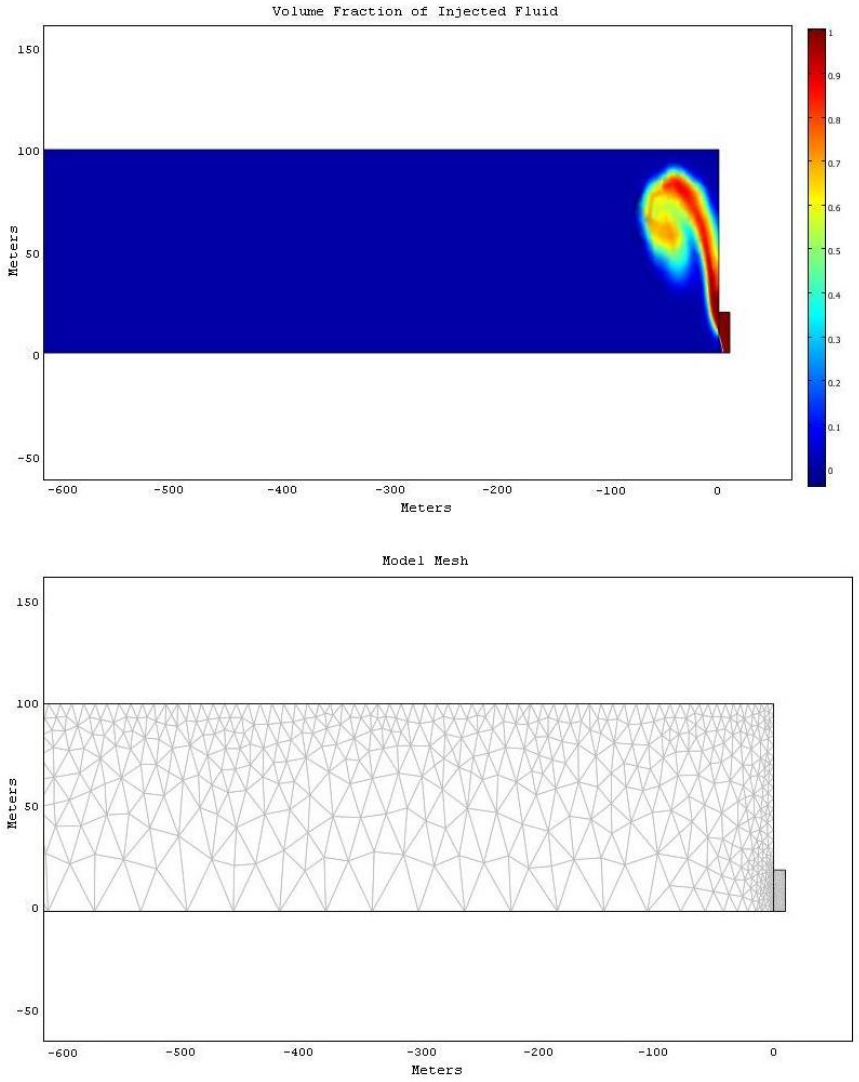

Figure C.5: A preliminary multiphase (two phase) fluid flow model. The upper image is a sample CO_2 injection scenario while the lower image is the model mesh (the grid structure that the numerical code COMSOL uses to solve multiphase fluid flow scenarios). Only the left half of the model is pictured as the model is symmetric about the right edge. CO_2 is injected into the large rectangular unit from the small unit in the lower right. The color scale indicates the fraction of fluid that is CO_2 at any point - dark red is entirely the injected CO_2 while dark blue is entirely the fresh-water that was in the unit prior to CO_2 injection. The CO_2 and water are immiscible. This model shows that buoyant, supercritical CO_2 rises and ponds underneath the caprock. At this point, the fluids flow through an open conduit rather than porous media and, thus, permeability and porosity are not modeled. Work is in progress to simulate porous media flow in a multiphase system with brine and supercritical CO_2, more representative of fluid flow in deep saline aquifers.

edge since only the left half of the symmetric two-dimensional aquifer is shown).

As previously noted, a range of geologic parameters and injection schemes need to be simulated to evaluate the likely CO_2 behavior upon injection. And as discussed throughout this section on numerical modeling, many additional parameters and conditions - as illustrated by the different stages of modeling - need to eventually be included in simulations so that they become better representations of the natural system. Nevertheless, the current (very limited) model does provide some insights into conceivable CO_2 migration scenarios. Much more has to be done, however, both with respect to numerical modeling and field-measurement of geologic conditions and parameters that can be used as model input data.

C.5 Conclusion - Summary, Results and Recommendations

C.5.1 Summary

Of the three principle methods for geologic storage of CO_2 - storage in oil reservoirs, coal beds, and deep saline aquifers - deep saline aquifers offer the most promise for significant global reduction of CO_2 [98]. Considering global CO_2 emissions through 2050, coal beds worldwide could store approximately 2% of emissions (40 to 150 Gtons), oil reservoirs could store approximately 42% of emissions (up to 920 Gtons), and saline aquifers could store approximately 500% of emissions (up to 10,000 Gtons [98]). Furthermore, saline aquifers are very prevalent worldwide and offer favorable proximity to large CO_2 sources while oil reservoirs and coal beds are notably more sparsely located. This discussion of numerical modeling of CO_2 injection and storage is thus constrained to deep saline aquifers.

Numerical modeling is essential to the process of determining a deep saline aquifer's potential for CO_2 injection and storage and analyzing associated risks. Experimental investigations of deep geologic processes are expensive and difficult, and often impossible, because of associated depths and the large spatial extent requiring investigation. First-hand observation of deep aquifer behavior is typically impossible and remote observation techniques are expensive but do provide useful (yet indirect and incomplete)

information about subsurface structures and processes. In addition, temporal effects of CO_2 injection are not constrained to short time periods immediately following injection; thus, injection sites would have to be studied in the field for hundreds of years after experimental injection ceases. Clearly, such long durations of experimental investigation are impractical. While some experimental studies are fully justifiable if a deep aquifer appears promising for CO_2 storage, the viability of such experimental analysis cannot be determined without some initial study.

Numerical modeling of CO_2 injection and storage, while not without its own limitations that are primarily the result of incomplete geologic model input data, can be applied to complete such initial, as well as subsequent, investigations. The true potential of numerical modeling is its ability to relatively easily examine numerous CO_2 injection and storage scenarios as well as ranges of geologic parameters to address necessarily incomplete three-dimensional subsurface data. For example, geologic geometries can be varied, aquifer characteristics can be adjusted, and fracturing of sealing units might be induced to study CO_2 leakage, to name only a few scenarios and parameters. Such exploration of model parameter space counteracts the uncertainty caused by incomplete knowledge of subsurface conditions, thus ultimately improving our understanding of the feasibility, effects, benefits, and risks of geologic CO_2 storage.

Recent numerical modeling of CO_2 injection and storage has examined both individual, detailed aspects of the process and simplifications of entire injection scenarios. CO_2 storage in a deep saline aquifer is inherently a multiphase process - i.e., multiple fluids, including supercritical CO_2, gaseous CO_2, and aquifer brine exist in the storage system - and hence, multiphase modeling is a principle concern of this type of numerical modeling. Work at present includes investigation of multiphase fluid flow (e.g., [101]) and brine displacement following CO_2 injection [103]. Ultimately, CO_2 storage projects seek permanent trapping of CO_2 in subsurface geologic features. A number of methods contribute to such storage - including stratigraphic trapping [106], solubility trapping [110], residual trapping [109], as well as precipitation of carbon-containing minerals, referred to as mineral trapping [104] - and modeling is ongoing to study each. Permanent CO_2 storage in saline aquifers can only be accomplished if leakage is minimal, and thus, various leakage assessment models (e.g., [111], [103]) have been established. Finally, several numerical exercises (e.g., [112], [105]) integrate individual elements of the

CO_2 storage problem in order to develop more comprehensive models with real-world geologic geometries and conditions.

Due to the necessary integration of numerous geologic processes, CO_2 injection and storage is a complex subject to model and is made more so by the natural variability of geologic structures. As such, numerical modeling should begin with very simplified injection scenarios and geologic units, gradually evolving as information regarding geologic structures become more abundant and realistic and as different types of model parameters are added. Each stage of the modeling process contributes additional information about the storage reservoir and injected fluid, eventually providing a general sense of how CO_2 may behave following injection.

Modeling begins with the injection of a dilute CO_2 solution into a simple, two dimensional aquifer geometry, at this stage avoiding the complexities of multiphase behavior and three dimensional modeling. Such basic models reveal the impact of pumping rate as well as aquifer and caprock permeability and porosity on the migration and potential leakage of injected CO_2 solute with time. Subsequent models are expanded to allow pure, supercritical CO_2 injection and examination of multiphase fluid flow, refining estimates of aquifer viability for CO_2 injection and storage. When data from field-based measurements become available, dissolution of the aquifer host-rock matrix, chemical reactions, mineral precipitation, and transport of associated aqueous species can be modeled. Further, inclusion of reactive transport considerably improves model estimates of an aquifer's CO_2 storage capacity and analysis of risks associated with injection. As numerical models are used to target field-based measurements and field-based measurements yield improved information concerning geologic conditions, numerical models can be further improved via refinements of model input parameters such as geologic structure, rock and brine composition, and pore-fluid pressure and host-rock stress fields.

C.5.2 Results and recommendations

Our preliminary numerical model is in the very initial stages of the type of modeling that needs to be completed in a comprehensive CO_2 project since a wide range of geologic conditions as well as injection and storage scenarios have yet to be fully explored.

The stage-1-type model (see Section 3) completed thus far is very simplistic. Significantly more detailed studies -both in the field and via numerical modeling are needed to determine whether the MRS has characteristics favorable to CO_2 storage.

The model currently developed injects a dilute CO_2 solution into a deep freshwater (not yet brine) aquifer for two years. A range of injection scenarios have been tested, varying solute injection rate as well as aquifer and caprock permeability and porosity between scenarios. Little leakage through caprock was observed, and injected material generally migrates less than ten kilometers (a relatively small distance) from the injection well. Within the ranges of geologic parameters we expect to encounter in the rift system, the stage-1-type model suggests that the following subsets would be feasible for CO_2 storage if indeed encountered in the subsurface: aquifer permeability, 10^{-15} to 10^{-13} m^2; aquifer porosity, 4% to 20%; caprock permeability, 10^{-21} to 10^{-18} m^2; and caprock porosity, 6% to 16%. Currently under way is an expansion of modeling capabilities to include multiphase behavior in addition to potentially existing, but less favorable, aquifer geometries and conditions.

A second phase numerical modeling program could proceed as follows. With additional time (three years), significant improvements could be made to a numerical multiphase fluid flow modeling environment. Initial work would be possible without the aid of simplified field studies to gain information about the potential CO_2 storage units in the continental rift system. Model geology could be improved by analysis of existing rock cores from the Iowa Deep Drilling Project as well as shallow cores that intersect rift system sedimentary units from locations around Minnesota. Shallow wells in the state and near the rift that intersect saline brines could be sampled in order to begin reactive transport modeling, further improving CO_2 storage models.

After an initial modeling study, results from such improved models could then be used to suggest sites in Minnesota to complete geophysical (seismic, electromagnetic, and gravity) field studies, if funding is available. Geophysical data would assist in the development of geologic unit geometries that can then be used to better constrain the next generation of numerical models. If, following this additional modeling, the rift seems to offer viable sites for CO_2 storage, deep boreholes that intersect geologic units of interest would be required, with the recent modeling aiding borehole site selection. Direct information on host-rock composition and geometric structure together with brine

composition from deep borehole sampling could then be applied to numerical models. This 3-year iterative process of geologic investigations in the field and numerical modeling continues until reasonable, predefined confidence levels concerning the feasibility of CO_2 injection and storage are reached. If studies suggest acceptable storage potential, field tests of actual CO_2 injection and storage may begin.

C.5.3 Conclusions

A preliminary numerical model of CO_2 injection into deep sedimentary structures of the Midcontinental Rift System (MRS) has been developed. The model injects a dilute CO_2 solution into a deep fresh-water (not yet brine) aquifer for two years. A range of injection scenarios have been tested, varying solute injection rate as well as aquifer and caprock permeability and porosity between scenarios. Little leakage through caprock was observed, and injected material generally migrates less than ten kilometers (a relatively small distance) from the injection well. Within the ranges of geologic parameters we expect to encounter in the rift system, the stage-1-type model suggests that the following subsets would be feasible for CO_2 storage if indeed encountered in the subsurface: aquifer permeability, 10^{-15} to 10^{-13} m^2; aquifer porosity, 4% to 20%; caprock permeability, 10^{-21} to 10^{-18} m^2; and caprock porosity, 6% to 16%. An expansion of modeling capabilities to include multiphase behavior is underway, as is model expansion to account for less favorable aquifer geometries and formation parameters. Significantly more detailed studies – both in the field and via numerical modeling – will be required to ultimately determine whether the MRS has characteristics favorable to CO_2 storage.

	aquifer porosity	max concentration of solute in aquifer (kg/m^3)	distance in aquifer from injection well horizontally to liquid with a concentration of 1 kg/m^3 (m)	leakage through caprock?
value used when other parameters are varied:	0.1			
range:	0.02	150	14000	yes
	0.04	150	13139	no
	0.06	150	11588	no
	0.08	150	10214	no
	0.1	150	9075	no
	0.12	150	8150	no
	0.14	150	7391	no
	0.16	150	6749	no
	0.18	150	6225	no
	0.2	150	5761	no
	aquifer permeability			
value used when other parameters are varied:	10^{-13} m^2			
range:	10^{-13}	150	9075	no
	10^{-14}	153	8927	no
	10^{-15}	186	7665	some
	10^{-16}	430	3656	some
	10^{-17}	1261	1167	yes
	10^{-18}	3472	360	yes
	10^{-19}	14080	170	yes
	10^{-20}	62970	123	yes
	pumping rate			
value used when other parameters are varied:	5 m^3/s			
range:	5	150	9075	no
	10	292	9101	no
	15	499	9134	no
	20	623	9150	some

Table C.1: See caption of Table C.2

	caprock porosity			
		max concentration of solute in aquifer (kg/m^3)	distance in aquifer from injection well horizontally to liquid with a concentration of 1 kg/m^3 (m)	leakage through caprock?
value used when other parameters are varied:	0.08			
range:	0.02	150	9160	yes
	0.04	150	9133	yes
	0.06	150	9101	some
	0.08	150	9075	no
	0.1	150	9031	no
	0.12	150	9024	no
	0.14	150	8997	no
	0.16	150	8963	no
	caprock permeability			
value used when other parameters are varied:	10^{-18} m^2			
range:	10^{-18}	150	9075	no
	10^{-19}	158	8904	no
	10^{-20}	192	7820	no
	10^{-21}	317	5684	no

Table C.2: The results of the stage-1-type, CO_2 solute injection model runs with a total of 30 simulations conducted. An explanation of a sample run: under "pumping rate", range 10 m^3/s. For this run, aquifer and caprock permeability and porosity were given the values next to "value used when other parameters are varied" in their respective locations in the chart. Pumping rate was set to 10 m^3/s, which is equivalent to the amount of carbon produced by a 500 MW coal-fired power plant (similarly, 5 m^3/s corresponds to a 250 MW power plant, 15 m^3/s to a 750 MW power plant, and 20 to a 1000 MW power plant). We then measured the maximum solute concentration in the aquifer (292 kg/m^3, column 3), the distance from the solute injection point to liquid in the aquifer with a solute concentration of 1 kg/m^3 (9101, column 4), and whether CO_2 leaked through the caprock (no, column 5). The 1 kg/m^3 value used in column 4 is an arbitrary value chosen because it indicates a dilute solution and provides a simple measure of solute migration.

Appendix D

Additional Material Relevant to Chapter 2.

A sample TOUGH2 input file, corresponding to the base-case model described in Chapter 2, is provided below. Note that TOUGH2 does not have a graphical user interface, rather requiring fixed-format input files. Similarly, model output is provided in the form of a fixed-format file.

```
*cpg* Flow from a CO2 Injection Well, reservoir, constant pressure drop
ROCKS----1----*----2----*----3----*----4----*----5----*----6----*----7----*----8
POMED          2650.       .10    5.E-14    5.E-14    5.E-14      2.10     1000.
well1       2650.e40       .50    5.E-14    5.E-14    5.E-14      2.10     1000.
well2       2650.e00       .50    5.E-14    5.E-14    5.E-14      2.10     1000.

MULTI----1----*----2----*----3----*----4----*----5----*----6----*----7----*----8
    3    4    3    6
SELEC....2....3....4....5....6....7....8....9...10...11...12...13...14...15...16
    1                                        0    0    0    0    0    0    0    0
        .8        .8
SOLVR----1----*----2----*----3----*----4----*----5----*----6----*----7----*----8
3  Z1   OO    8.0e-1    1.0e-7
START----1----*----2----*----3----*----4----*----5----*----6----*----7----*----8
----*----1 MOP: 123456789*123456789*1234 ---*----5----*----6----*----7----*----8
PARAM----1----*----2----*----3----*----4----*----5----*----6----*----7----*----8
   1 999     9991000300000000 14    3
          1.5768E8       -1. 3.15576E7 KA 1
       1.
     1.E-5     1.E00                                1.E-8
          250.e5                 0.0                  1.0                 100.
RPCAP----1----*----2----*----3----*----4----*----5----*----6----*----7----*----8
    7           .457       .30        1.       .05
    7           .457       .00    5.1e-5      1.e7      .999
FOFT ----1----*----2----*----3----*----4----*----5----*----6----*----7----*----8
 AA 1              1 .1745E+04 .2685E+03           .2570E+02          -.6500E+01
 KA 1              1 .3080E+08 .4738E+07           .1080E+04          -.6500E+01

GOFT ----1----*----2----*----3----*----4----*----5----*----6----*----7----*----8
 KA 1

GENER----1----*----2----*----3----*----4----*----5----*----6----*----7----*----8
 KA 1PRO 1                   1     DELV    6.4e-11   268.0e5      305.

INCON----1----*----2----*----3----*----4----*----5----*----6----*----7----*----8
 AA 1
          288.e5                 0.0                  1.0                  32.
 KA 1
          250.e5                 0.0                  1.0                 100.


TIMES----1----*----2----*----3----*----4----*----5----*----6----*----7----*----8
    1
  1.5768E8
ELEME ---   435    1    1  434   0.00000100000.000
 AA 1          well10.1906E+500.1250E+04          0.        0.        0.1525E+03
 BA 1          POMED0.7625E+060.5000E+04          0.7071E+020.        0.1525E+03
 CA 1          POMED0.7625E+060.5000E+04          0.1414E+030.        0.1525E+03
 DA 1          POMED0.7625E+060.5000E+04          0.2121E+030.        0.1525E+03
 EA 1          POMED0.7625E+060.5000E+04          0.2828E+030.        0.1525E+03
 FA 1          POMED0.7625E+060.5000E+04          0.3536E+030.        0.1525E+03
 GA 1          POMED0.7625E+060.5000E+04          0.4243E+030.        0.1525E+03
 HA 1          POMED0.7625E+060.5000E+04          0.4950E+030.        0.1525E+03
 IA 1          POMED0.7625E+060.5000E+04          0.5657E+030.        0.1525E+03
 JA 1          POMED0.7625E+060.5000E+04          0.6364E+030.        0.1525E+03
 KA 1          well20.7625E+060.1250E+04          0.7071E+030.        0.1525E+03
 BB 1          POMED0.7625E+060.5000E+04          0.7071E+020.7071E+020.1525E+03
 CB 1          POMED0.1525E+070.1000E+05          0.1414E+030.7071E+020.1525E+03
```

Figure D.1: Sample TOUGH2 input file, part 1, for CPG simulation at base-case conditions of 250 bar and 100 ^{o}C.

```
 CB 1          POMED0.1525E+070.1000E+05          0.1414E+030.7071E+020.1525E+03
 DB 1          POMED0.1525E+070.1000E+05          0.2121E+030.7071E+020.1525E+03
 EB 1          POMED0.1525E+070.1000E+05          0.2828E+030.7071E+020.1525E+03
 FB 1          POMED0.1525E+070.1000E+05          0.3536E+030.7071E+020.1525E+03
 GB 1          POMED0.1525E+070.1000E+05          0.4243E+030.7071E+020.1525E+03
 HB 1          POMED0.1525E+070.1000E+05          0.4950E+030.7071E+020.1525E+03
 IB 1          POMED0.1525E+070.1000E+05          0.5657E+030.7071E+020.1525E+03
 JB 1          POMED0.1525E+070.5000E+04          0.6364E+030.7071E+020.1525E+03
 CC 1          POMED0.7625E+060.5000E+04          0.1414E+030.1414E+030.1525E+03
 DC 1          POMED0.1525E+070.1000E+05          0.2121E+030.1414E+030.1525E+03
 EC 1          POMED0.1525E+070.1000E+05          0.2828E+030.1414E+030.1525E+03
 FC 1          POMED0.1525E+070.1000E+05          0.3536E+030.1414E+030.1525E+03
 GC 1          POMED0.1525E+070.1000E+05          0.4243E+030.1414E+030.1525E+03
 HC 1          POMED0.1525E+070.1000E+05          0.4950E+030.1414E+030.1525E+03
 IC 1          POMED0.1525E+070.5000E+04          0.5657E+030.1414E+030.1525E+03
 DD 1          POMED0.7625E+060.5000E+04          0.2121E+030.2121E+030.1525E+03
 ED 1          POMED0.1525E+070.1000E+05          0.2828E+030.2121E+030.1525E+03
 FD 1          POMED0.1525E+070.1000E+05          0.3536E+030.2121E+030.1525E+03
 GD 1          POMED0.1525E+070.1000E+05          0.4243E+030.2121E+030.1525E+03
 HD 1          POMED0.1525E+070.5000E+04          0.4950E+030.2121E+030.1525E+03
 EE 1          POMED0.7625E+060.5000E+04          0.2828E+030.2828E+030.1525E+03
 FE 1          POMED0.1525E+070.1000E+05          0.3536E+030.2828E+030.1525E+03
 GE 1          POMED0.1525E+070.5000E+04          0.4243E+030.2828E+030.1525E+03
 FF 1          POMED0.7625E+060.2500E+04          0.3536E+030.3536E+030.1525E+03
HTX00          POMED        0.
                                                                               
CONNE                                                                          
 AA 1 BA 1                  10.3536E+020.3536E+020.1078E+05
 BA 1 CA 1                  10.3536E+020.3536E+020.1078E+05
 BA 1 BB 1                  20.3536E+020.3536E+020.2157E+05
 CA 1 DA 1                  10.3536E+020.3536E+020.1078E+05
 CA 1 CB 1                  20.3536E+020.3536E+020.2157E+05
 DA 1 EA 1                  10.3536E+020.3536E+020.1078E+05
 DA 1 DB 1                  20.3536E+020.3536E+020.2157E+05
 EA 1 FA 1                  10.3536E+020.3536E+020.1078E+05
 EA 1 EB 1                  20.3536E+020.3536E+020.2157E+05
 FA 1 GA 1                  10.3536E+020.3536E+020.1078E+05
 FA 1 FB 1                  20.3536E+020.3536E+020.2157E+05
 GA 1 HA 1                  10.3536E+020.3536E+020.1078E+05
 GA 1 GB 1                  20.3536E+020.3536E+020.2157E+05
 HA 1 IA 1                  10.3536E+020.3536E+020.1078E+05
 HA 1 HB 1                  20.3536E+020.3536E+020.2157E+05
 IA 1 JA 1                  10.3536E+020.3536E+020.1078E+05
 IA 1 IB 1                  20.3536E+020.3536E+020.2157E+05
 JA 1 KA 1                  10.3536E+020.3536E+020.1078E+05
 JA 1 JB 1                  20.3536E+020.3536E+020.2157E+05
 BB 1 CB 1                  10.3536E+020.3536E+020.2157E+05
 CB 1 DB 1                  10.3536E+020.3536E+020.2157E+05
 CB 1 CC 1                  20.3536E+020.3536E+020.2157E+05
 DB 1 EB 1                  10.3536E+020.3536E+020.2157E+05
 DB 1 DC 1                  20.3536E+020.3536E+020.2157E+05
 EB 1 FB 1                  10.3536E+020.3536E+020.2157E+05
 EB 1 EC 1                  20.3536E+020.3536E+020.2157E+05
 FB 1 GB 1                  10.3536E+020.3536E+020.2157E+05
 FB 1 FC 1                  20.3536E+020.3536E+020.2157E+05
 GB 1 HB 1                  10.3536E+020.3536E+020.2157E+05
 GB 1 GC 1                  20.3536E+020.3536E+020.2157E+05
```

Figure D.2: Sample TOUGH2 input file, part 2.

```
113   GB 1 GC 1                  20.3536E+020.3536E+020.2157E+05
114   HB 1 IB 1                  10.3536E+020.3536E+020.2157E+05
115   HB 1 HC 1                  20.3536E+020.3536E+020.2157E+05
116   IB 1 JB 1                  10.3536E+020.3536E+020.2157E+05
117   IB 1 IC 1                  20.3536E+020.3536E+020.2157E+05
118   CC 1 DC 1                  10.3536E+020.3536E+020.2157E+05
119   DC 1 EC 1                  10.3536E+020.3536E+020.2157E+05
120   DC 1 DD 1                  20.3536E+020.3536E+020.2157E+05
121   EC 1 FC 1                  10.3536E+020.3536E+020.2157E+05
122   EC 1 ED 1                  20.3536E+020.3536E+020.2157E+05
123   FC 1 GC 1                  10.3536E+020.3536E+020.2157E+05
124   FC 1 FD 1                  20.3536E+020.3536E+020.2157E+05
125   GC 1 HC 1                  10.3536E+020.3536E+020.2157E+05
126   GC 1 GD 1                  20.3536E+020.3536E+020.2157E+05
127   HC 1 IC 1                  10.3536E+020.3536E+020.2157E+05
128   HC 1 HD 1                  20.3536E+020.3536E+020.2157E+05
129   DD 1 ED 1                  10.3536E+020.3536E+020.2157E+05
130   ED 1 FD 1                  10.3536E+020.3536E+020.2157E+05
131   ED 1 EE 1                  20.3536E+020.3536E+020.2157E+05
132   FD 1 GD 1                  10.3536E+020.3536E+020.2157E+05
133   FD 1 FE 1                  20.3536E+020.3536E+020.2157E+05
134   GD 1 HD 1                  10.3536E+020.3536E+020.2157E+05
135   GD 1 GE 1                  20.3536E+020.3536E+020.2157E+05
136   EE 1 FE 1                  10.3536E+020.3536E+020.2157E+05
137   FE 1 GE 1                  10.3536E+020.3536E+020.2157E+05
138   FE 1 FF 1                  20.3536E+020.3536E+020.2157E+05
139
140 ENDCY----1----*----2----*----3----*--- -4----*----5----*----6----*----7----*----8
```

Figure D.3: Sample TOUGH2 input file, part 3.

Appendix E

T(z) Profile Background Information

First and foremost, why do we choose to use T(z) profiles to investigate subsurface fluid and heat flow instead of other means? In order to gain insight into groundwater flow, one can use temperature data or hydraulic head measurements (among other means), but the former is much more easily obtained [66] [31]. Moreover, thermal data can be used in conjunction with hydraulic head information to constrain porous media hydraulic parameters such as permeability, and T(z)-determined groundwater flow parameters (such as velocity) provide an independent check of parameters determined by other methods. In addition, thermal conductivity (required in T(z) theory) of porous materials varies over a much smaller range than hydraulic conductivity (needed in hydraulic head theory) [66], and thus T(z) profile theory has the potential to very accurately determine groundwater flow parameters. Furthermore, T(z) profile studies have tremendously wide applicability – for example, to geothermal energy research (e.g., [114]), groundwater contamination studies (e.g., [115]), volcanic hazard assessment (e.g., [116]), paleoclimate reconstructions (e.g., [71]), and climate change studies (e.g., [68]) – so T(z) research is valuable to the scientific and wider communities.

E.0.4 History and development of temperature-depth profile theory: Initial observations

The potential use of heat in groundwater flow investigations was realized long before T(z) profiles were utilized. Slichter (1905)[117] noted that heat can serve as a groundwater tracer, and Collins (1925) [118] recognized that groundwater temperature is a water quality parameter. Van Orstrand (1934) [119] observed that heat flow variations in geologic units can be used to constrain geologic parameters and wrote that vertical groundwater movement can affect the amount of heat reaching the earth's surface because the natural heat flux density of the earth is small. In a 1948 publication, Birch [65] explained that the shallow subsurface records past climate change as a deviation in the thermal regime from steady state conditions. In 1960, then, Suzuki [56] reported one of the first uses of T(z) profiles in groundwater studies, estimating recharge rates in rice paddies from near surface vertical temperature distributions. Early recognition of the coupling between subsurface heat and groundwater flow formed a basis upon which the fundamental T(z) profile theories were developed.

E.0.5 Fundamental papers

Stallman's [120] differential equation for three dimensional conduction and convection in terms of groundwater velocity and temperature in a saturated porous medium is fundamental to T(z) profile theory, so it is here briefly derived.

Begin with a representative elementary volume, $dxdydz$ (see Figure E.1), of a saturated, isotropic, homogenous porous medium. Temperature is assumed to be smoothly continuous through space regardless of the fluid/solid distribution. For the very low fluid flow velocities of natural systems, this is a valid assumption. Let ρ_f be fluid density and μ, fluid viscosity. Let v and T be the seepage velocity (or specific discharge) and fluid/rock temperature, respectively, at the center of the volume. To note, though having similar units, v it is not actual fluid velocity because fluid moves only through volume pore space. Rather, it is the velocity at which the fluid appears to move through the volume, and pore-scale fluid velocity equals v divided by pore fraction. The temperature and velocity at face 1 (see Figure E.1) are $T_1 = T - \frac{1}{2}\frac{\partial T}{\partial x}dx$ and $v_1 = v - \frac{1}{2}\frac{\partial v_x}{\partial x}dx$, respectively. Similarly, at face 2 the temperature and velocity are $T_2 = T + \frac{1}{2}\frac{\partial T}{\partial x}dx$ and

$v_2 = v + \frac{1}{2}\frac{\partial v_x}{\partial x}dx$.

Fourier's law gives the rates q_{c1} and q_{c2} at which heat is conducted through faces 1 and 2, respectively: $q_{c1} = -k_t\frac{\partial T_1}{\partial x}dydz$ and $q_{c2} = -k_t\frac{\partial T_2}{\partial x}dydz$ (essentially, these equations are Fourier's law integrated over the very small area of faces 1 and 2) where k_t is the thermal conductivity of the saturated volume. Substituting into these equations the just-derived equations for T_1 and T_2, integrating, and subtracting q_{c2} from q_{c1}, we get the heat added to (or subtracted from) the volume by conduction in the x direction: $q_{c1} - q_{c2} = k_t\frac{\partial^2 T}{\partial x^2}dxdydz$. Applying this derivation to the y and z directions and summing the values along all axes, the total rate at which heat enters (or leaves) the volume by conduction is

$$q_c = k_t\left(\frac{\partial^2 T}{\partial x^2} + \frac{\partial^2 T}{\partial y^2} + \frac{\partial^2 T}{\partial z^2}\right)dxdydz.$$

Next, advection. The rate q_{f1} at which moving fluid brings heat into (or out of) the volume through face 1 is $q_{f1} = (c_f\rho_f v_1 T_1)dydz$ where c_f is the specific heat of the fluid. Substituting in the equations for v_1 and T_1 then expanding gives $q_{f1} = c_f\rho_f(v_x T - \frac{1}{2}v_x\frac{\partial T}{\partial x}dx - \frac{1}{2}T\frac{\partial v_x}{\partial x}dx + \frac{1}{4}v_x\frac{\partial T}{\partial x}\frac{\partial v_x}{\partial x}dx^2)dydz$. The same can be applied to face 2, giving q_{f2}. Subtracting q_{f2} from q_{f1} gives the rate at which heat is advected into (or out of) the volume in the x direction: $q_{f1} - q_{f2} = -c_f\rho_f\frac{\partial v_x T}{\partial x}dxdydz$. Applying the same derivation to the y and z directions then summing the values for all there axes gives the total rate at which heat is advected into (or out of) the volume:

$$q_f = -c_f\rho_f\left(\frac{\partial v_x T}{\partial x} + \frac{\partial v_y T}{\partial y} + \frac{\partial v_z T}{\partial z}\right)dxdydz.$$

Now, if $q_c + q_f \neq 0$, the temperature within the volume varies as a function of time in addition to space, with the time variance given by $q_c + q_f = c\rho\frac{\partial T}{\partial t}dxdydz$, where c is the specific heat and ρ is the density of the saturated volume. Substituting equations for q_c and q_f into this last equation gives Stallman's [120] equation for coupled heat and groundwater flow in a porous medium:

$$\frac{\partial^2 T}{\partial x^2} + \frac{\partial^2 T}{\partial y^2} + \frac{\partial^2 T}{\partial z^2} = \frac{c_f\rho_f}{k_t}\left(\frac{\partial(v_x T)}{\partial x} + \frac{\partial(v_y T)}{\partial y} + \frac{\partial(v_z T)}{\partial z}\right) + \frac{c\rho}{k_t}\frac{\partial T}{\partial t},$$

or in a more condensed form, rearranged to include spacial derivatives on one side of the equation and the time derivative on the other,

$$k_t\nabla^2 T - c_f\rho_f\nabla\cdot(vT) = c\rho\frac{\partial T}{\partial t}. \tag{E.1}$$

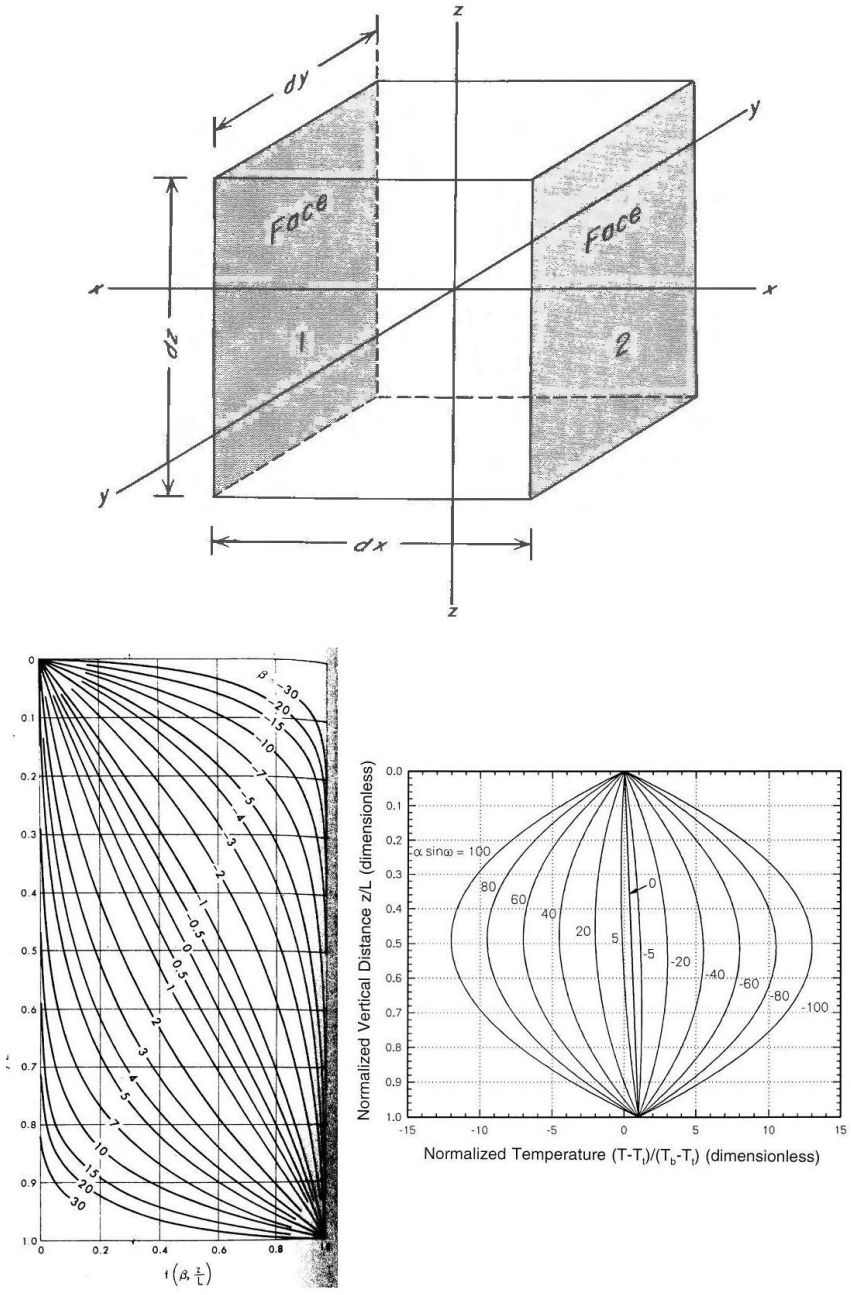

Figure E.1: The top figure is the representative elementary volume of porous medium, after [120]. Below, on the left are the type curves presented by Bredehoeft and Papadopulos (1965) [121] while in the right plot are the type curves presented by Ge (1998) [87]. T(z) profiles are fit to the former in order to determine vertical groundwater flow, while T(z) profiles are fit to the latter to determine (near) horizontal groundwater flow.

Note that this form assumes k_t, c_f, ρ_f, c, and ρ are constants. Furthermore, equation (E.1) can be formulated in terms of enthalpy rather than temperature and can be generalized to permit fluid density and viscosity variation, rock matrix compressibility, etc. [86].

Analysis of vertical temperature distributions in the subsurface was first discussed in hydrologic literature by Suzuki (1960) [56]. In 1965, Stallman [122] improved upon Suzuki's results for the effects of one dimensional groundwater flow on the vertical temperature distribution in the shallow subsurface. He together with Bredehoeft and Papadopulos [121] that same year – who solved Stallman's 1963 [120] equation analytically for one dimensional steady-state coupled groundwater and heat flow through a semiconfining layer deep enough to not be significantly affected by surface temperatures (sometimes called the geothermal zone [66]) – established the potential of T(z) profiles for subsurface heat and fluid flow studies and created the fundamental papers on which most following T(z) work is built [66].

The 1965 paper of Bredehoeft and Papadopulos [121], because of its importance in T(z) profile research, is briefly described. Bredehoeft and Papadopulos [121] consider the case of vertical, steady-state, anisothermal groundwater flow through an isotropic, homogeneous, fully saturated semiconfining layer in an aquifer system. To note, while Bredehoeft and Papadopulos [121] considered only flow in a semiconfining layer, their model is broadly applicable to vertical flow in porous media [66]. A semiconfining layer is likely to have vertical groundwater flow; Hubbert [123] demonstrated, using the law of tangents, that for a change in permeability of two orders of magnitude or greater between adjacent layers of porous medium, the direction of fluid flow across the layer boundary will be deflected by about 90^o. Thus, if we assume to first approximation that groundwater flow is horizontal in an aquifer bounded by a semiconfining layer and that the permeabilities of aquifer and semiconfining layer differ by at least two orders of magnitude (realistic), then flow will be approximately vertical in the semiconfining layer (for sample profile, see Figure E.2). Stallman's [120] equation thus reduces to

$$\frac{\partial^2 T_z}{\partial z^2} = \frac{c_f \rho_f v_z}{k_t} \frac{\partial T_z}{\partial z}. \tag{E.2}$$

While v_z, the vertical groundwater specific discharge, is assumed to be constant over the thickness of the semiconfining layer, T_z can change with depth.

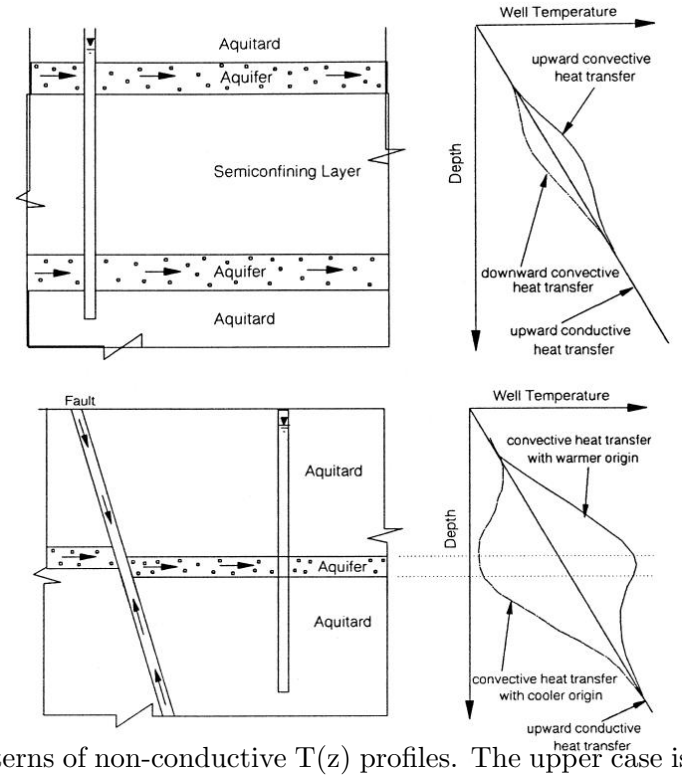

Figure E.2: Patterns of non-conductive T(z) profiles. The upper case is an example of a T(z) profile affected by vertical groundwater movement through a semiconfining layer, as in the case of Bredehoeft and Papadopulos [121], while the lower case is a profile affected by horizontal groundwater flow in which the groundwater is warmer or cooler than the local geothermal temperature. From Ge (1998) [87].

The boundary conditions $T_z = T_0$ at $z = 0$ (the uppermost temperature measurement) and $T_z = T_L$ at $z = L$ (the lowermost temperature measurement) are applied. Then, the solution to equation (E.2) is

$$\frac{T_z - T_0}{T_L - T_0} = f(\beta, z/L) = \left(exp\frac{\beta z}{L} - 1 \right) / \left(exp(\beta) - 1 \right), \quad \beta = \frac{v_z L c_f \rho_f}{k_t}.$$

Bredehoeft and Papadopulos [121] sought to determine the vertical groundwater velocity using this equation and T(z) profiles, which is accomplished by a type-curve matching technique. Plots of $\frac{T_z - T_0}{T_L - T_0}$ vs. z/L are created for measured T(z) profiles then matched to type-curves created by plotting z/L vs. $f(\beta, z/L)$ (both of which run from 0 to 1) for different values of β (see Figure E.1). The type-curve that best fits the

measured profile provides a value for β, from which v_z can be calculated if c_f, ρ_f, and k_t can be measured or estimated.

E.0.6 T(z) research continues

Bredehoeft and Papadopulos [121] proposed a visual approach to type-curve matching, which has since been examined and improved upon. Stallman [124] suggested plotting z/L vs. $z/L - (T_z - T_0)/(T_L - T_0)$ and using type curves of z/L vs. $z/L - f(\beta, z/L)$ for T(z) profiles in which the vertical groundwater flow velocity is less than 30 cm/yr, providing improved sensitivity. Sorey [67] fit type curves to data by Kunii and Smith [125] for the vertical temperature distribution in a column of glass beads and sand with helium flowing counter to the temperature gradient; T(z) profile-determine flow rate agreed well with directly measured values. Furthermore, Sorey [67] demonstrated that the theory of Bredehoeft and Papadopulos [121] is capable of detecting upward groundwater flow velocities of as little as 10^{-8} m/s. Lachenbruch and Sass [126] used the Bredehoeft and Papadopulos [121] method but with thermal boundary conditions specified in terms of heat flux rather than temperature, while Reiter et al. [127] plotted conducted heat flow vs. temperature rather than temperature vs. depth. Taniguchi et al. [61] and [62] created type curves to determine shallow vertical groundwater flow in the case of a linear or step increase in mean annual surface temperature.

Schneider [128] and Cartwright [129] were some of the first to investigate regional groundwater flow systems using T(z) profiles. Later researchers used the lag time between seasonal temperature waves in a recharge basin and aquifer, determined using T(z) profiles, to examine basin scale artificial groundwater recharge [130]. Ingebritsen et al. [86] noted that spacial variations in basin-scale heat flow can often be attributed to causes other than groundwater flow.

Numerous analytical solutions for coupled heat and groundwater flow in porous media have been published: regarding transient heat and steady state groundwater flow in the shallow subsurface (e.g., [131] [132] [133] [134] [135] [136]), horizontal groundwater flow [137], two dimensional groundwater flow from precision T(z) logs [138], and flow in fractures (e.g., [139] [55] [87]).

Parsons [140] was one of the first researchers to numerically demonstrate the impact

of groundwater flow upon the thermal structure of a basin, modeling groundwater-induced deflection of basin scale isotherms. Saleem [141], using the theory of Bredehoeft and Papadopulos [121], defined the function to be minimized when numerically solving for groundwater flow velocities from T(z) profiles. Several numerical studies relying heavily on T(z) profiles followed: to model coupled heat and fluid flow in porous media (e.g., [142] [143]), to analyze vertical groundwater flow through a semiconfining layer (e.g., [144] [145]), to estimate shallow groundwater recharge (e.g., [146] [60] [64] [147]), and to study climate (e.g., [75] [74]).

The impact of surface temperatures on the subsurface thermal regime has been analyzed in detail: to correct groundwater flow calculations for surface temperature effects (e.g., [57] [144] [148]), to correct geothermal heat flux estimates for groundwater flow effects (e.g., [149]), to estimate shallow vertical groundwater recharge rates (e.g., [58]; [75]), and to estimate changes in mean annual surface temperature associated with climate change (e.g., [81] [68] [148] [69] [70] [82] [71] [73] [74] [76]).

Finally, several other applications of T(z) profiles warrant note. T(z) profiles have been used to locate aquifers in glacial till (e.g., [150]), to identify preferential pathways for contaminants migrating through porous media (e.g., [115]), to assess eruption hazard in volcanic areas [116], to estimate submarine recharge to coastal aquifers [151], and to assess geothermal energy resources (e.g., [114]).

For further information concerning T(z) profiles and geothermal heat and subsurface fluid flow in general, see Anderson [66] and Saar [31].

Appendix F

Brief overview of Long Valley Caldera

F.0.7 Geology and History

Long Valley caldera is an elliptical depression located on the eastern boundary of the Sierra Nevada province, just inside the Basin and Range province. It extends about 32km east-west and about 17 km north-south and has a total area of approximately 450 km^2. The eastern half of the caldera, considered Long Valley proper, consists of a grass and sage covered valley of low relief with an average elevation of 2070 m. The western half is a forested area with higher relief and an average elevation of 2440 m. The caldera is drained predominately by four rivers or creeks – Deadman Creek, the Owens River, Mammoth Creek and Hot Creek – all of which drain into Crowley Lake in the southeastern corner of the caldera. The caldera walls are well-defined except in the southeast, rising to maximum elevations of 2550 m in the west, 3050 m in the south, 2300 m in the east, and 3350 m in the north and northeast. Mammoth Mountain, in the southwestern corner of the caldera, has an elevation of 3371 m [152]. See Figure F.1 for a map of the caldera.

The caldera was formed approximately 0.76 Ma [153] by the eruption of approximately 600 km^3 of the Bishop Tuff. The eruption partially emptied the Long Valley magma chamber, which resulted in collapse of the chamber roof. Potassium-argon dating indicates that almost immediately following caldera subsidence, eruptions resumed.

The rocks that accumulated on the caldera floor between 0.7Ma and 0.63Ma are known as the early rhyolites – crystal-poor rhyolite tuffs, flows, and domes. They cover the intracaldera Bishop Tuff to an average depth of 500 m. During emplacement of the early rhyolites, the resurgent doming began in the west central part of the caldera. The dome has a generally circular shape and is approximately 10 km in diameter. Bailey [152] suggests that doming ended about 0.63 Ma, though recent studies indicate that the area is inflating today [154].

Following the resurgent doming, three sets of eruptions occurred in the caldera moats (regions comprising all of the caldera floor surrounding the dome). The earliest eruption took place at 0.5 Ma with subsequent events following at 0.2My intervals. The emplaced material comprises the moat rhyolites, coarsely porphyritic hornblende-biotite type rhyolites [152]. Their location around the resurgent dome suggest that they reached the surface along the caldera ring faults. On the caldera rim and the outer edges of the caldera moat are hornblende-biotite rhyodacites, which are less silicic and more crystal rich than the moat rhyolites. The rhyodacites were emplaced from 0.37 Ma to 0.05 Ma, concurrent with and following latter moat rhyolite eruptions. The youngest are near or on Mammoth Mountain. The mountain was formed between 111 ka and 57 ka from a series of approximately 30 overlapping eruptions of trachydacitic to rhyodacitic lava flows [152].

Mafic volcanic rocks and cinder cones extend from the western caldera moat north into the Mono Craters region, which is approximately 10 km north of Long Valley Caldera. Intracaldera basaltic rocks were emplaced at the same time as the younger moat rhyolites and the rim rhyodacites. Also associated with the region extending from the west moat to the Mono Craters are the youngest volcanic features near Long Valley, the Inyo domes and craters. The domes, the youngest of which is approximately 700 years old, are rhyolitic to rhyodacitic lava domes while the craters are phreatomagmatic explosion pits likely created by rhyolitic magma rising near the surface and causing groundwater to flash to steam [152].

Following caldera subsidence, Long Valley was filled with water, possibly as a result of hot ash speeding melt of Sierra Nevada glaciers. The resulting Long Valley Lake reached its highest level shortly after forming, then gradually drained over the next 0.6 My as it cut through the rock holding it in place. The pleistocene lake outflow was in

the southeast corner of the caldera, near the present-day outflow of Lake Crowley (to note, Lake Crowley is not a remnant of Long Valley Lake but the result of the 1941 damming of the Owens River). Long Valley Lake drained completely within the last 0.1 My [152].

Considering all sources, caldera fill averages 2000 m to 2500 m thick, as estimated above precaldera materials. The deepest 1000 m to 1500 m is Bishop Tuff, none of which is exposed within the caldera (though it is exposed outside the caldera floor boundary) [152]. The materials that comprise the rest of the fill and are exposed within the caldera (as seen in Figure F.1) include the early and moat rhyolites, rim rhyodacites, basaltic rocks, rhyolites and rhyodacites of the Inyo domes, and glacial deposits and lake sediments.

Recent seismic activity in the caldera includes a magnitude 5.7 earthquake in late 1978 followed a year and a half later by four magnitude six earthquakes within two days. These earthquakes are worth noting because between the 1978 and 1980 periods of seismic activity, the resurgent dome began to inflate [155]. The unrest that began with these five large earthquakes continued through 1999 with numerous moderate earthquakes primarily during the periods of 1983, 1989 to 1990, 1996, and 1997-1998 [79]. Total resurgent dome uplift by 1999 was approximately 0.80m [153], approximately half of which took place during the initial earthquake activity [79]. Strongly correlated with periods of seismic activity was resurgent dome inflation; weeks to months before the onset of earthquakes, the rate of dome inflation tended to increase [79].

F.0.8 The Hydrothermal System

A geothermal system could be described as a groundwater circulation system with relatively deep circulation paths and high temperatures that is driven mainly by thermal buoyancy, according to Blackwell [84]. The lower segments of a system remain open as cold water moves towards a deep heat source while upper sections are often sealed as hot water rises and cools, precipitating minerals. Because of this precipitation, hydrothermal flow paths change frequently and rock permeability varies as a function of space and time. In a seismically active region such as Long Valley, flow paths may be opened by faulting; paths may remain open for hundreds to thousands of years before mineral precipitation seals them.

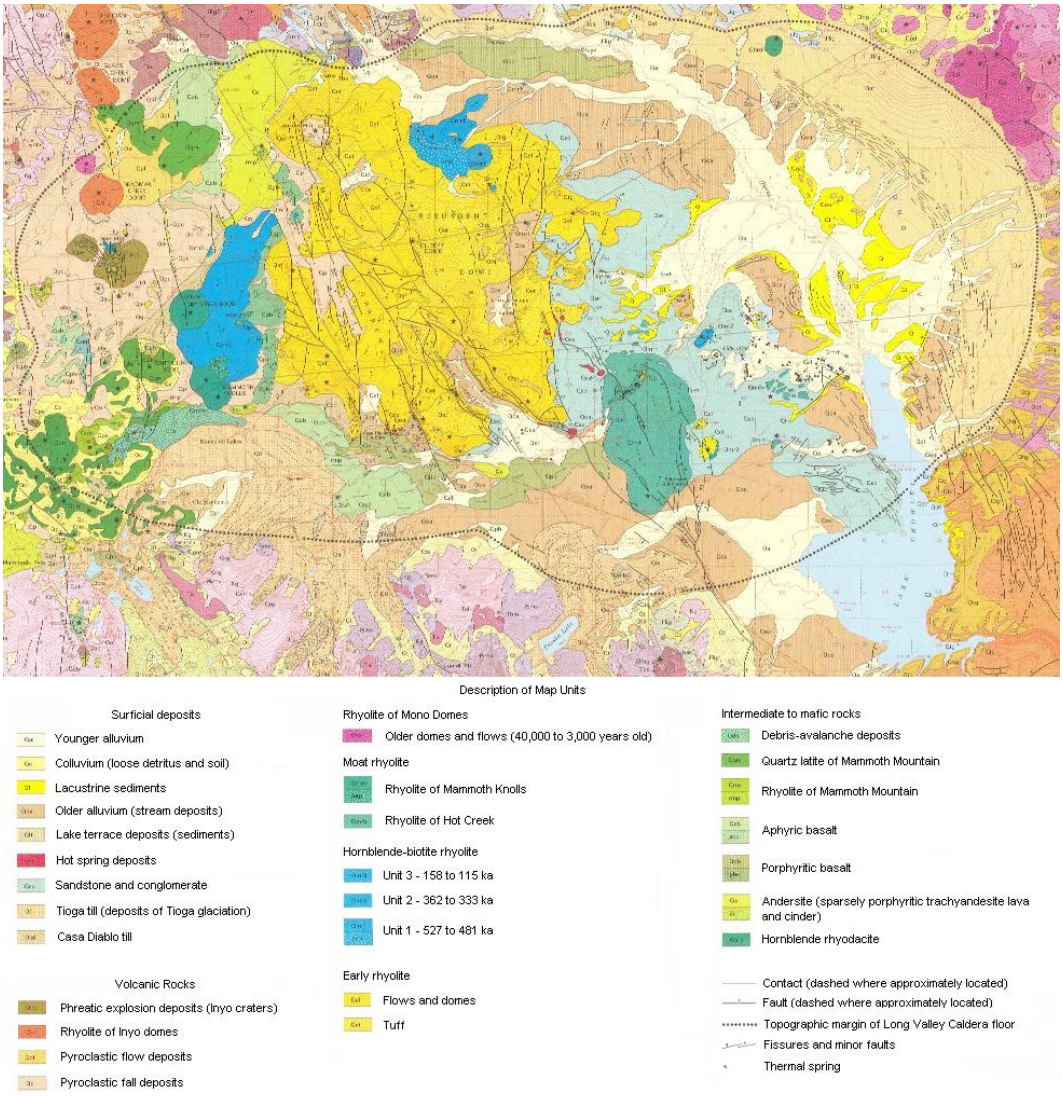

Figure F.1: Long Valley Caldera, outlined with the dotted line, with rock types. From [2].

Long Valley Caldera is located between the Sierra Nevada and the Basin and Range heat flow provinces, specifically, just inside the Basin and Range province. The regional background heat flow there is 80 mW/m^2 [84]. Common to Basin and Range

and many other geothermal systems is intermittent injection of hot hydrothermal waters into a cold, shallow hydrologic system from a deep reservoir or path. Using data obtained during the late 1980's, Sorey et. al. [80] determined that a high temperature hydrothermal reservoir exists beneath the west moat. The system, in which hot water flows upward from the reservoir into shallow aquifers then laterally through the caldera, seems to have been continuously active in some form of its present state for the last 40 ky. The activity of 40 ka corresponds well with the onset of Mono-Inyo craters rhyolitic volcanism, according to Bailey [2]. Additionally, the shallow aquifer flow established 600 B.P. corresponds well with the most recent volcanic activity of the Inyo craters and domes [84].

The thermal fluid reservoir underlying the caldera has an estimated temperature of 210 ^{o}C (using chemical geothermometry) [156]. Based on the boron concentration in Lake Crowley, which as the lowest point of the hydrologic gradient within Long Valley receives essentially all the thermal discharge from the caldera, the total surficial discharge of thermal water into Long Valley from the deep reservoir is approximately 370 L/s [157]. Approximately 248 L/s of the discharge is from springs, determined from individual spring discharge measurements [158]. The caldera exhibits a total conductive and convective heat loss of approximately $2.9 * 10^8$ W [159]. This corresponds to an average heat flux of 640 mW/m^2 over the caldera floor, similar to many North American calderas [80]. Comparing this value to the value of 1500 mW/m^2 for the Hot Creek region clearly indicates that caldera heat flow is not uniform. Approximately half the heat, $1.2 * 10^8$ W, is lost by convective flow through springs. A comparable amount of heat, $1.5 * 10^8$ W, is lost by conductive cooling of thermal fluid aquifers. Some dissipates by way of subsurface boiling, and the remainder flows into Lake Crowley via warm water [157].

A general summary of the chemistry of the waters inside and outside the caldera is provided by Mariner and Willey [85]. Outside the caldera, non-thermal waters are calcium bicarbonate in form and have low total dissolved solids. Caldera hot springs, typical of geothermal hot springs, have high chloride concentrations compared to non-thermal waters. The discharge is sodium bicarbonate to sodium bicarbonate-chloride in form; it typically has high concentrations of dissolved solids. Trace element – boron, arsenic, and fluoride – concentrations are also high compared to fresh waters. Warm

springs within the caldera have compositions between that of fresh water and that of hot springs.

To summarize, the hydrothermal system of Long Valley caldera is dominated by heating of waters, recharged along the western rim, in a deep thermal reservoir beneath the western moat. This water rises and travels laterally from west to east within two main caldera aquifers, a shallow one that has been active in its present form for approximately 600 years and a deep one that has been active for an estimated 3100 years. Hot waters mix with meteoric groundwater, conductively cool, and boil and condense before being discharged. Heat loss in the caldera is approximately $2.9 * 10^8$ W while the thermal water discharge is around 248 L/s. The present system seems to have been active for the last 40ky, concurrent with volcanic activity in the Mono-Inyo craters region.